MBE Growth and Characterisation of II-VI Semiconductor Materials and Devices

by

Gordon Horsburgh B.Sc.

Submitted for the degree of Doctor of Philosophy in the Department of Physics, Heriot-Watt University, December 1997

LIST OF FIGURES

LIST OF TABLES

PUBLICATIONS

1. S.Y. Wang, G. Horsburgh, P. Thompson, I. Hauksson, J. Mullins, K.A. Prior and B.C. Cavenett. Room temperature ZnSe/ZnCdSe self-electro-optic effect device (SEED) operating at 488nm. Appl. Phys. Lett. 63 (1993) 857-859
2. J.T. Mullins, G. Horsburgh, J. Simpson, P. Thompson, M.R. Taghizadeh, I. Hauksson, S.Y. Wang, K.A. Prior, B.C. Cavenett, G.M. Williams and A.C. Cullis. Laser induced doping profiles in MBE grown ZnSe doped with iodine. J. Crystal Growth 138 (1994) 357-361
3. K.A. Prior, B. Murdin, C.R. Pidgeon, S.Y. Wang, I. Hauksson, J.T. Mullins, G. Horsburgh, and B.C. Cavenett. Compensation processes in MBE grown zinc selenide doped with nitrogen. J. Crystal Growth 138 (1994) 94-98
4. S.Y. Wang, P. Thompson, G. Horsburgh, J. Mullins, I. Hauksson, K.A. Prior and B.C. Cavenett. A ZnSe/ZnCdSe Quantum-well Symmetric Self-Electro-Optic Effect Device (SEED) operating in the Blue-Green region. J. Crystal Growth 138 (1994) 647-651
5. S.Y. Wang, P. Thompson, G. Horsburgh, J. Mullins, M. Livingstone, I. Galbraith, K.A. Prior and B.C. Cavenett, Quantum confined Stark effect in ZnSe/ZnCdSe single quantum wells. 22nd Int. Conf. on the Physics of Semiconductors, Ed D.J. Lockwood, World Scientific, Singapore, 1995, p1536-1539
6. C. Trager-Cowan, A.M. Paterson, R.W. Martin, K.P. O'Donnell, J.T. Mullins, G. Horsburgh, K.A. Prior and B.C. Cavenett. 3-D mapping of strain and defects in a ZnSe epilayer using a variable energy electron beam. Materials Science Forum 182-184 (1995) 163-166
7. J.S. Massa, G.S. Buller, A.C. Walker, G. Horsburgh, J.T. Mullins, K.A. Prior and B.C. Cavenett. Carrier recombination studies of ZnCdSe/ZnSe quantum wells grown by molecular beam epitaxy. Appl. Phys. Lett. 66 (1995) 1346-1348
8. Z. Zhu, G. Brownlie, G. Horsburgh, P.J. Thompson, S.Y. Wang, K.A. Prior and B.C. Cavenett. Compensating acceptors and donors in nitrogen δ-doped ZnSe

layers studied by photoluminescence and photoluminescence excitation spectroscopy. Appl. Phys. Lett. 67 (1995) 2167-2169

9. Z. Zhu, G. Horsburgh, P.J. Thomson, G.D. Brownlie, S.Y. Wang, K.A. Prior and B.C. Cavenett, Nitrogen doping during atomic layer epitaxial process of ZnSe Appl. Phys. Lett. 67 (1995) 3927-3929

10. P.J. Thompson, S.Y. Wang, G. Horsburgh, T.A. Steele, K.A. Prior and B.C. Cavenett. II-VI ternary and quaternary quantum confined stark effect waveguide modulators. Appl. Phys. Lett. 68 (1996) 946-948

11. Z. Zhu, G. D. Brownlie, G. Horsburgh, P.J. Thompson, S.Y. Wang, K.A. Prior and B.C. Cavenett. Compensation Processes in Nitrogen δ-doped ZnSe Layers studied by Photoluminescence and Photoluminescence Excitation Spectroscopy. J. Crystal Growth 159 (1996) 248-251.

12. G.D. Brownlie, Z. Zhu, G. Horsburgh, T.A. Steele, P.J. Thompson, J.M. Wallace, K.A. Prior and B.C. Cavenett. Photoluminescence excitation spectroscopic studies of Nitrogen-Doped ZnSe J. Crystal Growth 159 (1996) 321-324

13. J.S. Massa, G.S. Buller, A.C. Walker, J. Simpson, G. Horsburgh, J.T. Mullins, K.A. Prior and B.C. Cavenett, A Study of the Excess Carrier Dynamics in ZnSe Based Structures Grown by Molecular Beam Epitaxy. J. Crystal Growth 159 (1996) 402-405

14. S.Y. Wang, P.J. Thompson, G. Horsburgh, T.A. Steele, G.D. Brownlie, K.A. Prior and B.C. Cavenett, Piezoelectric Effect in ZnSe/ZnCdSe Quantum Wells Grown on (211)B GaAs. J. Crystal Growth 159 (1996) 459-462

15. C. Trager-Cowan, D.M. Bagnall, F. McGow, W. McCallum, K.P. O'Donnell, P.C. Smith, P.J. Wright, B. Cockayne, K.A. Prior, J.T. Mullins, G. Horsburgh and B.C. Cavenett. Electron Beam Pumping of Cd(Zn)Se Quantum Well Laser Structures using a Variable Energy Electron Beam. J. Crystal Growth 159 (1996) 618-622

16. P.J. Thompson, S.Y. Wang, G. Horsburgh, T.A. Steele, G.D. Brownlie, K.A. Prior and B.C. Cavenett. ZnSe/ZnCdSe Quantum Confined Stark Effect Waveguide Modulators. J. Crystal Growth 159 (1996) 902-905

17. C.M. Townsley, J.J. Davies, D. Wolverson, P.J. Boyce, G. Horsburgh, T. Steele, K.A. Prior and B.C. Cavenett. Spin-flip Raman Scattering Studies of Compensating Donor Centres in Nitrogen-doped Zinc Selenide grown by molecular beam epitaxy, Phys Rev B, 53 (1996) 10983-10987

18. K.A. Prior, W. Meredith, G.D. Brownlie, Z. Zhu, P.J. Thompson, J.S. Milnes, I.S. Hauksson, G. Horsburgh, T.A. Steele, S.Y. Wang and B.C. Cavenett, Compensation in p-type ZnSe based semiconductors. Materials Sci. and Eng. B43 (1997) 9-15

19. G. Horsburgh, K.A. Prior ,W.Meredith, I Galbraith, B.C. Cavenett, G. Lacey, A.G. Cullis, C. R. Whitehouse, P. Parbrook and P. Möck, Topography Measurements of the Critical Thickness of ZnSe Grown on GaAs, submitted to APL.

20. S.A. Telfer, G. Horsburgh, J.S. Milnes, C. Morhain, P.J. Thompson, K.A. Prior and B.C. Cavenett, Growth of ZnSe and ZnCdSe on (211) GaAs substrates. J. Crystal Growth, accepted

21. C.B. O'Donnell, G. Lacey, G. Horsburgh, A.G. Cullis, C. R. Whitehouse, P.J. Parbrook, W.Meredith, I Galbraith, P.Möck, K.A. Prior and B.C. Cavenett, Measurements By X-Ray Topography Of The Critical Thickness Of ZnSe Grown On GaAs. J. Crystal Growth, accepted.

22. C. Trager-Cowan, A.M. Paterson, R.W. Martin, K.P. O'Donnell, J.T. Mullins, G. Horsburgh, K.A. Prior and B.C. Cavenett, 3-D mapping of strain and defects in a ZnSe epilayer using a variable energy electron beam. JAP submitted.

23. P.J. Thompson, J.S. Milnes, G.D. Brownlie, G. Horsburgh, W. Meredith, T.A. Steele, K.A. Prior, B.C. Cavenett and C. Trager-Cowan, Photoelectrolytic Etching Techniques for Defect Revealing in MBE Grown ZnSe, in preparation.

ACKNOWLEDGEMENTS

I would like to thank both my supervisor Kevin Prior and Brian Cavenett for all of the help and guidance which they offered during the course of my PhD.

My thanks also go to the many colleagues who I have worked beside over the years in the MBE lab, including John Simpson, John Mullins, Tim Steele and Wyn Meredith. Also, Isak Hauksson, Shouyin Wang, Paul Thompson, Glen Brownlie and James Milnes who provided the expertise for the PL and CV characterisation. I must also thank Paul Brown at Cambridge University for the TEM work, G. M. Williams of DERA for the CL results and Colin Whitehouse and Gareth Lacey from Sheffield University for their help with the X-ray topography.

A special thanks must go to the technical staff in the Physics Department for their support and assistance over the years, in particular Jimmy Smith, Peter Hearn and Euan Nelson.

I would also like to acknowledge both EPSRC and DRA Malvern for their financial support between 1992 and 1995.

A special thanks also to Samantha Telfer for all her help over the duration of this write-up.

Finally, thanks to my Mum and Dad without whose support and encouragement I would never have finished this thesis.

ABSTRACT

The work presented in this thesis is a study of the growth and characterisation of II-VI wide bandgap ZnSe based semiconductors by molecular beam epitaxy, (MBE). The materials investigated were ZnSe, ZnCdSe, ZnSSe and ZnMgSSe due to their potential application towards the development of blue emitting laser diodes. The doping of these compounds using an electrochemical iodine source and a nitrogen R.F. plasma source is also reported.

It was also shown that by using above band gap illumination a pattern could be grown into a ZnSe:I layer with micron scale definition which could potentially be used to form isolation between separate device structures.

A study of MBE grown ZnSe on (100) GaAs using asymmetric double crystal X-ray topography revealed that the critical thickness is 100±5 nm which is lower than previous estimations obtained by X-ray diffraction and photoluminescence studies. This has implications for the design of heterostructures regarding the thickness of a mismatched epilayer which could be grown before misfit dislocations form.

The growth of a quaternary laser diode which lased under pulsed operation was achieved. Although room temperature operation was not demonstrated, areas of device growth critical to the production of such a structure were identified. Subsequently, the DCXRD and PL quality of ZnSSe and ZnMgSSe grown was improved.

1. INTRODUCTION

1.1 RELEVANCE OF II-VI COMPOUND SEMICONDUCTORS

The research of II-VI semiconductors is basically split into two fields; narrow bandgap and wide bandgap compounds. The former group of compounds are largely (Hg,Cd)Te based materials and are used for the fabrication of infrared devices, in particular for optical isolators, modulators and switches to be used in high speed optical communications. These compounds also lend themselves to the formation of dilute magnetic semiconductors (DMS) which have large magneto-optic effects (eg CdMnTe). Wide bandgap II-VI semiconductors, based on ZnSe, are of particular interest due to their potential applications as LEDs, semiconductor heterostructure (SCH) laser diodes, self electro-optic effect devices (SEEDs) and modulators which operate in the blue and near UV region of the spectra. It is the investigation of these ZnSe based compounds which forms the basis of this thesis.

All of the II-VI compound semiconductors have direct bandgaps at room temperature in the range 1.52 eV to 3.54 eV corresponding to CdTe and ZnS respectively. This diversity also extends to the structural properties with lattice parameters from 6.49 Å for CdTe, to 5.41 Å for ZnS which allows for the lattice matching of II-VI ternary and quaternary alloys to a wide variety of commercially available substrates (Figure 1-1).

Figure 1-1: Bandgap vs lattice parameters of II-VI wide bandgap compounds

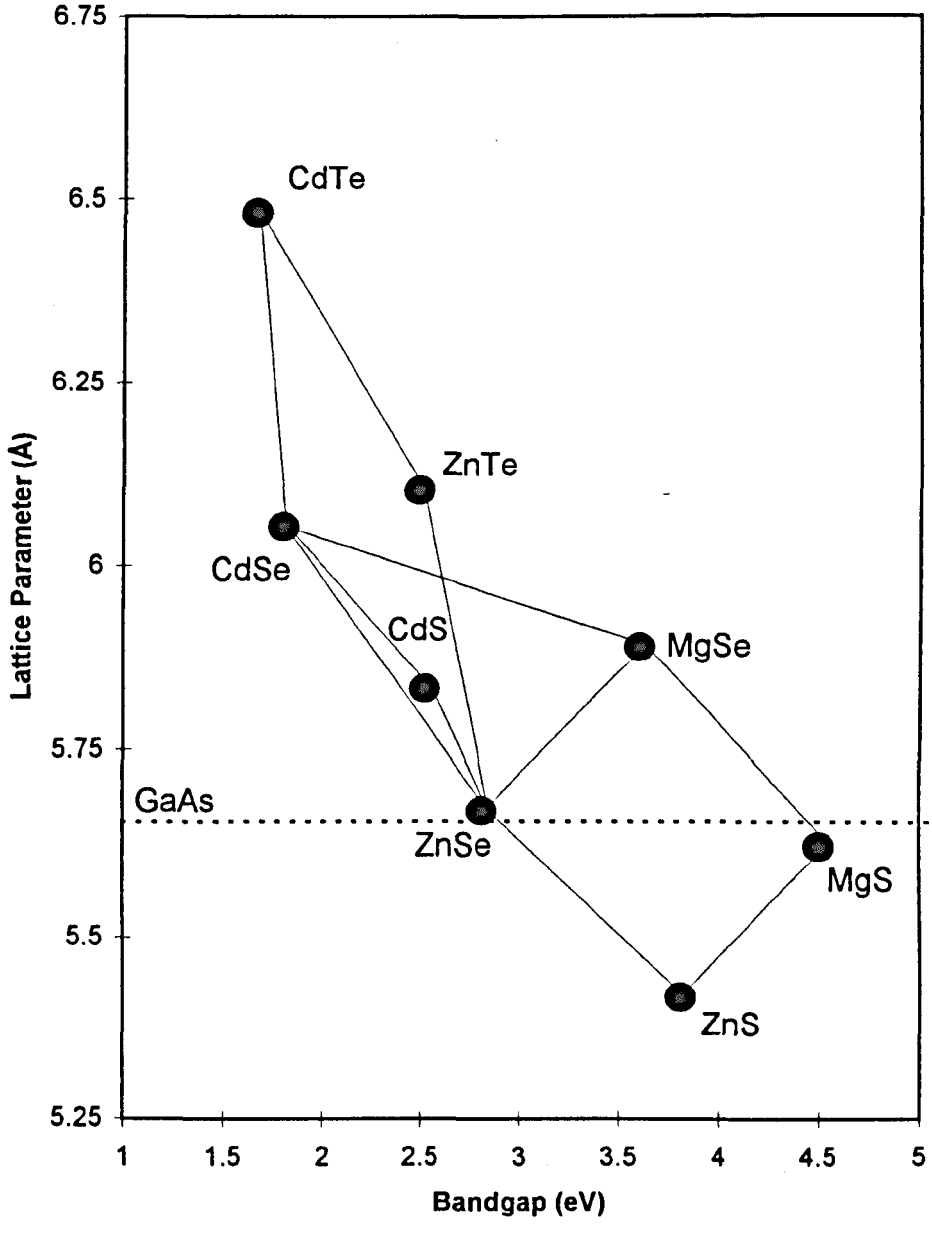

ZnSe with a room temperature bandgap of 2.71 eV and lattice parameter of 5.6681 Å is towards the middle of the bandgap range making it an ideal starting point for the development of wide bandgap devices. Ideally, the homo-epitaxy of ZnSe would be the preferred route for the epitaxial growth of devices as this approach would ensure the minimum defect levels in the grown material. However, as ZnSe substrates were not, until recently, available with suitable defect densities the majority of research undertaken on ZnSe based compounds has been performed on GaAs substrates. Both materials share the same zincblende structure and with a lattice mismatch of only 0.26% the hetero-epitaxial growth of ZnSe on GaAs is possible.

There is of course a premium to be paid for the use of GaAs substrates and that is the formation of misfit dislocations. These occur when the thickness of the epilayer exceeds the critical thickness which is determined by the magnitude of the misfit strain.[1] Although the misfit strain is small between GaAs and ZnSe it still results in a critical thickness of ~1500 Å as determined by XRD[2] and PL.[3] This is well below the required thickness for a typical device structure (approx. 3 μm). The formation of misfit defects at the GaAs/ZnSe interface results in the generation and propagation of defects throughout the structure and, critically, through the active region of any device. This severely limits the device lifetime.[4] Lattice matching through the use of ternary and quaternary compounds can help to alleviate this problem[5], but further complicate the device structure as shown in Figure 1-2.[6] The determination of the critical thickness of ZnSe on GaAs and its implications to device growth is discussed in detail in chapter 5 of this thesis.

Figure 1-2: Schematic of Quaternary Laser Structure

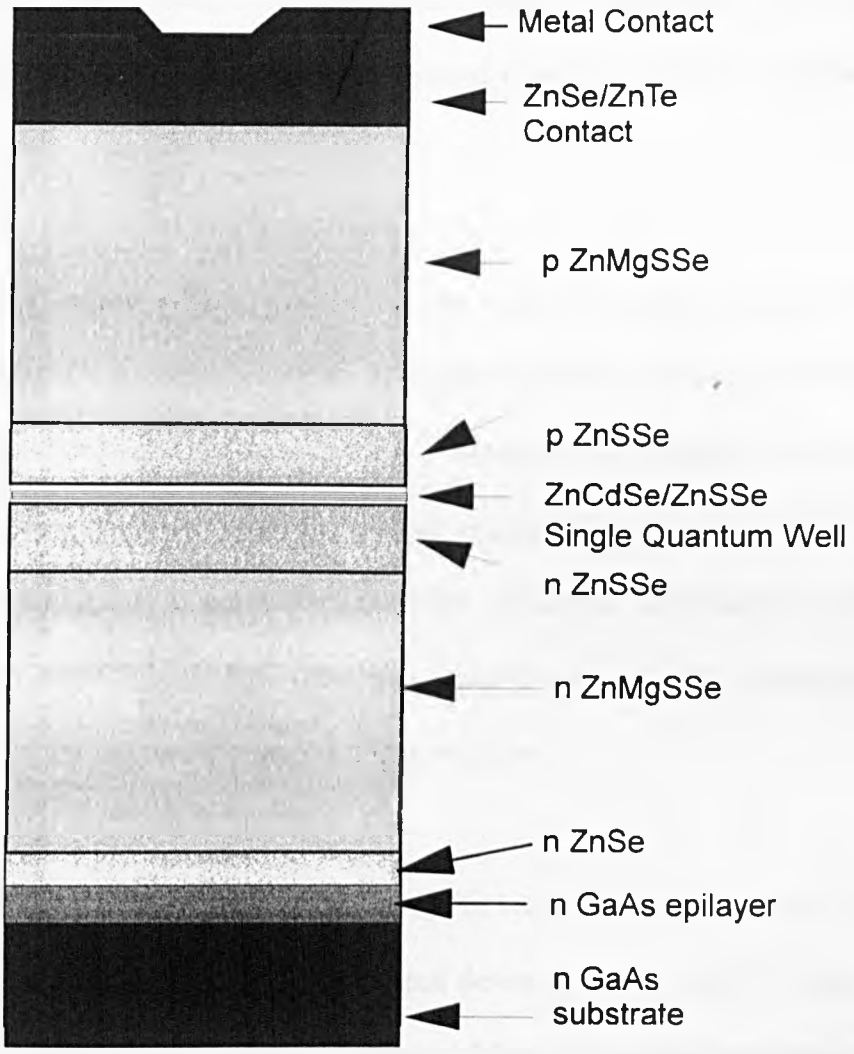

1.2 ZNSE BASED LIGHT EMITTING DIODES AND LASERS

The commercial interest in solid state diode lasers stems from their high optical output power, small physical dimensions and low power consumption which allows them to be integrated in a wide variety of miniaturised electrical equipment. A considerable scientific and commercial effort has been focused upon the realisation of blue emitting devices.

The renewal of interest in II-VI materials at the start of the eighties stemmed from the belief that using the growth techniques successful in III-V technology, II-VI materials could also be fabricated in the same fashion.[7] Although the potential of II-VI materials for the production of blue emitting devices was recognised, the early inability to produce material with p-type doping made this impossible. However, this changed in 1990 when first Park[8] and then Ohkawa[9] reported p-type material with acceptor concentrations, N_a-N_d, of 3-4x10^{17} cm^{-3} using a RF plasma nitrogen source.

LEDs emitting at 465 nm were produced using this technique[8] and it was not long before the first demonstration of lasing in ZnSe based devices came in 1991.[10] Since then the improvement in the characteristics and lifetimes of these devices has been steady.

By 1993 lasers which exhibited 77K CW and room temperature pulsed operation with threshold currents as low as 2.5 mA had been reported.[11,12] However, the lifetime of these devices was short and was measured in minutes. In order to be of viable commercial interest devices required room temperature CW operation and must have lifetimes of 10000's of hours. A step towards this goal was made in 1993 when lasers

with CW room temperature operation were reported by the Sony corporation.[13] This was achieved through the use of lattice matched laser structures containing ZnMgSSe and ZnSSe. The same group currently hold the record of 100 hours lifetime for room temperature CW lasing, reported in 1996.[14]

Although the majority of current II-VI devices have been grown by hetero-epitaxy on GaAs substrates, there has been an advance in homo-epitaxy on ZnSe substrates. Using ZnSe substrates supplied by Eagle-Picher Co., Schetzina has developed MBE grown II-VI LEDs.[15]

1.3 APPLICATIONS OF BLUE LIGHT EMITTERS

The practical applications envisaged for devices which emit in the blue region of the spectra include optical data storage, LED displays, various applications in the automotive industry and for traffic signals. Of these possible applications it is the potential impact that blue light would have on optical data storage which attracts the most commercial interest. As current systems use infrared lasers (λ=780 nm) to read/write to optical media the benefits of being able to use blue emitting laser diodes (λ=450 nm) would result in a four-fold increase in the storage density (as densities scale as $1/\lambda^2$). It is predicted that storage densities of 10 Gbit/in^2 will be reached by the year 2000.[16] However, it should be noted that the data storage density for magnetic storage systems is predicted to increase to a similar figure in the same timescale using technology which is already available.

A large number of the 20-30 million LEDs produced annually are used for display applications. These displays require red, blue and green LEDs which can then be used in various combinations to produce the desired images. Such systems are already in use as multi-pixel displays, road and rail signs in Japan and South Korea.

Another use of II-VI materials is for optoelectronic devices. A number of such devices have been grown and investigated at Heriot-Watt University including modulators[17] and SEEDs which exhibited optical bistability at room temperature for the first time in II-VI materials.[18,19] A ZnSe/ZnCdSe MQW longitudinal waveguide modulator, using the Quantum Confined Stark Effect (QCSE), was also demonstrated for the first time.[20] More recently an investigation of the piezoelectric effect of II-VI materials on (211)B GaAs substrates has been undertaken.[21]

1.4 PROBLEMS ASSOCIATED WITH II-VI DEVICE MANUFACTURE

The biggest problem facing the marketing of all II-VI based light emitters is their reduced lifetime due to defect multiplication during device operation. A high density of dislocations, typically greater than 10^6 cm^{-2} develop at the interface with the first grown ZnSe layer[22], but the defect level is reduced enormously in lattice matched systems. However, even for lattice matched systems defects at the 10^4 cm^{-2} level are still generated at the interface.[23] These then propagate through the active region, leading to rapid failure of the device. The other major problem is that of the contact to the p-type ZnSe. If a metal contact is directly applied there is a resistive barrier present between the metal contact layer and the p-type ZnSe which generates substantial amounts of heat. It has been estimated that during pulsed operation of a laser with such a contact that 80-

90% of the input power was lost at the contact corresponding to an estimated temperature increase of up to 12K during one pulse.[24] One method used for the improvement of the electrical contacts has been the growth of a ZnTe/ZnSe superlattice structure which is graded from ZnSe to ZnTe.[25] The advantage of this is that whereas ZnSe can only be doped p-type to a level 1-2x10^{18} cm^{-3}, ZnTe has been shown to have a maximum of 1x10^{19} cm^{-3} which forms a good ohmic contact.

1.5 OTHER TECHNOLOGIES

The field of blue emitting devices is not confined to II-VI ZnSe based technology. In particular, devices based on the III-V GaN system are already a viable alternative. GaN based lasers with a lifetime of 27 hours and operating at 405 nm have been fabricated by Nichia Chemical Industries.[26] The same company also has commercially available green, blue and violet LEDs which have equivalent performance to the more established AlGaAs devices currently available.[27]

1.6 CONTENTS OF THIS THESIS

In this thesis the results of investigations into a number of aspects of II-VI growth and characterisation are presented. The focus is toward the issues which affect the molecular beam epitaxial (MBE) growth of II-VI blue edge emitting laser diodes. In chapter 2 the ex-situ optical and electrical characterisation techniques and the in-situ monitoring and analytical techniques used in MBE are described. A description of the standard growth technique for obtaining high quality ZnSe material is reported. Chapter 2 also includes a comparison between the two MBE systems used describing the advantages of the current

system over the previous one. Chapter 3 and 4 report the results of double crystal X-ray diffraction and topographic analysis of ZnSe epilayers. Reported in chapter 5 is a description of the different approaches which have been attempted to find the growth conditions of ZnSSe and ZnMgSSe which would yield the quality of material required to produce edge emitting blue diode lasers. A summary of edge emitting lasers grown is also included. Chapter 6 is a discussion of the doping, both n- and p-type, of ZnSe and ZnSe based compounds and the range over which this doping can realistically be controlled. The laser patterning of n-type doped ZnSe is also included in this chapter.

1.7 REFERENCES

[1] J. H. Van der Merwe, J. Appl. Phys. 34 (1962), 123

[2] J. Petruzello, B. L. Greenberg, D. A. Cammack and R. Dalby, J. Appl. Phys. 63 (1988), 2299

[3] G. D. Brownlie, Z. Zhu, G. Horsburgh, T. A. Steele, P. J. Thomson, J. M. Wallace, K. A. Prior and B. C. Cavenett, J. Crystal Growth 159 (1196), 321

[4] C. C. Chu, T. B. Ng, J. Han, G. C. Hua, R. L. Gunshor, E. Ho, E. L. Warlick, L. A. Kolodziejski and A. V. Nurmikko, Appl. Phys. Lett. 69 (1996), 602

[5] H. Okuyama, K. Nakano, T. Miyajima and K. Akimoto, Jap. J. Appl. Phys., 30 (1991), 1620

[6] J. M. Gaines, R. R. Drenten, K. W. Haberern, T. Marshall, P. Mensz and J. Petruzello, Appl. Phys. Lett. 62 (1993), 2462

[7] T. Yao, Y. Makita and s. Maekawa, Appl. Phys. Lett. 35 (1979), 97

[8] R.M. Park, M. B. Troffer, C. M. Rouleau, J. M. DePuydt and M. A. Haase, Appl. Phys. Letts. 57 (1990), 2127

[9] K. Ohkawa, T. Karasawa and T. Mitsuyu, J. Cryst. Growth 111 (1991), 797

[10] M. A. Haase, J. Qui, J. M. DePuydt and H. Cheng, Appl. Phys. Lett. 59 (1991), 1272

[11] A. V. Nurmikko, R. L. Gunshor, N. Otsuka and M. Kobyashi, Int. Conf. Solid State Devices and Materials, Tsukuba (1992), 342

[12] H. Cheng, J. M. DePuydt, M. A. Haase and J. Qui, LEOS Meeting on Epitaxial Materials for Optoelectronic Devices, Newport, CA (1991)

[13] N. Nakayama, S. Itoh, H. Okuyama, M. Ozawa, T. Ohata, K. Nakano, M. Ikeda, A. Ishibashi and Y. Mori, Electron. Lett. 29 (1993), 2194

[14] S. Taniguchi, T. Hino, S. Itoh, K. Nakano, N. Nakayama, A. Ishibashi and M. Ikeda, Electron. Lett. 32 (1996), 552

[15] J. F. Schetzina, Int. Symp. on Blue Laser and Light Emitting Diodes, Chiba 1996

[16] Compound Semiconductor, Volume 1; Number 1 (1995), 26

[17] S. Y. Wang, Y. Kawakami, J. Simpson, H. Stewart, K. A. Prior and B. C. Cavenett, Appl. Phys. Lett., 62 (1993), 1715

[18] S. Y. Wang, G. Horsburgh, P. Thompson, I. Hauksson, J. Mullins, K. A. Prior and B. C. Cavenett, Appl. Phys. Lett. 63 (1993), 857

[19] S. Y. Wang, P. Thompson, G. Horsburgh, J. Mullins, I. Hauksson, K. A. Prior and B. C. Cavenett, J. Cryst. Growth 138 (1994), 647

[20] P. J. Thompson, S. Y. Wang, G. Horsburgh, T. A. Steele, G. D. Brownlie, K. A. Prior and B. C. Cavenett, J. Cryst. Growth 159 (1996), 459

[21] S. Y. Wang, P. J. Thomson, G. Horsburgh, T. A. Steele, G. D. Brownlie, K. A. Prior and B. C. Cavenett, J. Cryst. Growth 159 (1996), 459

[22] H. Jeon, J. Ding, W. Patterson, A. V. Nurmikko, W. Xie, D. C. Grillo, M. Kobyashi and R. L. Gunshor, Appl. Phys. Lett. 59 (1991), 3619

[23] L. H. Kuo, L. Salamanca-Riba, B. J. Wu, J. M. DePuydt, G. M. Haugen, H. Cheng, S. Guha and M. A. Haase, Appl. Phys. Lett. 65 (1994), 1230

[24] H. Jeon, J. Ding, A. V. Nurmikko W. Xie, D. C. Grillo, M. Kobyashi, R. L. Gunshor, G. C. Hua and N. Otsuka, Appl. Phys. Lett. 60 (1992), 2045

[25] Y. Fan, J. Han, L. He, J. Saraie, R. L. Gunshor, M. Hagerott, H. Jeon, A. V. Nurmikko, G. C. Hua and N. Otsuka, Appl. Phys. Lett. 61 (1992), 3160

[26] S. Nakamura, M. Senoh, S. Nagahama, N. Iwasa, T. Yamada, T. Matsushita, Y. Sugimoto and H. Kiyoku, Appl. Phys. Lett. 70 (1997), 1417

[27] III-Vs Review, Vol 9; No 1, (1996), 48

2. MBE GROWTH AND CHARACTERISATION

2.1 INTRODUCTION

Molecular beam epitaxy (MBE) is an ultra high vacuum technique for the growth of semiconductor materials of high chemical purity and structural perfection. The technique typically uses solid elemental or compound sources of high purity (typically ≥ 6N i.e. better than 99.9999% pure).

The requirement for high purity source materials for II-VI growth was first reported in 1984 by Yoneda et al[1], where after subjecting the selenium to repeated purification cycles the optical and electrical properties of the ZnSe grown improved with each cycle. The purification process involved the sublimation of the source material in a sealed evacuation chamber prior to installation in the growth chamber. After a total of nine purification cycles the net electron concentration (at room temperature) for samples grown with this material had fallen to $5x10^{14}$ cm^{-3} from an initial value of $1x10^{17}$ cm^{-3} for the as bought selenium. The photoluminescence (PL) from these samples mirrored the improvement in electrical characteristics with the PL spectra being increasingly dominated by free exciton emission, with no bound exciton emission.

Ultra high vacuum pressures, $<10^{-11}$ mbar, are achieved through the use of high performance pumps and extensive cryogenic cooling panels within stainless steel chambers. The design of these chambers varies, but essentially they are as shown in

Figure 2-1. As can be seen from this schematic the growth chamber, containing the source cells is isolated from atmosphere by a dedicated preparation chamber and entry lock. The entry lock provides a rapid and convenient means of transporting the sample from atmosphere to vacuum, and vice versa. A preparation chamber between the entry lock and the growth chamber provides a buffer which allows thermal treatment of the substrate wafer prior to entry into the growth chamber in order to minimise the risk of contamination. Also, this chamber gives provision for additional analysis techniques such as XPS which can be used prior to sample exposure to atmosphere and any subsequent oxidation of the surface. In this way a machine capable of ultra high vacuum performance can be constructed.

An ultra high vacuum allows thermally effused molecules to travel with long mean free paths before reacting at a crystalline surface. The impact of this is the fact that material evaporated by an effusion source will be transported as a beam, with no scattering from background gas (the molecular flow regime). Also, it is possible to have beams of different elements or compounds and to direct them towards a substrate material in the correct ratio to allow a surface reaction to occur and a material to form. Hence the use of the term *molecular beam.*

Epitaxial growth describes a reaction mechanism whereby a material is formed in layers, one upon the other, adopting the crystal structure of the preceding layer. In the ideal case the material grown is the same as the substrate material, *homoepitaxy.* However, it is also possible to grow different materials on the substrate material which is known as *heteroepitaxy.*

Figure 2-1: Schematic of MBE Machine

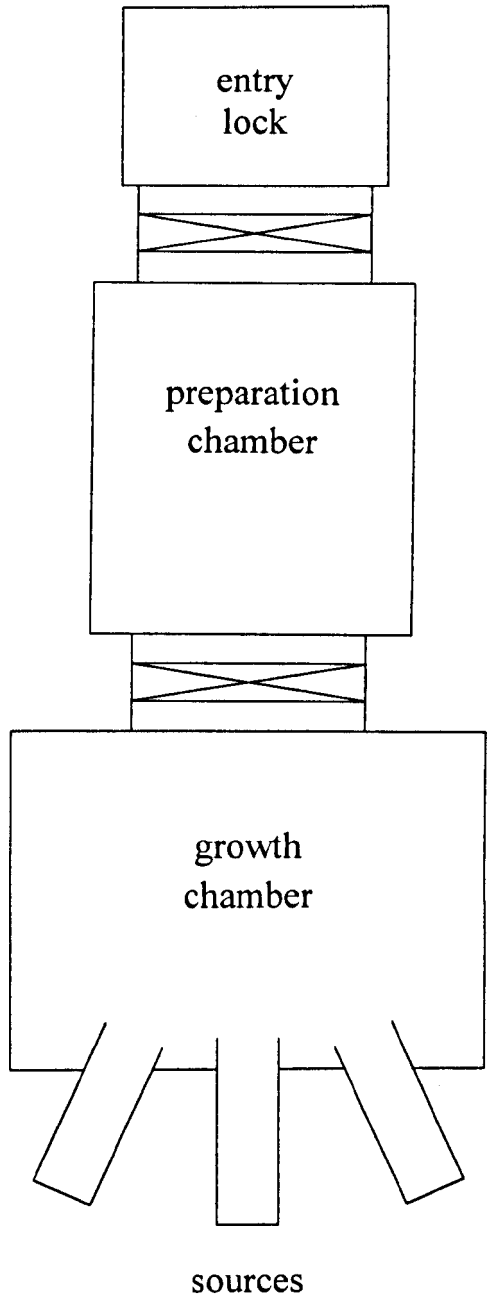

The reason for using epitaxial growth techniques is that they provide a means of precisely controlling the crystal structure, chemical composition and level of electrical doping throughout a structure allowing the formation of complex devices. In particular, the ability to grow superlattices by MBE has allowed the fabrication of a number of devices including high electron mobility transistors (HEMT's), semiconductor lasers and self electro-optic devices (SEED's) which would not have been otherwise possible using bulk growth techniques.

Another advantage that MBE has over other growth techniques, such as chemical vapour deposition (CVD) and metal-organic chemical vapour deposition (MOCVD), is the availability of in-situ growth monitoring via reflection high energy electron diffraction, RHEED. RHEED allows the growers the advantage of being able to continuously monitor the growing surface which is invaluable in the development of new materials and is only possible in high vacuum systems.

2.2 HERIOT-WATT MBE SYSTEMS

In the first year of this study a Vacuum Generators MB 288 Molecular Beam Epitaxy (MBE) system was used. This machine was commissioned in 1980 for the British Telecom Research Laboratories for the study of III-V GaAs based materials. In 1988 this vacuum system was donated to Heriot-Watt University for the study of II-VI ZnSe based compounds. Obviously, the machine required extensive cleaning and refurbishment for the conversion between the two material systems. This work was detailed in a previous study.[2]

One of the most notable achievements was in 1992, when the first II-VI ZnSe based blue-green laser diode in Europe was grown using this machine.[3] In addition, a study of quantum confined Stark effect modulators[4] culminated in the fabrication of the first ZnSe structures to exhibit SEED properties[5]. However, as II-VI material research progressed it became apparent that the MB 288 reactor did not have the necessary capacity to enable the fabrication of a room temperature blue laser diode. The system simply did not have enough cell ports to enable growth of the ZnMgSSe quaternary[6], which will be described further in chapter 5.

In 1993 a system was acquired from the GEC Hirst Laboratories. Not only did this system have the necessary number of growth ports, but it also had the added benefit of twin growth chambers. This machine had been extensively used in the fabrication of III-V devices. Indeed it had been used in production for many years. Consequently, a complete overhaul was required as many of the components were not only badly contaminated, but were also badly worn. Approximately 15 months after the start of this work, samples were again being produced.

In the following sections a comparison of the two systems will be presented detailing in particular, the differences in the vacuum pumping, sample entry, sample transportation and the source flange cell port arrangement. Also in this chapter is a description of the standardised technique employed to fabricate high quality ZnSe layers at Heriot-Watt University, including substrate etching prior to loading, the thermal heat clean of the substrate and the initiation of growth with examples of the RHEED patterns obtained.

2.3 VACUUM GENERATORS MB 288

This system was the first commercial system ever produced by Vacuum Generators. It consisted of a growth chamber, a preparation chamber and an entry lock. The layout of the system was such that rather than all three chambers being in-line, the growth chamber and entry lock were at an angle of about 30° to the preparation chamber (Figure 2-2).

Pumping of the growth and preparation chambers was exclusively achieved via oil diffusion pumps fitted with liquid nitrogen cryogenic traps. Roughing and diffusion pump backing of the system was achieved using rotary vane pumps which were fitted with foreline traps to prevent rotary oil contamination of the system.

Pressure measurement was performed using Bayard-Alpert type ionisation gauges for pressures below 10^{-3} mbar. Pirani gauges were used for the pressure range 0 to 10^{-3} mbar.

Sample transport was achieved by means of a trolley system manually driven by pulleys via external rotary drives. There were two independent trolleys, one in the entry lock and the second in the preparation chamber to enable the use of a gate valve between the chambers. The sample was mounted on a molybdenum block shaped to engage in a receptor located on the preparation and growth chamber manipulator arms as shown in Figure 2-3. The trolleys themselves were designed as shown in Figure 2-4 and held the molybdenum block vertically throughout the transfer procedure. In order to move the sample block between chambers, through gate valves, it was necessary to first locate the

Figure 2-2: Schematic diagram of MB 288 MBE system

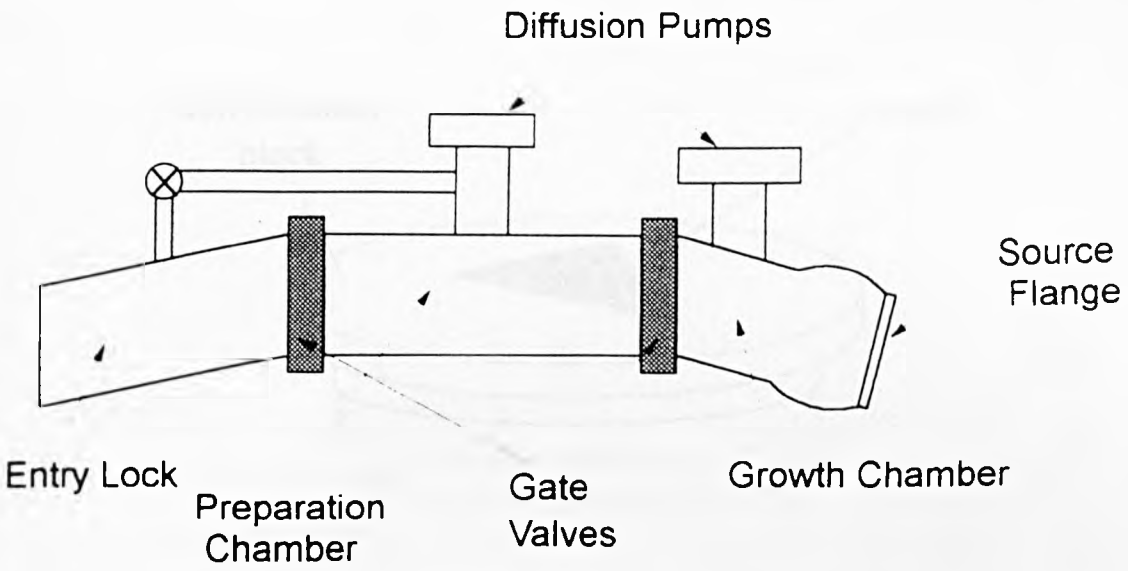

Figure 2-3: 288 Molybdenum Block

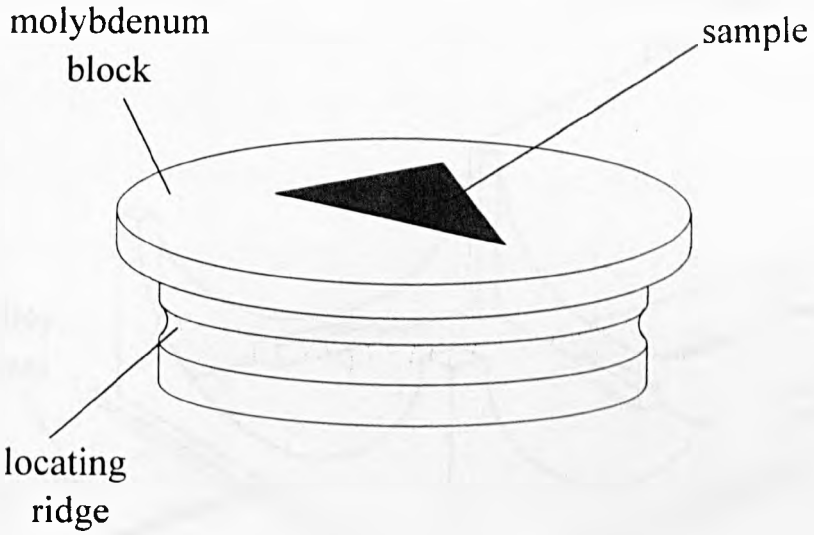

Figure 2-4: 288 Trolley

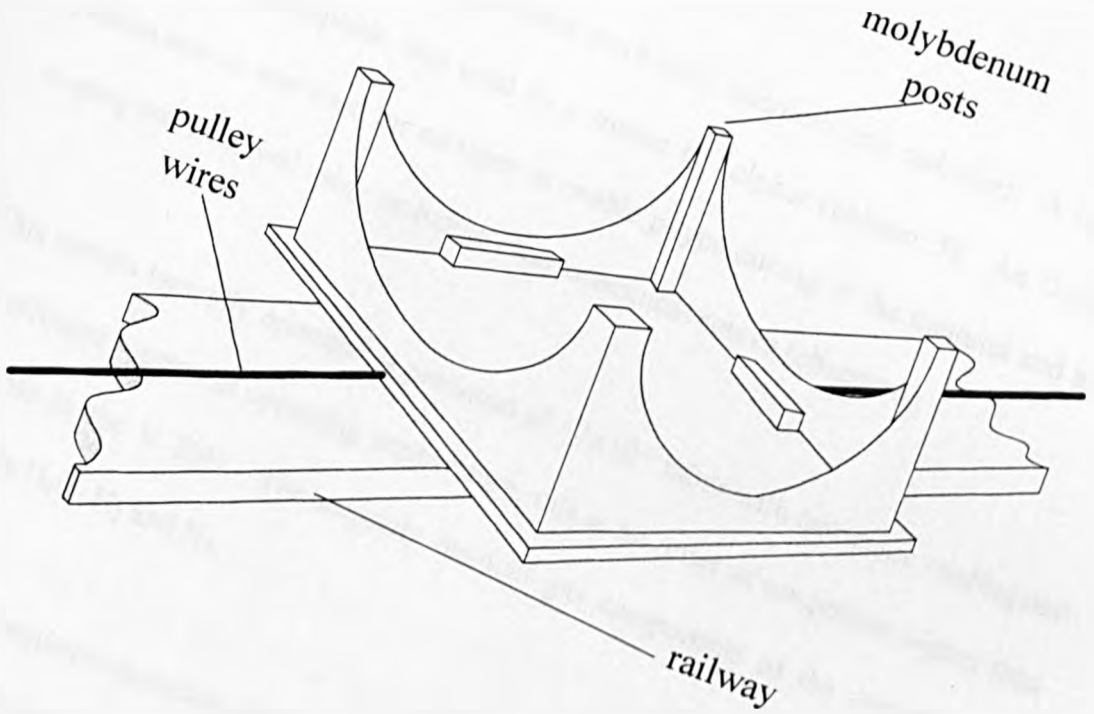

block in the receptor on the manipulator and then lift it from the first trolley. Subsequently, it was lowered into the other trolley and disengaged from the manipulator receptor.

The growth chamber had space for six V 80 standard 40cc VG effusion cells. An ancillary port for an optical pyrometer was also provided, this enabled the direct measurement of substrate temperature during growth.

The elemental effusion sources used were zinc, selenium and cadmium. A compound source of zinc-sulphide was used as a source of sulphur (chapter 5). An Oxford RF plasma source was used for nitrogen to enable p-type doping of the material and n-type doping was achieved using an iodine electrochemical source (chapter 6).

This system typically operated at pressures of ~$1x10^{-9}$ mbar with cryogenic cooling and all effusion sources at operating temperature, this is an order of magnitude higher than possible in the V 80H. The majority residual gas components of the vacuum were typically H_2O, H_2 and N_2.

The semiconductor materials grown in this chamber were ZnSe, ZnCdSe and ZnSSe. All of the devices grown used ZnSe with ZnCdSe as the active layer. Initial growth conditions of ZnSSe were investigated, but the material was not optimised to a standard where it could be incorporated in any device in this chamber. In addition there was no substrate rotation facility available which meant that samples grown in this chamber had a thickness variation across the wafer of approximately 5% which could be observed in the form of an interference pattern on the surface. Uniformity was improved by

adjusting the cell support mounts which attached the cell assembly to the cell vacuum flange by means of three rods, to try and ensure an even coverage of the beam across the sample.[7] This was particularly important for devices with quantum wells in order to ensure uniformity in the active region.

One advantage of the lack of rotation of the sample meant that it was possible to check the growth rate by mounting a GaAs bar on the wafer surface using indium. Then, by using a depth profiler, the step left when the bar was removed could be measured. In this way a direct measurement of growth rate could be made for one point on the surface of the sample.

2.4 VACUUM GENERATORS V 80H

In contrast to the MB 288, the V 80H is a modular multichamber MBE machine and the V 80H MBE machine used at Heriot-Watt was a double ended machine, meaning that there were two deposition chambers (HWA and HWB) sharing a common preparation chamber and fast entry lock shown schematically in Figure 2-5. The facility for substrate rotation is provided for in both chambers. All of the work contained in this thesis was obtained using samples grown on the A end of the growth system. Samples grown on the MB 288 have the prefix MBE whereas samples grown in the A chamber of the V 80H system have the prefix HWA.

The system is pumped using a combination of both ionisation pumps and turbomolecular pumps which are particularly useful when doping with a nitrogen plasma source due to the continuous gas flow required. This combination is particularly

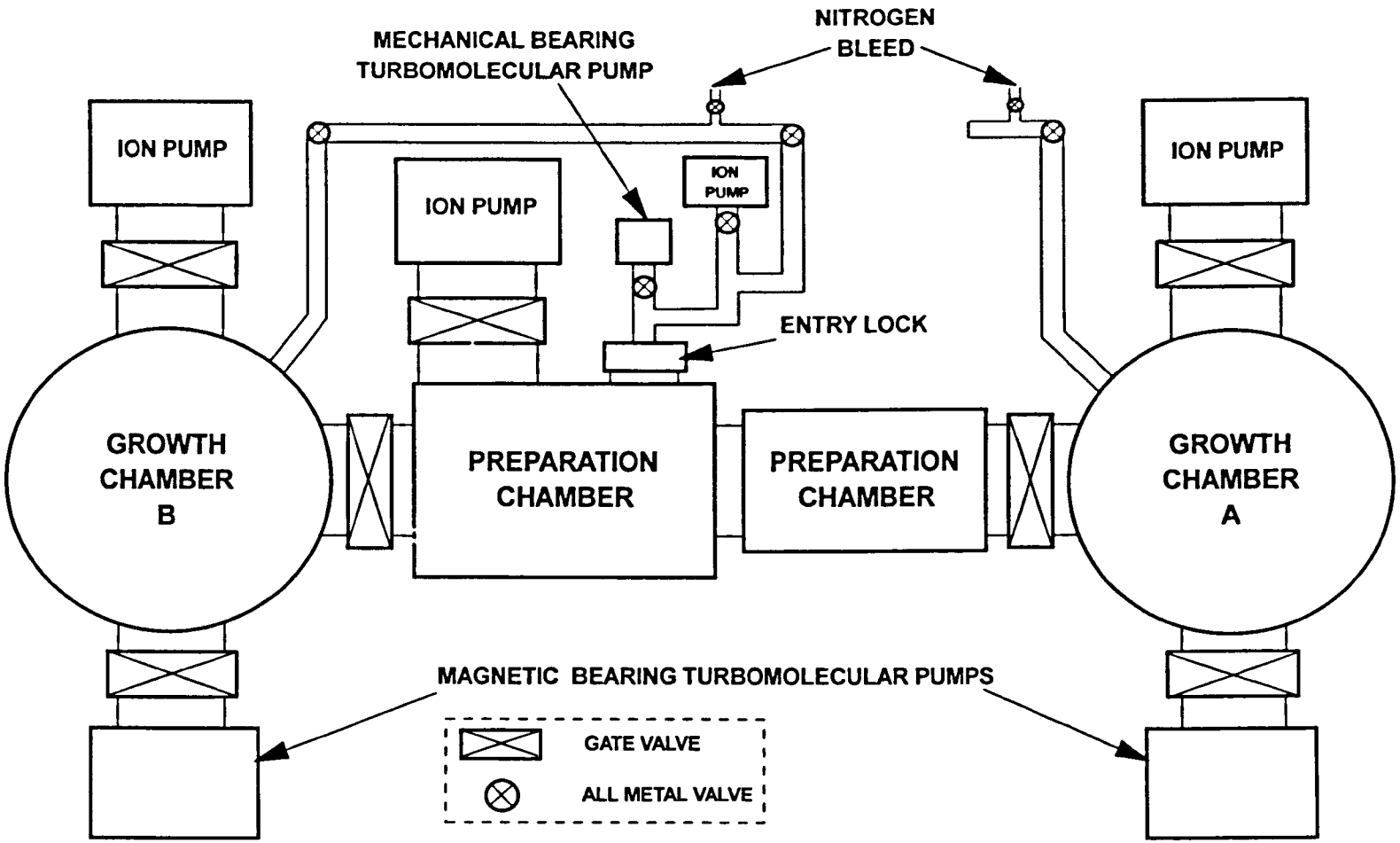

FIGURE 2-5: SCHEMATIC DIAGRAM OF VACUUM GENERATORS
TWIN-CHAMBER V80

successful in that the ionisation pump is an excellent holding pump which will keep the chamber at about 10^{-9} mbar ensuring that a contamination free vacuum is maintained when the system is idling. This pumping arrangement is supported by the use of large area liquid nitrogen cryopanels during growth as was the MB 288. Typically, pressures of approximately 10^{-10} mbar are achieved during growth in the V 80H system.

On this system, the entry lock is pumped using a 250 l/s turbomolecular pump which allows relatively rapid transport of the sample from entry lock to preparation chamber. Also in this system there is a substrate heater in the preparation chamber which was used to degas the substrates before entry into the growth chamber, reducing the risk of the vacuum within the deposition chamber being contaminated from outside the machine.

Again, pressure measurement is performed using Bayard-Alpert type ionisation gauges for pressures below 10^{-3} mbar and Pirani gauges for the pressure range 0 to 10^{-3} mbar.

Sample transport is achieved by means of a pulley driven railway with a trolley that carries the molybdenum block on which the substrate is mounted. The molybdenum block is transferred horizontally with the sample face down. Any sample manipulation required is performed using wobble sticks that have a peg at the end which locates in a hole in the molybdenum block allowing it to be lifted and transferred.

As the V 80H was designed to accommodate 3" wafers, sample uniformity over the quarter 2" wafers used during this study is maintained, providing the substrate rotation facility is used.

As mentioned above, this system had been used as a commercial production tool for GaAs devices for a number of years. Therefore, the machine required to be cleaned as well as overhauled. The entire system was dismantled and each individual component inspected for wear and was then cleaned or replaced as necessary. In addition to this the chambers were also chemically and mechanically etched using a combination of ammonia:hydrogen-peroxide mixture and abrasive material to remove all III-V deposits from the system. The top flange of the deposition chamber was also modified by removing the existing titanium sublimation pump and cryopanelling, then a new 150mm port was machined to accept a magnetically levitated turbo molecular pump. Wherever possible aluminium alloy gaskets were used in place of the more common copper type as copper reacts with Se forming black flaky deposits. All of the titanium sublimation pumps were removed from the system due to their reaction with Se.

The growth chamber provided much more flexibility as it could accommodate eight standard V 80 40cc effusion cells as well as having a number of ancillary ports for a pyrometer and a mass spectrometer. The elemental sources used were zinc, selenium, cadmium and magnesium. These sources were arranged in the growth flange as shown in Figure 2-6(b) in comparison to the source arrangement in the MB 288, Figure 2-6(a). Again zincsulphide was used as a source of sulphur and a nitrogen plasma and an iodine electrochemical cell were used for the p-type and n-type doping respectively. The range of materials which could now be grown included ZnMgSSe allowing more advanced II-VI laser structures to be investigated. Both systems had the provision for reflection high energy electron diffraction (RHEED).

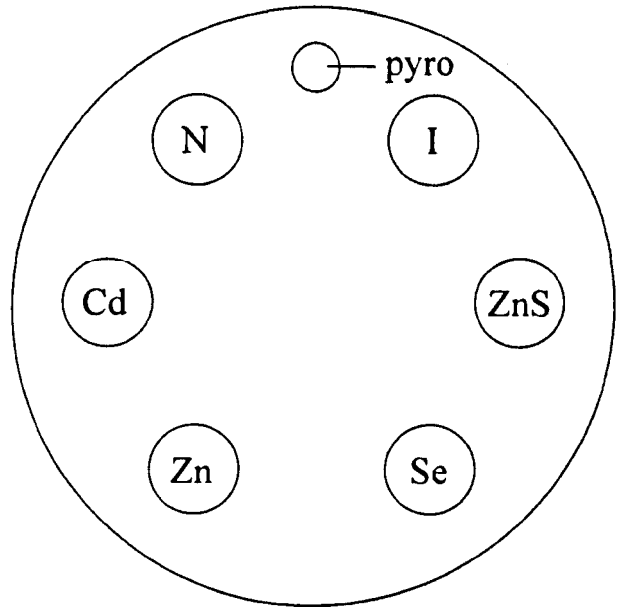

Figure 2-6(a): Arrangement of sources in 288

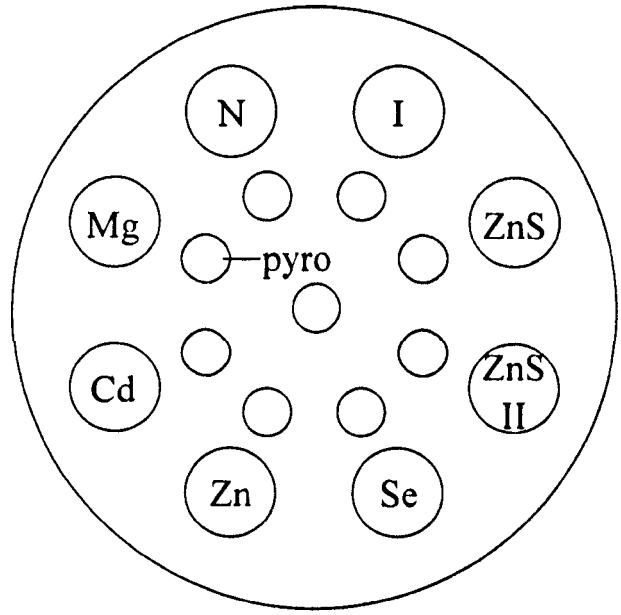

Figure 2-6(b)b: Arrangement of sources in V80H

2.5 ADVANTAGES OF THE V 80H OVER THE MB 288

Apart from the obvious age difference between the two machines, the V 80H is a far more versatile machine. A number of design modifications were made between the MB 288 and the V 80H which considerably improved the overall procedure for growth. These improvements were as follows:

2.5.1 Vacuum pumping

As the V 80H used a combination of turbomolecular pumps and ionisation pumps the risk of oil contamination was greatly reduced. The possibility of oil contamination on the MB 288 from the oil diffusion pumps was always a prime concern and it was necessary to keep the liquid nitrogen cryogenic traps cold at all times. Also, in the event of a backing rotary pump failure the diffusion pump would stall resulting in oil backstreaming into the vacuum chamber.

The use of a turbomolecular pump in the growth chamber made the use of the nitrogen plasma source far easier as the higher pumping rate allowed a greater degree of stability of the plasma, due to the far higher gas throughput capacity of the turbomolecular pump in comparison to a diffusion pump.

2.5.2 Sample entry

In contrast to the MB 288 the V 80H has an entry lock with an independent turbomolecular pump capable of pumping the chamber to a pressure of ~10^{-6} mbar within 15-30 minutes, whereas, the MB 288 entry lock was rough pumped using a rotary

pump then differentially pumped using the preparation chamber oil diffusion pump. At best, this arrangement managed to pump the entry lock to 10^{-5} mbar in a time of ~1 hour and resulted in a pressure burst in the preparation chamber when the gate valve was first opened. The lack of independent pumping of the entry lock was a major design fault of the MB 288 resulting in a far higher risk of vacuum contamination from sample loading than in the V 80H.

2.5.3 Sample transport

The vertical arrangement of sample transport in the MB 288 made the procedure cumbersome. It was necessary to clip the molybdenum block into the manipulator arm, then lift the whole manipulator assembly using micrometer drives to disengage the block from the trolley. In order to transport the sample to the next chamber the manipulator was rotated to face the next trolley, the manipulator arm was then lowered to locate the molybdenum block in the support on the trolley. The block was then disengaged from the manipulator and the trolley could then be rotated through 180° to face the next manipulator arm. However, as this process required the manual lowering of the manipulator using micrometer drives, it was possible for the operator to wind the assembly too far. Also, any indium which found its way to the edge of the block during growth inhibited the operation by causing greater friction at the contacting surfaces between the molybdenum blocks and the trolleys. This resulted in a splaying of the posts of the trolley between which the block was located. Eventually the gap between the posts became too large for the molybdenum block to be located precisely making sample transport impossible. The only way to repair this was to bring the machine to air and straighten the posts. However, as this operation had been done a number of times

over the years, the posts were relatively malleable requiring great care to be observed during sample transport.

In contrast the V 80H has a far more robust arrangement of horizontal transport which requires only that the block is located between four pegs on the trolley. Any block manipulation was performed using purpose designed wobble sticks not bulky manipulator arms. Also rather than being clipped in position, the block rests in a molybdenum support in the manipulator. The previous arrangement used on the MB 288 was prone to failure which often left the block in a precarious position.

2.5.4 Substrate rotation

The provision of substrate rotation in the V 80H leads to far better layer uniformity than was ever possible on the MB 288 which had no rotation. One slight drawback was that it was no longer possible to measure growth rate by masking the substrate, as any attempt at this resulted in graded growth away from the bar due to shadowing during rotation.

2.6 IN-SITU GROWTH MONITORING TECHNIQUES

2.6.1 Mass Spectrometry

The mass spectrometer is an invaluable tool for UHV component systems. It allows the analysis of the constituents of the residual gas in the UHV chamber from which a judgement can be made as to the condition of the vacuum. The data obtained can be displayed in the form of a chart of partial pressure versus mass number as in Figure 2-7. From this data it can be determined if there is a leak to atmosphere or if there is some

Figure 2-7: Mass spectra

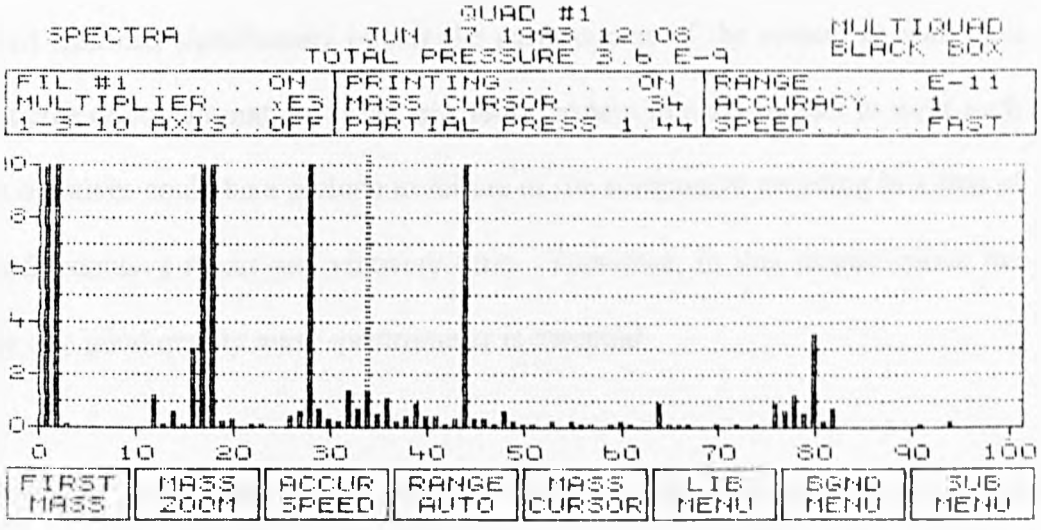

source of contamination present. The most commonly observed gases in any vacuum system are argon, carbon dioxide, carbon monoxide, nitrogen, helium, hydrogen, oxygen and water.

Leak checking of a vacuum system after it has been repaired is of paramount importance as any small leak can significantly impair the performance of the system as well as a potential source of contamination. Also, any leaks present in parts subject to wear such as bellows or valves could be a prelude to failure of the component resulting in a loss of vacuum and extensive repair and recovery time. Therefore, in this respect alone the availability of a good quality mass spectrometer is essential.

Contamination of the vacuum from sources such as rotary pump oil can be found quickly reducing the amount of time, and samples wasted finding the cause. Most common sources of contamination have characteristic cracking pattern mass spectra which allows their rapid identification through the use of a good quality residual gas analyser. Monitoring of the source cells during their degas cycle also enables the growers to ensure that the sources, or cells, have not been contaminated during filling, refurbishment or manufacture.

Throughout this study the mass spectrometer used was of the quadrupole type which has the advantages of being compact and sensitive in comparison to the magnetic field type of spectrometer. However, the technique does have a limit determined by the pressure of the system, if the upper limit of the vacuum pressure exceeds 1×10^{-4} mbar the mean free path of the ions is reduced such that they will experience collisions and will be lost

to the beam. Additionally if the pressure approaches 1 x 10^{-3} mbar oxidation and damage to the filament will occur.

2.6.2 Temperature Monitoring

Thermocouples are used extensively within the MBE system for monitoring and control of the temperature of all the heated components in the vacuum system which include effusion-cells, substrate heaters, preparation stage heaters and the LN_2 cryoshield. A thermocouple is formed at the junction of two dissimilar metals, due to the different work functions of these metals a small voltage is produced, typically in the mV range. This emf voltage is highly dependent on the temperature of the junction. Therefore, by choosing the correct thermocouple type to reflect the temperature range over which control is required a very effective means of temperature measurement is obtained. As the thermocouple is made from two strands of wire, connected only at the junction, the thermocouple can be designed into the vacuum component to provide the best position for temperature control.

The thermoelectric emf generated by the thermocouple is measured by a proportional integrating differentiating (PID) temperature controller which can remotely control the heater power supply to provide a stable measurement-control loop. The reason for using such a control circuit is to enable active control of the heater temperature through the means of a feedback loop. It is possible to tune the proportional, integrating and differentiating terms of the controller individually in order to match the power supply output to the heater characteristics to minimise overshoots and oscillations in the heater temperature. This is particularly important for the effusion cells as any variation in

temperature will have the effect of varying the molecular beam flux output resulting in unpredictable flux ratios and subsequently poor quality epitaxial growth.

A schematic diagram of such a control circuit is shown in Figure 2-8. Consideration must be made as to the type of wire which is used to connect the thermocouple with the PID controller as any further junctions, other than the intended thermocouple junction, between dissimilar metals at contacts can cause erratic and inaccurate measurements due to uncontrolled temperature fluctuations in the lab environment. This problem can be minimised through the use of the correct compensating cable for the particular thermocouple type used as they are designed to match the thermocouple material.

Low temperature cells commonly use the type K (chromel-alumel) thermocouple (Zn, Se, Cd) and for higher temperature cells (ZnS, Mg) and heaters type W5 (tungsten-rhenium) is more applicable.

Optical pyrometry also provides a valuable means of indirectly measuring the substrate growth temperature. This is necessary as the sample is mounted on a solid molybdenum block with the thermocouple behind the block and in front of the heaters with no thermal contact with either (Figure 2-9). Therefore, this temperature is valid only as a reference rather than as a direct measurement of substrate temperature. Typical offsets between the thermocouple and pyrometer readings were as shown in Figure 2-10.

The optical pyrometer used was an IRCON 500 with a wavelength range of 2-2.5μm which corresponds to a temperature range of 250-700°C. This covers the typical growth

Figure 2-8: Temperature Control Circuit Schematic

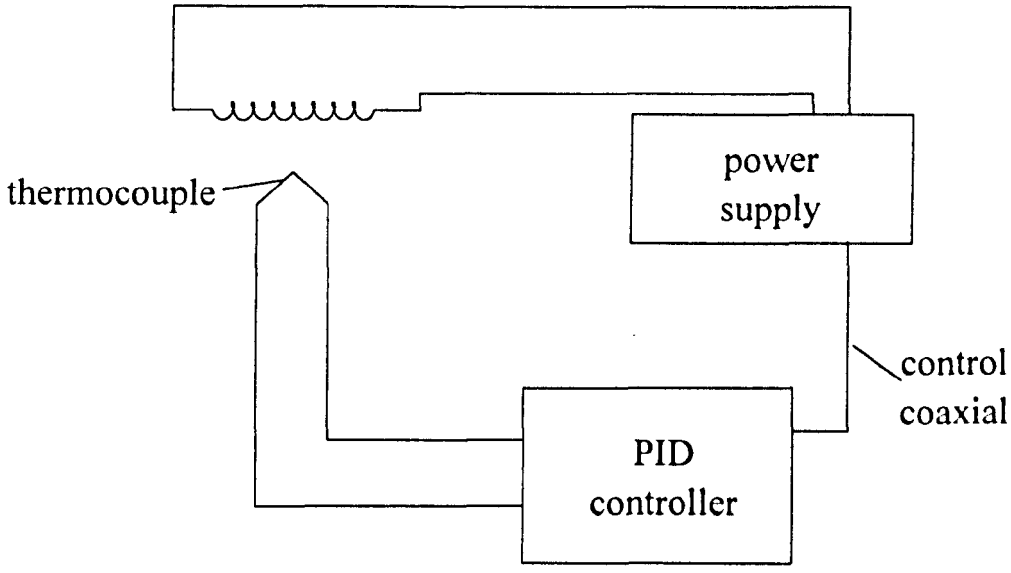

Figure 2-9: Schematic of Substrate Heater and Thermocouple Position

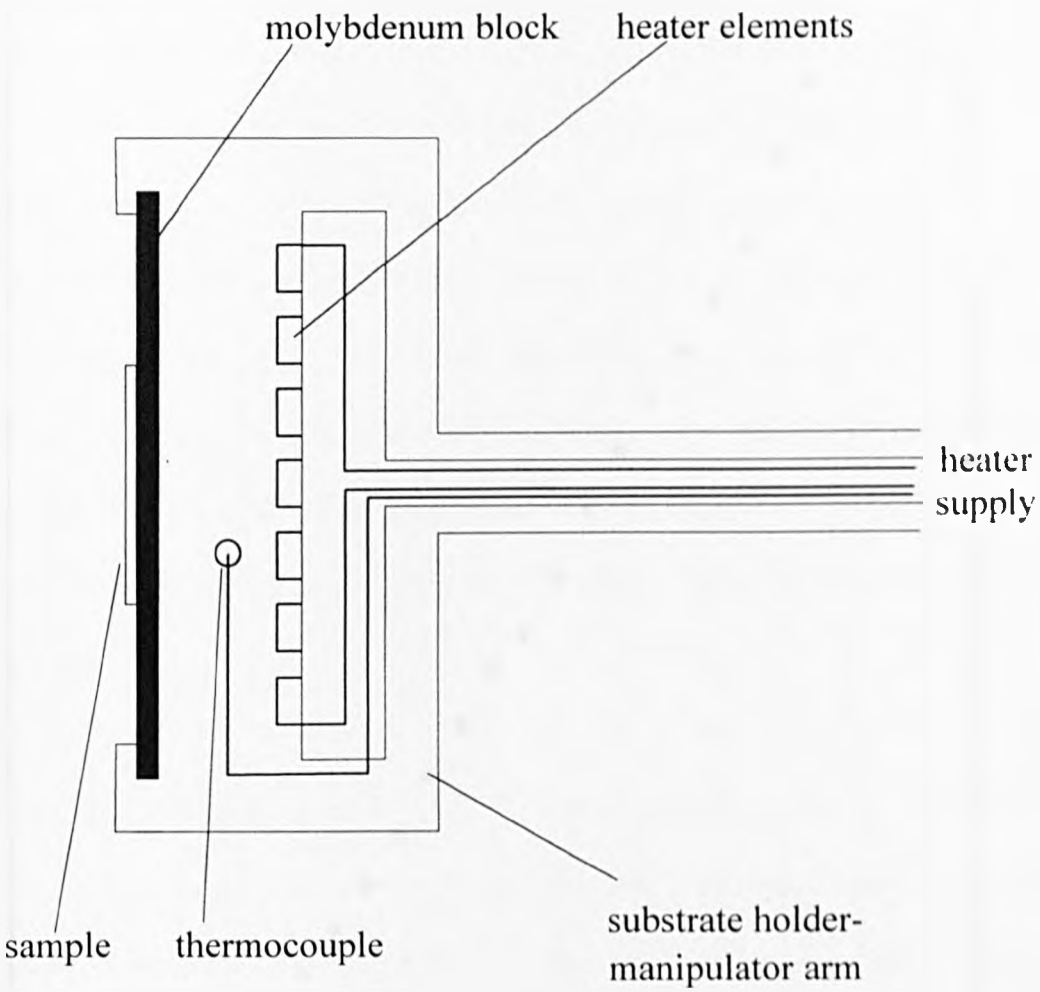

Figure 2-10: Graph of Thermocouple Temperature vs Pyrometer Reading

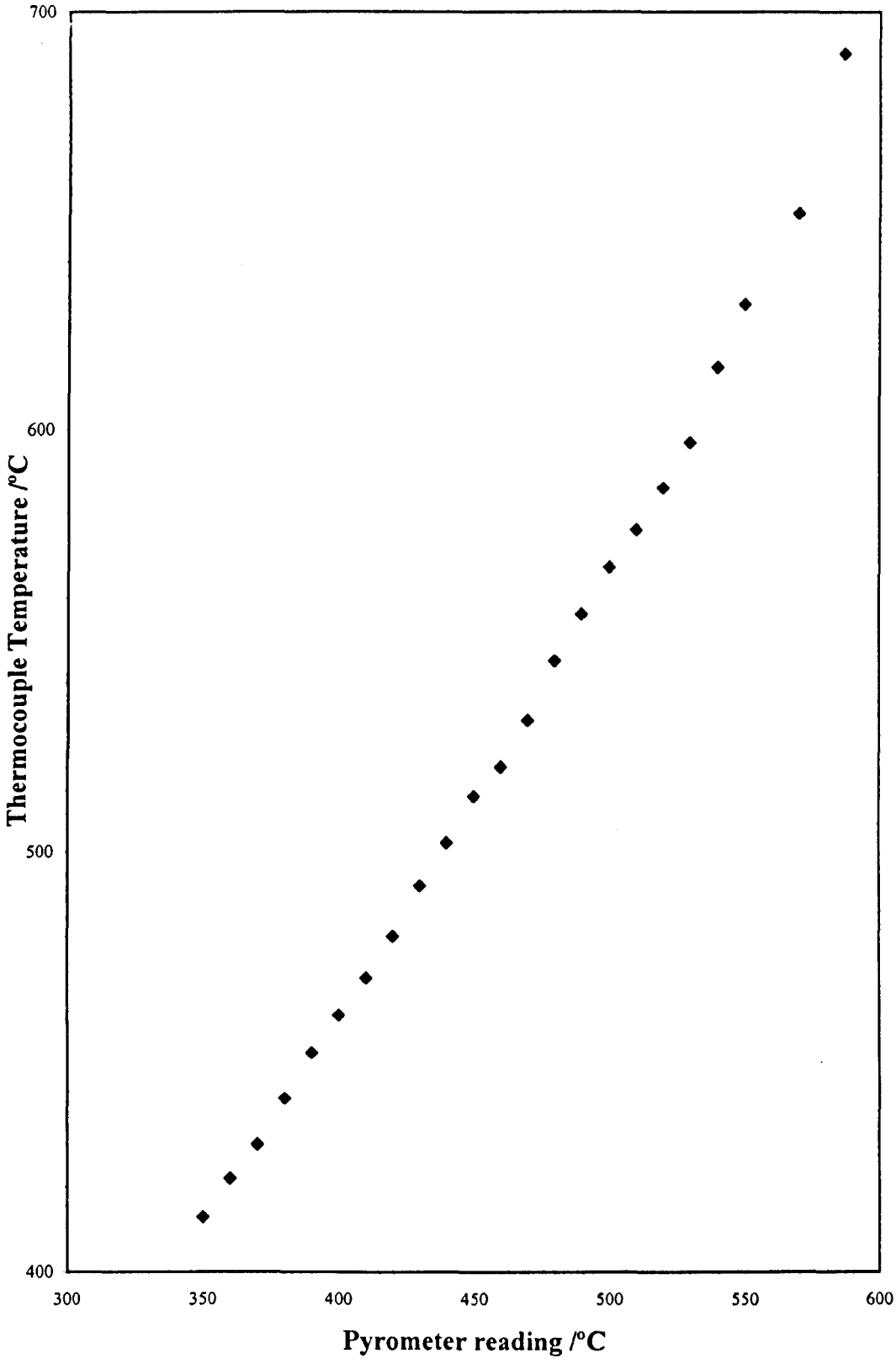

temperature in the range 280-350°C and thermal desorption of the GaAs oxide layer occurring in the region of 600°C.

An optical pyrometer works on the principal that the intensity of radiation emitted from a body is dependent on the temperature of the body as described by Stefan's law:

$$H = Ae\sigma T^4$$

where, H is the heat current due to radiation, A is the surface area, e is the emissivity, σ is Stefan's constant (=5.6699x10^{-8} Wm^{-2}K^{-4}) and T is the absolute temperature of the body.[8] In this way a temperature measurement can be made without direct contact to the substrate. However, it is necessary to have a clear optical path between the pyrometer and the sample, so to this effect a shuttered UHV window was installed on the growth flange facing the substrate. The shutter was necessary to minimise the build-up of growth deposits of absorbing films on the window to ensure reproducible measurements, which were taken at intervals throughout the growth. The window was also cleaned whenever the machine was brought to air as an additional precaution against deposition related effects.

Although GaAs (bandgap 1.090eV at 973K[9]) is largely transparent in the measurement range of the pyrometer (0.621-0.497eV) there is some free carrier absorption of long wavelength radiation. This necessitates the adjustment of the pyrometer emissivity setting for the GaAs substrate used. This setting is also dependent on doping as more heavily doped material will have greater absorption than semi-insulating substrates. However, the temperature measured is largely that of the indium used to mount the wafer. Emissivity settings used were as found previously in an earlier study and were e= 0.42 and e= 0.6 for semi-insulating and n-type substrates, respectively.[10]

2.6.3 Reflection High Energy Electron Diffraction (RHEED)

The apparatus shown schematically in Figure 2-11, is used to monitor the surface of a growing semiconductor. This consists of an electron gun unit capable of producing a beam of electrons with an energy of 30 keV and a phosphor screen. This technique is only available to UHV growth systems as it requires a collimated beam of electrons to impinge on the surface at a glancing angle producing a diffraction pattern which can be imaged. The incident and reflected beam angles are typically $< 1°$. This limits the penetration depth of the primary electrons to the top few monolayers of the surface under investigation.

The reciprocal lattice of the surface of a flat semiconductor is an array of rods, perpendicular to the real surface, in reciprocal space as the real lattice spacing is effectively zero in this direction[11]. Therefore, the electrons impinging the surface generate a diffraction pattern which is dependent on the lattice spacing and coherency of the surface. Figure 2-12 shows the reciprocal lattice of a simple square net, together with the Ewald sphere of the incident electrons. Constructive interference occurs wherever the Ewald sphere intersects with the reciprocal lattice rods. In practice, intersection occurs over an extended distance and a streaked pattern is obtained, firstly because the Ewald sphere is of finite thickness (as the incident electrons are never exactly monochromatic); secondly, because lattice vibrations and crystal imperfections cause the reciprocal lattice rods to be of finite thickness; and thirdly, because the diameter of the Ewald sphere is considerably larger than the spacing of the lattice rods.

Figure 2-11: Typical RHEED geometry

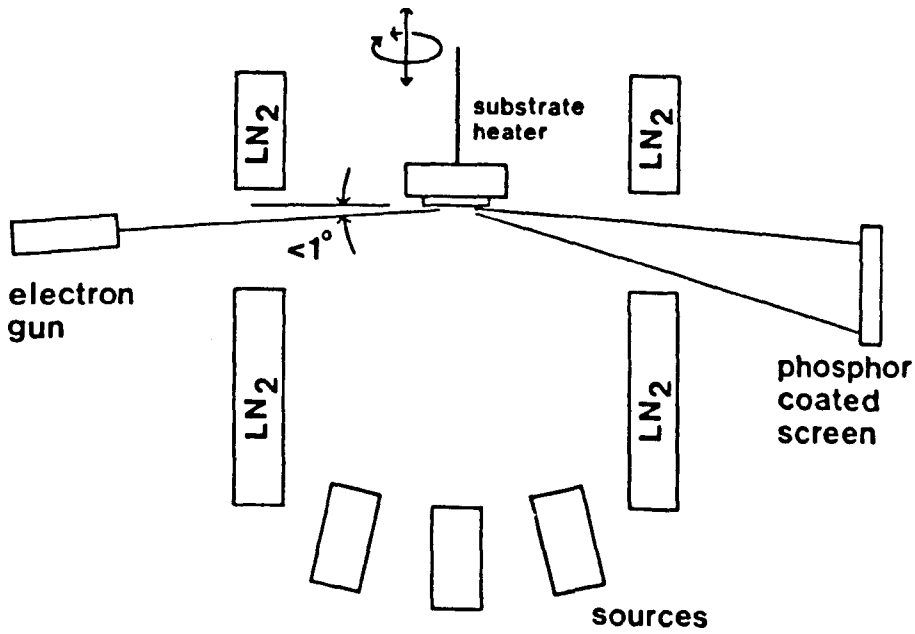

Figure 2-12: Origin of a RHEED pattern

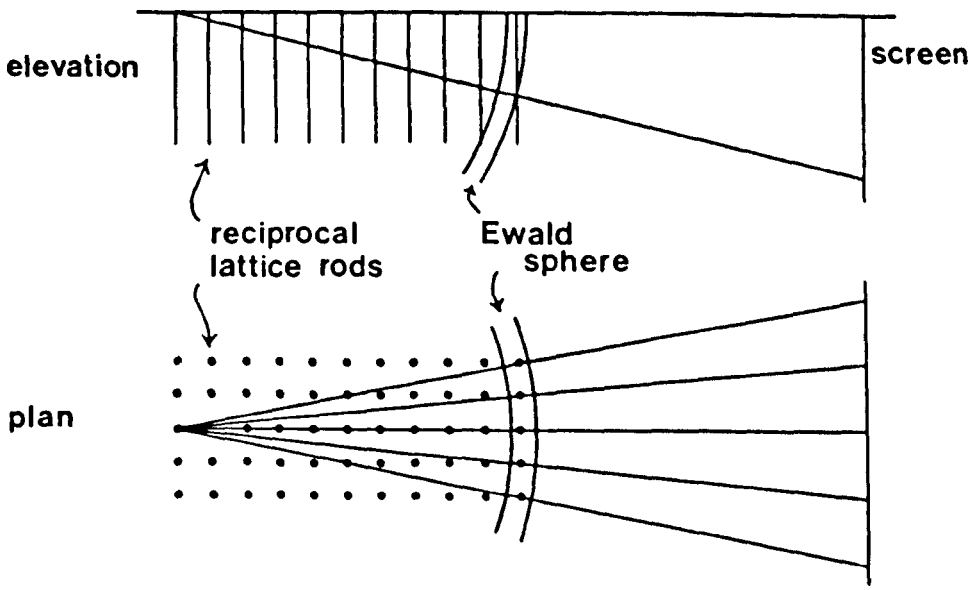

The reason that RHEED is such a useful tool for MBE is due to the phenomenon of surface reconstruction of semiconductor surfaces. Surface reconstruction is a re-ordering of the outermost atomic layer(s) of a crystal to reduce the energy of the free surface[12]. This surface reconstruction is dependent on factors such as flux ratios, surface species termination, growth rate and temperature. Therefore, unique surface reconstruction patterns for different conditions are obtained and can be used as a system-independent monitor of the growth conditions[13]. For this reason RHEED is routinely used for the monitoring of many of the most critical aspects of MBE growth such as:

1. Thermal cleaning of the substrate prior to growth.
2. Selection of the correct flux ratios.
3. Structural purity of the growing layer.

During the thermal desorption of the oxide layer from the substrate surface, the RHEED patterns change from an initial diffuse glow to a sharply reconstructed surface pattern consisting of narrow streaks. The surface reconstruction pattern of the substrate can be used to identify the terminating atomic species and can therefore be used to select a Ga or As rich surface (in the case of GaAs substrates) by the duration of the thermal treatment[14]. As these reconstructions are repeatable, once they have been characterised, it is possible to use them to ensure the consistency of the pre-growth treatment of the substrate and the standardisation of the starting surface.

RHEED is also used for observing the surface reconstruction during growth to monitor the quality of the growing layer. As the surface reconstruction during growth is dependent on the flux ratio and temperature, from the pattern obtained the growth parameters required for high quality crystal growth can be identified and reproduced.

The occurrence of any surface roughening causes the incident electron beam to be diffracted into a series of discrete spots rather than the streaks obtained from a flat surface. However, a streaked pattern can still be obtained if the epilayer surface undulates over distances appreciably greater than the e-beam coherence length[15] which is approximately 1500Å.[16] The use of RHEED as an analysis tool during the growth of ZnSe on a GaAs substrate is demonstrated in 2.9.4.

2.7 EX-SITU MEASUREMENT

2.7.1 Photoluminescence Spectroscopy (PL) of Undoped ZnSe

This particular technique provides sensitive analysis of material quality. Any impurities or defects which provide optical traps produce transitions at specific energies which show up on the spectra. Photoluminescence (PL) occurs when a semiconductor is subjected to above band gap radiation. This causes the generation of electron-hole pairs which then decay from their excited state to their ground state by radiative recombination. As PL is normally performed at 4K the exciton and low energy emission features can be observed as at this temperature PL features tend to be narrower as broadening due to lattice vibrations are minimised.

In the case of high purity ZnSe at 4K the decay of free and bound excitons occurs between 440-450nm (2.818-2.755eV). However, when there is a residual impurity present in the material which creates donors or acceptors then the excitons are bound to either ionised or neutral donors or acceptors. For nominally undoped ZnSe with a n-type residual background of ~ 10^{15} cm^{-3} this results in a PL spectra which is dominated by

donor bound and free exciton transitions. The energies of these transitions can be found from:

$$h\nu = E_g - E_x - E_B \qquad 2.1$$

where E_g is the bandgap, E_x is the binding energy of the exciton and E_B is the binding energy of the exciton to the donor or acceptor.

The PL from an early nominally undoped sample (HWA 436) grown in the A chamber of the V 80H after rebuild is shown in Figure 2-13a. These initial samples showed poor morphology and also had PL spectra indicating high levels of impurities and structural defects. The sample was grown with a Se:Zn ratio of ~1.5 and a growth temperature of 280 °C measured by pyrometer. It was approximately 1μm thick.

As well as a donor bound I_2 emission at 2.7967eV and a free exciton transition (2.8018eV)[17], this sample also exhibited other excitonic transitions (I_3, I_v^o) and deep level emission peaks due to impurities and structural defects (SA, M, Y_o). The existence of these transitions has been extensively investigated and reported in a number of publications.[18,19,20] The poor PL quality of this sample was attributed to contamination left in the system after cleaning possibly due to remaining III-V deposits or from the cleaning itself.

In contrast the PL from sample HWA 540 (Figure 2-13b) which was grown under similar conditions after the machine had been used for some time. The dominant features of the PL were the donor bound I_2 and free exciton transitions. The deep level transitions in this sample were very much lower indicative of very high quality ZnSe undoped material. This sample showed that the system was now capable of producing high quality ZnSe. The PL spectra from sample HWA 721 shown in Figure 2-13(c) was the

Figure 2-13: PL of ZnSe Grown in V 80H

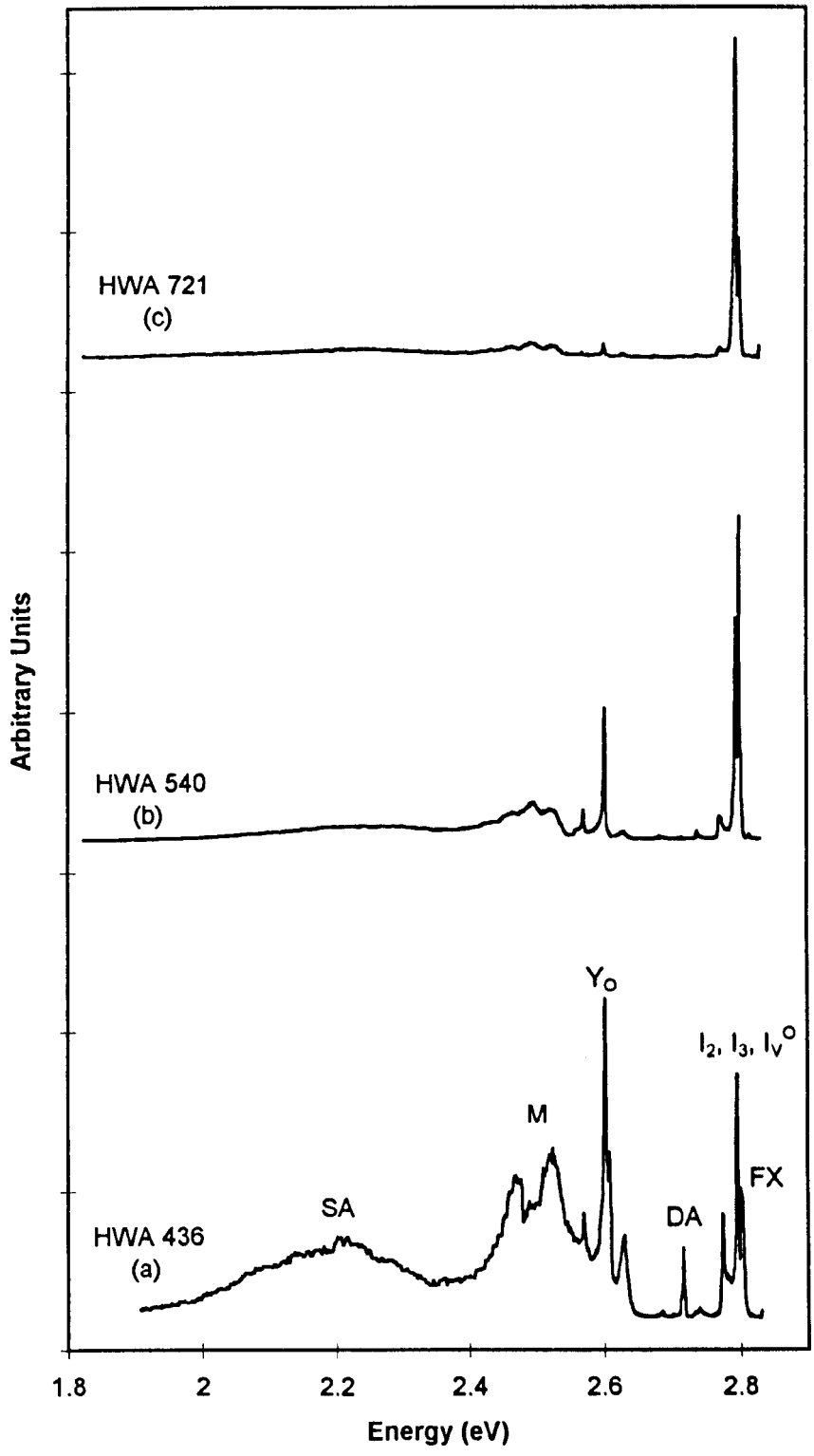

best optical quality undoped ZnSe sample produced in this system and shows very strong excitonic features.

2.7.2 Capacitance-Voltage (CV) Profiling

In order to fabricate an electrically pumped semiconductor device good control of impurity doping is required. To make this possible it is necessary to have a measurement technique which is capable of providing rapid feedback regarding the carrier concentration of the sample. Also the profile of the doping through the layer or structure is required to be measured to ensure that the doping is uniform as well as to the required carrier concentration. In the case of II-VI materials, CVD growth techniques are limited by the lack of a dopant capable of providing the level of p-type doping required for electrical devices. Whereas, in MBE the use of a nitrogen plasma gives sufficient doping for pn junction devices.[21,22]

Measurement of doping is performed using an electrochemical C-V profiling technique in which an electrolyte solution is used to establish contact with the semiconductor. For ZnSe the use of the electrolyte solution enables both the C-V measurements to be obtained and the etching of the material to provide a depth profile. The electrolyte solution used was NaOH:Na_2SO_3.[23] In practice, the conditions which favour etching and those for measuring are alternated allowing the carrier concentration to be measured as a function of depth. As the electrolyte is a concentrated solution the number of ions available is high, this means that the electrolyte/semiconductor interface behaves as a metal/semiconductor Schottky junction. Therefore, for a uniformly doped semiconductor the depletion width, W_d of the interface is given by:[24]

$$W_d = \sqrt{\frac{2(\phi - V)\varepsilon_o \varepsilon_r}{eN}}$$

and the barrier capacitance, C by:

$$C = A\sqrt{\frac{eN\varepsilon_o \varepsilon_r}{2(\phi - V)}}$$

where $\varepsilon_o\varepsilon_r$ is the permittivity of the material, e is the electronic charge, A is the area of the electrolyte/semiconductor contact, N is the net donor or acceptor concentration and ϕ is the flat band potential. The charge carrier density, N at the edge of the depletion layer is given by:

$$N = \frac{1}{e\varepsilon_o \varepsilon_r A^2} \frac{C^3}{dC/dV}$$

where dC/dV is the slope of the C-V curve at the edge of the depletion layer. The quantities C and dC/dV were obtained by using a slowly modulated high frequency voltage, typically between 1-25kHz to measure C and 0.01-2.55kHz to determine dC/dV. Typically the frequency is fixed at 3.2 and 0.04kHz to measure C and dC/dV, respectively. In normal materials the free carrier concentration is equal to the net donor or acceptor concentration as measured by the C-V profile at room temperature because the donors and acceptors are totally ionised. However, deep states or highly compensated doping can influence the measured profile.

Figure 2-14; Diagram of electrochemical cell used for C-V measurement

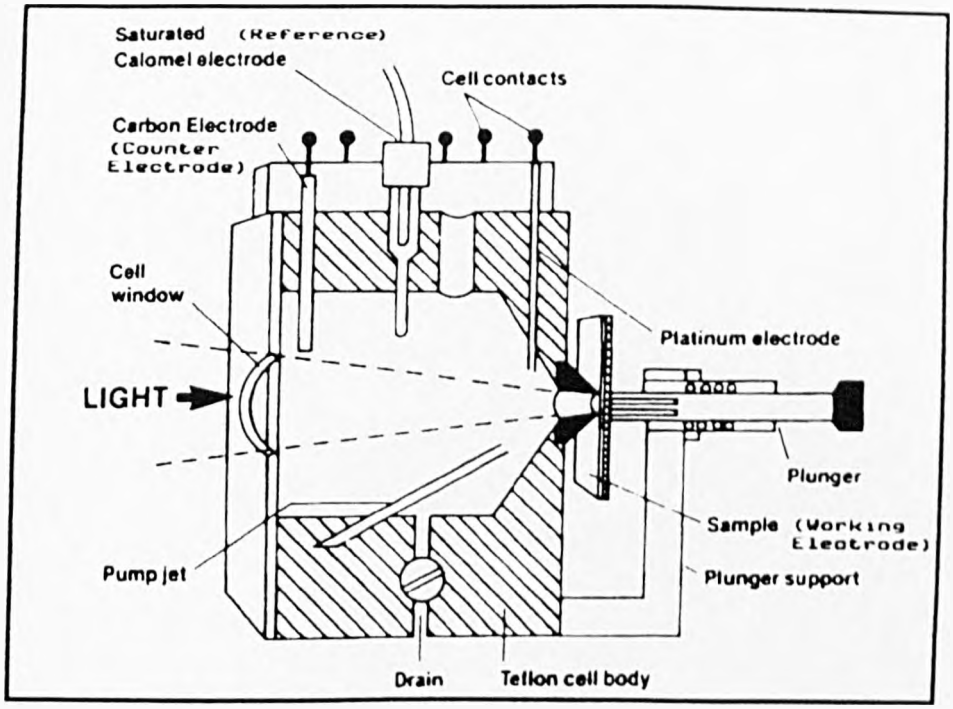

A schematic diagram of the electrochemical cell used to achieve these measurements is included in Figure 2-14. The sample was held on the Teflon cell by spring loaded pins that are used to provide an essentially ohmic contact. The electrolyte was in contact with the front surface of the semiconductor, the area of which is defined by the PVC sealing ring. Results obtained using this method are included in chapter 6.

2.8 ZnSe/GaAs INTERFACE

There are two possibilities when considering the interface between GaAs and ZnSe. The first is that ZnSe grows directly on the GaAs surface, the other is that there is some compound formed at the interface at the beginning of growth involving some or all of the species present which grades to ZnSe some time after the start of growth. Evidence for the latter being the case has been observed.

Prior to growth the protective oxide layer on the GaAs surface must be removed. As the oxide desorption of the GaAs surface occurs at an elevated temperature (~600°C) As is desorbed from the surface when the oxide is removed. In the case of III-V MBE this problem is addressed by thermally cleaning under an As ambient flux, in this fashion an As stabilised surface is maintained prior to growth. It has been shown that the As terminated surface provides the best conditions for initiating growth on the substrate. Arsenic desorption from the surface can be observed from the change in patterns obtained from RHEED, as shown in Table 2-1.[14] However, due to the constraints of the availability of source ports in the growth chamber on the machine at Heriot-Watt it is not possible to perform a thermal clean with an As ambient. Also the presence of arsenic in the chamber would unintentionally dope any layers produced. In this case the

Table 2-1: Surface structures observed by RHEED indicating Ga or As stabilised surfaces dependent on temperature and As background pressure

Background pressure		Substrate temperature (°C)	Surface structure
5×10^{-9} Torr As_4	Cooling	580	$c(8 \times 2)$Ga
		525	(4×6)a
		400	(6×6)a
		200	(2×6)a
	Heating	425	(2×4)As
		510	(3×6)a
		520	(6×6)a
		530	(4×6)a
		550	(4×2)Ga
		560	$c(8 \times 2)$Ga
1×10^{-7} Torr As_4	Cooling	600	$c(8 \times 2)$Ga
		560	(3×4)a
		530	(2×4)As
		150	(4×4)As
	Heating	415	$c(2 \times 8)$As
		470	(2×4)As
		530	(3×4)a
		560	(4×4)Ga
		580	(4×2)Ga
		590	$c(8 \times 2)$Ga

timing of the cessation of the thermal clean is paramount as the ambient species in the II-VI chamber is selenium. The method of heat clean used is explained further in section 2.9.2. Despite this it is inevitable that As will be lost from the surface due to the thermal lag time between the end of the heat clean and cooling to growth temperature (~300°C), typically 5-10 mins. Therefore, the substrate surface at the onset of growth will be As deficient. In order to regain stability the surface preferentially bonds with Se to form Ga_2Se_3 when the Se shutter is first opened. Hence a layer of Ga_2Se_3 is formed before the ZnSe can grow.

In Figure 2-15 the transmission electron microscopy (TEM) obtained from a ZnSe/GaAs interface is shown. This sample (HWA 475) was undoped ZnSe grown using the standard growth procedure outlined in Section 2.9. It was a very thin ZnSe sample (estimated 0.2 nm) grown specifically to investigate the interface region between ZnSe and GaAs. The TEM clearly shows a cross-section through a surface etch pit. The linear density of etch pits was estimated to be $200\mu m^{-1}$. EDX analysis of this sample failed to show any ZnSe. However, in the case of sample HWA 476 grown under the same conditions but to a thickness of ~2nm, no etch pits were observed (Figure 2-16). The existence of ZnSe at the surface was confirmed by EDX. Also, from a plan view image of HWA 476, there was no evidence of island formation.[25] However, the epilayer thickness varied between 0.57 and 3.97nm. It was possible that islands had formed at the very early stages of growth and had coalesced after further growth. Therefore, it would appear that the island coalescence occurs at an epilayer thickness $\leq$ 2nm indicating the onset of a layer by layer growth regime.

Figure 2-15: TEM through etch pit (HWA 475)

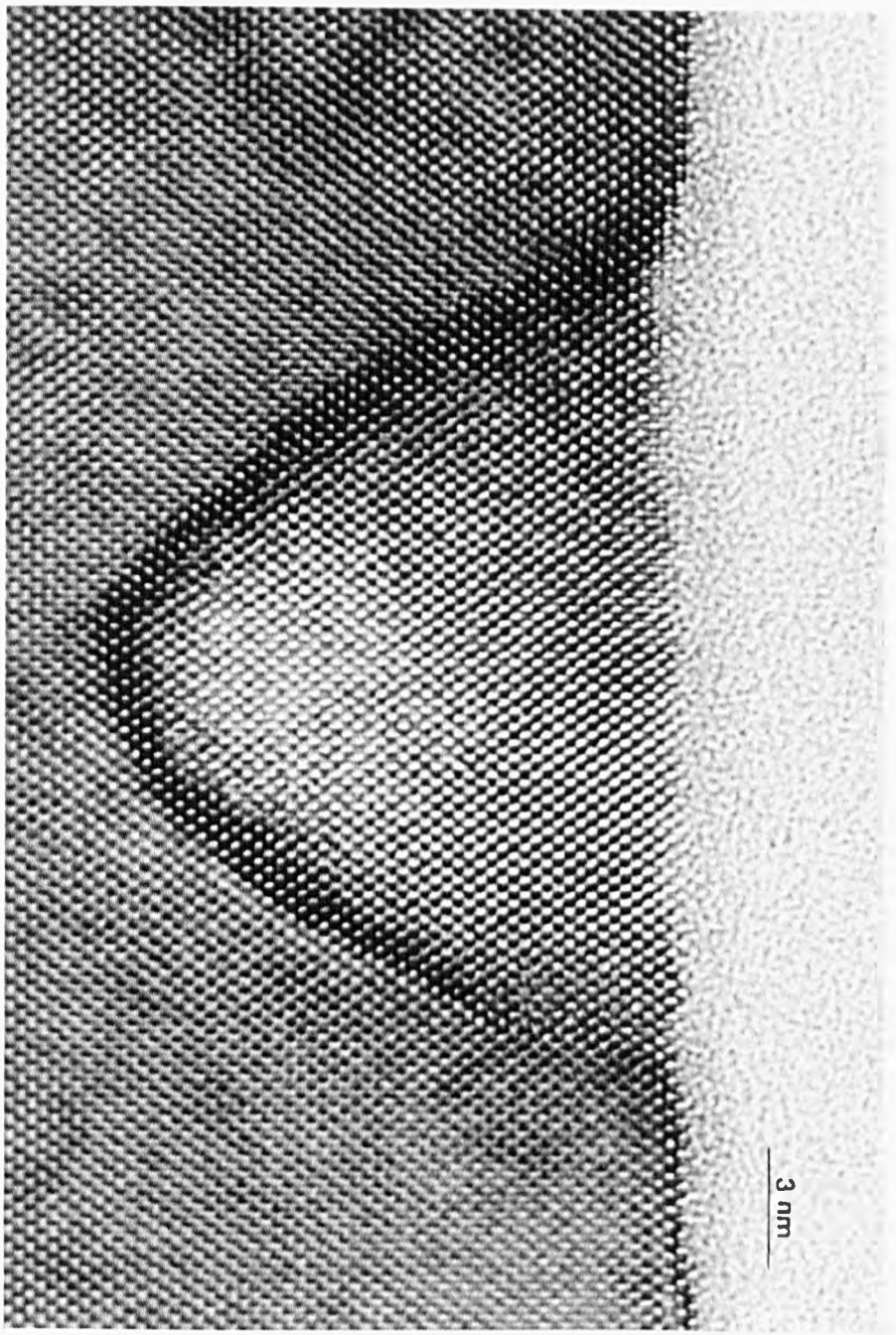

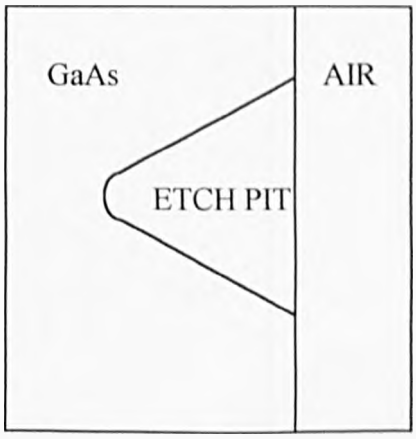

Figure 2-16: TEM of thicker sample (HWA 476)

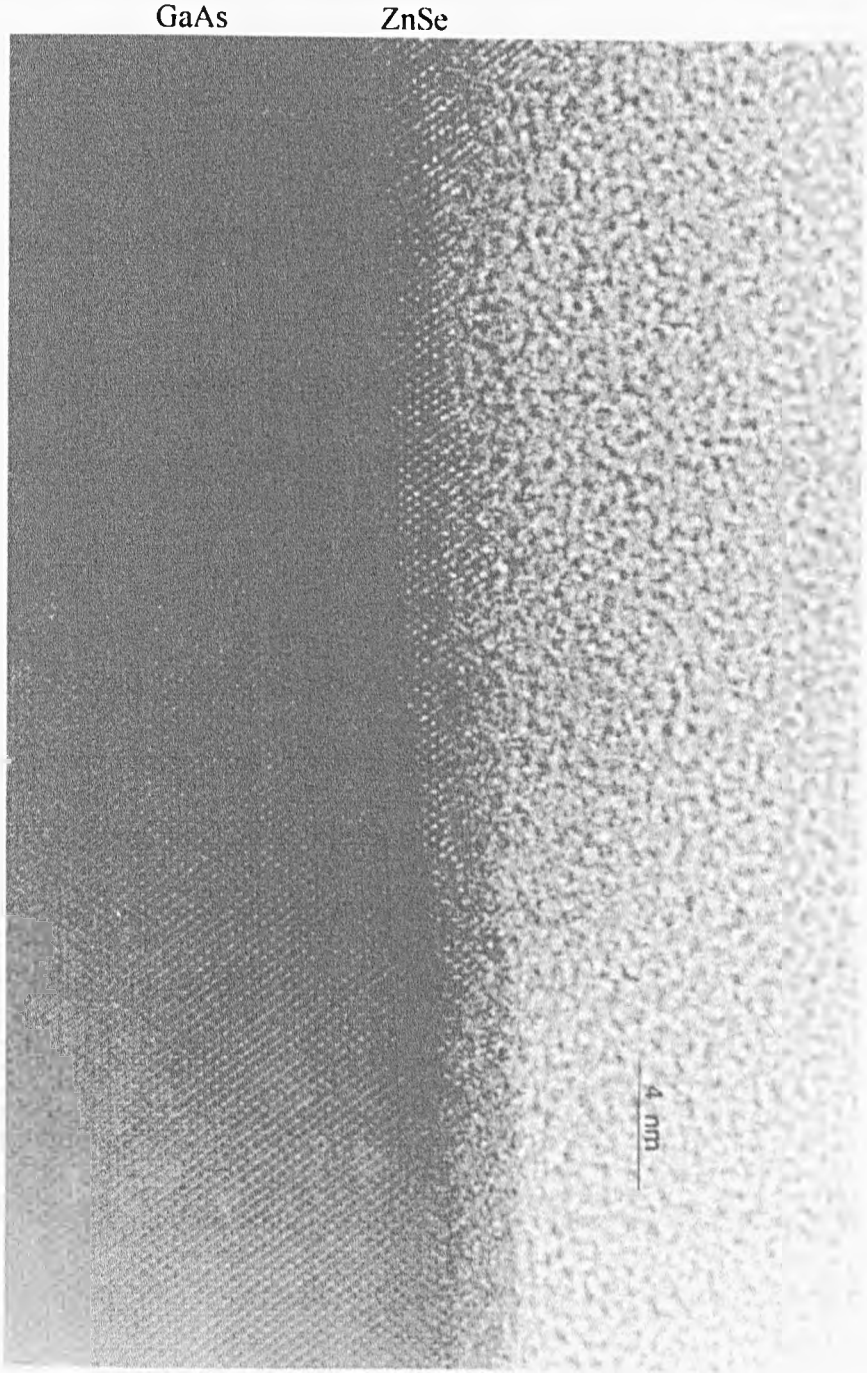

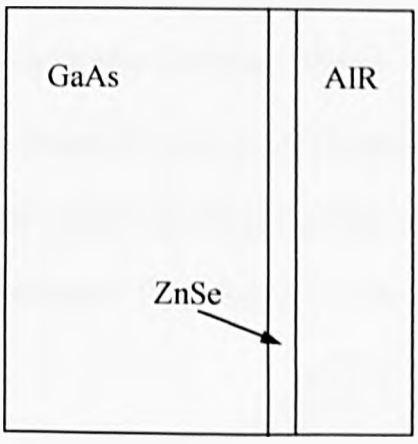

It was unclear whether the difference between this sample and the previous one which showed etch pits was due to a substrate etch problem or due to initial growth under group II and VI excess.

2.9 NORMAL GROWTH PROCEDURES

In both MBE systems, the procedures for preparing a substrate remained the same. The standard method used for loading a substrate through to start of growth is described below.

The substrate material used was GaAs of (001) orientation. Two suppliers were used; the first was the Sumitomo Mining Corporation of Japan. These were liquid encapsulated Czochralski (LEC)[26] wafers and were 500μm thick. The second type of wafers used were from American Crystal Technologies (AXT) and were grown by the vertical grade freeze method.[27] These wafers were 350μm thick.

2.9.1 Chemical etching

The cost of the wafers made it necessary that the wafers should be cleaved into quarters. In order to ensure that the initial surface was the same each quarter was etched separately using an identical procedure prior to entry to the MBE system (as each wafer was exposed to air after being quartered). The etch solution used consisted of 15ml sulphuric acid (H_2SO_4), 2ml hydrogen peroxide (H_2O_2) and 2ml de-ionised water. During the mixing of the etch chemicals there is an exothermic reaction. Therefore, to ensure consistency the substrate wafers are always etched when the solution cooled to 50°C for an etch time of 90 seconds. The solution is then quenched with de-ionised

water and the substrate rinsed. The wafer is then removed and blown dry using oxygen free nitrogen. This etch procedure is based on that proposed by Cho[28] and adopted as a standard preparation for epitaxial growth[29]. Following this procedure results in a chemisorbed oxide layer ~4-5Å thick[30],[31],[32]. The wafer is then mounted on the molybdenum block using indium. The temperature of the block during the mounting of the sample is limited to just above the melting point of indium (156.8°C) to minimise the thickening of the oxide layer on the surface of the wafer.

2.9.2 Thermal desorption

In the case of the V 80H, after the sample has been loaded and transported into the preparation chamber, the sample is degassed in the preparation stage heater. Typically this procedure takes 10 minutes at a thermocouple temperature of 400°C. As the thermocouple is positioned behind the block and in front of the heaters the measured temperature is higher than the front face temperature, estimated to be in the range 200-300°C. This procedure ensures that the excess water vapour is removed from the block before entry to the growth chamber. Unfortunately, the MB 288 did not have such a facility.

After transferring the sample to the growth chamber, the growth stage and sample are rotated to the growth position facing the cells. The RHEED beam is then turned on and the pattern observed shows amorphous rings from the oxide layer (Figure 2-17). If the oxide is thin enough a superimposed pattern of the primary diffraction rods of the underlying GaAs surface is also visible. At this stage the pyrometer position is also checked to ensure that the sample is visible in the measurement cone of the pyrometer.

Figure 2-17: Amorphous rings due to oxide layer on GaAs surface

True Image

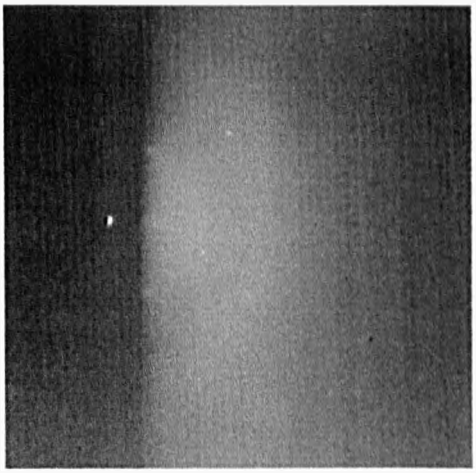

Inverted Image

The thermal desorption of the oxide layer is now started. Substrate temperature is increased to give a front face temperature of approximately 600°C, measured by the pyrometer. Once this temperature is reached an increase in intensity of the RHEED pattern is observed accompanied by a sharpening of the overall image. It has been found that for a GaAs (100) surface the pattern which indicates good thermal desorption is the 4x3 reconstruction.[33] As soon as this pattern is obtained, the substrate heater power is reduced and the sample allowed to cool to the desired growth temperature, typically 300°C. Figure 2-18(a) shows the reconstructed 4x RHEED pattern along the <110> direction and (b) the 3x reconstruction along the $<1\bar{1}0>$.

2.9.3 Start of growth

Once growth temperature is obtained the growth can commence. Typically, for ZnSe, the 4x3 RHEED reconstruction remains to growth temperature unless there is a large overpressure of selenium in the chamber, in which case a characteristic 2x1 pattern ensues.[34] Growth was started by opening both the zinc and selenium shutters in unison. Upon opening the shutters the RHEED is observed to become spotty, due to 3 dimensional growth. After some time the RHEED recovers to a streaky reconstruction indicative of 2-dimensional planar growth. This effect is greatly reduced by optimising the Zn:Se flux ratios to an extent that streaky reconstruction typically appears within 20 secs. On some occasions the RHEED pattern stays streaky from the start of growth indicating that the growth conditions are indeed optimum.

2.9.4 RHEED patterns for a typical ZnSe epilayer before and during growth

These patterns are highly dependent on the VI:II ratio used. The conditions which have been found to provide the highest quality layers are in the range of VI:II = 1-1.2 i.e.

Figure 2-18: 4x3 RHEED pattern after thermal desorption of oxide layer

(a) 4x RHEED pattern along <110>

True Image

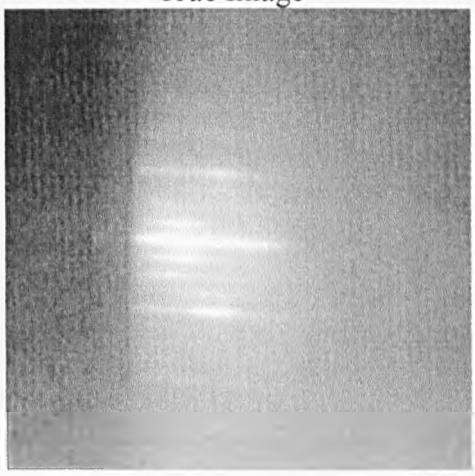

Inverted Image

(b) 3x RHEED pattern along $<1\bar{1}0>$

True Image

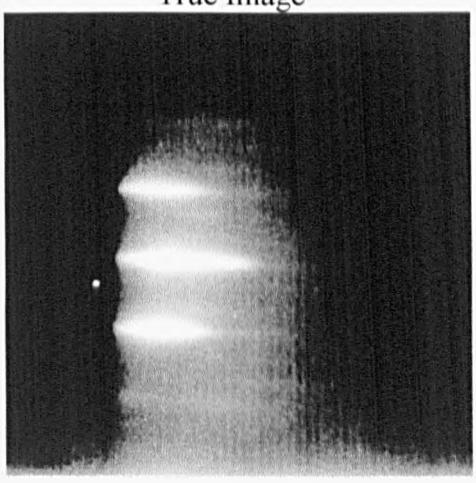

Inverted Image

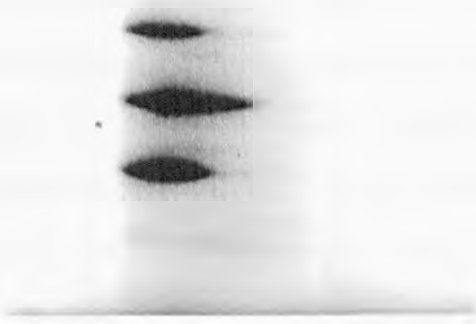

slightly Se rich. For these flux ratios the RHEED reconstruction pattern observed shows the characteristic (2x1) Se terminated surface mixed with a faint c(2x2) pattern Zn terminated surface. This particular mixed pattern is indicative of a Se:Zn surface ratio of 1:1 whereas, for a Se rich surface the 2x1 pattern is dominant and for the metal rich surface the c(2x2) pattern is stronger.[35]

Figure 2-19 are the RHEED patterns obtained during growth of a slightly Se rich surface where (a) is the 2x along <110>, (b) is the 1x along $<1\bar{1}0>$ giving a 2x1 reconstruction and (c) is the c(2x2) pattern observed in the {100} directions.

By following this recipe and ensuring that these RHEED patterns were observed through the growth it was possible to standardise the growth of high quality undoped ZnSe samples. If these growth conditions are not adhered to then this also shows in the RHEED in the form of a spotty pattern indicative of surface corrugations.

2.10 CONCLUSIONS

Although a considerable amount of progress had been achieved using the MB 288 vacuum system, the demands of II-VI SCH laser growth involving quaternary materials were such that this system no longer had the necessary source capacity to continue research in this field. Therefore, the upgrade to the V 80H system, although time consuming, was essential to the further development of the II-VI research at Heriot-Watt university. This involved the conversion from III-V materials, cleaning and refurbishment of the V 80H system.

In order to achieve this, considerable time was spent characterising and adjusting the system to investigate growth conditions which would give the high quality ZnSe samples required. Once this goal had been achieved it was then possible to investigate the

Figure 2-19: 2x1 and c(2x2) RHEED pattern typically seen during growth

(a) 2x RHEED pattern along <110>

True Image

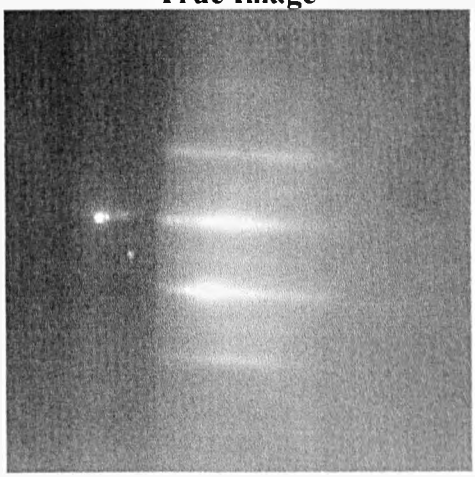

Inverted Image

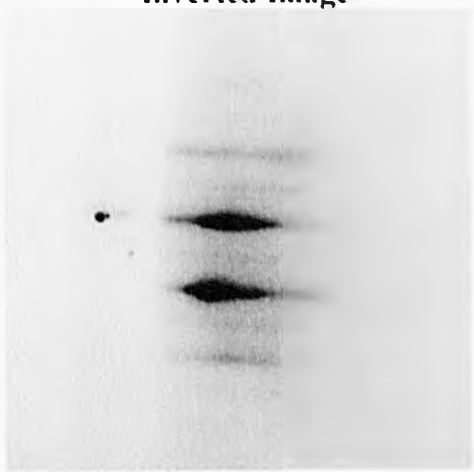

(b) c(2x2) RHEED pattern along {100} directions

True Image

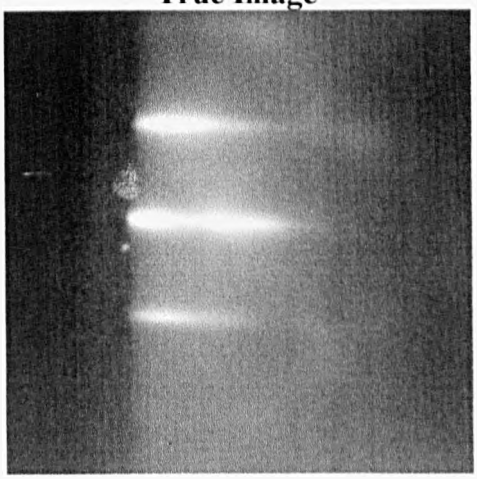

Inverted Image

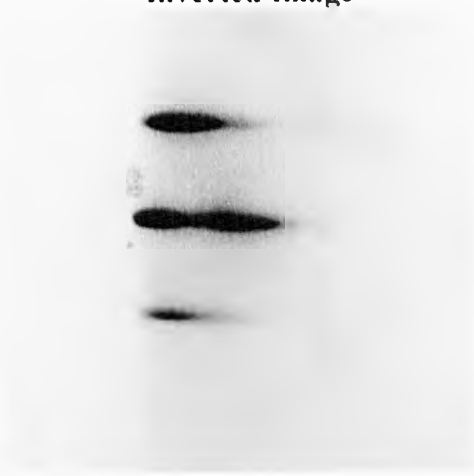

growth and characterisation of the ternary and quaternary materials important to the laser research described in Chapter 5.

Also included in this chapter were descriptions of the in-situ (RHEED) and ex-situ (PL, C-V profiling) characterisation techniques which were used throughout this study.

2.11 REFERENCES

[1] K. Yoneda, Y. Hishida, T. Toda, H. Ishi and T. Niina, Appl. Phys. Lett., 45 (1984) 1300

[2] J. M. Wallace, PhD Thesis 1992, Chapter 2, p1

[3] S. Y. Wang, I. Hauksson, J. Simpson, H. Stewart, S. J. A. Adams, Y. Kawakami, K. A. Prior and B. C. Cavenett, Appl. Phys. Lett., 61 (1992), 506

[4] S. Y. Wang, Y. Kawakami, J. Simpson, H. Stewart, S. J. A. Adams, K. A. Prior and B. C. Cavenett, Appl. Phys. Lett., 62 (1993), 1715

[5] S. Y. Wang, G. Horsburgh, P. Thompson, I. Hauksson, J. T. Mullins, K. A. Prior and B. C. Cavenett, Appl. Phys. Lett., 63 (1993), 857

[6] N. Nakayama, S. Itoh, T. Ohata, K. Nakano, H. Okuyama, M. Ozawa, A. Ishibashi, M. Ikeda and Y. Mori, Electronics Letters, 29 (1993), 1488

[7] J. Simpson, Personal communication

[8] University Physics, F. W. Sears, M. W. Zemansky and H. D. Young, 7th Edition, Addison-Wesley (1987), 381

[9] Landolt-Börnstein, Numerical Data and Functional Relationships in Science and Technology, Vol 17 Springer 1984.

[10] J. M. Wallace, PhD Thesis 1992, Chapter 2, p6

[11] M. Prutton, Surface Physics, 2nd ed, Clarendon Press, Oxford (1983)

[12] A. Y. Cho, Thin Solid Films, 100 (1983), 291

[13] S. M. Newstead, R. A. A. Kubiak and E. H. C. Parker, J. Crystal Growth, 81 (1987) 49

[14] R. Ludeke, R. M. King and E. H. C. Parker, Chapter 16 in *The Technology and Physics of Molecular Beam Epitaxy* ed E. H. C. Parker Published 1985 Plenum Press New York

[15] J. H. Neave, B. A. Joyce, J. Cryst. Growth, 44 (1978), 387

[16] K. A. Prior, Personal Communication

[17] R. M. Park, C. M. Rouleau, M. B. Troffer, T. Koyama and T. Yodo, J. Mat. Res. 5 (1990), 475

[18] T. Yao, M. Ogura, S. Matsuoka and T. Morishita, Jpn. J. Appl. Phys., 22 (1983), L144

[19] T. Yao, J. Cryst. Growth 72 (1985), 518

[20] K. Shazad, D. J. Olego and D. A. Cammack, Phys. Rev., B 39 (1989), 13016

[21] R. M. Park, M. B. Troffer, C. M. Rouleau, J. M. DePuydt and M. A. Haase, Appl. Phys. Lett., 57 (1990), 2127

[22] K. Ohkawa, T. Karasawa and T. Mitsuyu, J. Cryst. Growth, 111 (1991), 797

[23] S. Y. Wang, F. Haran, J. Simpson, H. Stewart, J. M. Wallace, K. A. Prior and B. C. Cavenett, Appl. Phys. Lett., 60 (1992) 344.

[24] I. C. Mayes, Bio-Rad Semiconductor Notes, No. 201 (1985)

[25] P. D. Brown, Personal Communication

[26] Advanced Crystal Growth, ed P. M. Dryburgh, B. Cockayne and K. G. Barraclough, Prentice Hall (1987), p75

[27] Advanced Crystal Growth, ed P. M. Dryburgh, B. Cockayne and K. G. Barraclough, Prentice Hall (1987), p141

[28] A.Y. Cho, Thin Solid Films, 100 (1983), 291

[29] J.D. Grange, The Technology and Physics of Molecular Beam Epitaxy, Plenum Press, 1985 Chapter 3, p52

[30] J. Massies and J.P. Contour, J. Appl. Phys., 58 (1985), 806

[31] J.P. Contour, J. Massies, H. Fronius and K. Ploog, Jap. J. Appl. Phys., 27 (1988) L167

[32] A. Salètes, J. Massies and J.P. Contour, Jap. J. Appl. Phys., 25 (1986) L48

[33] L. A. Kolodziejski, R. L. Gunshor, N, Otsuka and A. V. Nurmikko, Mat. Res. Soc. Symp., 102 (1988), 113

[34] H. J. Cornelissen, D. A. Cammack and R. J. Dalby, J. Vac. Sci. Technol., B6 (1988), 769

[35] J. M. Wallace, PhD Thesis (1992), Chapter 3, p9

3. DOUBLE CRYSTAL X-RAY DIFFRACTION

3.1 INTRODUCTION

It has been accepted for some time that the ability to produce an electrical device using semiconductors requires the tight control of the material parameters. These parameters include doping, chemical composition and structural quality of both the substrate and epilayer. A discussion of the doping of II-VI materials is included in Chapter 6 of this thesis. The control of the structural properties and composition of semiconductors is by no means trivial especially in the case of ternary and quaternary compounds. In these cases a number of techniques have to be used in conjunction in order that these epilayers can be fully characterised. The techniques used include photoluminescence spectroscopy (PL), energy dispersive X-ray spectroscopy (EDX), X-ray diffraction (XRD) and X-ray topography (XRT). In this chapter XRD and its use in the II-VI material system are described. The use of XRT is the subject of Chapter 4.

The fabrication of ZnSe based electro-optical devices requires the growth of II-VI alloys on single crystal substrates. Typically GaAs substrates are used in the study of the ZnSe system as they are readily available and have relatively low defect densities. The ideal case would be that of homoepitaxy using ZnSe substrates. However, ZnSe substrates of sufficiently high quality are relatively scarce.

In order that these devices may be realised the composition of these alloys must be carefully controlled to enable the selection of the bandgap of the active region. Also, the lattice parameter mismatch between the GaAs substrate and ZnSe leads to the generation of misfit dislocations. The mismatch (m) is given by:

$$m = \frac{a_r - a_o}{a_o} \qquad 3.1$$

where a_r is the relaxed bulk lattice parameter of the epilayer and a_o is the lattice parameter of the substrate. In the case of ZnSe on GaAs this mismatch is ~2600ppm (or 0.26%), leading to the formation of misfit dislocations at some epilayer thickness determined by the misfit strain. The thickness at which the first misfit dislocation is formed is defined to be the critical thickness and for ZnSe on GaAs has previously been determined by PL[1] and XRD[2] to be in the region of 1500Å. It is necessary to grow lattice matched compounds to keep these defects at a minimum. As the total thickness of a typical device is approximately 3μm the effects of this relaxation are highly undesirable and severely limit the performance and lifetime of the device. It is for this reason that a number of ternary and quaternary compounds have been studied (see Chapter 5) in order to minimise the effects of relaxation by lattice matching the epilayer to the substrate.

3.2 TERMINOLOGY AND CONDITIONS FOR DIFFRACTION

3.2.1 Lattice Planes in the Crystal and Bragg's Law

In order to measure the lattice parameters and the degree of relaxation of these epilayers, X-ray diffraction is used to measure the spacing of the crystallographic planes in the

crystal. Diffracted beams may only occur at an angle $2\theta_B$ to the incident beam according to the Bragg equation:[3]

$$\lambda = 2d_{hkl} \sin\theta_B \qquad 3.2$$

where λ is the wavelength of radiation used and d_{hkl} is the lattice plane spacing for the (hkl) planes. In general, for any right angled system the relation:

$$\frac{1}{d^2} = \frac{h^2}{a^2} + \frac{k^2}{b^2} + \frac{l^2}{c^2} \qquad 3.3$$

applies, where a, b, and c are the dimensions of the unit cell. ZnSe and its associated compounds assume a zinc-blende (cubic) structure. However, for strained or partially strained material grown on (001) substrates $a = b \neq c$. This is described as a tetragonal distortion of the cubic lattice. However, when the mismatch between epilayer and substrate is large and the thickness of the epilayer is such that it greatly exceeds the critical thickness, then it is possible to assume that the layer is fully relaxed and its structure is cubic in which case $a = b = c$.

3.2.2 Symmetric and Non-Symmetric Reflections

As X-ray diffraction occurs from the crystallographic planes in the crystal it is possible to obtain information from different diffraction planes simply by changing the orientation of the crystal with respect to the incident beam. The (004) planes are those most commonly used for diffraction from a (001) surface oriented crystal as this reflection gives an intense diffracted beam.[4] The conditions for such a reflection are as shown in Figure 3-1 where the Bragg angle is calculated for the GaAs substrate. As can be seen

from this diagram the angles of the incident and diffracted beams are the same with respect to the surface. Hence, this type of geometrical set-up is described as symmetric.

Figure 3-1: Symmetric Reflection

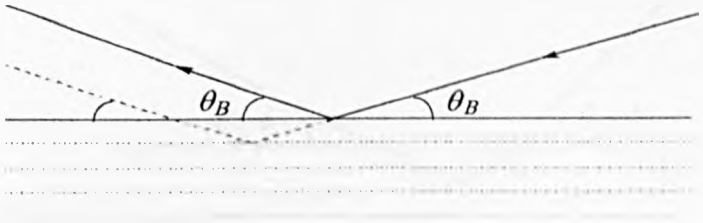

It is also possible to satisfy the Bragg conditions for planes which are non-parallel to the surface provided that the Bragg angle for these planes is such that both the incident and reflected beams exit from the front surface of the sample and is described as an asymmetric reflection, as depicted in Figure 3-2.

Also, it should be noted that the same set of planes can be observed from two distinct angles of incident and exit beam with respect to the crystal surface simply by reversing the direction of the beam (or rotating the sample by 180°). This gives rise to pairs of asymmetric reflections where in one case the incident beam is at a glancing angle and the other where the exit beam is at a glancing angle.

Figure 3-2: Asymmetric Reflection

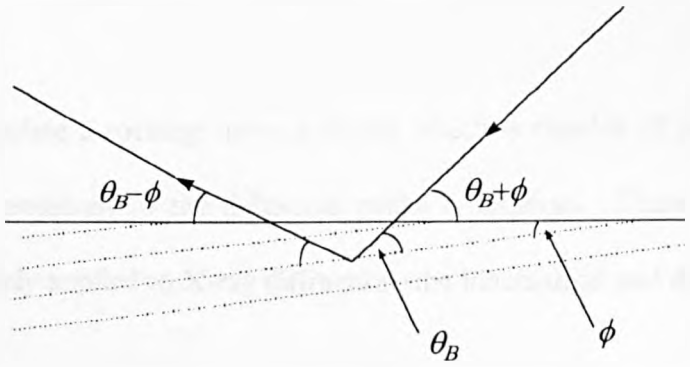

By utilising these asymmetric reflections any distortion of the unit cell can be directly measured as planes which are non-parallel to the sample surface have a lattice plane spacing which contains a component of both the lattice parameter perpendicular and parallel to the interface. This provides a method for measuring the amount of strain present in an epilayer.[5]

3.3 X-RAY DIFFRACTION THEORY

X-ray diffraction provides non-destructive characterisation information regarding the structural perfection of epilayers and substrates from the FWHM and composition from the relative splitting of the diffracted peaks. However, to extract the maximum information possible it is necessary to have a means of analysing the rocking curves obtained. One method of achieving this is to be able to simulate the results expected and

to be able to modify these to agree with the experimental results. Through the use of simulations layers and structures can be modelled so that the expected splitting and relative intensities of the diffracted peaks can be estimated prior to measurement and can be used to interpret the results obtained.

In order to effectively simulate a rocking curve a theory which is capable of predicting the intensity and angular positions of the diffracted peaks is required. There are two theories which are commonly applied to X-ray diffraction; the kinematical and dynamical.

3.3.1 Kinematical Theory

Following the discovery of X-ray diffraction by crystals the possibility of being able to characterise crystals by their diffraction spectra was soon recognised[6]. Diffraction of X-rays was considered to occur as the specular reflection of X-rays from lattice planes in the crystal. This is the Kinematical Theory. In this case the condition at which maxima of diffracted intensity occur are as given by Bragg's law (3.2) as described above. The intensity of the diffracted beam is calculated from the sum of the contribution from each unit cell calculated from the structure factor. Kinematical theory only takes into account the interaction of each atom with the primary, or refracted, wave in the crystal. This ignores the interaction of the diffracted waves with the refracted one and that there is no rediffraction. Also, this model assumes that each unit cell is subject to the same intensity of incident beam so the diffracted beam must be of negligible intensity to that of the incident beam. In the case of small crystals this is indeed found to be the case. Therefore, for techniques such as powder diffractometry the kinematical theory can be successfully used. However, in the case of a perfect, or near perfect, crystal with a large enough volume the summation of contributions to the diffracted beam from all of the unit

cells in the crystal would eventually predict a diffracted intensity greater than that of the incident beam. As this clearly cannot be the case, from an energy conservation point of view, a theory which takes account of all of the wavefields propagating within the crystal volume was required for semiconductor grade crystals of high structural perfection.

3.3.2 Dynamical Theory

The derivation of the dynamical theory for the diffraction of crystals in a perfect and nearly-perfect crystal is beyond the scope of this thesis, but has been covered in a number of reviews of the subject.[7,8,9] In brief, the dynamical theory is the solution of Maxwell's equations for a complex, dimensionally periodic electric susceptibility, χ (a model of the crystal lattice). Independently, Takagi[10] and Taupin[11] developed a generalised diffraction theory which can be used to describe the passage of X-rays through a crystal as two coupled second order partial differential equations expressing the propagating wavefronts along the forward and diffracted beam directions. These Takagi-Taupin equations can be used for the simulation of the diffraction of X-rays through a crystal as they directly predict the intensities of the direct and diffracted beams emerging from the crystal using an analytical method.[12] This formalism is the basis of the BEDE RADS simulation program used throughout this study for the investigation of II-VI epilayers.

In order to enable the RADS program to simulate the diffraction from II-VI epilayers, the properties of the binary endpoint compounds used had to be entered into the program database, these were as shown in Table 3-1. The Poisson's ratio for many of the compounds was taken as 0.333 due to the fact that none of these parameters have been experimentally determined. For each simulation the degree of strain present in the

epilayer, substrate material, orientation and the thickness of the epilayer could all be varied to allow accurate dynamical simulation of rocking curves.

Table 3-1: Properties of the Binary Endpoint Compounds used in RADS

MATERIAL	LATTICE PARAMETER (Å)	DENSITY (g/cm^3)	POISSONS RATIO
ZnSe	5.6686[14]	5.2630[13]	0.380[14]
CdSe	6.0520[14]	5.8569[13]	0.333
ZnS	5.4102[14]	4.0859[13]	0.333
MgSe	5.8900[15]	4.2100[13]	0.333
ZnTe	6.1037[14]	5.6410[13]	0.333

3.4 THE EFFECTS OF LATTICE MISMATCH ON THE EPITAXIAL LAYER

Heteroepitaxy is the epitaxial growth of a material on a substrate of different properties. Although ZnSe has the same crystal structure as GaAs (zinc-blende), its physical, electrical and optical properties are quite different. As has been previously discussed, the difference in lattice parameter results in a lattice mismatch between ZnSe and GaAs. This has the effect of causing a strain between the two materials. As the substrate (≥350 μm) is much thicker than the epitaxial layer (<10 μm), then it will experience a much lower average in-plane stress than the epitaxial layer[16]. Therefore, it is possible to make the assumption that all of the lattice parameter misfit is accommodated by the strain in the epitaxial layer, rather than the substrate. For low values of misfit (ZnSe/GaAs ~ 0.27%) the creation of the first misfit dislocation does not occur immediately, but at some finite thickness of the epilayer known as the critical layer thickness (CLT). This leads to the possibility of the epilayer having three distinct physical states dependent on the thickness of the layer.

These three states are:

1) Pseudomorphic (coherent)

2) Partially relaxed (semi-coherent)

3) Totally relaxed.

Figure 3-3 shows these three states schematically. The terms coherent and semi-coherent are also used for cases (a) and (b) and refer to the registry between the epilayer and substrate atoms parallel to the growth interface.

Figure 3-3: Three States of Strain due to Mismatch for a Compressed Epilayer

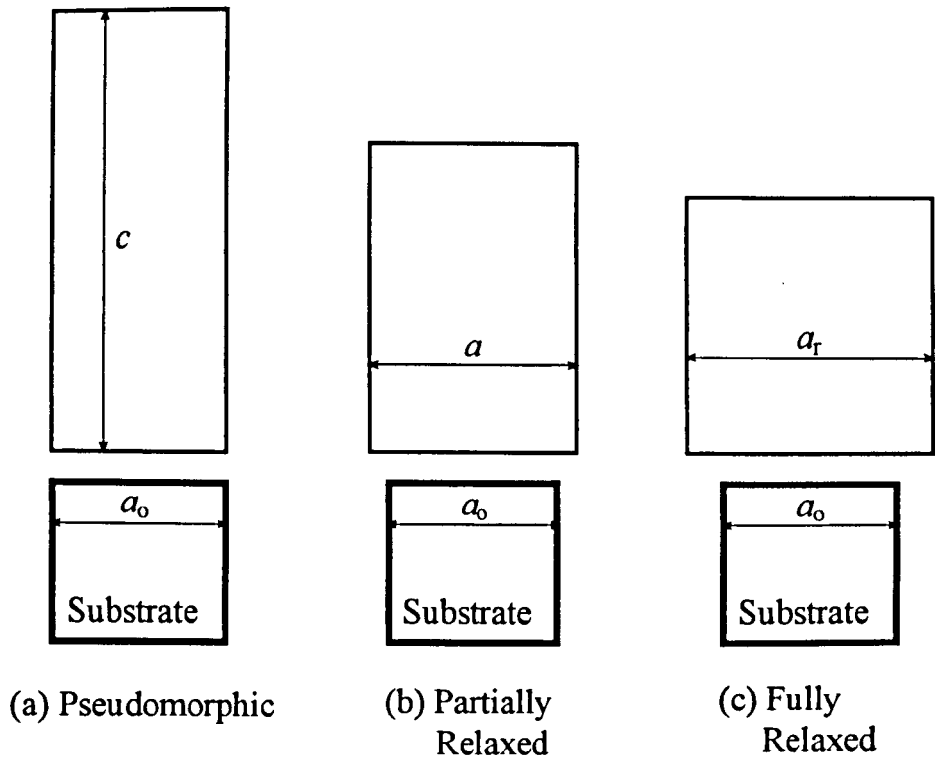

3.4.1 Pseudomorphic ZnSe

A pseudomorphic (strained) layer is one which assumes the same lattice parameter as that of the substrate parallel to the interface through an elastic deformation, resulting in tetragonal distortion in the case of a cubic structure. Below the CLT no misfit dislocations will have formed in the epilayer and the crystal structure should be as free from defects as possible, provided growth conditions and surface pre-treatments have been chosen to maximise the structural quality of the epilayer. Defects such as those resulting from etch pits at the substrate surface and substrate threading dislocations will still exist[17].

In the case where the epilayer material has a relaxed lattice parameter greater (smaller) than that of the substrate the layer will be under a compressive (tensile) strain. This means that the epilayer lattice parameter perpendicular to the interface will be greater (smaller) than that parallel to the interface. This tetragonal distortion can be described using the equation:[5]

$$a_r = a + (c-a)\frac{(1-\nu)}{(1+\nu)} \qquad 3.4$$

where: a_r is the bulk lattice parameter of the epilayer

a is the lattice parameter parallel to the growth interface

c is the lattice parameter perpendicular to the growth interface

υ is Poisson's ratio.

This equation is only valid under the approximation that the distortion along the <110> directions parallel to the interface are equal. This type of distortion is described as tetragonal.

Provided that the strain is indeed tetragonal (i.e. that relaxation is equal along the axes parallel to the interface) then the fractional relaxation can be calculated from:

$$R = \frac{a - a_o}{a_r - a_o} \qquad 3.5$$

where a, a_o and a_r are as defined previously. This provides a simple method of measuring the relaxation present in the epilayer simply by measuring the perpendicular lattice parameter provided that the bulk lattice parameter is known. However, in the case of ternary and quaternary materials such as ZnSSe and ZnMgSSe which are approximately lattice matched to the substrate, the lattice parameter is a variable function of composition and must be measured using asymmetric reflections.

In the case of ZnSe grown on GaAs where the ZnSe has the larger lattice parameter the tetragonal distortion will be as shown in Figure 3-3 resulting in a greater lattice parameter in the perpendicular direction.

Using the RADS simulation program it is possible to model layers of ZnSe, of varying thickness, pseudomorphic to a GaAs substrate. These simulations are of (004) symmetric reflections with a Si(111) reference crystal and are representative curves as shown in Figure 3-4. It can be seen from this figure that the ZnSe peak becomes larger

Figure 3-4: Simulated rocking curves of pseudomorphic ZnSe for different layer thickness

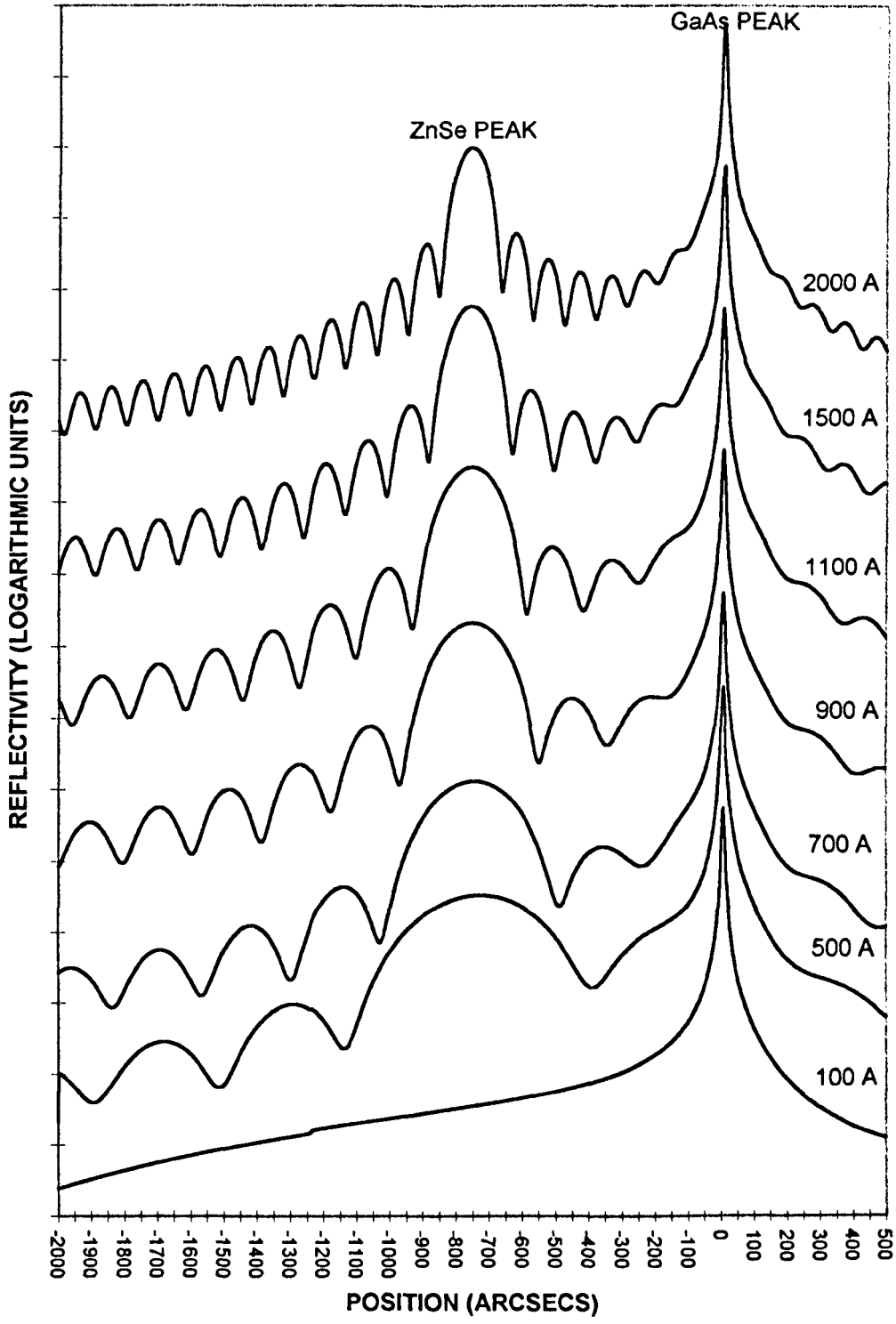

and the FWHM decreases as the thickness of the epilayer increases. The relative position of the ZnSe peak with respect to the GaAs peak is as defined using equation 3.4 above. However, close inspection of Figure 3-4 reveals that the peak of the 500 Å ZnSe layer is slightly offset towards the GaAs layer due to the effect of the boundary between the epilayer and the substrate as described by Fewster and Curling.[18]

In addition to these features a periodic oscillation is superimposed on the rocking curve. These oscillations are known as thickness (or Pendellösung) fringes and originate from interference of the X-ray waves between the layers. The existence of these interference fringes is indicative of crystal of good structural quality as the formation of these fringes requires a large structural coherence length. As the layer thickness increases the period of these oscillations decreases. It is possible to calculate the thickness of the layer, t from the period of the fringes ($\Delta\theta_L$) using the formula[19,20]:

$$t = \frac{\lambda}{2\Delta\theta_L \cos\theta_B} \qquad 3.6$$

where λ is the wavelength of the X-rays and θ_B is the Bragg angle of the symmetric reflection used. Also, as the coherence length of X-rays is of the order of 1 μm[21], the structural coherence of the epilayer has to be at least of the same order for the fringes to be so clearly observed. This ability to measure the thickness is particularly useful in the case of ZnSe on GaAs when dealing with thin layers (<2500 Å) where other measurement techniques, such as optical reflectivity are limited.

An estimate of the error with which the thickness of a pseudomorphic layer can be determined using the above method can be found by differentiating 3.6 w.r.t. $\Delta\theta_L$:

$$\frac{dt}{d(\Delta\theta_L)} = -\frac{\lambda}{2\cos\theta_B} \cdot \Delta\theta_L^{-2} \qquad 3.7$$

Therefore, the magnitude of the error in thickness due to the error in determining the period, $d(\Delta\theta_L)$, will be:

$$|dt| = \left| \frac{\lambda}{2\cos\theta_B} \cdot \Delta\theta_L^{-2} \cdot d(\Delta\theta_L) \right| \qquad 3.8$$

In the case of a layer with $\Delta\theta_L$ = 189.5 arcsecs (corresponding to a layer thickness of 100nm) and taking a reasonable uncertainty, $d(\Delta\theta_L)$, of 10 arcsecs then $|dt|$ = 5.28 x 10^{-9} m. Therefore, for epilayers in the range of 100nm in thickness the estimated error in the thickness measured by DCXRD will be approximately ±5nm.

3.4.2 Partially and Fully Relaxed ZnSe

As the thickness of the epilayer exceeds the CLT, the epilayer begins to relax through the formation of misfit dislocations. These dislocations serve to relieve the strain parallel to the interface by causing localised regions of misalignment between the epitaxial and substrate atoms. The effects of this misalignment between the substrate and epitaxial layer atoms is as shown in Figure 3-5. Misfit dislocations and their effect on the epilayer are discussed further in Chapter 4.2. Eventually the epilayer will become thick enough that it will be completely relaxed and should assume its bulk lattice parameter (that of a free-standing crystal of ZnSe).

Again, using the simulation program, the effect on the epilayer peak FWHM of relaxation of the epilayer was calculated and is shown in Figure 3-6 where it can be seen that as the epilayer thickness increases the FWHM should decrease to 9.3 arcsecs, similar to that of a bulk ZnSe crystal.[22] However, it should be noted that the Takagi-Taupin formalism is not valid for relaxed structures. A comparison with the experimentally determined values is given in section 3.6.1.

Figure 3-5: Pure edge and pure screw dislocations lying in the epilayer substrate interface

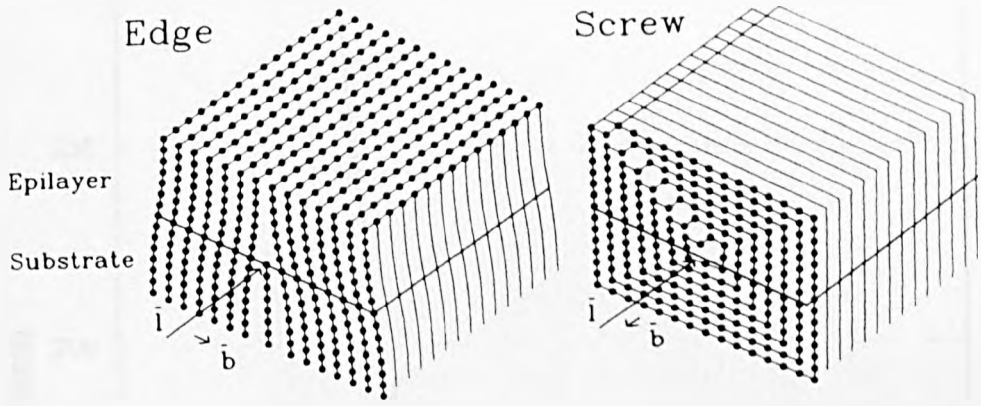

Figure 3-6: Simulated ZnSe rocking curve FWHM vs layer thickness

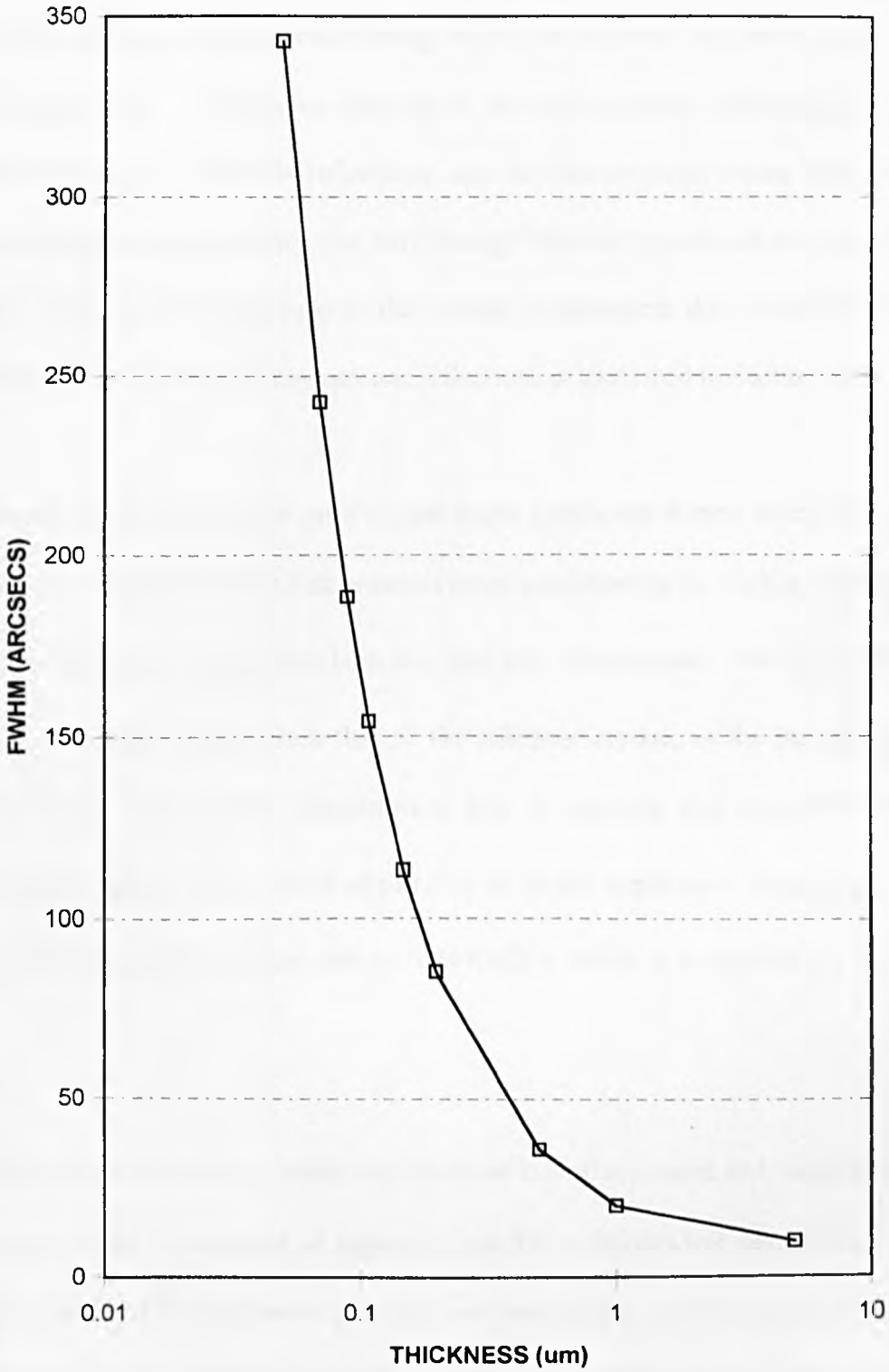

3.5 EXPERIMENTAL MEASUREMENT OF DOUBLE CRYSTAL X-RAY DIFFRACTION ROCKING CURVES

The apparatus used was a double crystal diffractometer (BEDE 200) which is capable of precisely orienting crystals to obtain Bragg reflections, in order that lattice plane spacing may be measured. A schematic diagram of the double crystal diffractometer used is shown in Figure 3-7. The 004 reflections are the most common planes used for GaAs (001) oriented substrates as they give very strong diffracted signals and are parallel to the surface of the crystal which reduces the amount of alignment that would otherwise be required. These are known as symmetric reflections as described in Section 3.2.2.

Accelerated electrons impinge on a copper target producing X-rays which then enter a channel cut collimator (CCC) that provides beam conditioning for Cu $K\alpha_1$ radiation. At this point the beam still contains both $K\alpha_1$ and $K\alpha_2$ components. The CCC allows the use of a dissimilar crystal, from that of the substrate crystal, as the monochromating crystal.[23] Only the Cu $K\alpha_1$ characteristic line is required and monochromation is performed by using a thick crystal of Si (111) set at the appropriate Bragg angle for the (111) reflection and the Cu $K\alpha_1$ line (λ=1.540562Å), which is approximately 14° in this case.

The diffractometer base, on which are mounted both the sample and monochromating crystals, is rotated by an angle of approximately 28° to the incident beam from the CCC in order that the diffracted beam from the monochromating crystal propagates along the centreline of the base towards the sample crystal. The sample crystal is then oriented at an angle of θ_S to this beam where θ_S is the appropriate Bragg angle for the lattice spacing

Figure 3-7: Schematic of double crystal diffractometer

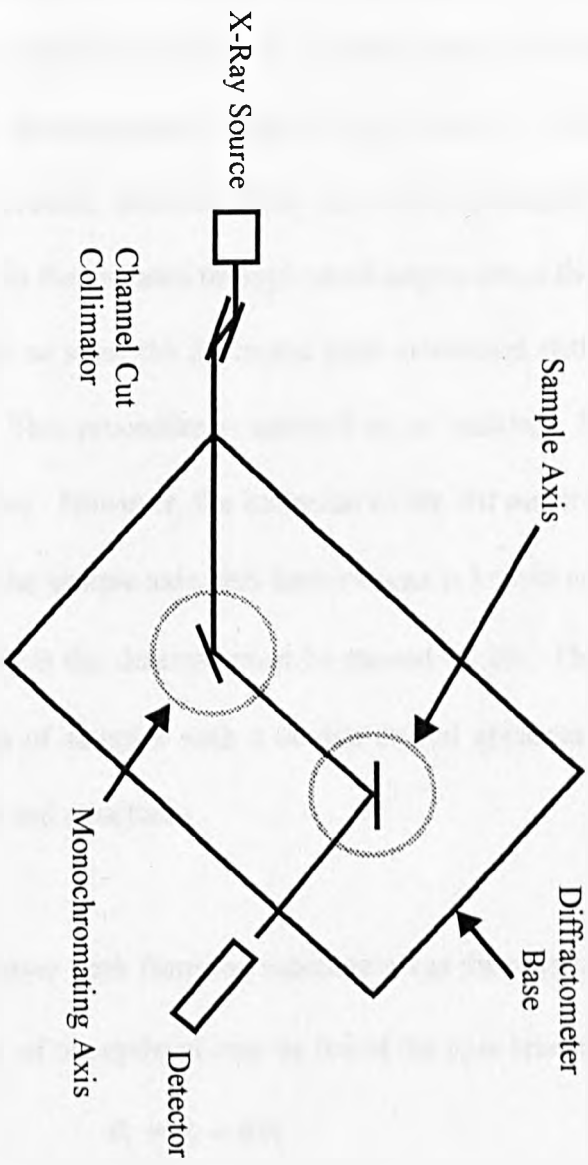

of the substrate, in this case GaAs. In order that the diffracted beam may be observed the detector must be positioned at an angle $2\theta_S$ to the centreline of the diffractometer.

Double crystal rocking curves (DCRC) are obtained after maximising the substrate diffracted peak through a series of iterative steps by rotating the sample about both the vertical rotation axis and the tilt axis of the sample stage. Once this is achieved a vertical slit is placed in front of the detector in order to reduce background and scattered radiation by reducing the acceptance angle of the detector. The width of the slit is chosen such that the counts detected from the GaAs diffracted peak are only just curtailed. The sample is then rotated through small angles about the vertical axis around the GaAs peak in order to view the diffracted peak associated with the growth layer as shown in Figure 3-8. This procedure is referred to as 'rocking', hence the term X-ray diffraction rocking curve. However, the inclusion of the slit requires that the detector is moved in unison with the sample axis, this form of scan is known as a θ,2θ scan as when the sample is moved by θ the detector must be moved by 2θ. This method allows the highest resolution scan of samples with a double crystal apparatus and is essential for examining II-VI layers and structures.

The separation of the layer peak from the substrate gives the angular splitting ($\Delta\theta_L$), and thus the Bragg angle θ_L of the epilayer may be found (as θ_S is known) from:

$$\theta_L = \theta_S + \Delta\theta_L \qquad 3.9$$

Then from equation 3.2 the lattice plane spacing, d_{hkl} can be found. From equation 3.2 and 3.3 the lattice parameter perpendicular to the diffraction planes can be found, as the indices of the diffraction planes are set by the geometry of the reflection, from:

Figure 3-8: Schematic of movement axis on diffractometer

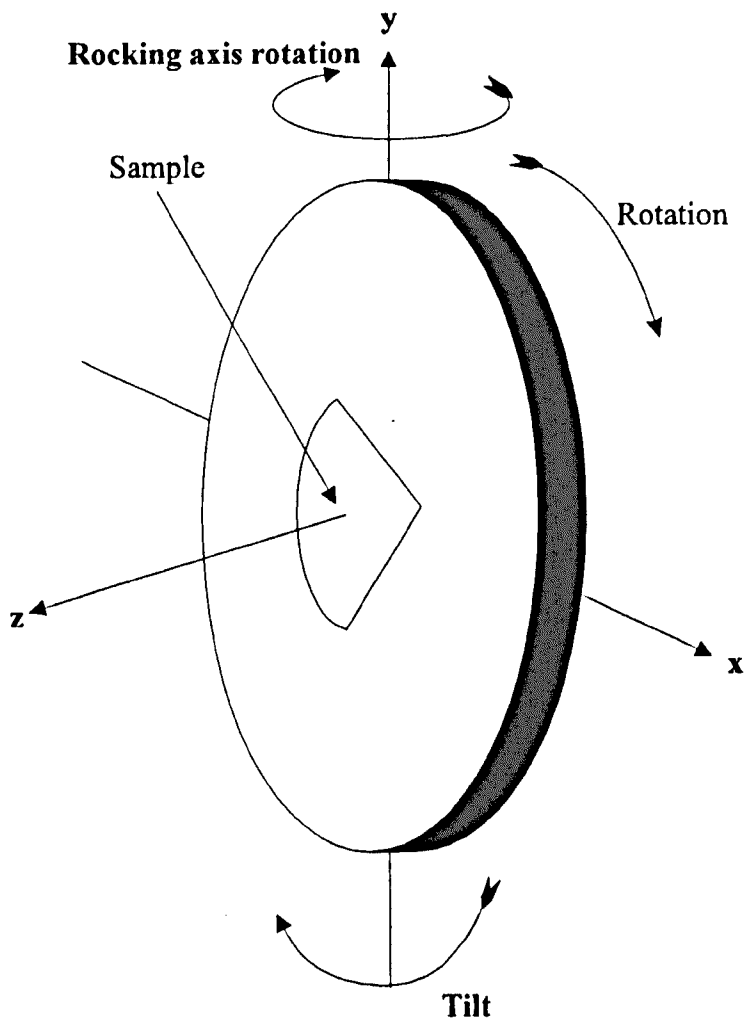

$$\sin\theta_L = \frac{\lambda}{2}\sqrt{\frac{h^2}{a^2}+\frac{k^2}{b^2}+\frac{l^2}{c^2}} \qquad 3.10$$

So for (004) symmetric reflections:

$$\sin\theta_L = \frac{\lambda}{2}\sqrt{\frac{4^2}{c^2}}$$

$$\therefore c = \frac{2\lambda}{\sin\theta_L} \qquad 3.11$$

Therefore, the lattice parameter perpendicular to the interface, c can be directly measured using a symmetrical reflection such as (004). In order to obtain a the use of an asymmetric reflections would be required.

If the layer is a ternary compound and the degree of relaxation can be either measured (again using asymmetric reflections) or assumed, the composition can be found using Vagard's Law from the lattice parameter measured. This assumes a linear variation of lattice parameter between the two binary compounds which constitute the ternary. In the case of $Zn_{(1-x)}Cd_xSe$ it is safe to assume that the epilayer is relaxed as the mismatch to a GaAs substrate is 1.6% for a typical value of x=0.2, this is ~6 times the mismatch of ZnSe hence the critical thickness is very small, so the composition x is given by:

$$x = \frac{a_{ZnCdSe} - a_{ZnSe}}{a_{CdSe} - a_{ZnSe}} \qquad 3.12$$

where: a_{CdSe} is the lattice parameter of CdSe (6.052Å)

a_{ZnSe} is the lattice parameter of ZnSe (5.6682Å)

and a_{ZnCdSe} is the lattice parameter for the layer calculated from the rocking curve.

The above calculation assumes that the layer is thick enough to be fully relaxed to its bulk value lattice parameter, a_r. This is true for ZnCdSe, but for ternaries and quaternaries capable of lattice matching, ZnSSe and ZnMgSSe, there could be a partial relaxation which would result in residual strain in the epilayer. Any residual strain in the layer would affect the splitting, $\Delta\theta_L$ as the unit cell would be subject to a tetragonal distortion due to the lattice mismatch between the layer and substrate. As a result of this distortion the unit cell would be of dimensions a x a x c where a and c are now the dimensions of the epilayer unit cell parallel and perpendicular to the growth interface respectively, and c is the lattice constant measured by the (004) reflections. In order to measure the degree of relaxation (distortion) asymmetric reflections must be used. However, in the case of this study the important issue was to investigate the lattice matching conditions of these compounds and for this (004) reflections are adequate.

3.6 RESULTS OF DCXRD STUDIES ON II-VI MATERIALS

3.6.1 Measurements of Typical ZnSe Layers

In section 3.4 above the effect of lattice mismatch on the epilayer was discussed and the rocking curves for varying thickness of ZnSe were simulated. The critical test for any simulation method must be whether it can reliably predict the outcome of the physical experiment.

A number of pseudomorphic layers were grown for the purpose of determining the critical thickness of ZnSe on GaAs by X-ray topography and shall be discussed further in

Chapter 5. However, these samples also provide the perfect basis for the DCXRD investigation of the early stages of ZnSe growth. Using the experimental method described above (section 3.5) these layers were measured by DCXRD.

A typical rocking curve obtained for a pseudomorphic layer is shown in Figure 3-9. As expected from the simulation the ZnSe and GaAs peaks are clearly visible with the thickness fringe oscillations superimposed upon the rocking curve.

Also shown in Figure 3-9 is the simulated rocking curve for this sample. Therefore, it can be seen that the scattering of X-rays from a pseudomorphic layer can be described by the Takagi-Taupin formalism of the dynamical theory used in the simulation program. Through the use of the simulation program the thickness of the layer was found to be 165 nm.

Symmetric (004) rocking curves were obtained from a number of pseudomorphic epilayers of varying thickness grown on (001) GaAs the results of which are shown in Figure 3-10 and should be compared with the corresponding simulations shown in Figure 3-4. It can be observed that the measured pseudomorphic ZnSe results do indeed follow the simulated trend with the FWHM of the ZnSe epilayer reducing with increasing thickness. Again the simulation program was used to calculate the thickness of the layers from the thickness fringes observed. From the layer to substrate peak splitting it can be observed that even for the thickest sample in this set no appreciable relaxation has taken place as this reduces the layer to substrate peak splitting. However, the layer peak remained at a constant splitting of ~ 790 arcsecs indicative of fully strained, tetragonally distorted ZnSe as calculated from equation 3.4.

Figure 3-9: Measured and simulated rocking curves of HWA 589 ZnSe 1650Å

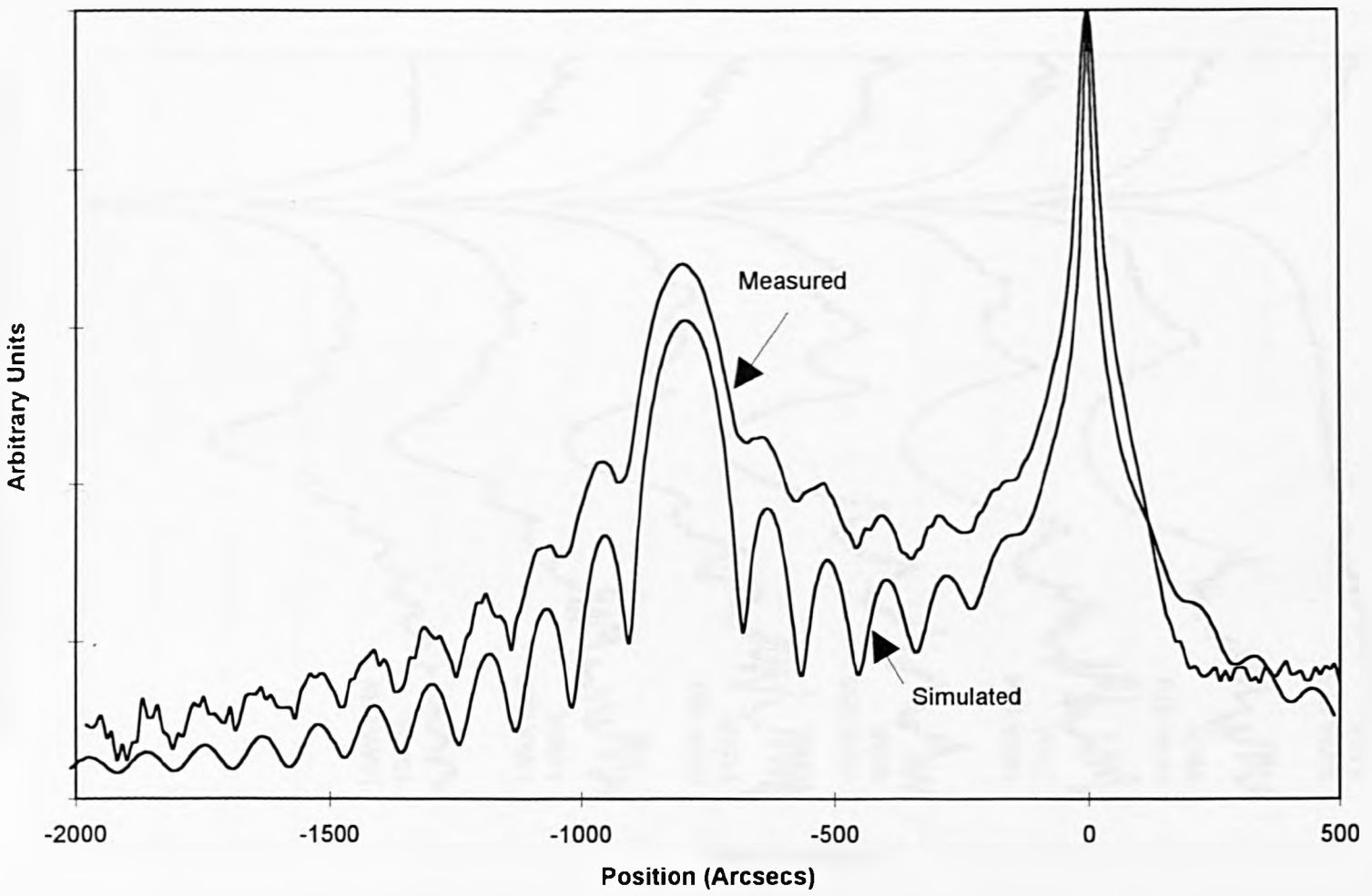

Figure 3-10: XRD of pseudomorphic ZnSe layers

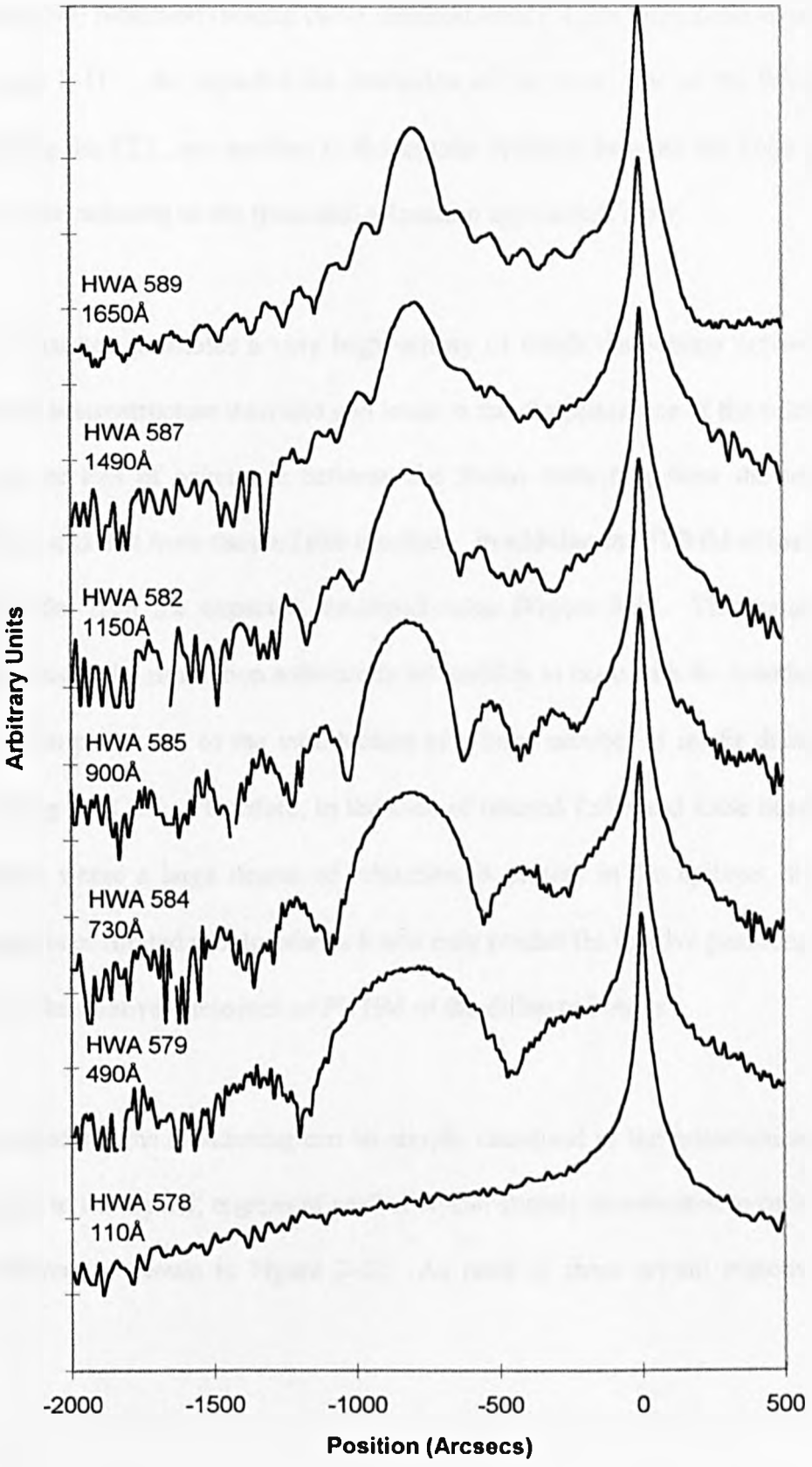

As well as these pseudomorphic samples, a number of thicker samples were also grown under similar growth conditions as the previous set in the range 0.49 μm to 4.5 μm. A typical (004) reflection rocking curve obtained from a 1 μm thick ZnSe layer is as shown in Figure 3-11 . As expected the relaxation of the layer, due to the thickness greatly exceeding the CLT, has resulted in the angular splitting between the ZnSe peak and the GaAs peak reducing as the fractional relaxation approaches unity.

This relaxation generates a very high density of misfit dislocation networks initiating from the heterostructure interface and leads to the disappearance of the thickness fringes due to the loss of coherence between the X-rays reflecting from the heterostructure interface and that from the air/ZnSe interface. In addition the FWHM of the layer peak is far broader than the expected simulated value (Figure 3-6). This result shows the limitations of the simulation software in its inability to cope with the broadening of layer diffraction peaks due to the introduction of a large number of misfit dislocations after exceeding the CLT. Therefore, in the case of relaxed ZnSe and ZnSe based compound epilayers where a large degree of relaxation is present in the epilayer, the simulation program is of limited use, insofar as it will only predict the relative positions of the peaks and not the relative intensities or FWHM of the diffracted peaks.

The reason for the broadening can be simply visualised as the introduction of a mosaic structure to the crystal; regions of perfect crystal slightly misoriented to each other due to dislocations as shown in Figure 3-12. As each of these crystal regions will have a

Figure 3-11: Measured and simulated rocking curves for HWA 751 4.5um thick

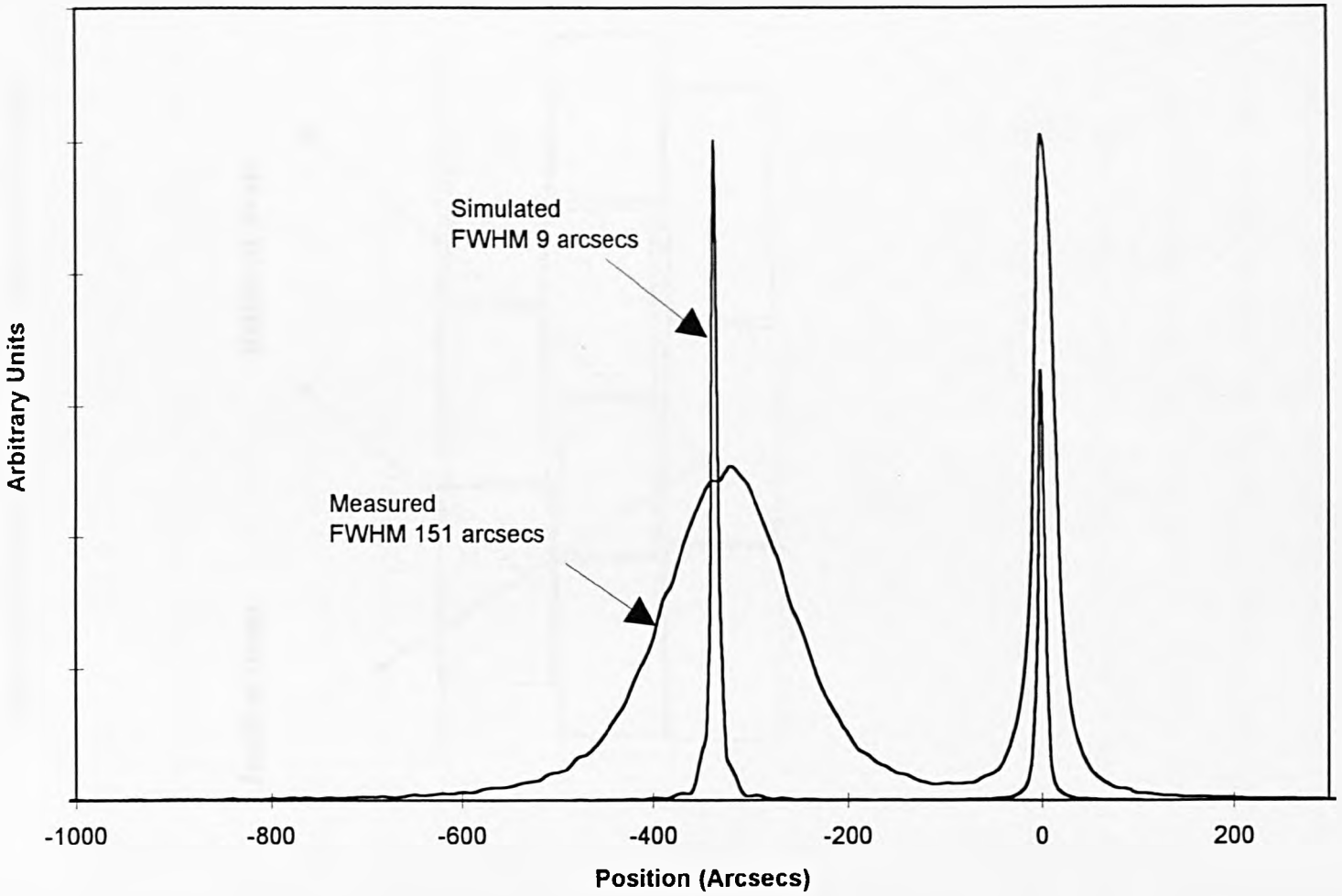

Figure 3-12: Mosaic structure of non-perfect crystal

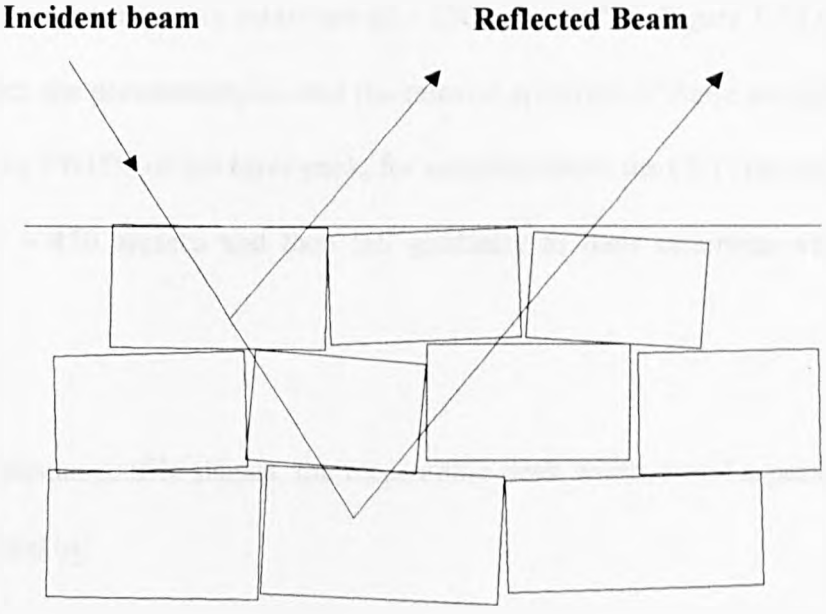

slightly different solution to the Bragg conditions for diffraction the resultant rocking curve is broadened.

Although the FWHM of the diffracted peak from the epilayer does reduce with increasing layer thickness, it does not approach the theoretical minimum of FWHM of ~ 9 arcsecs but instead reaches a minimum of ~ 150 arcsecs.[24] In Figure 3-13 the measured FWHM of both the pseudomorphic and the relaxed epilayers of ZnSe are plotted. It can be seen that the FWHM of the layer peak, for samples above the CLT, increase sharply to a maxima of ~ 450 arcsecs and then fall gradually to their minimum value of ~150 arcsecs.

Assuming Gaussian profile shapes, the measurable peak width $\Delta\omega$ of a perfect layer can be approximated by:

$$\Delta\omega = \sqrt{\Delta\theta^2 + \Delta\varepsilon^2} \qquad 3.13$$

where, $\Delta\theta$ is the intrinsic reflection width (dependent on t, the thickness of the layer) and $\Delta\varepsilon$ is the FWHM of the apparatus function and is dependent on the Bragg angle. The broadening due to the finite resolution of the diffractometer becomes important if the intrinsic width itself becomes smaller than the resolving power. However, in the case where the layer is not perfect due to the defects introduced from the generation of misfit dislocations it is possible to estimate the broadening, $\Delta\xi$, from these imperfections using:

$$\Delta\omega^2 = \Delta\xi^2 + \Delta\theta^2 + \Delta\varepsilon^2 \qquad 3.14$$

Figure 3-13: Measured FWHM vs thickness for ZnSe

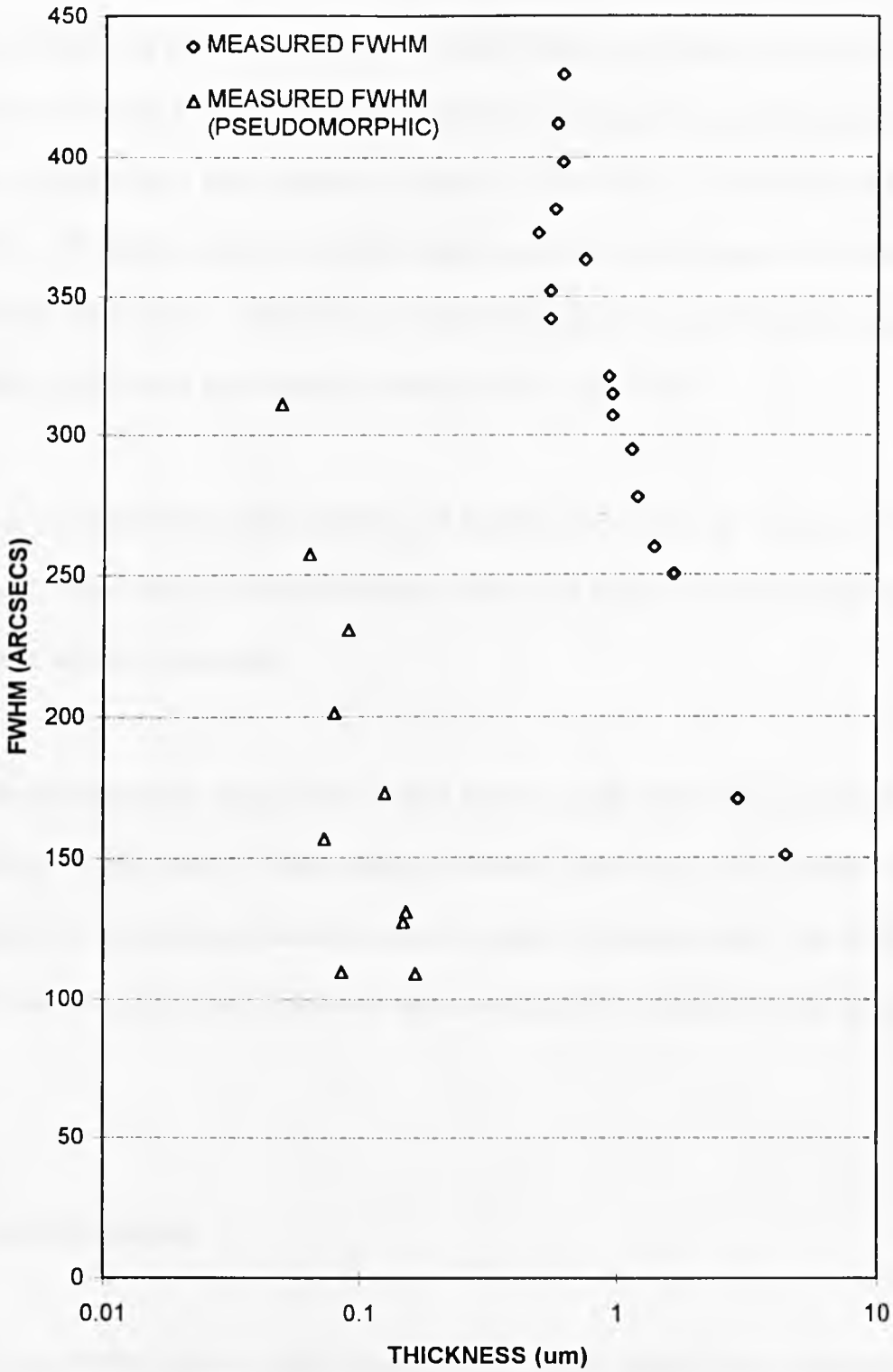

where, $\Delta\omega$ is now the observed FWHM.[25]

An estimate of the number of dislocations required to relieve the strain of ~0.26% in the ZnSe/GaAs system can be obtained. The magnitude of the Burgers vector is $a/\sqrt{2}$ which corresponds to the predominant 60° misfit dislocation common to the zinc-blende structure. Consider a 1cm length of strained ZnSe crystal grown on a GaAs substrate. In order to fully relax it must expand by ~0.26% (2.6×10^{-3}cm). Given that the Burgers vector is ~4Å then the number of misfit dislocations which would require to be generated would be $\sim 6.5 \times 10^{4}$cm^{-1}. Therefore, this yields a minimum density of misfit dislocations to enable a ZnSe layer to become fully relaxed to be $\sim 4 \times 10^{9}$cm^{-2}.

This is a considerable defect density and highlights the case for the use of lattice matched compounds for device fabrication where the formation of misfit dislocations should be kept to a minimum.

For the pseudomorphic samples the FWHM almost exactly follows the predicted value. Therefore, in the case of lattice matched material where any misfit strain will be negligible the theory should indeed be able to predict the correct result. The DCXRD of lattice matched ternary and quaternary compounds shall be discussed further in Chapter 5.

3.7 CONCLUSIONS

It has been shown that as a routine analysis tool, double crystal X-ray diffraction is an invaluable technique for the rapid characterisation of epilayers. Information regarding

the lattice parameter, strain and, in the case of pseudomorphic material, the thickness of an epilayer can all be routinely measured. Also from the FWHM of the diffracted peaks a judgement can be made regarding the structural perfection of the epilayer. As it is also non-destructive extensive studies can be carried out without detriment to other analysis techniques.

3.8 REFERENCES

[1] G. D. Brownlie, Z. Zhu, G. Horsburgh, T. A. Steele, P. J. Thomson, J. M. Wallace, K. A. Prior and B. C. Cavenett, J. Crystal Growth 159 (1196), 321

[2] J. Petruzello, B. L. Greenberg, D. A. Cammack and R. Dalby, J. Appl. Phys. 63 (1988), 2299

[3] *Elements of X-Ray Diffraction*, B. D. Cullity, Addisson-Wesley (1978)

[4] M. A. G. Halliwell, J. B. Childs and S. O'hara, 1972 Symp. on GaAs, 98

[5] M. A. G. Halliwell, *Advances in X-ray Analysis*, Vol. 33, Plenum Press, New York, 1990

[6] M. F. C. Ladd and R. A. Palmer, in *Structure Determination by X-ray Crystallography*, Plenum Press, New York 1977

[7] B. W. Batterman and H. Cole, Rev. Mod. Phys. 36 (1964), 681

[8] R. W. James, *The Optical Principles of the Diffraction of X-Rays*, Ox Bow Press, Connecticut, 1982

[9] Z. G. Pinsker, *Dynamical Scattering of X-rays in Crystals*, Springer-Verlag, New York, 1978

[10] S. Takagi, J. Phys. Soc. Japan, 26 (1962), 1311

[11] D. Taupin, Bull. Soc. Fr. Mineral. Cristallography, 87 (1964), 469

[12] M. A. Halliwell, M. H. Lyons, M. J. Hill, J. Cryst. Growth, 68 (1984), 523

[13] Handbook of Chemistry and Physics, Ed. D. R. Lide, CRC Press, 1991

[14] Landolt-Bornstein, Springer-Verlag, Vol. 17b, New York (1982)

[15] H. Okuyama, K. Nakano, T. Miyajima and K. Akimoto, J. Cryst. Growth, 117 (1992), 139

[16] Z. C. Feng and H. D. Liu, J. Appl. Phys., 54 (1983), 83

[17] C. R. Whitehouse, A. G. Cullis, S. J. Barnett, B. F. Usher, G. F. Clark, A. M. Keir, B. K. Tanner, B. Lunn, J. C. H. Hogg, A. D. Johnson, G. Lacey, W. Spirkl, W. E. Hagston, J. H. Jefferson, P. Ashu, G. W. Smith and T. Martin, J. Cryst. Growth, 150 (1995), 85

[18] P.F. Fewster and C. J. Curling, J. Appl. Phys. 62 (1987), 4154

[19] W. Bartels, J. Vac. Sci. Technol. B1 (1983) 338

[20] L. Tapfer, M. Ospelt and H. von Kanel, J. Appl. Phys. 67 (1990) 1298

[21] M. O. Möller, V. Beyersdorfer, D. Hommel, T. Behr, H. Heinke, T. Lippmann and G. Landwehr, J. Crystal Growth 143 (1994) 162

[22] Y. Okuno, H. Tamura and T. Maruyama, J. Elect. Mat. 22 (1993), 685

[23] N. Loxley, D. K. Bowen and B. K. Tanner in Proc. Mat. Res. Soc. Symp. J. Fall MRS Meeting 1990

[24] T. Reisinger, M. J. Kastner, K. Wolf, E. Steinkirchner, W. Hackl, H. Stanzl and W. Gebhardt, Mat. Sci Forum, 182-184 (1995), 147

[25] C. Dunn and E. Koch, Acta Met. 5 (1957), 548

4. DOUBLE CRYSTAL X-RAY TOPOGRAPHY

4.1 INTRODUCTION

Double crystal X-ray topography is a technique used to image the defects in the crystal structure of a crystal.[1] The term topography does not refer to the surface morphology but to the effects of defects propagating through the crystal structure. The conditions for X-ray diffraction are as described in section 3.2 in the previous chapter where diffraction only occurs where the crystal planes are oriented to the incident beam such that the conditions of Bragg's law are satisfied. However, in the case of a dislocation or defect in the crystal, the planes through which the dislocation passes will be deformed in that region such that the solution for Bragg's law will occur at a different angle than from the rest of the plane. This different solution provides the opportunity to image the dislocation using X-ray diffraction as the diffracted intensity from the region of the dislocation will be different from that of the rest of the sample. This technique has been used successfully for a number of years for the imaging crystal defects in other semiconductor systems.

As it is necessary to image an area of the sample and to have enough diffracted X-ray intensity to expose some recording medium to produce a topograph, a high intensity source of X-rays is required. Although topography is possible using a conventional laboratory X-ray source, the beam intensity after broadening is low which leads to the

requirement of very long exposure times (hours) to achieve the contrast required. A far better solution is to use a synchrotron based system where the intensity is far in excess of any possible in the laboratory allowing very much shorter exposure times of the order of minutes. One advantage of this is to minimise the effect of machine vibration and long-term drift of mechanical components which would otherwise limit the resolution of the technique. Also, as the beam intensity is so much higher for synchrotron radiation, the positioning of the sample to produce diffraction is far easier. A synchrotron essentially provides white radiation where the wavelength required can be tuned using the orientation of the first monochromating crystal. For this study the synchrotron resonator at Daresbury was used.

4.2 CRITICAL THICKNESS AND MISFIT DISLOCATIONS

In the case of heteroepitaxy where an epilayer is grown on a substrate of a material with a different lattice parameter a strain parallel to the interface results. The magnitude of this misfit is found from Equation 3.1, the effect of this is to deform the epilayer unit cell to achieve the same lattice parameter as the substrate parallel to the interface which causes a subsequent change of the perpendicular lattice parameter as described by Equation 3.4. As the layer thickness increases during growth the strain energy due to the deformation of the unit cell also increases until at some thickness it becomes energetically favourable to form misfit dislocations to relieve the strain. The critical thickness of an epilayer is defined as that thickness where the very first misfit dislocation is formed and is dependent on the initial misfit.[2]

The determination of this critical thickness for the material system used is an important aspect of device design and growth as it has implications for the level of defects present in the semiconductor material. Ideally, any device structure should be free from defects in order to obtain the maximum performance. However, in the case of a strained layer, such as a quantum well of ZnCdSe or InGaAs in an otherwise lattice matched structure, the potential exists for generating a large number of defects due to the formation of misfit dislocations if the critical thickness is exceeded is introduced. X-ray topography is the ideal tool for the measurement of the critical thickness and subsequent relaxation processes as using this technique it is possible to image individual misfit dislocations.[3]

A misfit dislocation can be described as a localised region of disregistry in the crystal structure as shown in Figure 4-1 for the case of a pure edge and a pure screw dislocation. It can be seen that in the case of the edge dislocation the Burgers vector of the dislocation, $\boldsymbol{b}$, is both perpendicular to the line of the dislocation and in the plane of the interface whereas for the screw dislocation the Burgers vector is parallel to the line of the dislocation. This is the reason why pure edge dislocations are the most efficient method of relieving strain in the lattice and screw dislocations do not relieve strain. In the event of a mixed dislocation having both a screw and an edge nature, it is only that component of the Burgers vector which is edgelike and in the plane of the interface which acts to relieve the misfit strain. However, in order to be efficient at relieving strain a misfit dislocation must have a component of its Burgers vector out of the interface so that it may glide through the crystal. Otherwise the misfit would only be able to glide parallel to the interface which would not result in any relaxation of the strain.[3]

Figure 4-1: Pure edge and pure screw dislocations lying in the epilayer substrate interface

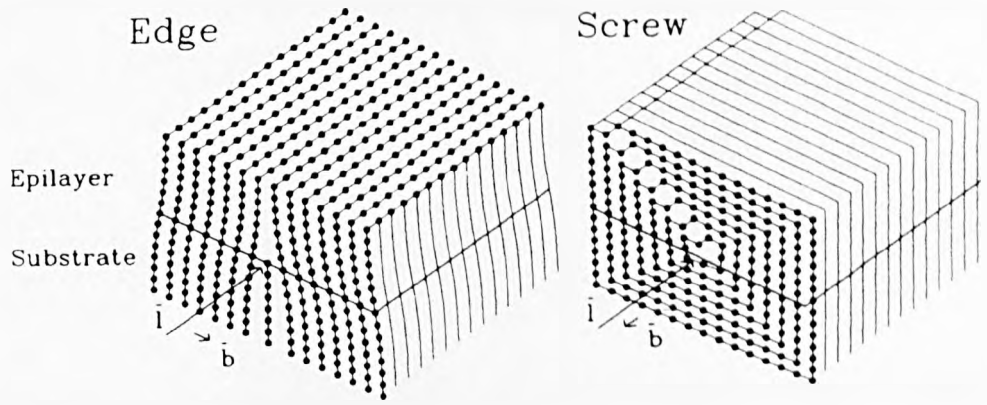

The principal lattice vectors, and therefore the most likely Burgers vectors for dislocations in a face centred cubic structure, are of the type $(a/2)<110>$ and $a<001>$. Since the energy of a dislocation is proportional to the square of the length of its Burgers vector, b^2, the energy of $(a/2)[110]$ dislocations will be only half that of $a[001]$. Therefore, the most energetically favourable dislocation is of $(a/2)[110]$ type.[4] Indeed, electron microscopy studies have shown that mismatch dislocations which cause relaxation at (001) interfaces are predominantly 60° in nature and glide in the inclined {111} slip planes to form long segments lying along the <110> directions parallel to the interface.[5]

4.3 X-RAY TOPOGRAPHY

It has been known for some time that X-ray double crystal topography (XRDCT) can be used to image defects in thin films or in the subsurface region of crystals.[6] Indeed XRDCT was successfully used to image very low levels of strain in silicon.[7,8] X-ray imaging techniques have an advantage over electron techniques as they allow the imaging of samples with macroscopic dimensions (areas of a few mm^2 to tens of cm^2) and also they offer very high strain sensitivity. X-ray diffraction is able to reveal lattice strains as small as 10^{-6} - 10^{-7}.[9] These characteristics make X-ray diffraction topography an ideal tool for the investigation of defect configurations and their evolution in as-grown and processed semiconductor materials.

XRT has been used in the investigation of III-V compounds, in particular the crystal quality of both the substrate and epilayers and the effects of the relaxation processes in strained epilayers. As whole wafers can be imaged by asymmetric XRT using

relatively short exposure times, it is an ideal tool for pre-screening of substrate wafers. The reason for using asymmetric reflections is to provide sufficient beam broadening to allow the imaging of large area samples.[10]

More recently studies of III-V strained layer relaxation processes have been carried out which highlight the important role played by the pre-existing substrate dislocation structure in the subsequent generation of misfit dislocations.[11,12,13] From this work it was found that there was a substantial difference in the threading dislocation distribution between GaAs substrates grown by the liquid encapsulated Czochralski (LEC) and by the vertical-gradient freeze Bridgeman (VGF) techniques.[14] In the case of LEC undoped GaAs substrates a cellular structure of threading dislocations is observed with typical dimensions of 100 μm across.[15] Although the average threading dislocation density of these substrates is 10^4 cm^{-2}, the distribution is highly non-uniform with densities of the order 10^5 cm^{-2} in the walls and less than 10^2 cm^{-2} in the centres of the cells, respectively. In contrast, VGF undoped GaAs substrates exhibit a much more uniform distribution of threading dislocations with an average density of typically < 3000 cm^{-2}. However, in the case of Si doping of the VGF substrates the resultant hardening of the lattice leads to a substantial reduction in the average threading dislocation density to < 20 cm^{-2} with relatively large areas observed to be totally free of threading dislocations. This difference between GaAs substrates grown by different techniques makes it necessary, where possible, to pre-screen the wafers used to ensure that any subsequent measurements are not affected by poor quality substrate material with a high density of threading dislocations. This is achieved by performing topography on one or two substrate wafers from a particular substrate boule rather than analysing every wafer in the batch which would be time consuming.

Studies of $In_{0.185}Ga_{0.815}As$ layers grown on LEC GaAs substrates analysed by *ex-situ* XRT resulted in a direct determination of the critical thickness of the epilayer from the observation of the formation of the first misfit dislocation at a thickness of 16.6 ± 0.2 nm.[16] Also, from the XRT data it was observed that in excess of 95% of the misfit dislocations formed subsequently were generated by the turning over of threading dislocations emanating from the substrate. The same group performing *in-situ* XRT studies of $In_{0.185}Ga_{0.815}As$ layers on VGF substrates during growth using a purpose built MBE chamber[12] again showed that the initial formation of misfit dislocations occurred due to the bending over of the substrate threading dislocations. However, for Si doped VGF GaAs substrates the density of threading dislocations present were not enough to generate the misfit dislocations observed in the subsequent relaxation of the epilayer, unlike the LEC case. In the case of epilayers grown on VGF substrates a secondary source for the formation of misfit dislocations was attributed to local morphological and/or compositional variations in the growing layer. Therefore, for the topography samples grown for the purpose of determining the critical thickness of ZnSe for this thesis, Si doped VGF GaAs substrates were used due to their relatively low threading dislocation density.

4.4 TOPOGRAPHY OF ZnSe SAMPLES

As explained above, XRT is able to image the formation of the first misfit dislocation which allows a direct measurement of the critical thickness to be made. The upper limit of dislocation density measurable by X-ray topography occurs when the spacing between the dislocations is less than the resolution of the technique. The resolving

power is limited by the angular dispersion of the source and by the grain size of the photographic medium. In the case of synchrotron radiation the angular dispersion is very small as the source is far removed from the diffractometer and the resolution is limited by the grain size of the film. Photographic plates were used throughout this study, these were made from glass slides coated with Ilford L4 nuclear emulsion on one side. The nuclear emulsion used had a grain size of 0.15μm.

X-ray topography images presented in this thesis were obtained using beam station 7.6 at the Daresbury synchrotron facility. The beam used was operated at 2 GeV with the wiggler source at 5 T and a beam current of 150 mA. A wavelength of 1.54 Å was selected using a very low defect density Si (111) wafer.

Experimental values for the onset of relaxation for ZnSe on GaAs have previously been determined by X-ray double crystal rocking curve measurements[17] and photoluminescence (PL)[18]. In both cases, values for the critical layer thickness of ≈150 nm were obtained. More recently, a value of 250 nm was obtained for a ZnSe layer grown by migration enhanced epitaxy[19].

As the critical layer thickness was suspected to be in the region of 150 nm for conventional MBE ZnSe, a range of samples was proposed. These nominally undoped ZnSe layers were grown on Vertical Gradient Freeze Bridgeman (VGFB) GaAs substrates, with low threading dislocation densities, using elemental Zn and Se sources. The substrates were etched and the oxide removed by thermal cleaning as described in chapter 2.9.

All of these samples were grown under the same conditions, consecutively on the same day. The growth rate, which had previously been determined by growing a thick calibration layer, was set at 0.5 μm/hour. Also, the Se/Zn ratio was maintained at 1:1 confirmed by the presence of mixed 2x1 & c(2x2) RHEED patterns (as discussed in Section 2.9.4). The growth temperature was maintained at 350°C as measured using an optical pyrometer. In addition to this, the samples were grown under continuous rotation throughout the entire process to try to ensure the best uniformity possible, including during the thermal heat clean and cool down and initial start of growth. This was necessary as each samples total growth time was measured in terms of minutes. The thickness of the films was determined using X-ray rocking curve simulation as described in Section 3.4 as the thickness fringes for all of the samples were easily visible, indicative of structurally sound material. It was also necessary to remove the indium used to mount the wafer during growth from the back surface in order that the substrate would be as flat as possible to allow good imaging of the sample during XRT.

As the CLT appeared to be in the region of 150nm a set of samples were proposed in the range 30 to 170 nm. There were 13 samples grown in this range with thickness as shown in table 4.1.

Table 4.1: Results of Sample Set 1

SAMPLE SET 1: MEASURED THICKNESS FROM XRD SIMULATION	
SAMPLE NO.	THICKNESS ±5(nm)
577	79
578	11
579	49
580	63
581	30
582	115
583	40
584	73
585	90
586	126
587	149
588	153
589	168

The X-ray topographs for these samples were obtained using the apparatus previously described with the 620 reflection from the GaAs substrate as shown in Figure 4-2. The substrate peak was used to image the dislocations as it gave the strongest reflected intensity from the incident beam.

The X-ray topographs obtained are shown in Figure 4-3 from which it can be seen that below 90 nm (a) no dislocations can be seen, but for the 115 nm (b) sample a misfit dislocation network is clearly visible indicating that the sample has begun to relax through the generation of misfit dislocations. Therefore, from this initial set of samples it can be seen that the CLT is in the region 90 to 115 nm, considerably less than the 150 nm found previously.

Now that the critical thickness had been determined to within 25 nm a narrower range of samples were grown using the same conditions as for the first set. These samples covered the range 85 to 99 nm (table 4.2) as from the previous set it looked as if the critical thickness was nearer to the lower end of the range than the higher. However, it

Figure 4-2: Angles used for <620> glancing incidence reflection

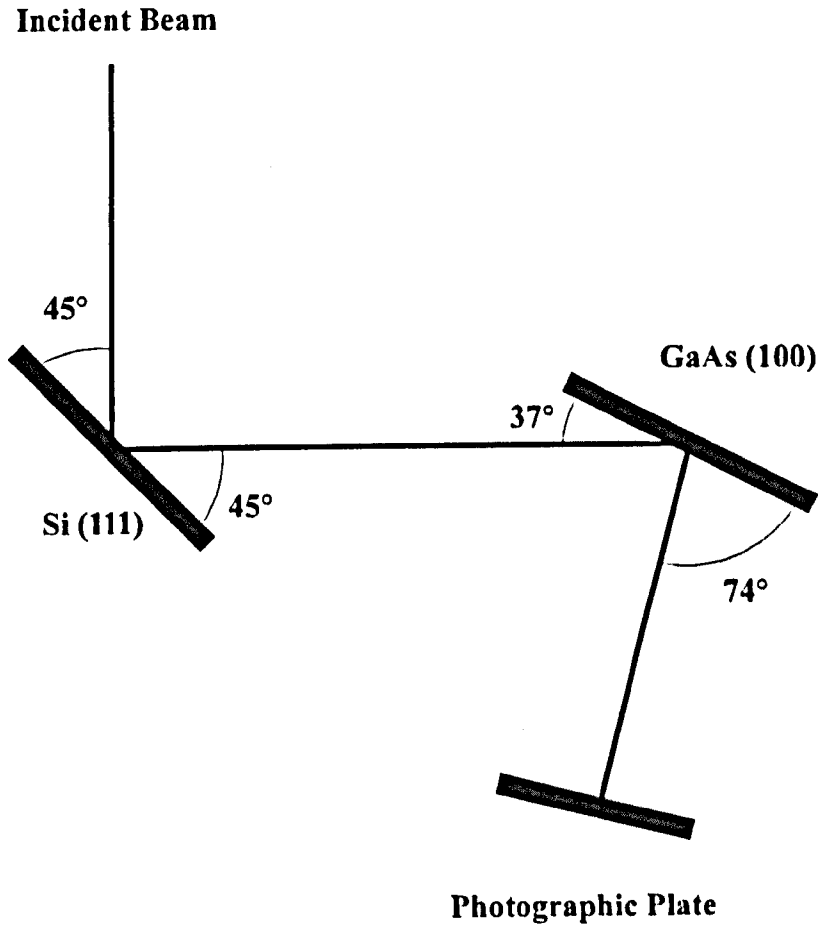

Figure 4-3: Topography results from sample set 1

a) HWA 585 90nm

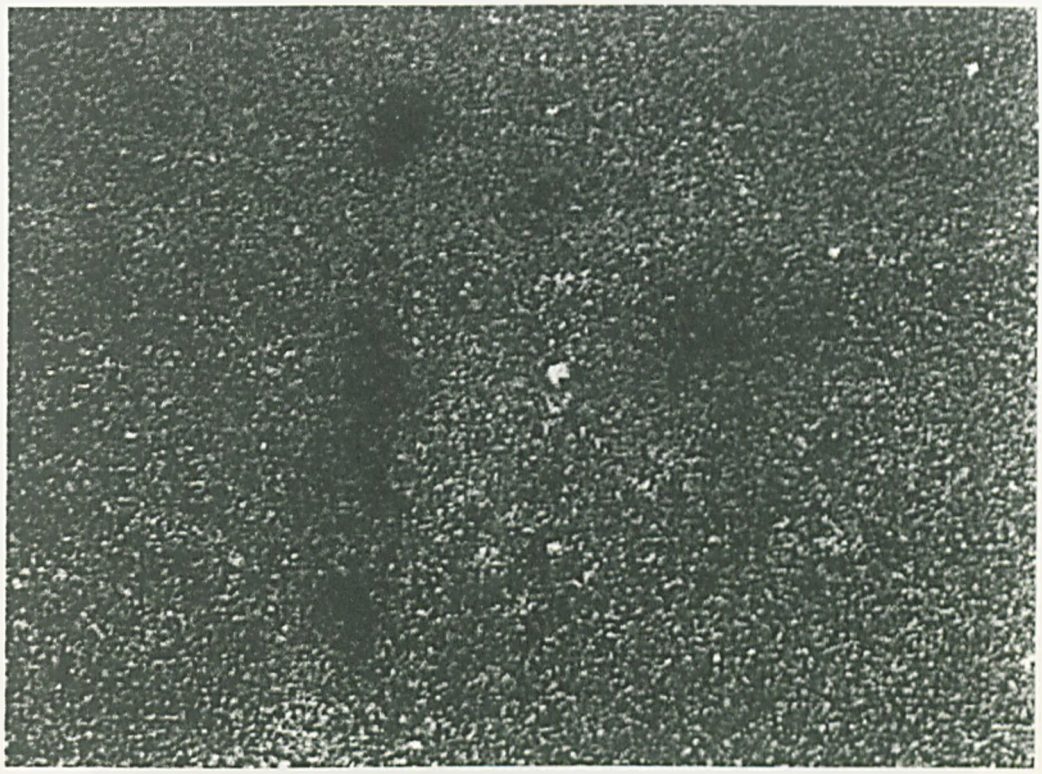

b) HWA 582 115nm

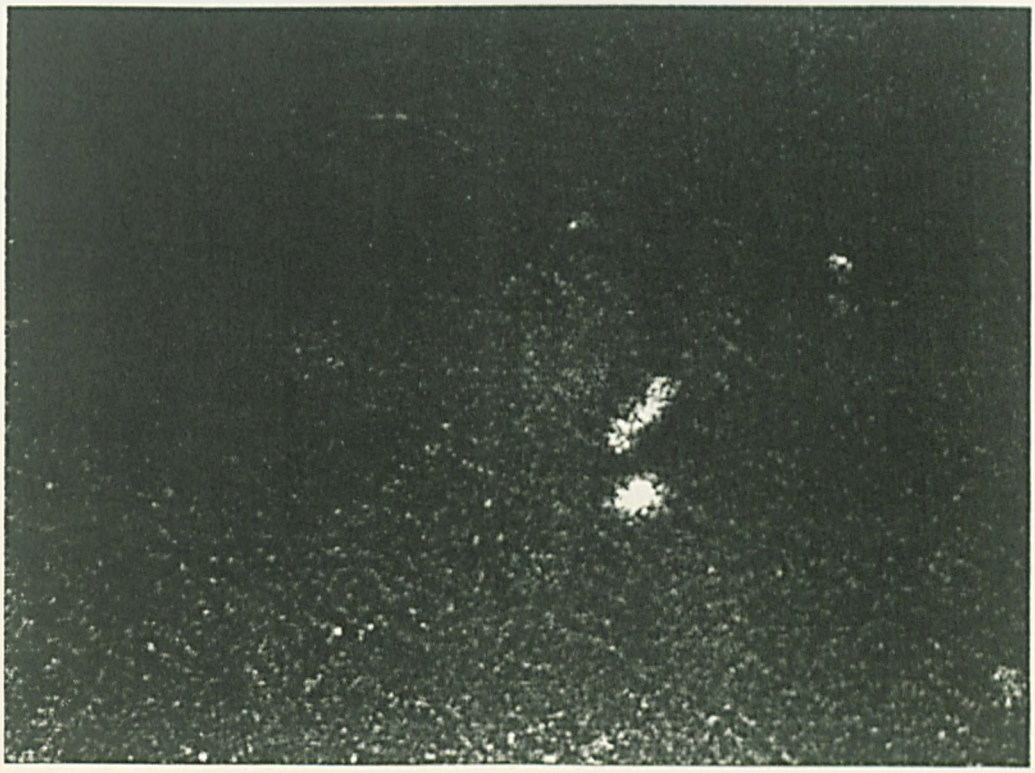

Figure 4-4: XRT of HWA 734 ZnSe (99 nm)

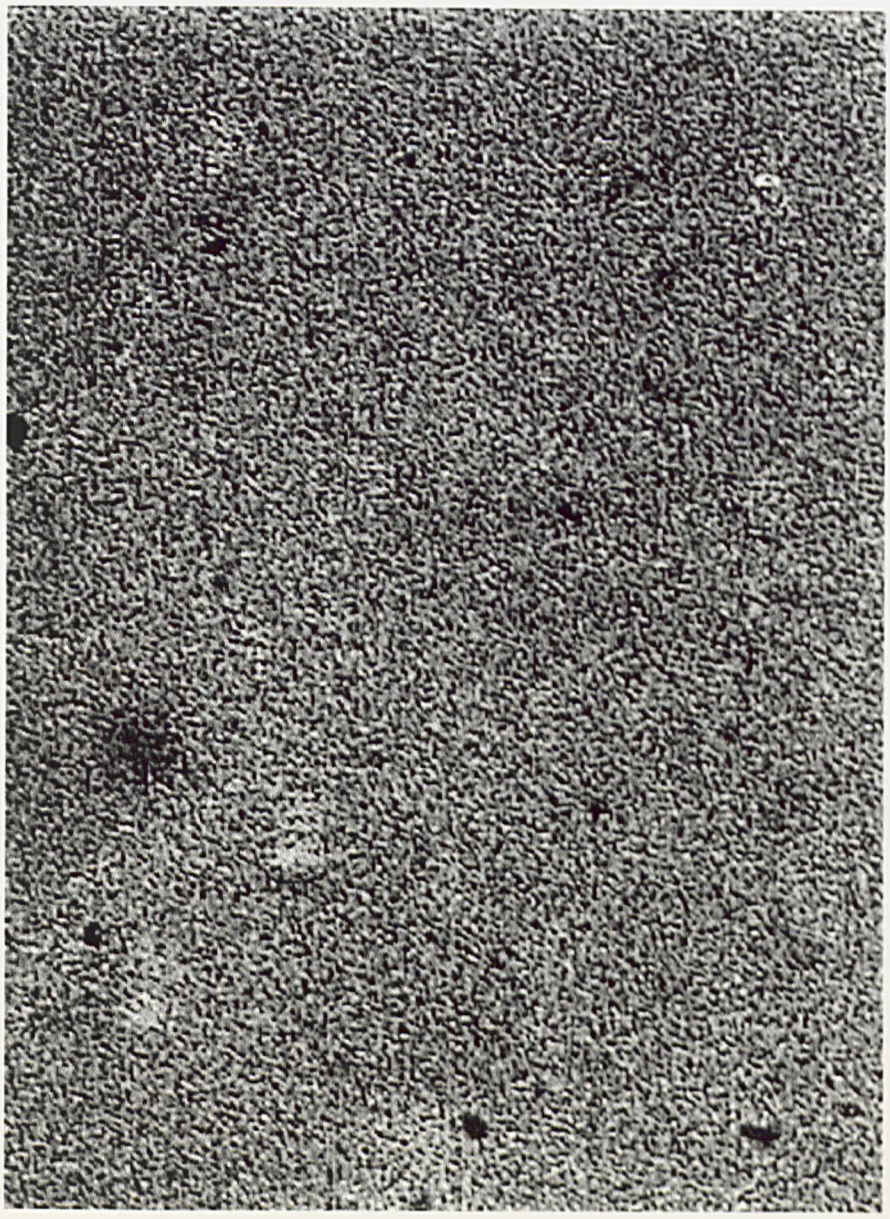

can be seen from the results of sample HWA 734 (Figure 4-4) that there are no dislocations present in this range of samples.

Table 4.2: Results of Sample set 2

SAMPLE SET 2: MEASURED THICKNESS FROM XRD SIMULATION	
SAMPLE NO.	THICKNESS ±5(nm)
731	85
732	90
733	94
734	99

As the topography results from this set of samples had shown that the CLT was greater than 99 nm it was necessary to grow a further set, but to ensure continuity between the sets the first sample thickness of this set was chosen to lie within the range of the second set. These 4 samples and their measured thickness are shown in table 4.3.

Table 4.3: Results of Sample set 3

SAMPLE SET 3: MEASURED THICKNESS FROM XRD SIMULATION	
SAMPLE NO.	THICKNESS ±5(nm)
807	95
808	100
809	105
810	110

Again the 620 reflections were obtained using synchrotron radiation. From these results it can be seen that the 95nm sample (Figure 4-5) has no strain-relieving misfit dislocations, as expected from the previous set. However, the topograph of the 100nm sample (Figure 4-6) clearly shows dislocations with a spacing of 14 μm. This figure also shows that the dislocation glide velocity is markedly different in the two orthogonal <110> directions, as evidenced by the very different extensions of the misfit segments. However, careful study of these topographs also indicate that some dislocation lines are in non-<110> directions. These are caused by repeated cross-

Figure 4-5: XRT of HWA 807 ZnSe (95 nm)

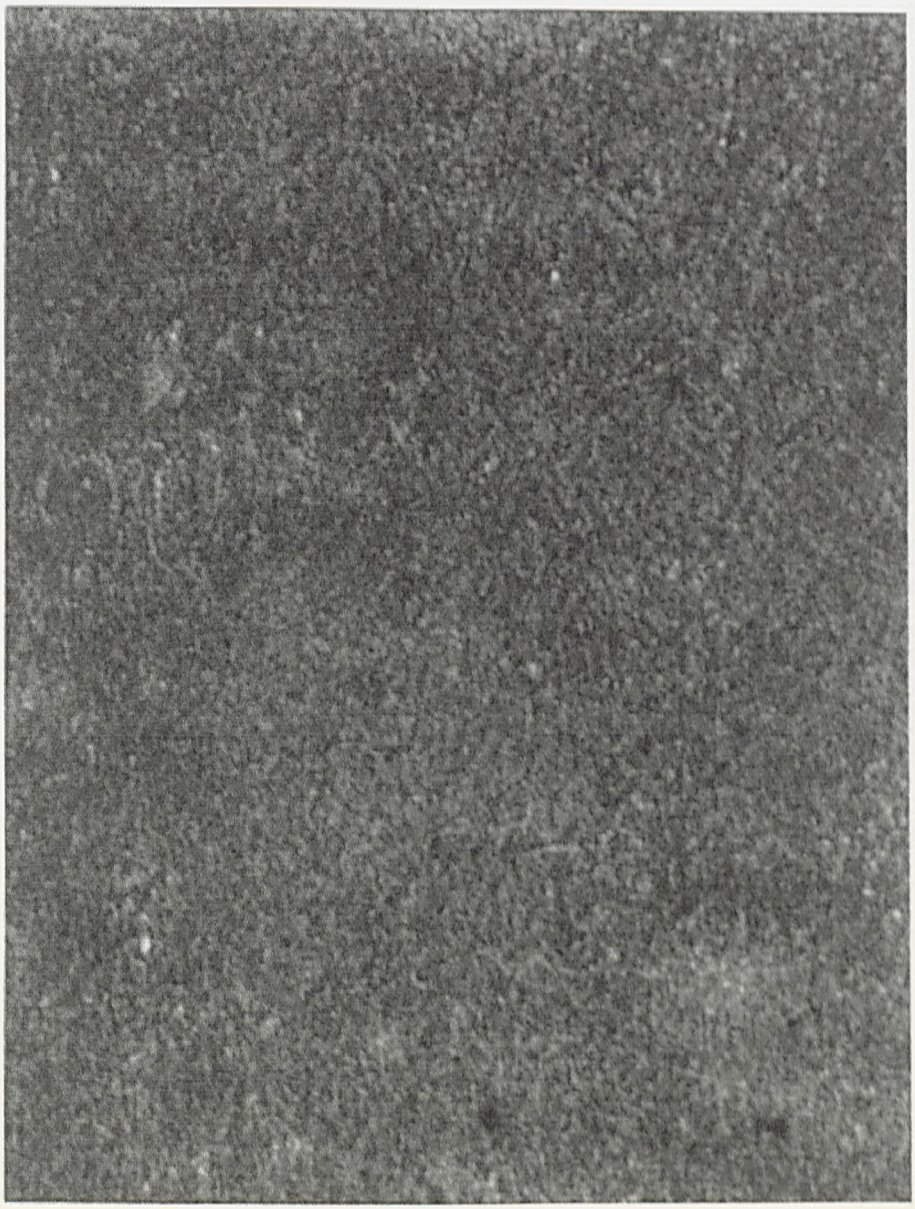

50μm

Figure 4-6: XRT of HWA 808 ZnSe (100 nm)

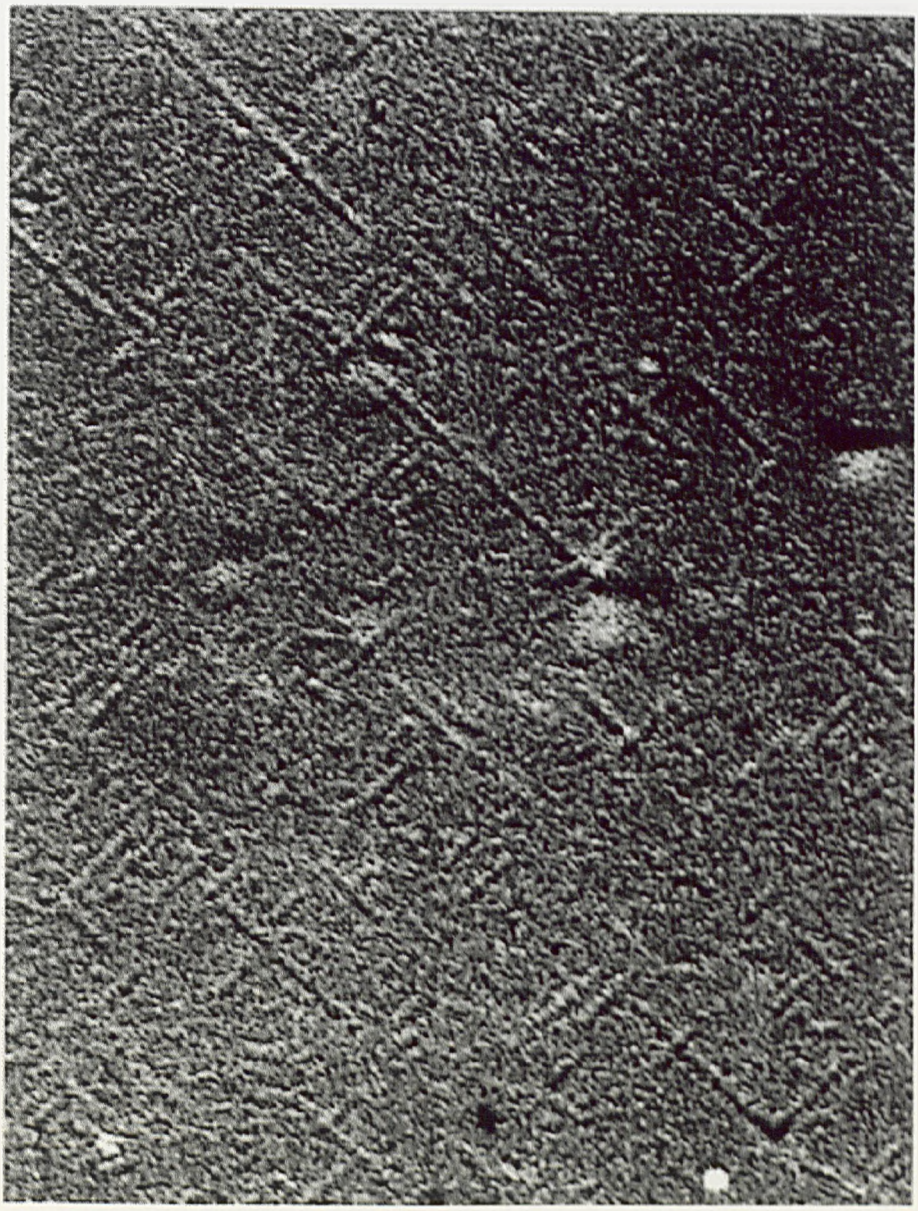

Figure 4-7: XRT of HWA 809 (105 nm)

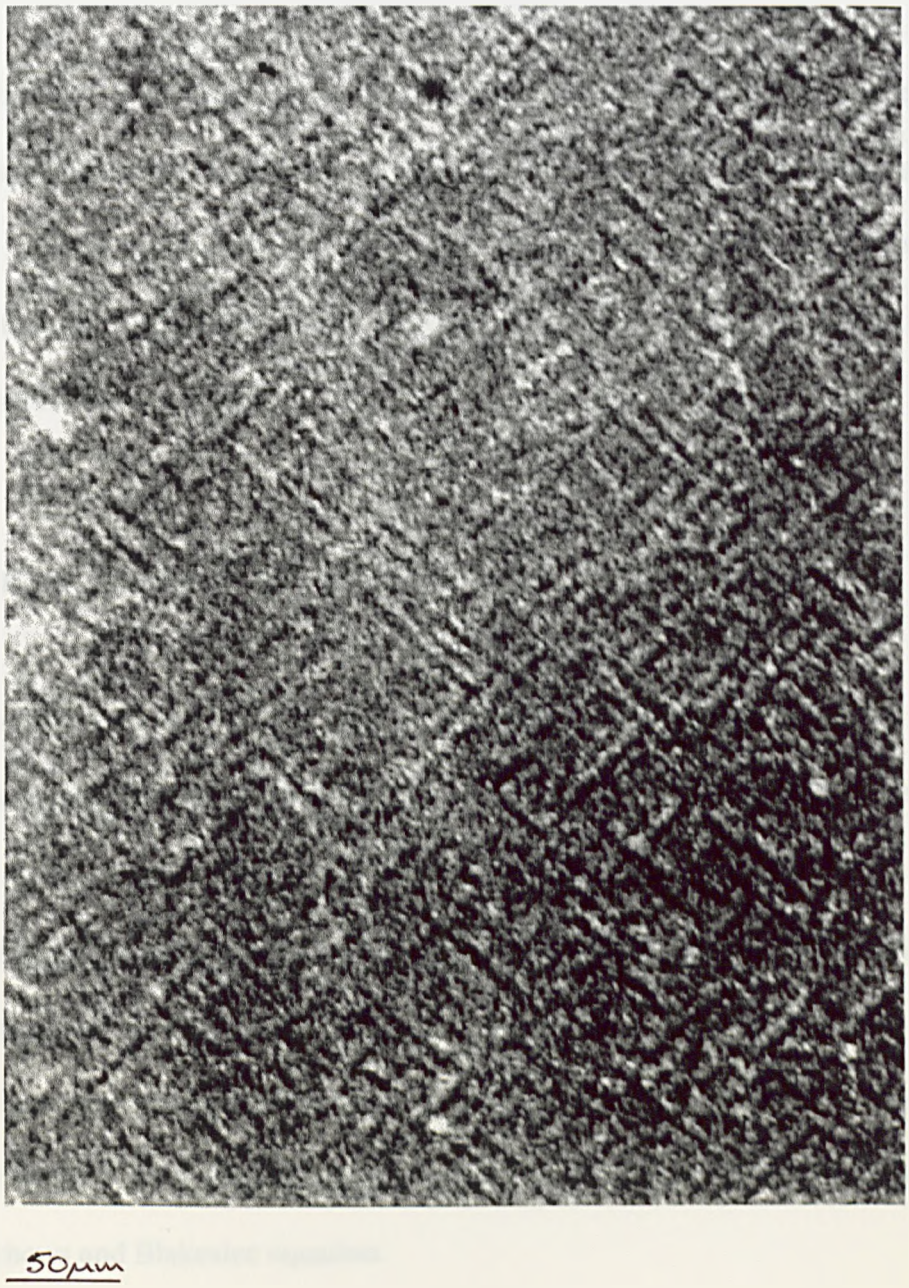

slipping of dislocations between orthogonal <110> directions as has been discussed by Guha et al[20]. The topograph obtained for the 105nm (Figure 4-7) sample shows an extensive dislocation network exhibiting even more clearly the non-<110> dislocation lines.

Although the first misfit dislocation has not been directly observed, from the XRT results obtained the critical thickness of ZnSe on GaAs has been directly measured as 100±5nm. This is much less than previously found from DCXRD and PL studies which put the critical thickness at 150 nm. The implications of this for device design are discussed in the next section.

4.5 CRITICAL THICKNESS CALCULATIONS

The most widely accepted model for the calculation of critical thickness, h_c, of a lattice mismatched overlayer is that of Matthews and Blakeslee.[21,22,23] In this model h_c is calculated as the epilayer thickness in which the force exerted by misfit stress on an existing grown-in threading dislocation equals the tension in the dislocation line (mechanical equilibrium). However, when the epilayer thickness exceeds h_c it becomes more energetically favourable for a dislocation to exist and the threading dislocation bends over producing a misfit dislocation. This leads to the simplest form of the Matthews and Blakeslee equation:

$$h_c = \frac{b}{8\pi m \cos\lambda}\left(\frac{1-\nu\cos^2\beta}{1+\nu}\right)\ln\left(\frac{4h_c}{b}\right) \qquad 5.1$$

where, b is the Burgers vector of the dislocation, m is the misfit, ν is Poisson's ratio, λ is the angle between b and the direction that is both normal to the dislocation line, l, and that lies within the plane of the interface and β is the angle between b and the

Figure 4-8: Angles commonly used to define misfit dislocations and their Burgers vectors

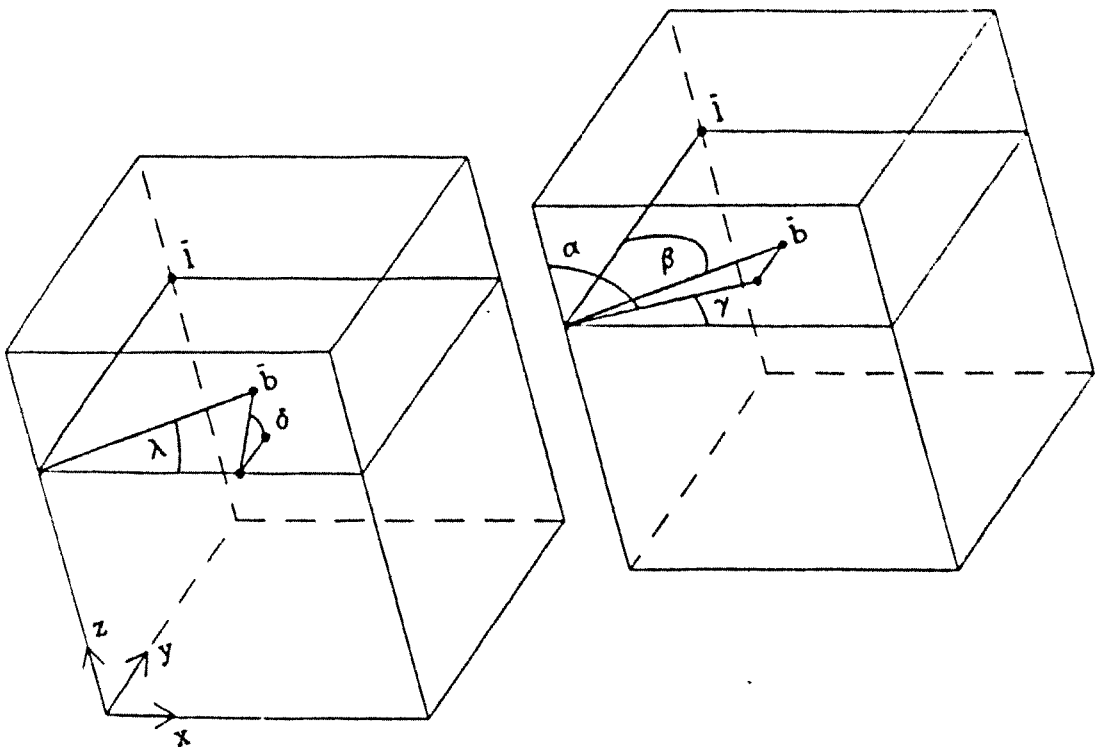

dislocation line (as shown in Figure 4-8). For a FCC or ZB structure the misfit dislocation is predominantly of the 60° type and $\lambda = \beta = 60°$. Using the material parameters defined in Table 3.1 for the II-VI compounds and $b = a/\sqrt{2}$, the critical thickness of ZnSe on GaAs was calculated to be 49.4 nm. This is considerably lower than the experimental value obtained of 100±5nm. The reason for this is due to the assumption in the model that the misfit dislocations formed are pure edge dislocations. Unfortunately, in a real structure it is far more likely that the dislocations formed are of a mixed variety and that the energy required to form them is modified from the ideal case, but if the energy is lower then h_c will also be lower.

Although the Matthews and Blakeslee model does not provide an agreement for the measured critical thickness, it can be used to calculate the critical thickness expected for ternary layers of differing composition (misfit strain). Then normalising with respect to the known value of the ZnSe critical thickness gives an indication of the mismatch which can be tolerated in a nominally lattice matched structure before misfit dislocations are formed. For the case of ZnSSe the critical thickness versus incorporation of S is as shown in Figure 4-9, from which it can be seen that the compositional fluctuation which can be tolerated is ±2%of S. This corresponds to a critical thickness of ~200 nm which is less than the 250 nm layers of ZnSSe used in a typical SCH laser structure. Therefore, the fact that the ZnSe critical thickness is much lower than previously thought has implications for device structure design for ensuring that the active region is free from defects.

4.6 CONCLUSIONS

Through the use of X-ray double crystal topography the critical thickness of ZnSe has been directly measured for the first time to be 100±5nm, considerably less than the 150nm previously measured using XRD and PL. This has implications for the design

Figure 4-9: Estimated critical thickness of ZnSSe vs S incorporation

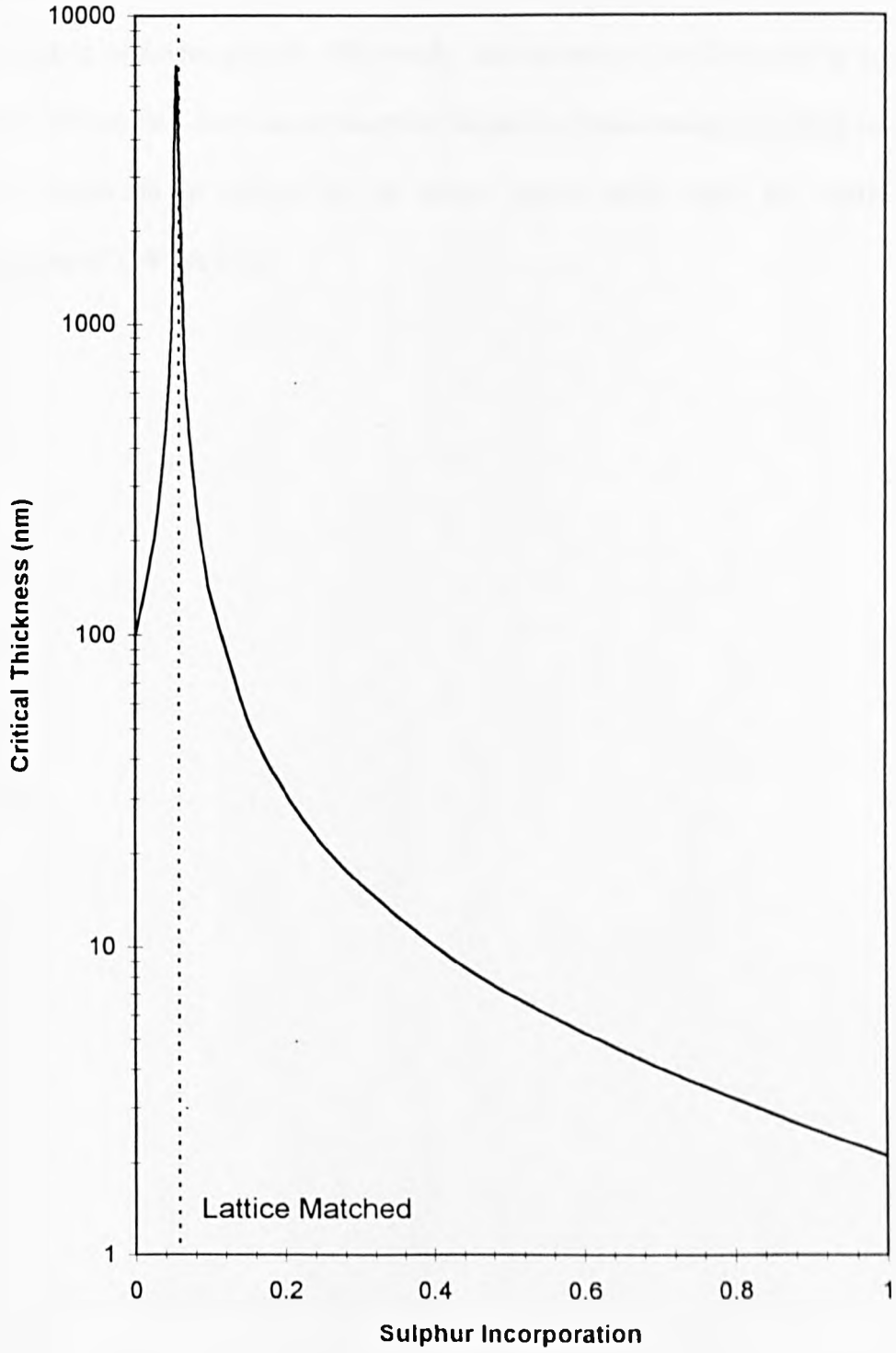

of lattice matched structures in the amount of compositional drift from lattice match which can be tolerated.

The measurement of the critical thickness of ZnCdSe, ZnSSe and ZnMgSSe for varying concentrations could be measured using DCXRT which could help to improve understanding of device growth. Ultimately, this technique could be used to image the structural defects in a laser device structure before and after lasing providing an insight into the formation of defects in the active region which limit the lifetime and performance of II-VI devices.

4.7 REFERENCES

[1] B. K. Tanner, *X-Ray Diffraction Topography*, Pergamon Press, Oxford 1976

[2] J. H. Van der Merwe, J. Appl. Phys. 34 (1962), 123

[3] D. J. Eaglesham, E. P. Kvam, D. M. Mayer, C. J. Humphreys, G. S. Green, B. K. Tanner and J. C. Bean, Appl. Phys. Lett. 53 (1988), 2083

[4] D. Hull, *Introduction to Dislocations*, Pergamon Press (1969), 86

[5] M. A. G. Halliwell, *Advances in X-ray Analysis*, Vol. 33, Plenum Press, New York, 1990

[6] U. Bonse, Direct Observations of Imperfections in Crystals, New-York: Wiley, (1962) 431

[7] M. Hart, Science Progress Oxford 56 (1968) 429

[8] K. Kohra and T. Matsushita, Semiconductor Silicon 1977, Princeton: Electrochemical Society, 441

[9] M. Sauvage, A. Authier and J. F. Petroff, Proc. Microsc. Semicond. Mater. Conf., (1981) 249

[10] I.C. Bassignana, D.A. Macquistan and D.A. Clark, Advances in X-ray Analysis, Vol. 34, Edited C.S. Barrett, Plenum Press, New York 1991

[11] G. S. Green, B. K. Tanner, S. J. Barnett, M. T. Emeny, A. D. Pitt and C. R. Whitehouse, Phil. Mag. Lett. 62 (1990), 131

[12] C. R. Whitehouse, S. J. Barnett, D. E. J. Soley, J. Quarell, S. K. Aldridge, A. G. Cullis, M. T. Emeny and A. D. Johnson, Rev. Sci. Instr. 63 (1992), 634

[13] S. J. Barnett, C. R. Whitehouse, A. M. Keir, G. F. Clark, B. F. Usher, B. K. Tanner, M. T. Emeny and A. D. Johnson, J. Phys. D (Appl. Phys.), 26 (1993), A45

[14] Advanced Crystal Growth, Ed. P. M. Dryburgh, B. Cockayne and K. G. Barraclough, Prentice Hall (1987)

[15] D. J. Stirland, Microscopy of Semiconducting Materials, Inst. Phys. Conf. Ser. 117, Eds. A. G. Cullis and N. J. Long (Inst. Phys., Bristol 1991), 327

[16] C. R. Whitehouse, A. G. Cullis, S. J. Barnett, B. F. Usher, G. F. Clark, A. M. Keir, B. K. Tanner, B. Lunn, J. C. H. Hogg, A. D. Johnson, G. Lacey, W. Spirkl, W. E. Hagston, J. H. Jefferson, P. Ashu, G. W. Smith and T. Martin, J. Cryst. Growth, 150 (1995), 85

[17] J. Petruzello, B.L. Greenberg, D.A. Cammack and R. Dalby, J. Appl. Phys. 63 (1988) 2299

[18] G.D. Brownlie, Z. Zhu, G. Horsburgh, T.A. Steele, P.J. Thomson, J.M. Wallace, K.A. Prior and B.C. Cavenett, J. Crystal Growth 159 (1996) 321

[19] J.M. Gaines, J. Petruzello and B. Greenberg, J. Appl. Phys. 73 (1993) 2835

[20] S. Guha, H. Munekata, F.K. LeGoues and L.L. Chang, Appl. Phys. Lett. 60 (1992) 3221

[21] J. W. Mathews, S. Mader and T. B. Light, J. Appl. Phys. 41 (1970), 3800

[22] J. W. Mathews and A.E. Blakeslee, J. Cryst. Growth, 27 (1974), 118

[23] J. W. Mathews, J. Vac. Sci. Technol. 12 (1975), 126

5. GROWTH OF ZnSSe AND ZnMgSSe

5.1 INTRODUCTION

In order to produce state of the art II-VI laser diodes it is necessary to grow an active region as free from defects as possible. The use of GaAs substrates in II-VI growth introduces the complication of misfit strain due to the lattice parameter mismatch (see Chapter 4) resulting in the formation of misfit dislocations.

The threading dislocations generated from these misfit dislocations propagate through the subsequent material producing defects in the active region of the device and therefore, this is a major limiting factor on the lifetime of any device fabricated from ZnSe based materials on a GaAs substrate.[1]

Although homoepitaxy is the simplest way of preventing the formation of misfit dislocations, there is another option available, which is to lattice match the epilayer to the GaAs substrate. This is achieved by alloying to reduce the ZnSe lattice parameter through the use of ZnSe based ternary and quaternary compounds. In this way the compounds can be engineered to optimise optical and electronic properties, while still remaining lattice matched to GaAs to minimise the formation of misfit dislocations. However, this introduces further variables into the growth process and the control of alloy compositions needs to be addressed. In the band diagram of Figure 5-1 the most

Figure 5-1: Bandgap vs lattice parameters of II-VI wide bandgap compounds

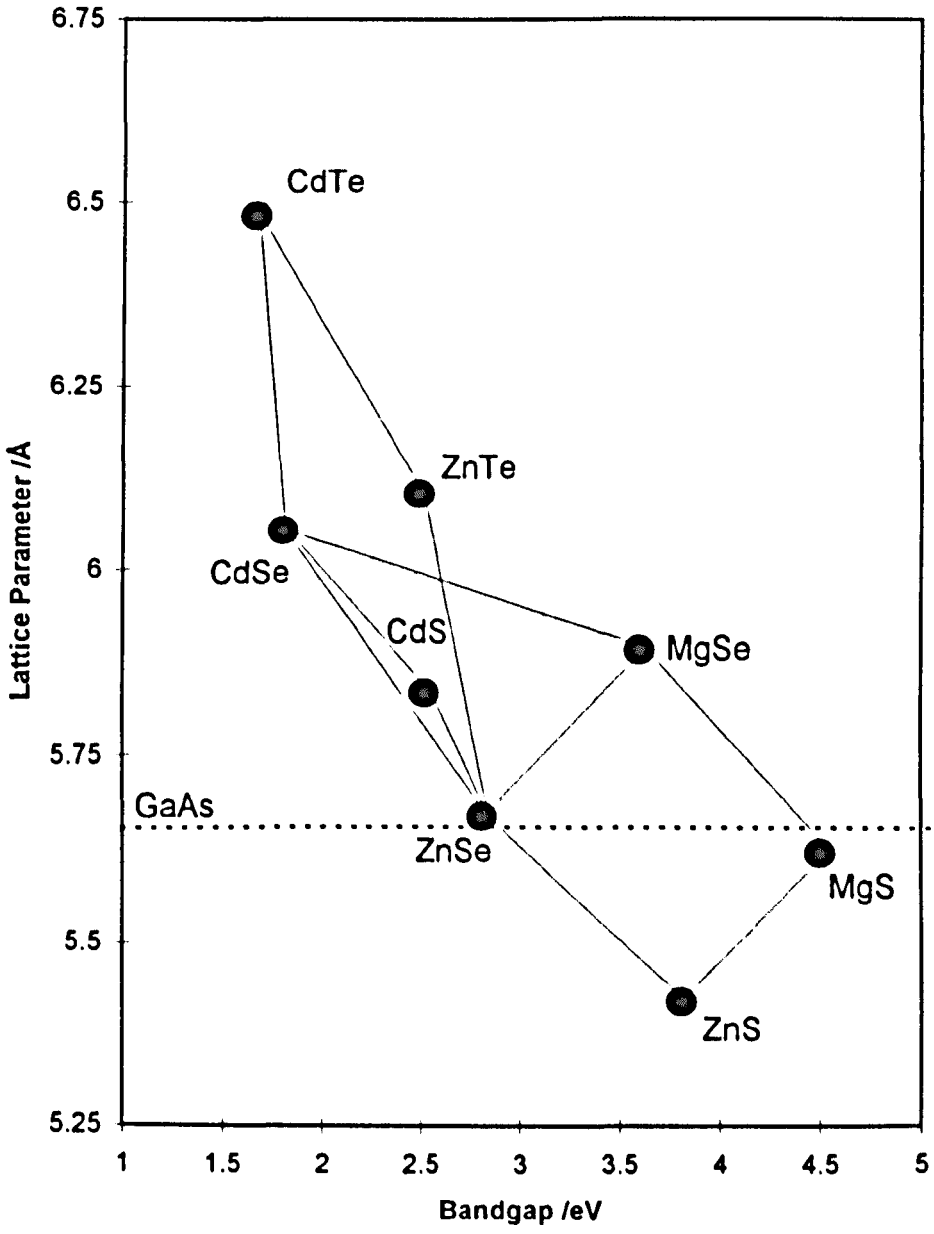

commonly used material combinations are shown. As can be seen from this, it is possible to engineer $Zn_{(1-x)}Mg_xS_ySe_{(1-y)}$ of varying composition with a lattice constant equal to GaAs. Also, for one sulphur content in $ZnS_ySe_{(1-y)}$, lattice matching is achieved. In the case of MBE $ZnS_ySe_{(1-y)}$ grown at a growth temperature of 300°C, y = 5.68%.

Another factor affecting the quality of early II-VI lasers was the absence of sufficient optical confinement between ZnSe and the active ZnCdSe quantum wells. However, the addition of magnesium into the material allows the refractive index of the material to be sufficiently increased to provide a suitable cladding layer. It is also possible to keep this layer lattice matched by using sulphur to offset the increase in lattice parameter occasioned by the use of magnesium.

For this reason the compounds $ZnS_ySe_{(1-y)}$[2,3] and $Zn_{(1-x)}Mg_xS_ySe_{(1-y)}$[4,5] are commonly used in the fabrication of lattice matched II-VI structures on GaAs substrates. However, sulphur is not an easy material to deal with for MBE purposes due to its relatively low melting point of 120°C[6] and its high vapour pressure. A compound source of zinc sulphide is the most common source of sulphur in II-VI MBE, although elemental sulphur has been used in cracker cells.[7] Magnesium, on the other hand rapidly oxidises with H_2O or O_2 to form $Mg(OH)_2$ and MgO, respectively. Therefore, magnesium is supplied in sealed glass ampoules to prevent reaction in atmosphere and must be loaded into the chamber in a controlled atmosphere and then baked thoroughly to remove any water.

In this chapter the growth of lattice matched ZnSSe and ZnMgSSe with the required properties for use in II-VI devices is described. Also some of the problems associated

with the growth of these materials and their subsequent incorporation in device structures is discussed.

5.2 MEASUREMENT OF TERNARY AND QUATERNARY COMPOUND COMPOSITIONS

In order for any alloy to be used in a device structure, the relative composition of the constituent elements must be tightly controlled. The two main considerations to achieve this are as follows:

i) How are the beam pressures controlled ?

ii) How are the compositions reliably measured ?

Beam pressure control is achieved using a combination of growth calibrations, flux measurements and precise temperature control of the source cells.

Measurement of the resultant compositions of the compounds poses another problem. This is due to the fact that no one technique can definitively measure the alloy compositions due to the approximations which have to be made. The techniques routinely used in this study included x-ray diffraction, photoluminescence spectroscopy and energy dispersive x-ray spectroscopy. However, in the case of the measurement of ternary compound materials (see Section 3.5) the problem is considerably less complex than for quaternary compounds.

5.2.1 Quaternary Compounds

Unfortunately, the measurement of quaternary compounds is not so straightforward. The reason for this becomes clear on considering the band diagram for $Zn_{(1-x)}Mg_xS_ySe_{(1-y)}$ of Figure 5-2 which shows that the same lattice parameter can be obtained from a range of compositions. In the case of quaternary compounds it is not possible to directly determine the composition from the X-ray diffraction curves themselves as there are two unknowns: the Mg, (x) and S, (y) compositions. However, when measured in conjunction with PL it is possible to determine x and y, provided that the relationship between the band edge emission, lattice parameter and composition is known (as shown in Figure 5-3).[4] In order to directly measure the composition another technique must be employed, in this case energy dispersive x-ray spectroscopy, (EDX). This technique, provided the necessary calibration standards are available, allows the direct measurement of the compositions, however for this study EDX was not routinely available.

Fortunately the absolute measurement of the compositions is not essential as the only parameters that are of interest from a growth point of view are the lattice parameter and the bandgap of the quaternary. As long as the alloy is lattice matched and of sufficient bandgap the quaternary is suitably optimised for device fabrication, provided the cell fluxes and substrate temperature are repeatable. Examples of ZnSSe and ZnMgSSe layers grown during this research are shown later in this chapter. Therefore, by using a combination of XRD and PL the growth conditions can be continually evaluated to ensure that compositions stay constant as the source fluxes change (as the material in the cell is depleted).

Figure 5-2: ZnMgSSe lattice parameter vs composition

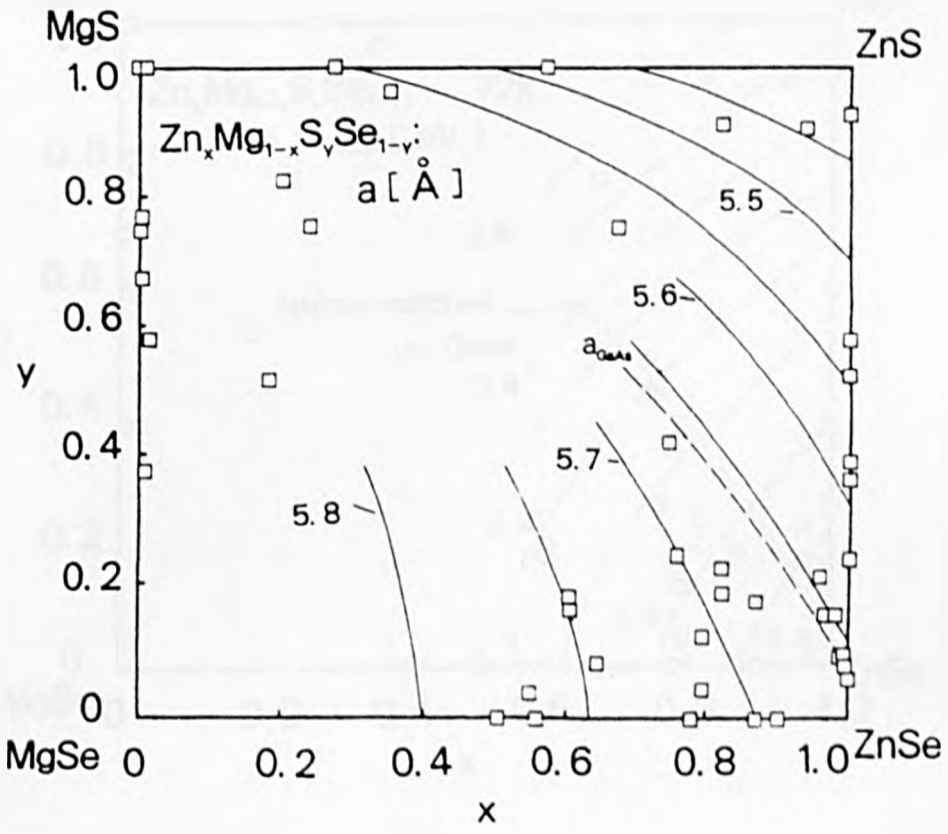

(from Ref. 4)

Figure 5-3: Relationship between band edge and lattice parameter

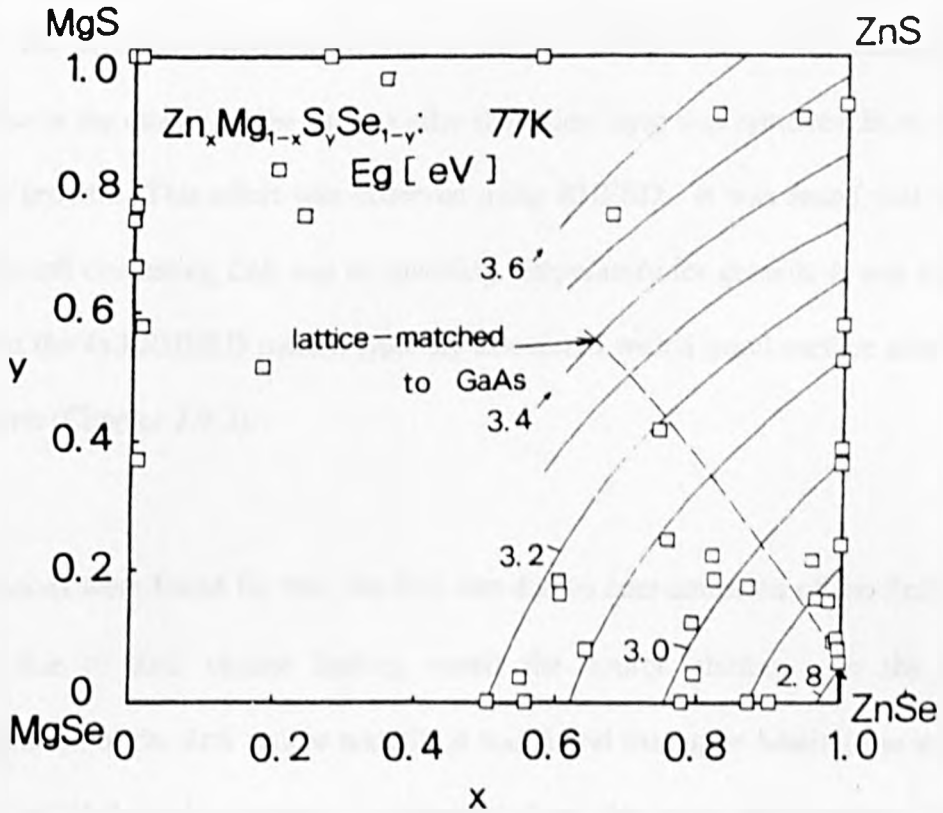

(from Ref. 4)

5.3 PROBLEMS ASSOCIATED WITH THE USE OF ZnS IN MBE

5.3.1 Effect on thermal desorption of Oxide on GaAs Substrates

One of the problems encountered due to the use of ZnS in a II-VI chamber was a reduction in the quality of the surface after the oxide layer was removed from the GaAs prior to growth. This effect was observed using RHEED. It was found that when the Knudsen cell containing ZnS was at operating temperature for growth, it was impossible to obtain the 4x3 RHEED pattern typically associated with a good surface after thermal desorption (Chapter 2.9.2).

Two reasons were found for this; the first was due to contamination of the ZnS; and the second due to ZnS vapour leaking round the source shutter. In the case of contamination of the ZnS source material it was found that upon heating the source the pressure of H_2S in the system, as measured from the mass spectrometer, increased proportionately as can be seen in Figure 5-4. The reaction between the H_2S and the GaAs results in the formation of Ga_2S_3. This effect was also observed by other II-VI groups.[7,8] The solution to this problem is of course to install uncontaminated ZnS. Unfortunately, this did not solve the whole problem of degradation of the GaAs surface after thermal oxide desorption when the ZnS cell was at operating temperature.

The ZnS operates at a temperature in the region of 750°C, about 350°C hotter than the other sources. This elevated temperature appears to cause a substantial increase in chamber pressure as this cell is first heated, despite an extensive degas after bakeout.

Figure 5-4: Hydrogen sulfide partial pressure vs ZnS cell temperature

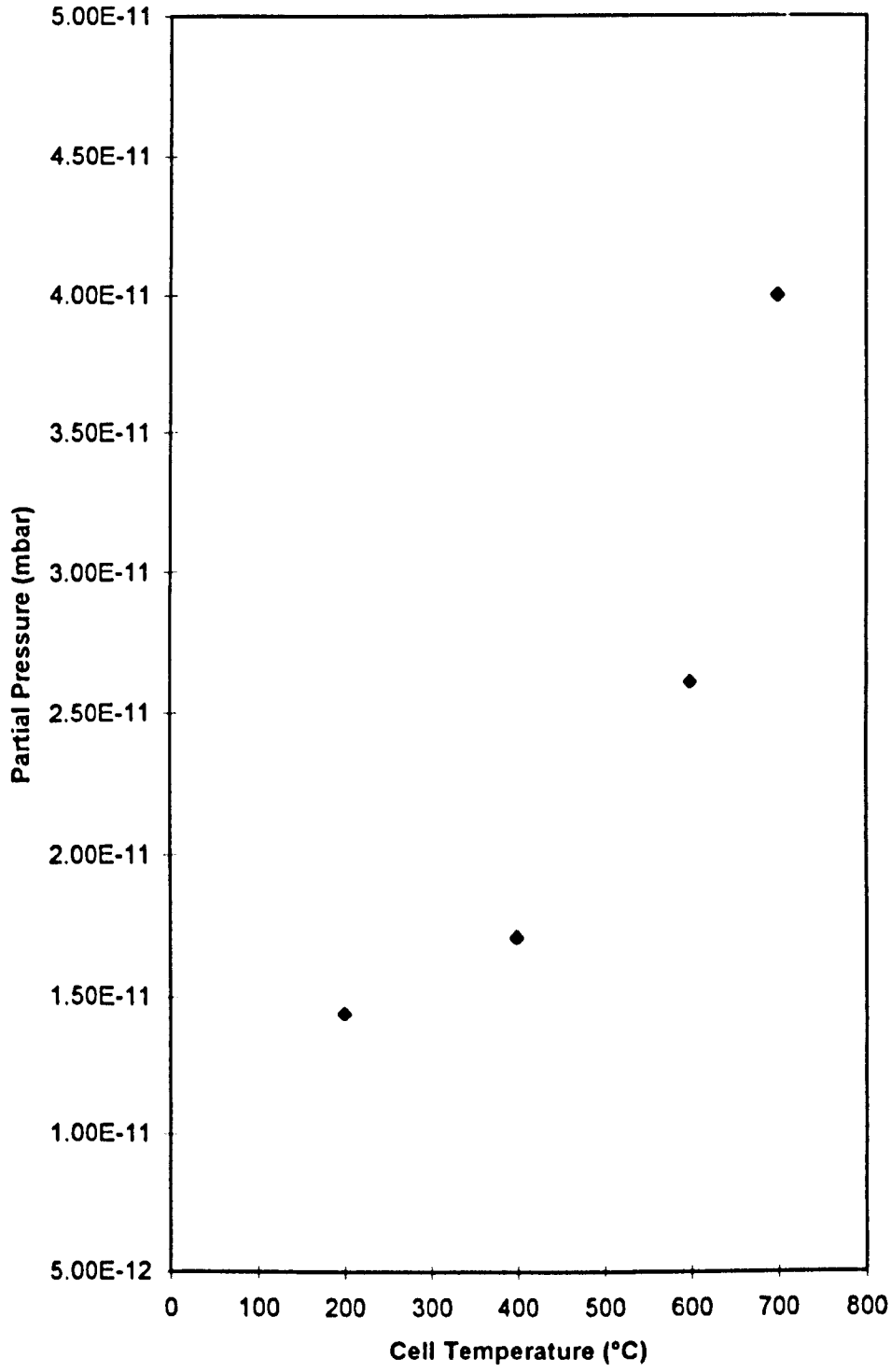

This was attributed to the evaporation of material deposited around the cell during previous growths not requiring sulphur, particularly material deposited on the baffles between the cells. The baffles are plates of molybdenum bolted to the cryoshield, but without independent liquid nitrogen cooling, therefore as the cells warm up so do the baffles. Unfortunately this is unavoidable as it is not possible to leave the ZnS cell at an idling temperature above 200°C for any length of time, to prevent deposition on the baffles, as the thermal stress on the cryogenic shielding without coolant would be substantial.

5.3.2 Pyrometer readings

As a consequence of the ZnS cell being so hot, there is an increased heat load on the substrate due to radiated heat from the front of the cell. This effect is measurable using an optical pyrometer and results in an increase in the measured substrate temperature of about 12°C after the ZnS shutter is first opened. Such behaviour requires that some form of compensation technique be employed to maintain a stable growth temperature during the initial growth period. This effect is highly undesirable as in order to grow the best quality material careful control of the ratio of reactant species on the growth surface is required and temperature fluctuations of this order will alter that ratio The methods which were employed to overcome these problems are discussed in Section 5.4.

5.4 GROWTH OF ZnSSe AND ZnMgSSe

5.4.1 First approach

As described above, one of the problems encountered was the temperature loading effect of the ZnS cell on the substrate after opening of the ZnS shutter. Also the RHEED pattern after thermal desorption of the oxide layer was indicative of a poor quality surface showing a spotty 2x1 pattern as described in Chapter 2.9. Obviously this was not desirable as even before the subsequent layer was grown the surface morphology was poor, so in order to compensate for these problems the following approach was initially adopted. The ZnS cell was held 100°C below its operating temperature at the start of growth as at this temperature the material being evaporated from the cell would be minimal. This was indeed found to be the case.

It had previously been reported by Möller[9], that in order to obtain good quality ZnSSe a 100-200Å buffer of ZnSe was required. As the thickness of this buffer layer was well below the critical thickness of ZnSe on GaAs this layer would be pseudomorphic. The cooling down of the substrate after thermal desorption and subsequent growth of this buffer layer provided a suitable time for the heating of the ZnS cell to its operating temperature. In this way a streaky 2x1 RHEED pattern was obtained after thermal desorption. However, the effect on the beam flux due to rapid temperature changes of the cell would in itself affect the sulphur composition, causing oscillations in the cell temperature. These oscillations die out as the cell temperature stabilises to its set-point over the period of 5-10 minutes allowing overall material quality to be improved.

There still remained the heating effect of the ZnS cell upon the substrate after the shutter was opened. As this was purely due to the ZnS cell's high operating temperature, it was thought that by using a dummy heat load this effect could be compensated. A cell port next to the ZnS cell port was fitted with another Knudsen-cell, which contained only an empty PBN crucible. Once it had been fully degassed, this dummy cell was heated to the same temperature as the ZnS source. The shutter for this cell was kept open during the cooling down period after the thermal desorption and while the substrate was allowed to settle at growth temperature. A buffer layer of ZnSe was then grown before the ZnS shutter was opened in conjunction with the dummy cell shutter being closed allowing the heat load on the substrate to be kept constant. This did indeed work and allowed a stable substrate temperature to be maintained at the start of growth, one of the most critical periods of the overall structure.

Lattice matched material was achieved by an iterative process which involved growing many layers and measuring their lattice parameter using x-ray diffraction and photoluminescence. Throughout these growths the beam pressure ratio VI:II was maintained at approximately unity corresponding to mixed 2x1 and c(2x2) RHEED patterns.

5.4.2 Results of samples grown using this method

A number of samples were grown using this method in order to determine the conditions for lattice matched ZnSSe and ZnMgSSe with a growth rate of approximately 0.5 μm/hr.

The best quality ZnSSe sample grown using this method (HWA 610) was lattice matched with a DCXRD peak FWHM of ~70 arcsecs as shown in Figure 5-5. The PL from this

Figure 5-5: XRD of HWA 610 ZnSSe

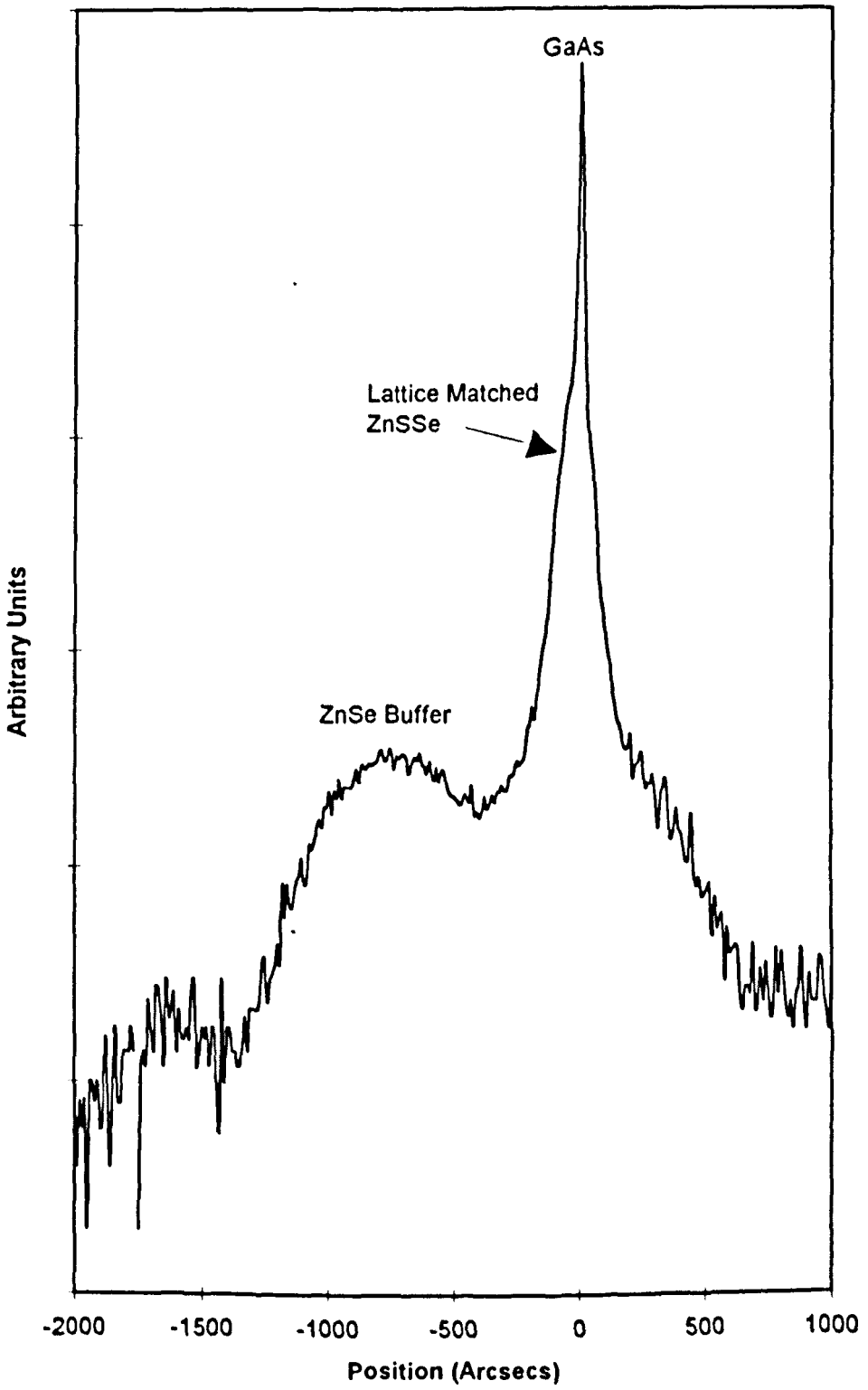

sample is shown in Figure 5-6 where the dominant feature is ascribed to the I_2 donor bound exciton and the peak on the lower energy side is due to donor-acceptor emission. In the case of ZnMgSSe, the best lattice matched sample grown was HWA 646. This sample had a DCXRD peak with FWHM of 100 arcsecs as shown in Figure 5-7. It can be seen from the PL shown in Figure 5-8 that in comparison to the PL from HWA 610, the exciton emission is now at a higher energy position indicative of the Mg incorporation in the layer. Both layers were ~0.5μm thick. In the XRD of HWA 646 the peak at ~ 500 secs is from a ZnSSe layer grown with the same ZnS flux as that used for the ZnMgSSe layer and corresponds to a S incorporation of ~11%.

5.4.3 Improved Method of Temperature Compensation

One of the major drawbacks of the first approach was the need to use a cell port for the dummy cell. This was not an ideal situation as the availability of cell ports is one of the ultimate limitations of any MBE system. Also, the rapid temperature adjustment made at the start of growth, as mentioned above, had an unknown effect on the ZnS flux and subsequently on the composition. Therefore, it was necessary to investigate another approach.

A liquid nitrogen cooled shutter was installed in front of the ZnS cell (Figure 5-9). The collar on this shutter acts as a cryogenic trap for volatile species emanating from the ZnS source at operating temperature. In this way it was now possible to stabilise the ZnS source at growth temperature prior to the start of growth and still be able to achieve a good 4x3 RHEED reconstruction. Obviously this removed the problem of flux transients from the ZnS source.

Figure 5-6: PL of HWA 610 ZnSSe

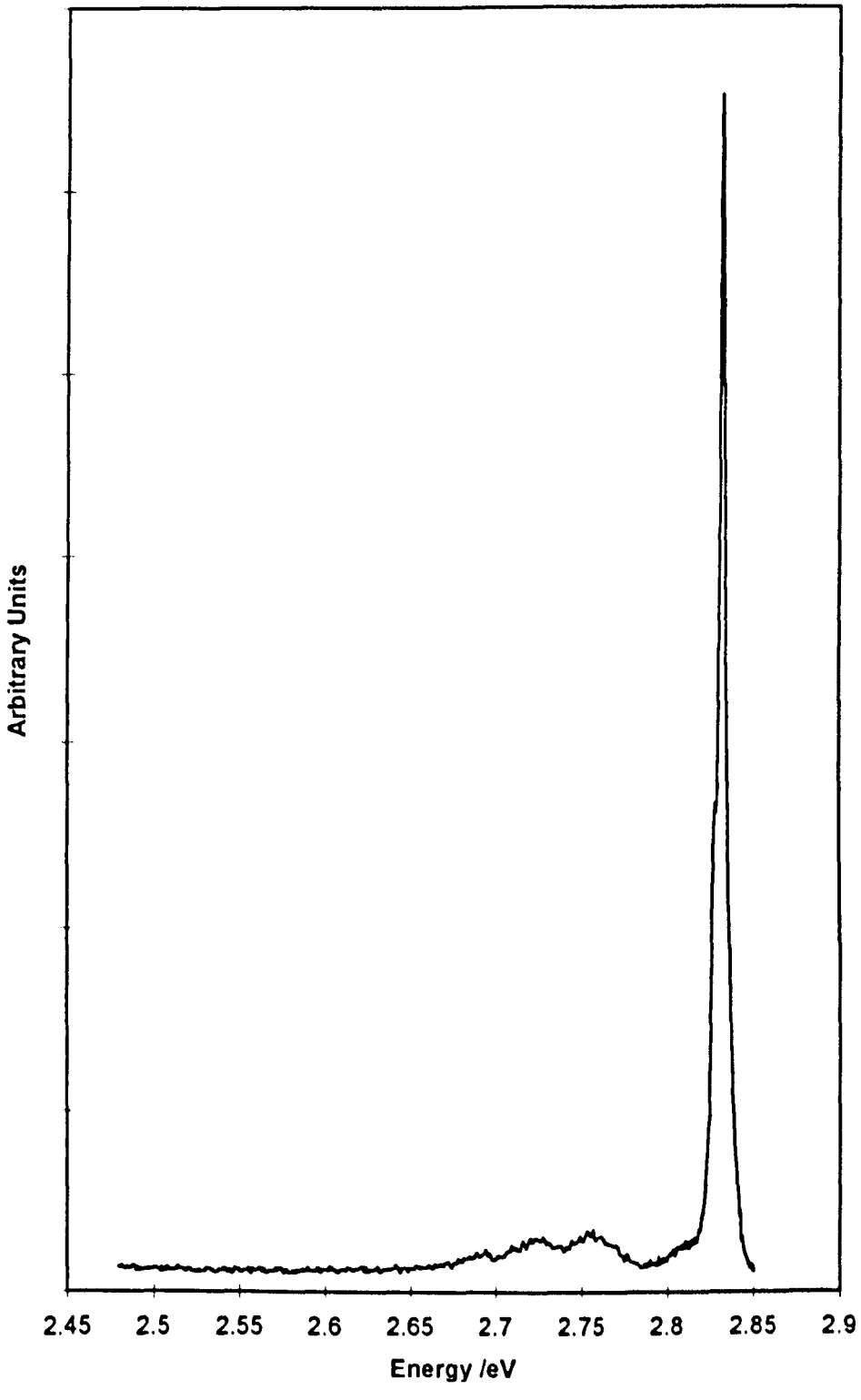

Figure 5-7: DCXRD of HWA 646

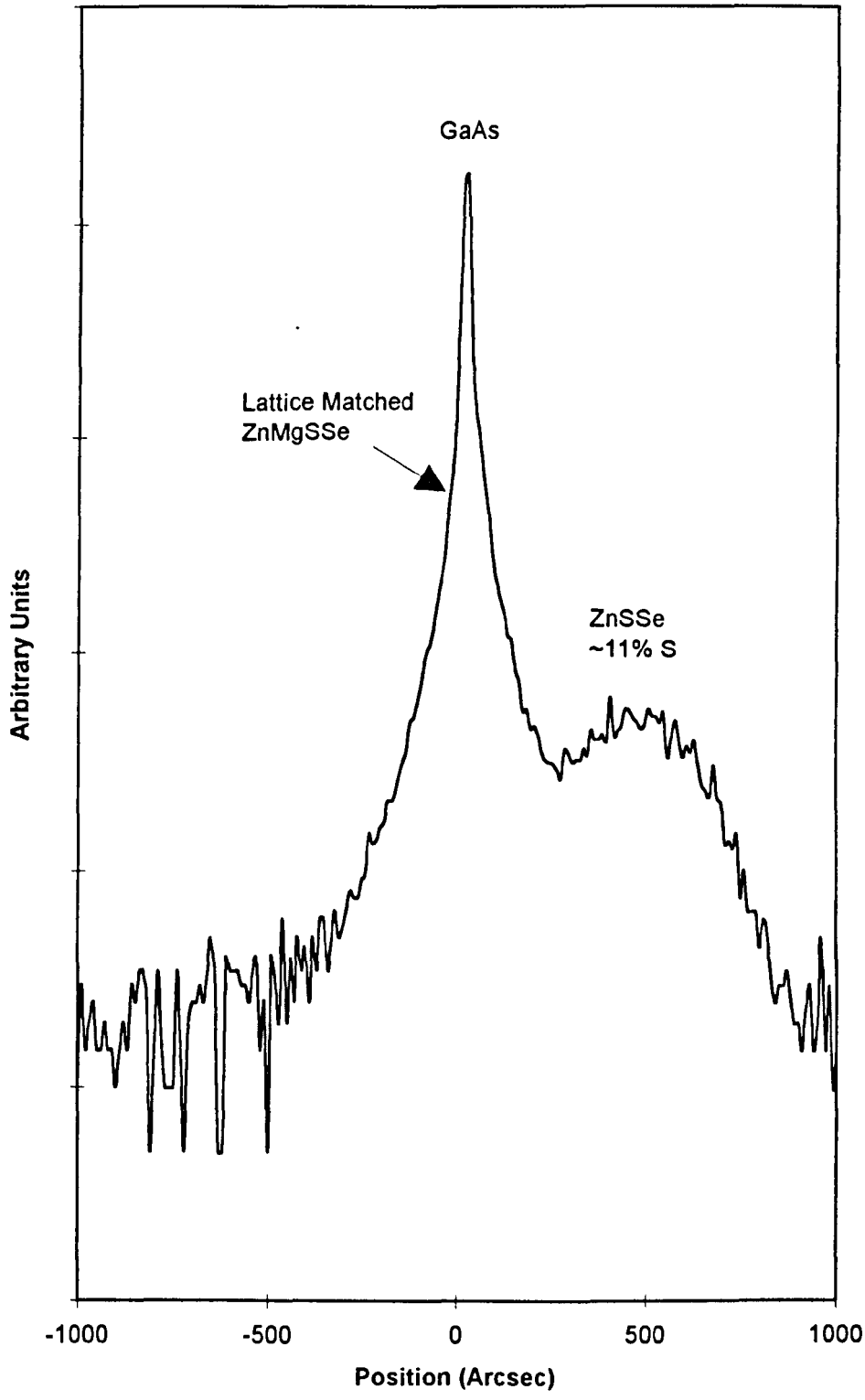

Figure 5-8: PL of HWA 646

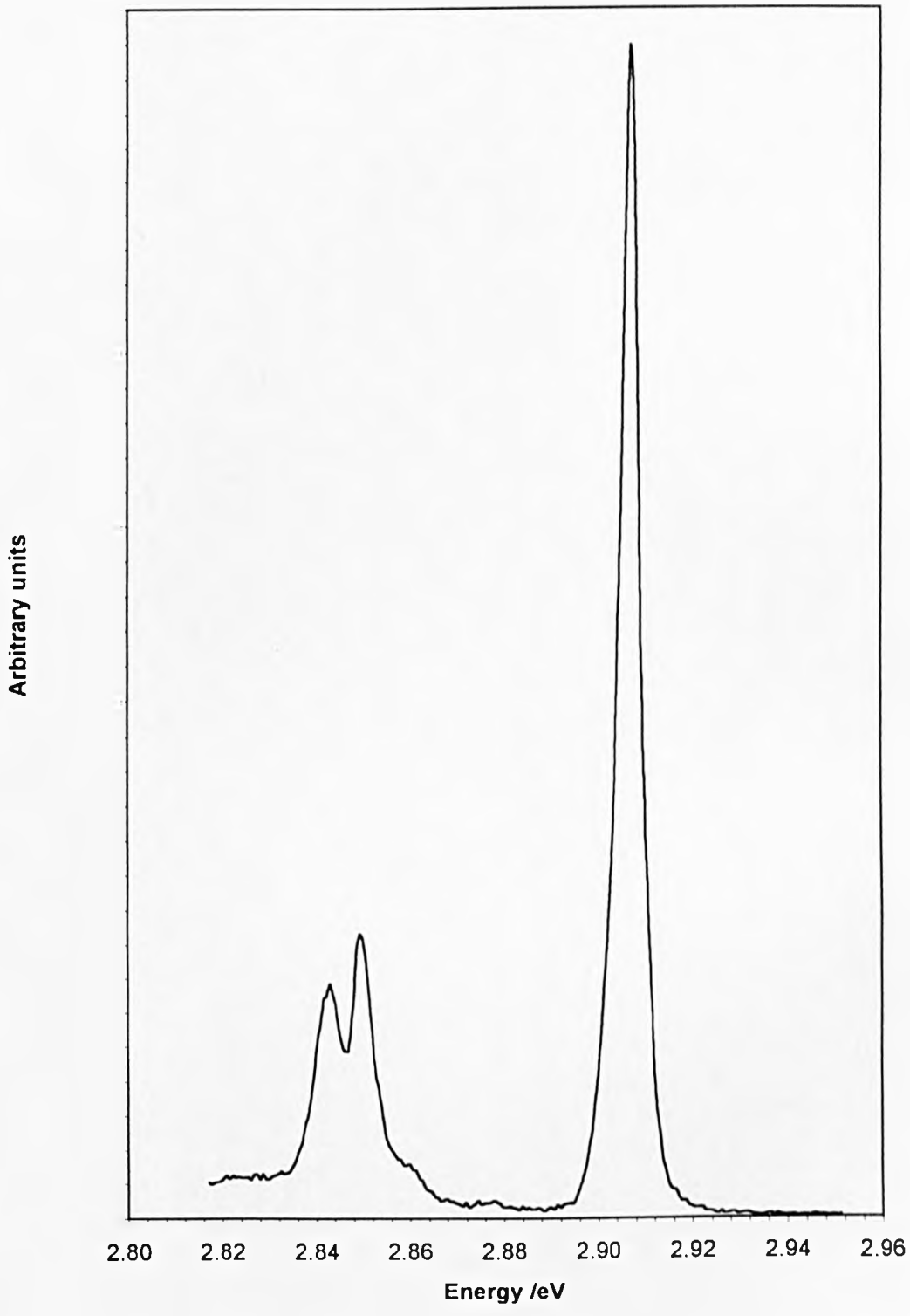

Figure 5-9: LN_2 Cooled Shutter

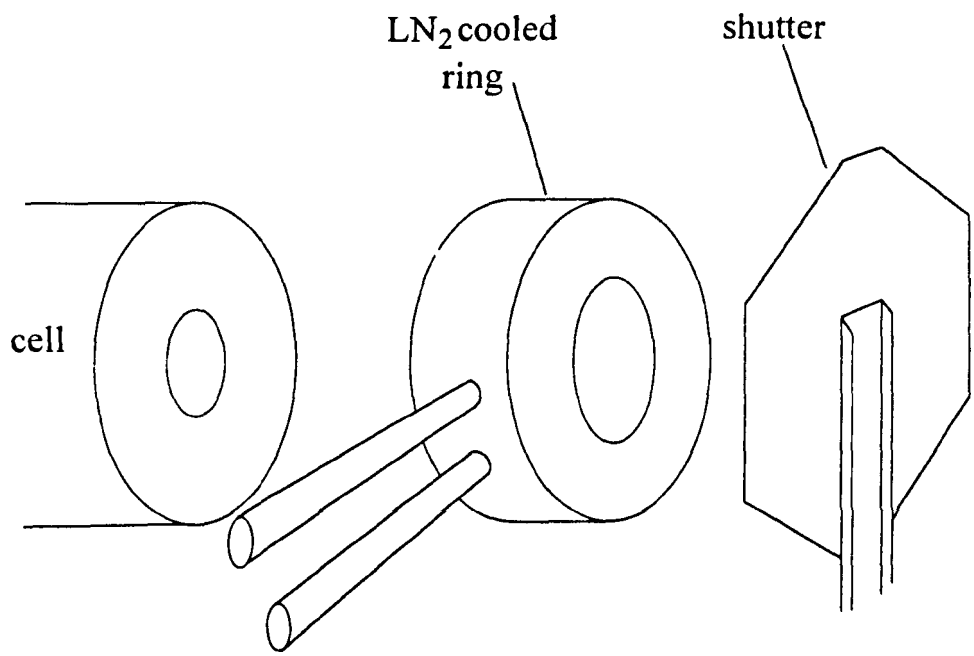

It was now noticed that although the heat clean produced a good 4x3 reconstruction, the RHEED pattern degenerated to a spotty 2x1 pattern on cool down to growth temperature. This was indicative of some sort of chemical reaction with the GaAs surface resulting in a roughening of the surface morphology. This affect had been reported by Kolodziejczyk[10] in a study of growth on GaAs epilayers. In this work it had been shown that the formation of intermediate compounds, such as Ga_2Se_3, was inhibited by cooling the sample under a zinc flux to stabilise the surface. This surface treatment prevents any further chemical reactions prior to growth. Therefore, after the 4x3 reconstruction was obtained after thermal desorption of the oxide layer, the Zn shutter was opened. The Zn flux used was the same as that normally used for growth, corresponding to a growth rate of 0.5 μm/hour. This allowed the RHEED pattern to remain a streaky 4x3 pattern during the cool down from thermal desorption temperature to growth temperature indicating a far better surface.

5.4.4 Results of Epilayers of ZnSSe and ZnMgSSe Grown using the Second Approach

In order to remove the need for a dummy cell to provide temperature compensation it was necessary to confirm that lowering the substrate temperature on opening the ZnS cell would produce material of the same quality as that previously grown. A comparison of this and the previous method was achieved by growing two thin ZnMgSSe samples in succession. The growth conditions for ZnMgSSe had already been found as described in Section 5.4.2. In order that the material structure could be compared, the two samples were thin enough that thickness fringes would be apparent on the x-ray diffraction rocking curves as the observation of these fringes is indicative of good quality material.

The samples were grown consecutively on the same day on GaAs (100) substrates with a 100Å buffer layer of ZnSe grown prior to the growth of a 1500Å layer of ZnMgSSe. Growth of the first sample, (HWA 682), was halted after the ZnSe layer and the substrate temperature stabilised under a Se flux at 280°C, measured by pyrometer with the dummy cell heat load incident on the substrate. Once this had been achieved, the ZnS shutter was opened and the empty cell shutter closed simultaneously. The Zn and Mg shutters were also opened, commencing growth of ZnMgSSe. The second sample, (HWA 683), was identical except that the substrate temperature was stabilised at 280°C prior to the ZnSe layer and there was no pause between this and the ZnMgSSe layer. Instead of compensating the substrate temperature with the empty cell, the substrate temperature controller was reduced by 14°C upon opening the ZnS and Mg shutters. The pyrometer temperature remained stable at 280°C. Both samples exhibited similar RHEED patterns during growth, mixed 2x1 and c(2x2) but HWA 683 had sharper RHEED diffraction features than HWA 682.

Both samples exhibited thickness fringes on the rocking curves as shown in Figure 5-10. Therefore, from these results it was apparent that the dummy heat load was no longer required in order to grow good quality ZnMgSSe. This allowed the possibility of using the empty cell position for another source material.

The next test of this method for compensating for the substrate temperature increase due to the ZnS cell was to grow good quality lattice matched ZnSSe. Growth conditions found to give the best quality ZnSSe using the previous growth method were used as a starting point for the optimisation of growth using the second temperature compensation method. To this end, the measured beam fluxes of Zn and Se were kept constant and

Figure 5-10: DCXRD of HWA 682 and HWA 683

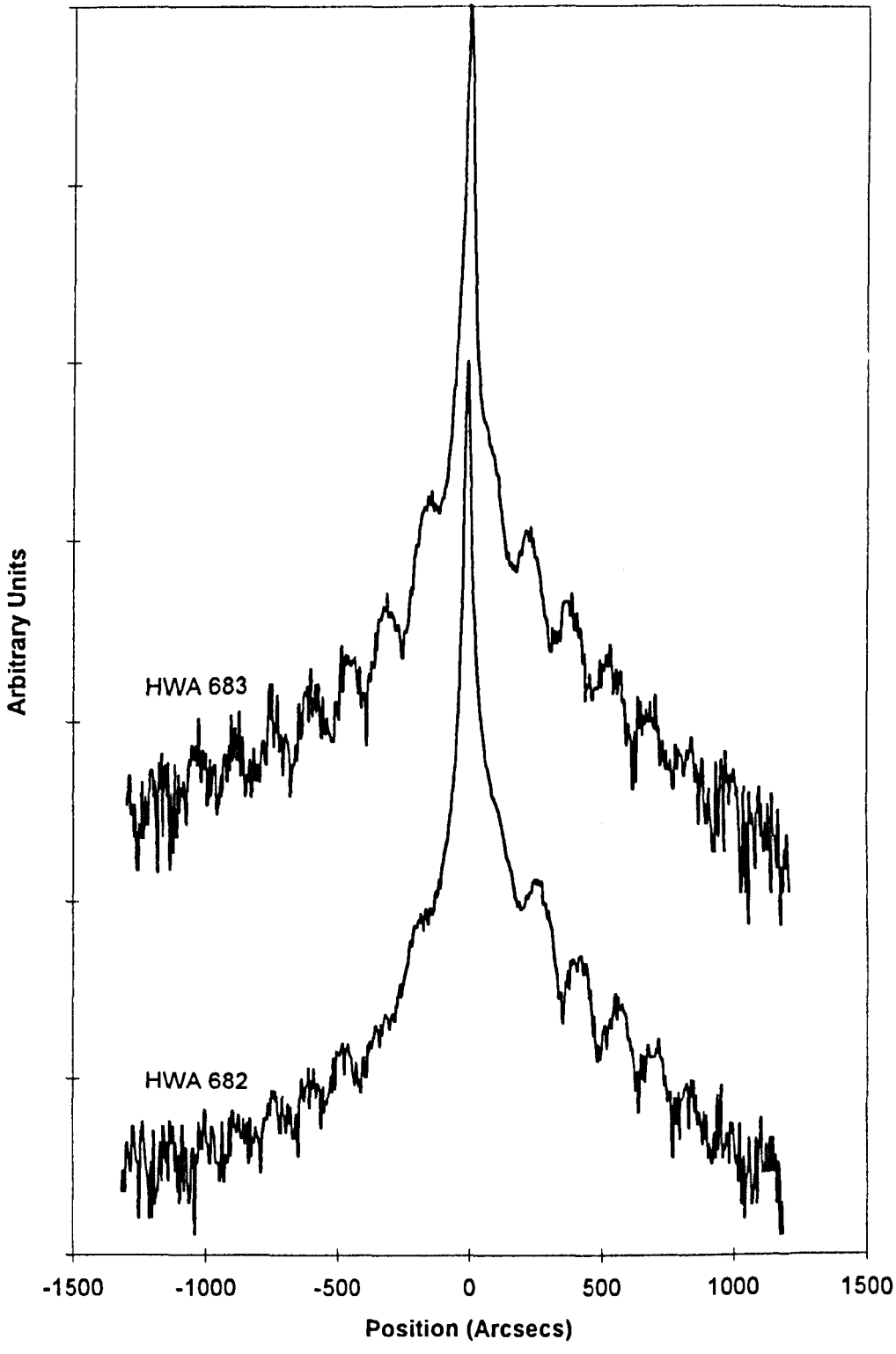

only the ZnS flux was varied, in this fashion the sample set shown in table 5.1 was grown. The target growth rate was in the range of 0.5μm per hour.

Table 5.1: ZnSSe samples grown to find lattice matched conditions

SAMPLE NUMBER	ZnS MEASURED FLUX	THICKNESS (μm)	INCORPORATED S % XRD
HWA 757	9.8	0.53	3.0
HWA 758	13.0	0.54	4.8
HWA 759	18.1	0.59	7.8
HWA 761	14.8	0.53	6.9
HWA 762	16.0	0.54	7.6
HWA 793	30.0	0.51	19.5
HWA 794	10.0	0.55	4.1

The sulphur composition was measured using double crystal x-ray diffraction. A graph of measured ZnS flux versus sulphur incorporation in ZnSSe was plotted and a line of best fit, through the origin, was calculated as in Figure 5-11. It is known that sulphur incorporation is linear with respect to the flux ratio P_{ZnS}/P_{se} up to a S composition of 35%.[11] Therefore, from this figure the flux of ZnS required for lattice matching ZnSSe to GaAs can easily be found, provided that the Se flux is kept constant.

HWA 796 was grown using the conditions found above at a temperature of 300°C (pyrometer reading). This sample was the best lattice matched ZnSSe grown with both excellent PL (Figure 5-12) and XRD (Figure 5-13) spectra. The XRD spectra shows clear thickness fringes indicative of high quality material with long range order. The angular separation between these thickness fringes is 33.33 arcsecs and using Equation 3.6 the thickness of the sample can be calculated to be 0.57μm.

Figure 5-11: Sulphur Incorporation vs ZnS Flux

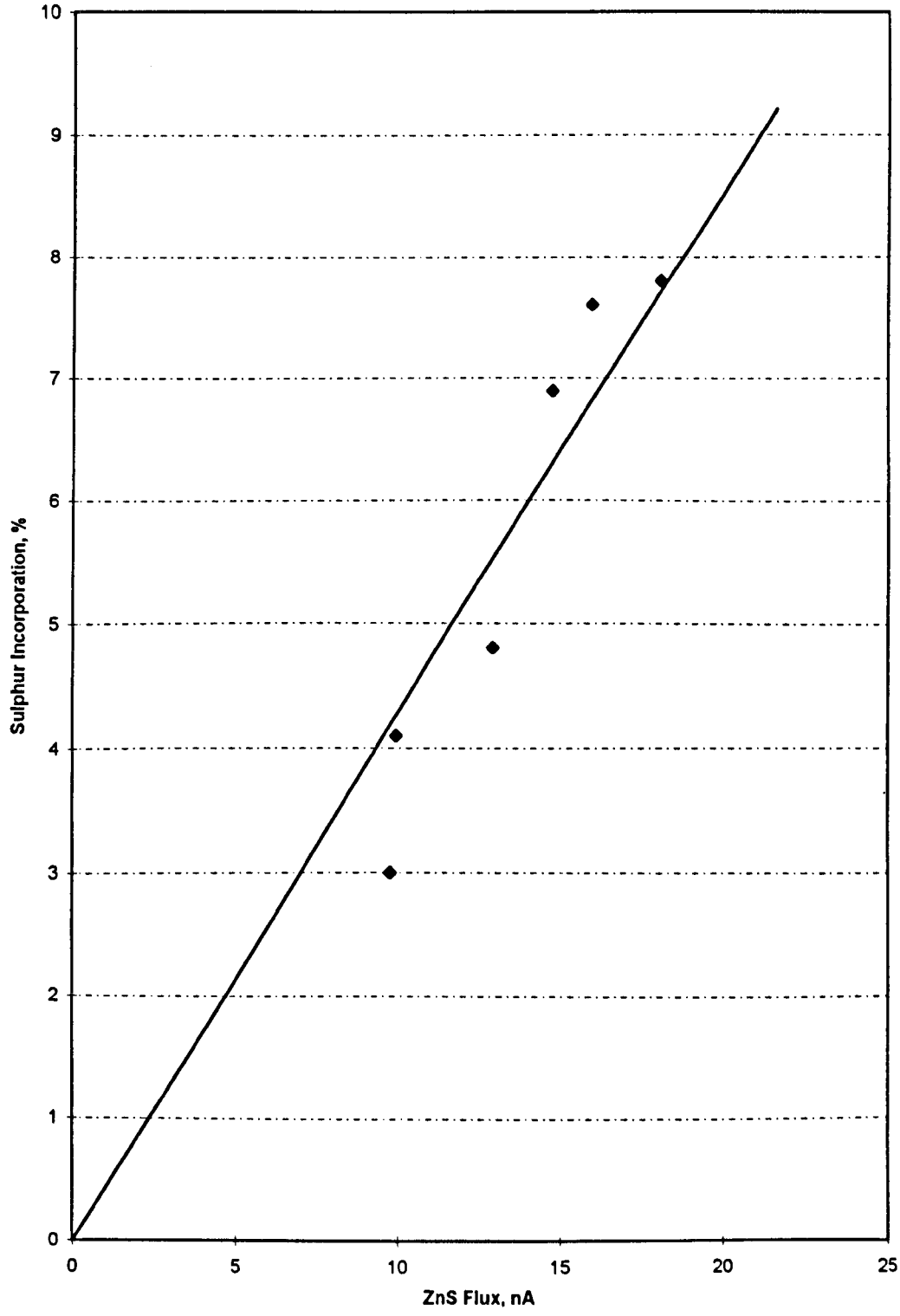

Figure 5-12: DCXRD of HWA 796 ZnSSe

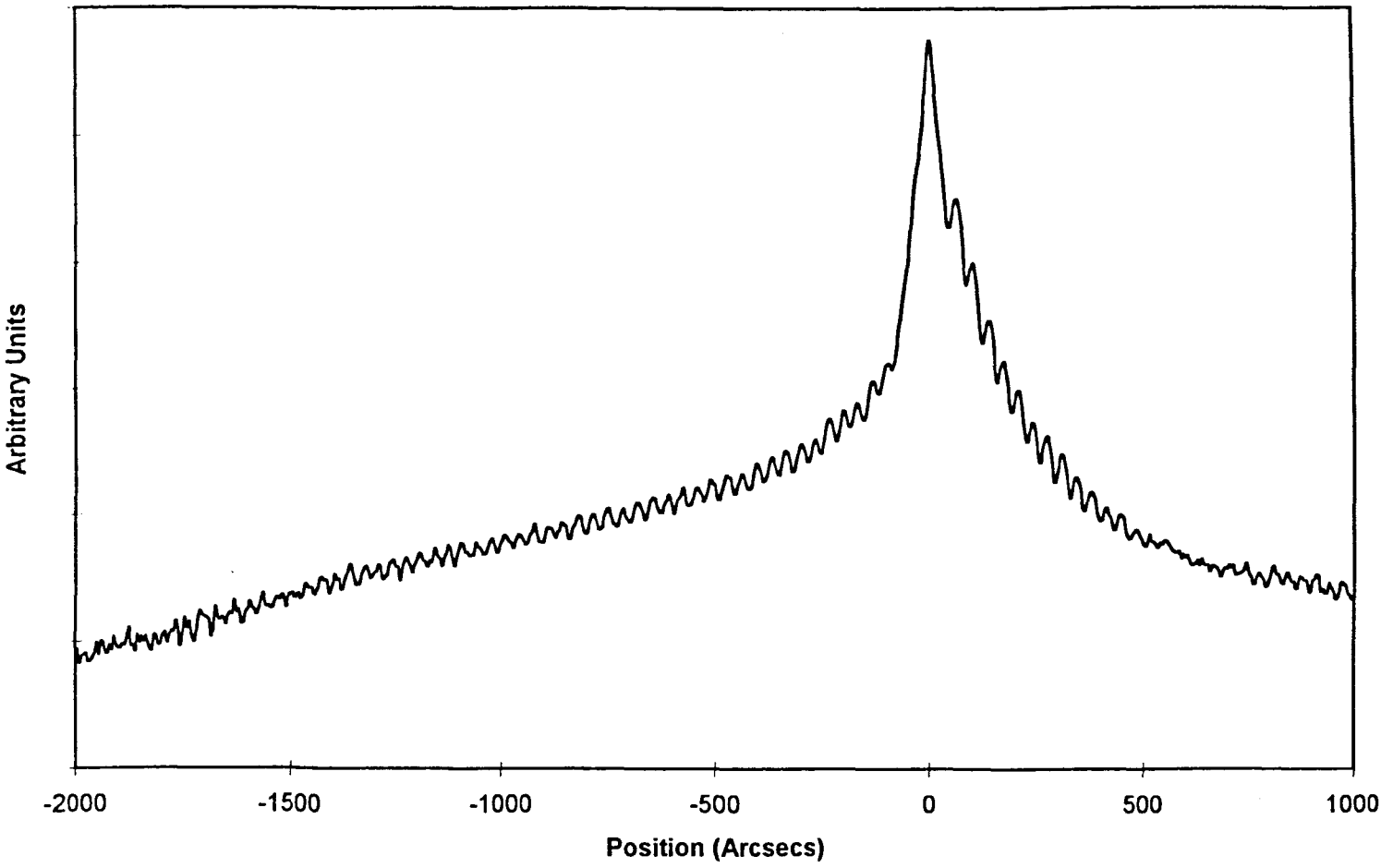

Figure 5-13: PL of HWA 796 ZnSSe

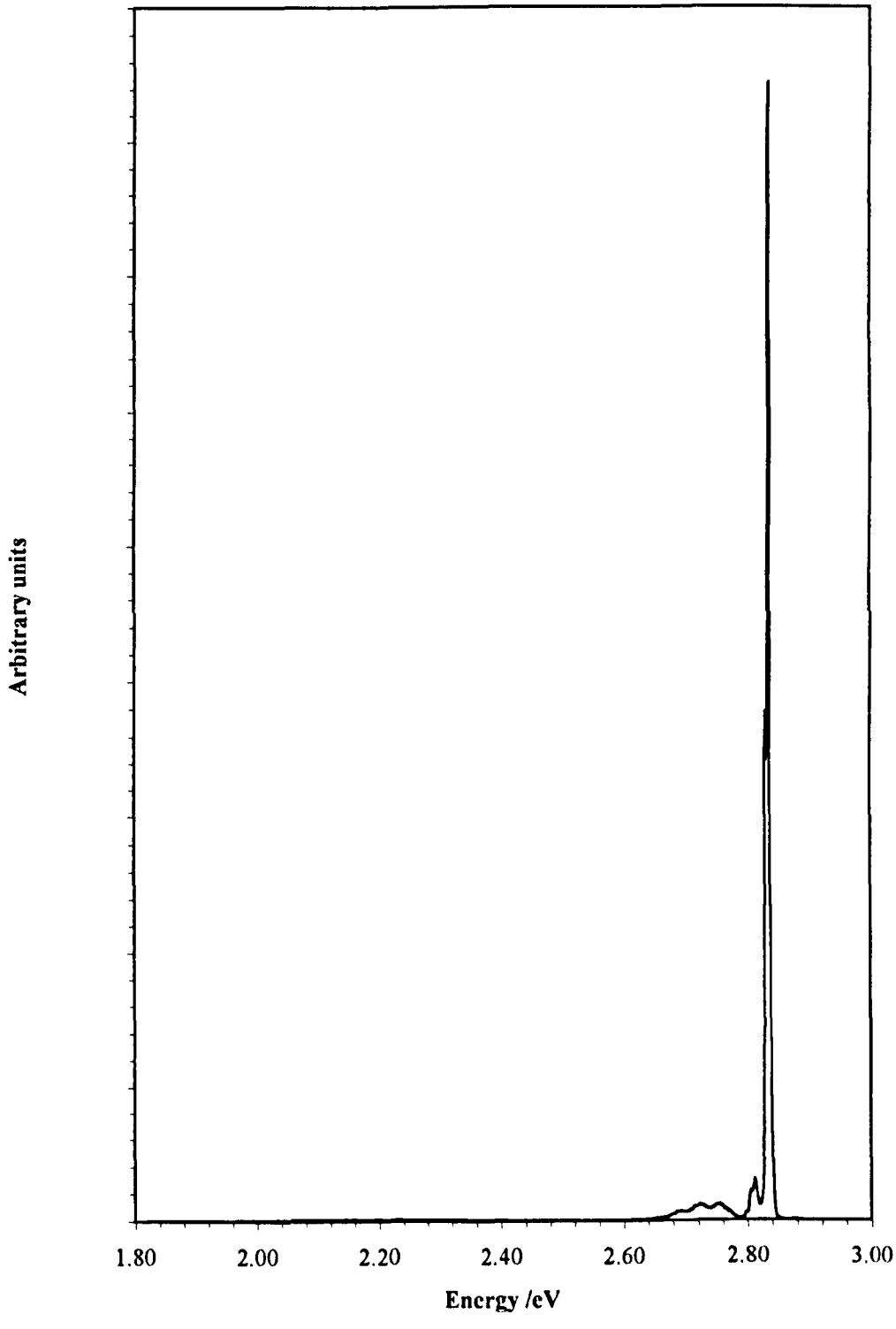

From the PL spectra it can be seen that the layer is of good quality with strong exciton emission at a peak position of 2.831eV.

It can be seen from this sample that it was now possible to grow good quality lattice matched ZnSSe. For an operating device, ZnSSe is only part of the requirement and it was now necessary to develop the lattice matched ZnMgSSe optical cladding layer required with the correct refractive index to provide cladding. Electrical confinement is also achieved through the use of ZnMgSSe.

The highest bandgap ZnMgSSe obtained using the previous method of growth was in the region of 2.9 eV at 4K, but for effective optical cladding the bandgap should be in the region of 3.1 eV at room temperature. The incorporation of Mg into ZnMgSSe is known to be linear proportional to the P_{Mg}/P_{ZnS} ratio.[11] Therefore, by increasing the ZnS flux and the Mg flux it was possible to incorporate more Mg and remain lattice matched. The highest bandgap achieved in this study was 3.2 eV at 4K (Figure 5-14)which is approximately 3.1 eV at room temperature. This was achieved by using the compound ZnS source as a source of both Zn and S during the growth of ZnMgSSe, previously the Zn source had also been used during the growth of the quaternary as well as ZnS, Mg and Se. Although this resulted in a reduction in growth rate of the quaternary to ~0.25 $\mu m\ hr^{-1}$, this was still acceptable and did provide the means to increase the bandgap to the required level.

Figure 5-14: PL of highest bandgap ZnMgSSe grown (HWA 777)

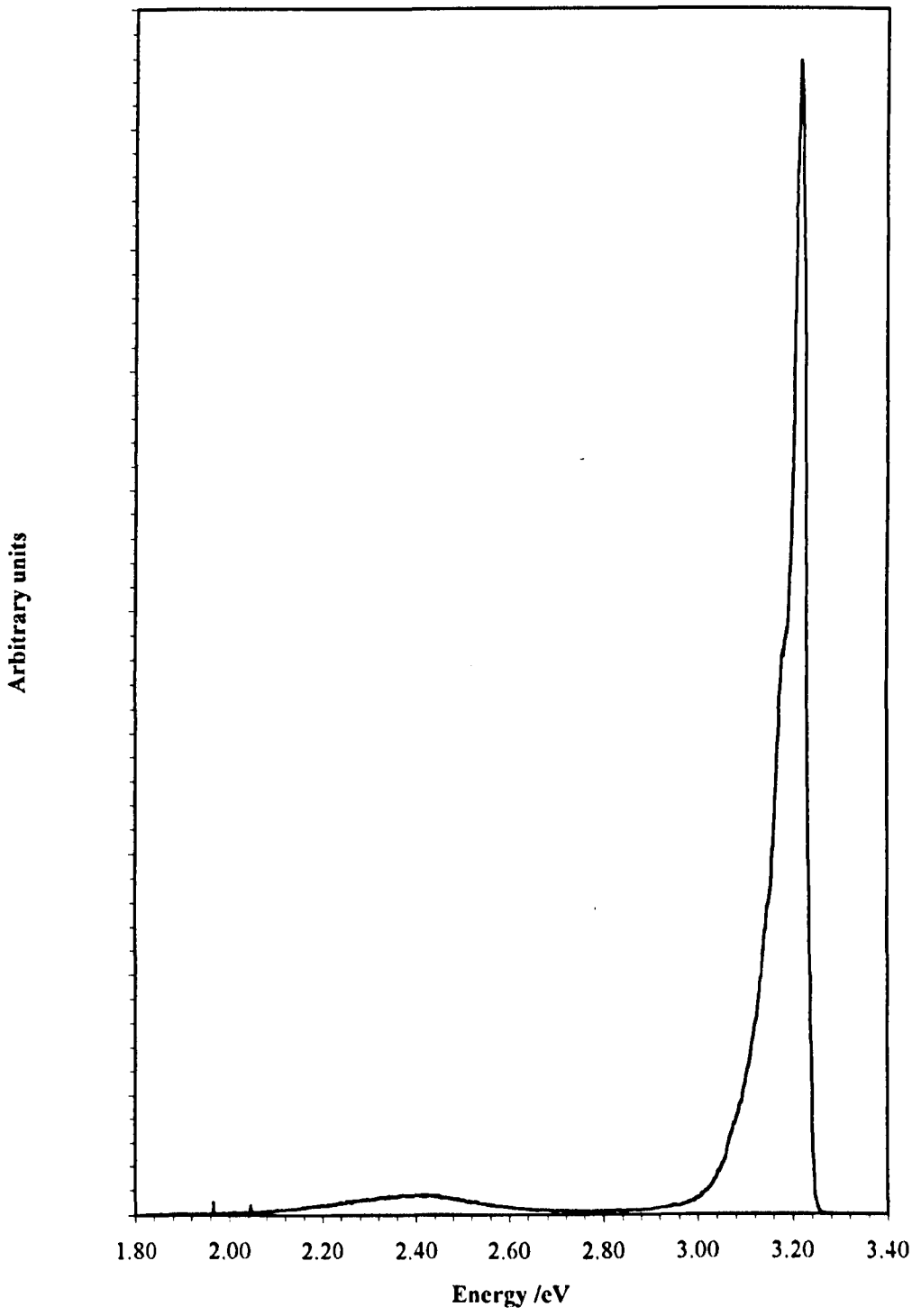

5.5 PROBLEMS ASSOCIATED WITH THE APPLICATION OF ZnSSe AND ZnMgSSe TO LASER STRUCTURES

It is not enough to grow good quality ZnSSe and ZnMgSSe in single layers, as in order to be of any real use these materials must be able to be incorporated in a real structure. As Sony have been the most successful of II-VI groups in terms of obtaining laser devices, the logical place to start in terms of laser structure growth is with a comparable device. A schematic diagram of such a device is shown in Figure 5-15. As can be seen from this schematic, there are a number of junctions between the different materials and the best way to change between them must be investigated.

The problem is that the sulphur composition which is required to lattice match ZnSSe (~6%) to GaAs is very much different from that for ZnMgSSe (typically 12-18%). In a growth reactor with an available cell port capacity of only eight cells there is only room for one source of sulphur (ZnS), (the other cells being Zn, Se, Cd, Mg, Te, N and AgI) and therefore, some method of changing the sulphur incorporation is required during growth. There are three possible methods of achieving this:

i) Change the ZnS cell flux.

ii) Change the substrate temperature (S incorporation is inversely proportional to substrate temperature).[12]

iii) Turn off the Zn flux.

As explained previously in this chapter, changing fluxes is a highly undesirable action due to the nature of thermally controlled effusion cells. Rapid temperature changes result in uncontrolled flux oscillations which ruin the integrity of the material structure. As the composition of the material changes, so the lattice mismatch will increase causing the

Figure 5-15: Schematic of quaternary laser

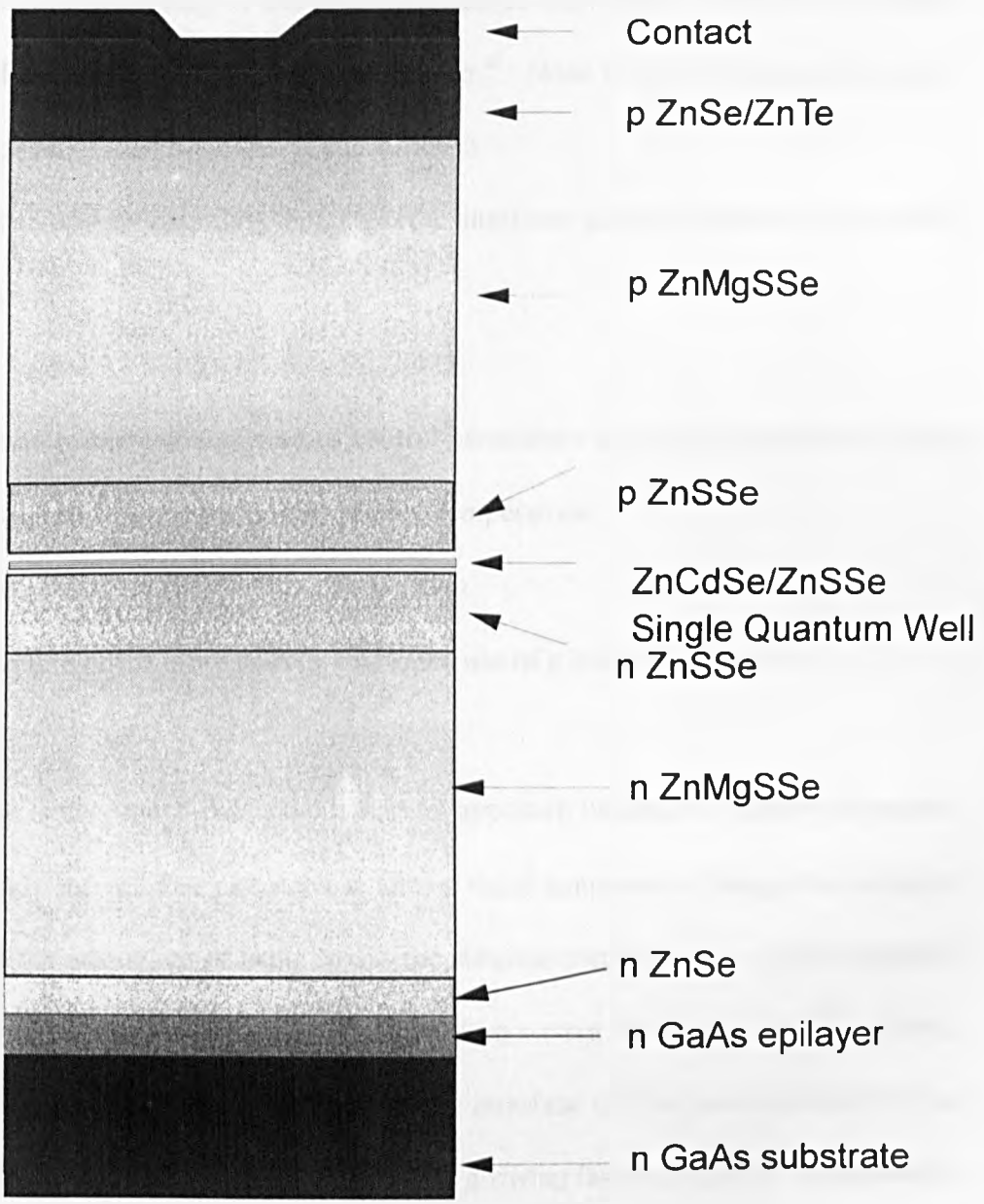

onset of relaxation if the layer thickness becomes of the same order as that of the critical thickness. The effect of this will be the formation of misfit dislocations that will act as recombination centres during device operation. This will seriously limit, or even prevent, the operation of the structure as a laser diode.

Of the other groups working in this field only Purdue University has actually published their method for attempting to solve this problem.[13] None of the other groups actually publish any detail of their approach to this problem.

There are three options regarding these material interfaces given the limits of the growth reactor available:

i) Optimisation of the cell temperature control parameters in order to minimise the flux transient caused by rapidly changing the cell temperature.

ii) Controlled grading of the junction composition.

iii) Removing one of the other cells to enable the use of a second ZnS source.

The first case is very much a damage limitation approach in that it is entirely dependent on how quickly the cell flux can stabilise after a rapid temperature change has occured. It does have the advantage of being by far the simplest method and as a first approach appears to be adequate for the task as working lasers were obtained using this method. However, as explained above the effects on the interface will be uncontrollable and as such is not a sound basis for use in reproducibly growing laser structures. Alternatively, rather than continuing to grow during the cell changes, the growth could be halted. However, stopping the growth in between layers can lead to interface problems due to the static surface being exposed to residual contaminants within the MBE chamber

resulting in unpredictable surface reactions with unknown effects. It has been shown previously by the Heriot-Watt group that when growing ZnSe:I epilayers that halting growth results in a dip in the CV carrier concentration at the epilayer thickness corresponding to this.[14] The reason for this dip is unclear however, the most likely cause is due to either the formation of point defects at the static surface or the incorporation of contaminants from the residual background in the vacuum.

Continuous grading of the previous layer to eventually match that of the subsequent layer is the approach reported by Purdue University[13]. In this method the fluxes are varied continuously at a rate slower than the thermal time constant of the cell thereby maintaining lattice match by grading the composition to provide a smooth transition between ZnSSe and ZnMgSSe. In the case of the ZnMgSSe to ZnSSe interface the Mg flux will gradually be reduced to zero while the S flux is decreased to that required for lattice matched ZnSSe. However, this method is complex requiring good control of cell temperatures through the use of either a temperature controller with a ramp option or computer control of cell temperatures. The problem with this technique is that if the material lattice parameter strays too far from lattice match during the grading process the formation of misfit dislocations is again inevitable. This approach was not feasible during this work due to the lack of an effective computer controller for the necessary grading of cell temperatures.

The third approach required the sacrifice of the ability to grow the ZnTe/ZnSe contact superlattice in the same chamber as the laser structure. As a second chamber was available on this system the ability to grow the ZnTe/ZnSe interface was not lost but required transfer of the sample between chambers. Providing that the other fluxes

required remained constant, a second ZnS source would provide the solution as two ZnS fluxes could be set, one for ZnSSe and one for ZnMgSSe providing a clean interface between the materials which would be repeatable. Unfortunately, the time available meant that this approach could not be tried for this study.

5.6 QUATERNARY LASERS

The interest in II-VI light emitters escalated after the announcement by Haase in 1991 that the first pulsed blue/green laser diode had been achieved.[15] This led to a race to produce a CW room temperature blue laser using either ZnSe/ZnCdSe or ZnSSe/ZnCdSe active regions. A number of groups, including Heriot-Watt, reported the operation of laser devices at cryogenic temperatures using structures similar to the double heterostructure (DH) shown in Figure 5-16 .[16,17,18]

The next step in device design came with the use of the quaternary ZnMgSSe in the laser structure. Of the groups working in this field, the most successful were the Sony[19] and the Philips[20] groups who developed the SCH structures shown in Figure 5-17. The Heriot-Watt quaternary laser structures grown were of a similar design to that used by Philips.

5.6.1 Heriot-Watt Quaternary Laser Diodes

These lasers were grown using the growth method described in Section 5.4.1. The structure of these devices and the growth conditions used are as shown in Figure 5-18. It can be seen from this figure that a number of changes were required to the sources and

Figure 5-16: Schematic of Heriot-Watt ZnSe/ZnCdSe laser structure

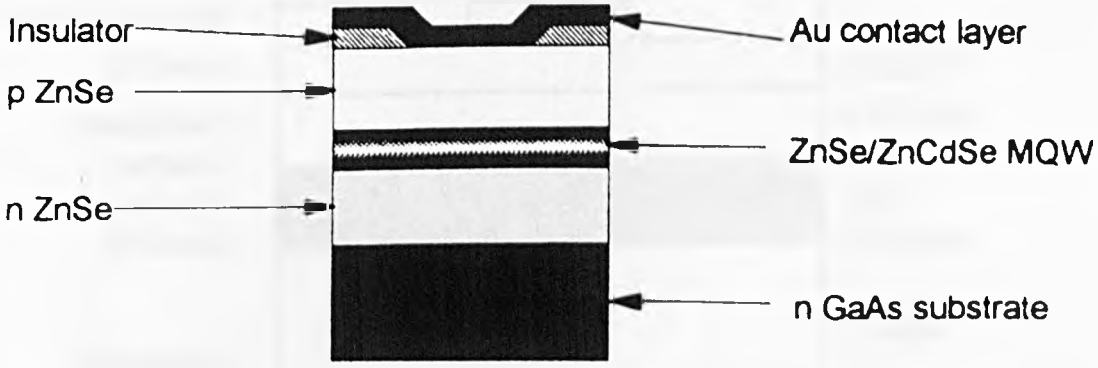

Figure 5-17: Schematic of Sony and Philips quaternary lasers

(a) Sony laser diode structure:

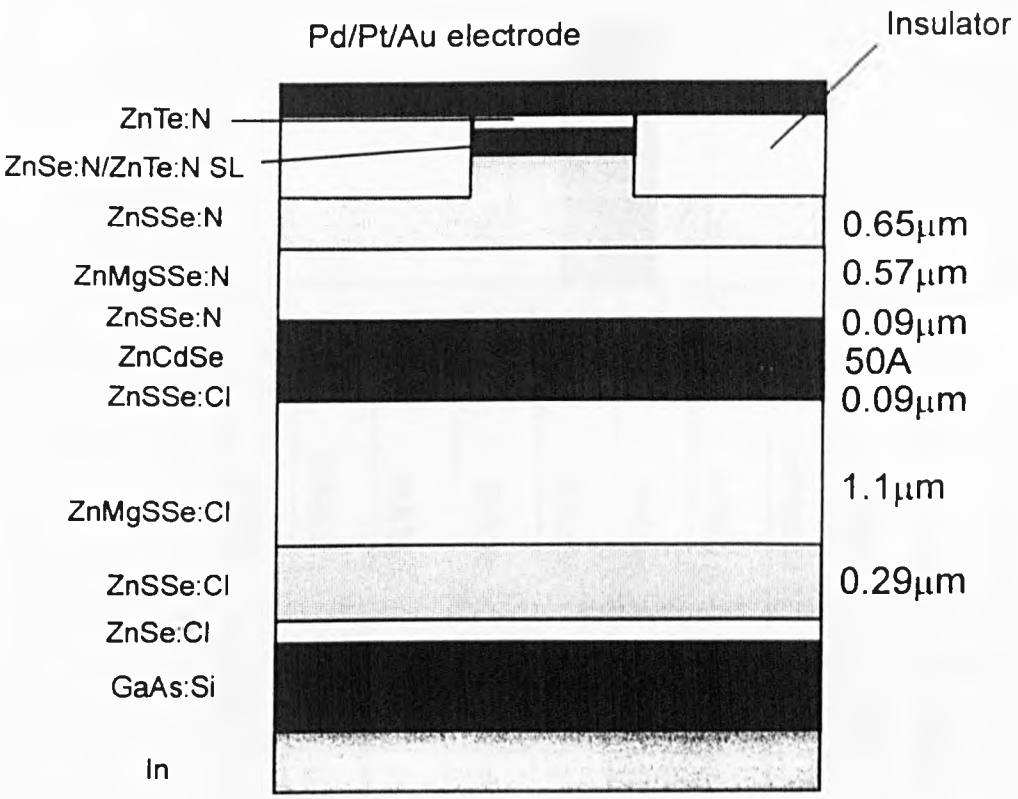

(b) Philips laser diode structure

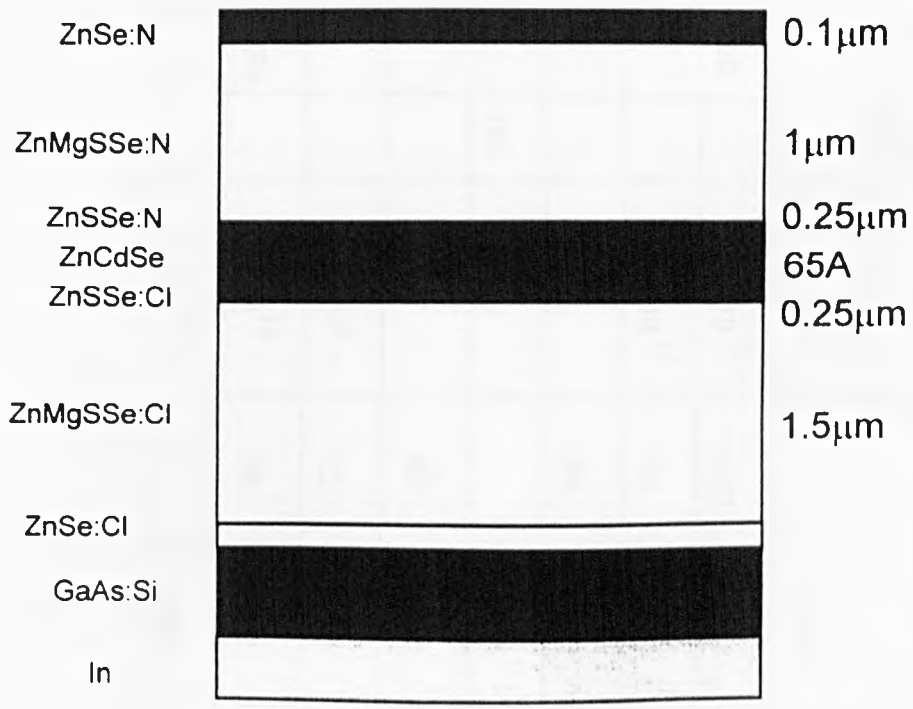

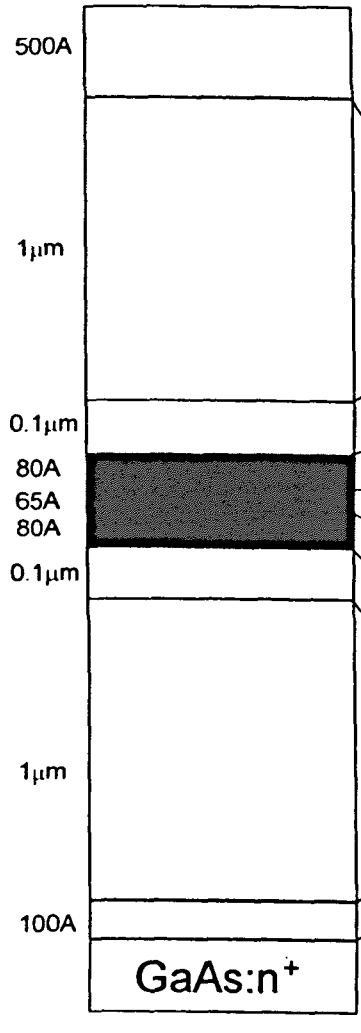

Layer	Cell Temperature °C						Carrier concentration cm^{-3}	DCXRD FWHM arcsec	T_{sub} °C
	Zn	Se	ZnS	ZnS	Mg	Cd			
ZnSe:N	300	177					$5x10^{17}$		250
ZnMgSSe:N	300	177		743	220		$1.5x10^{17}$	<100	280
ZnSSe:N	300	177	729				$2.2x10^{17}$	70	280
ZnSSe	292	177	737					66	280
ZnCdSe	292	177				183			280
ZnSSe	292	177	737					66	280
ZnSSe:I	292	177	737				$>10^{18}$	72	280
ZnMgSSe:I	292	177		748	220		$>10^{18}$	75	260
ZnSe:I	292	177					$>10^{18}$		280

Figure 5-18: Heriot-Watt quaternary laser diode structure and growth details

the substrate temperatures to compensate for composition changes between ternary and quaternary layers as discussed in Section 5.5. Despite this, there were a number of devices which operated as lasers. The DCXRD rocking curve of one such device (HWA 655) is shown in Figure 5-19 which operated under pulsed operation at 512nm near room temperature (290K). Unfortunately, the lifetime of this device was only a few seconds.

This device had an active region consisting of a 65Å single quantum well of ZnCdSe with a Cd incorporation of 23% (source flux estimate). The quaternary ZnMgSSe alloy had a bandgap of ~2.9 ev at 4K, estimated from prior growth calibrations. The rocking curve clearly shows three peaks which indicate that the structure is not lattice matched but, the degree of relaxation could not be determined as it is difficult to identify the layer which corresponds to each peak. However, the significant result was that the material quality grown was sufficient to produce semiconductor lasers.

It was apparent from these results that greater control over the growth parameters would be required if a room temperature CW laser was to be produced which was why the second method of growth described in Section 5.4.3 was investigated. Unfortunately, despite success in improving the quality of the ZnSSe and ZnMgSSe layers grown, it was not possible to incorporate this technique into a device structure in the time available.

5.7 CONCLUSIONS

The ability to grow good quality ZnSSe and ZnMgSSe had been achieved and quaternary laser structures had been grown. A number of problem areas had been identified in the

Figure 5-19: XRD of HWA 655 laser diode structure

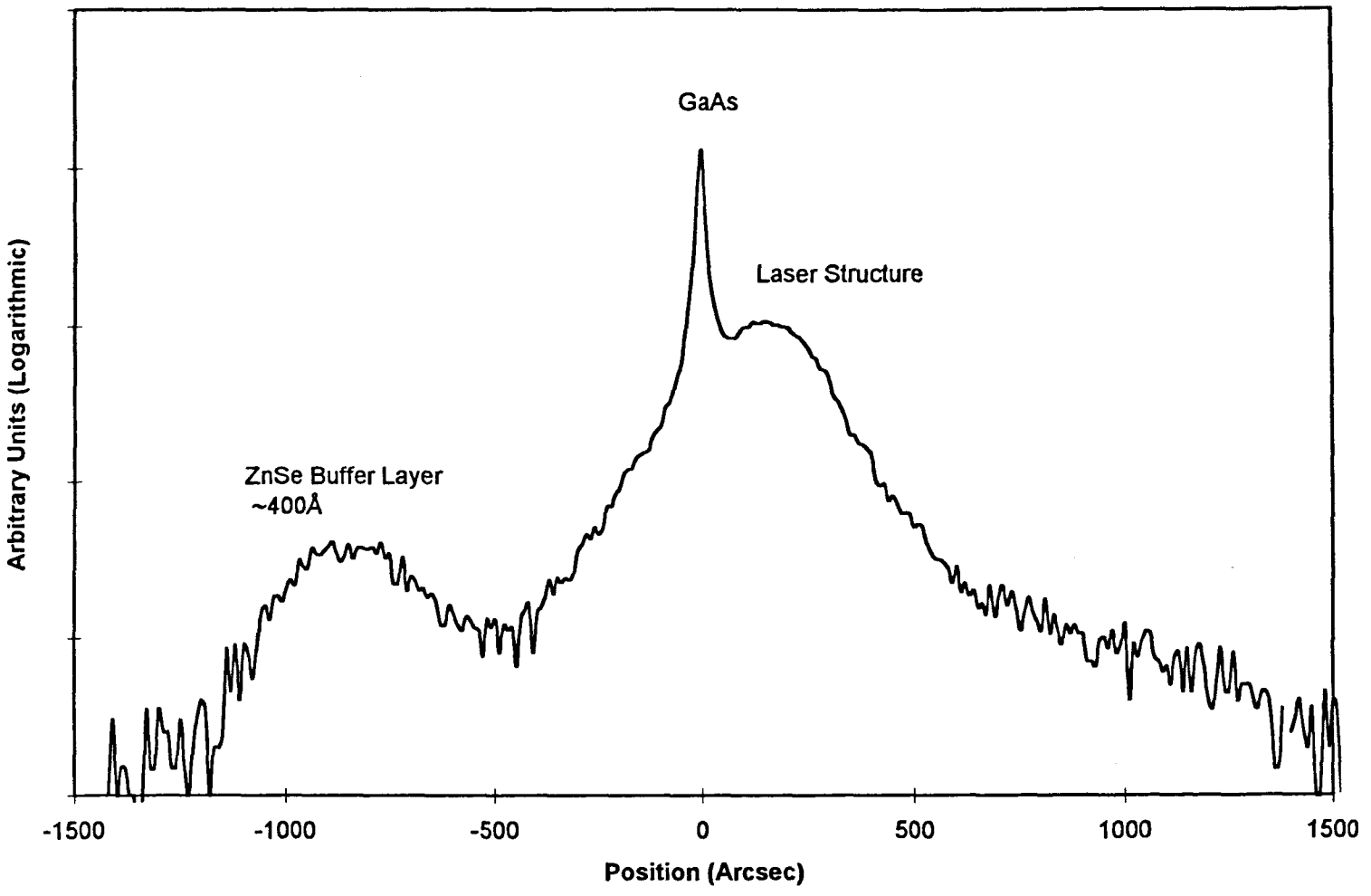

growth method regarding temperature stabilisation at the start of growth and interface problems when changing between materials. Methods of compensating for these problems were investigated. The installation of a liquid nitrogen cooled shutter solved the problem of poor thermal desorption of the GaAs while the adoption of a substrate temperature adjustment at the start of growth minimised the heat load effect of the ZnS source. The material quality of both the ZnSSe and ZnMgSSe was subsequently improved however, there was not sufficient time to incorporate these improvements into a laser structure before the end of this study.

5.8 REFERENCES

[1] A. Ishibashi, J. Cryst. Growth, 159 (1996), 555

[2] S. Colak, B. J. Fitzpatrick and R. N. Bhargava, J. Cryst. Growth, 72 (1985), 504

[3] D. A. Cammack, R. J. Dalby, H. J. Cornelissen and J. Khurgin, J. Appl. Phys., 62 (1987), 3071

[4] H. Okuyama, K. Nakano, T. Miyajima and K. Akimoto, Jap. J. Appl. Phys., 30 (1991), 1620

[5] H. Okuyama, K. Nakano, T. Miyajima and K. Akimoto, J. Cryst. Growth, 117 (1992), 139

[6] *Handbook of Chemistry and Physics 72nd Edition*, Ed. D. R Lide, 1991

[7] B. J. Wu, H. Cheng, S. Guha, M. A. Haase, J. M. De Puydt, G. Meis-Haugen and J. Qui, Appl. Phys. Lett., 63 (1993), 2935

[8] E. Tournié, Personal communication

[9] M. O. Möller, V. Beyersdorfer, D. Hommel, T. Behr, H. Heinke, T. Lippmann and G. Landwehr, J. Cryst. Growth, 143 (1994), 162

[10] M. Kolodziejczyk, T. Filz, A. Krost, W. Richter and D. Zahn, J. Cryst. Growth 117 (1992), 549

[11] B. J. Wu, J. M. DePuydt, G. M. Haugen, G. E. Höfler, M. A. Haase, H. Cheng, S. Guha, J. Qiu, L. H. Kuo and L. Salamanca-Riba, Appl. Phys. Lett., 66 (1995), 3462

[12] S. V. Ivanov, S. V. Sorokin, P. S. Kopev, J. R. Kim, H. D. Jong and H. S. Park, J. Cryst. Growth, 159 (1996), 16

[13] C. C. Chu, T. B. Ng, J. Han, G. C. Hua, R. L. Gunshor, E. Ho, E. L. Warlick, L. A. Kolodjziejski and A. V. Nurmikko, Appl. Phys. Lett., 69 (1996), 602

[14] J. Simpson, J. M. Wallace, S. Y. Wang, H. Stewart, J. J. Hunter, S. J. A. Adams, K. A. Prior and B. C. Cavenett, Semicond. Sci. Technol., 7 (1992), 464

[15] M. A. Haase, J. Qui, J. M. DePuydt and H. Cheng, Appl. Phys. Lett., 59 (1991), 1272

[16] Z. Yu, J. Ren, B. Sneed, R. A. Bowers, K. J. Gossit, C. Boney, Y. Lansari, J. W. Cook, J. F. Schetzina, G. C. Hua and N. Otsuka, Appl. Phys. Lett., 61 (1992), 1266

[17] D. C. Grillo, Y. Fan, J. Han, L. He, R. L. Gunshor, A. Salokatve, M. Hagerott, H. Jeon, A. V. Nurmikko, G. C. Hua and N. Otsuka, Appl. Phys. Lett., 63 (1993), 2723

[18] I. S. Hauksson, S. Y. Wang, J. Simpson, M. R. Taghizadeh, K. A. Prior and B. C. Cavenett, Physica B, 191 (1993), 124

[19] N. Nakayama, S. Itoh, T. Ohata, K. Nakano, H. Okuyama, M. Ozawa, A. Ishibashi, M. Ikeda and Y. Mori, Electron. Lett., 29 (1993), 1488

[20] J. M. Gaines, R. R. Denton, K. W. Haberern, T. Marshall, P. Mensz and J. Petruzello, Appl. Phys. Lett., 62 (1993), 2462

6. DOPING OF ZnSe, ZnSSe AND ZnMgSSe

6.1 INTRODUCTION

In order to fabricate any electrical device from semiconductor material it is essential to have good control of impurity doping.

Undoped ZnSe is of low resistivity (20 Ωcm), as estimated below, and exhibits n-type conductivity.

$$\rho = \frac{1}{ne\mu} \qquad 6.1$$

where ρ is resistivity (Ωcm), μ is mobility ($\approx$300 $cm^2V^{-1}s^{-1}$)[1] and n is the carrier density. For MBE grown nominally undoped ZnSe $n\approx10^{15}cm^{-3}$ which gives a resistivity, ρ = 20 Ωcm.

The n-type conductivity of nominally undoped ZnSe, was originally attributed to native donors as opposed to out diffusion of Ga from the GaAs substrates.[2] More recently SIMS studies on ZnSe epilayers have shown that Ga does out diffuse from the substrate into the epilayer.[3,4] Whatever the reason, the fact that nominally undoped ZnSe has an n-type character makes the production of p-type ZnSe more difficult.

6.2 N-TYPE DOPANT FOR ZnSe AND ZnSe BASED COMPOUNDS

As Zn and Se are elements from group II and VI of the periodic table respectively, the most appropriate donor dopant species lie in groups III and VII. Early doping studies, performed on MOCVD grown material, focused on the group III elements due to the experience already gained from the use of these elements in the more established III-V technology. In MBE, early studies were performed using Ga as a donor source.

The first n-type dopant tried was Al. Layers of ZnSe with carrier concentrations as high as $2x10^{18}$ cm^{-3} were grown by MOCVD using aluminium as the donor species. It was found that above a carrier concentration of $1.6x10^{17}$ cm^{-3} degenerate behaviour was observed.[5,6] However, in a comparison of group III and VII elements using triethylaluminium, and 1-chloro-octane as sources of Al and Cl it was found that the Al doped layers exhibited a non-linear relationship between dopant incorporation and carrier concentration.[7] A maximum carrier concentration of $1x10^{18}$ cm^{-3} was attained with Al but, any attempt to increase this resulted in degradation of the optical properties. In contrast the layers doped with Cl achieved higher carrier concentrations without the degradation to the optical properties.

Other elements studied as donors in MOCVD grown ZnSe include Ga (triethyl-gallium)[8], bromine (ethylbromide)[9] and iodine (ethyliodide and n-butyliodide).[10] In particular, the ethylbromide source produced maximum carrier concentrations of $1x10^{19}$ cm^{-3}.[11] Iodine was also successful, allowing the dopant concentration to be controlled between 10^{15} cm^{-3} and 10^{19} cm^{-3}. Therefore, from the MOCVD research the best dopant species lie in group VII of the periodic table as opposed to group III.

Unfortunately, from the point of view of ZnSe MBE growth, the gas sources used in MOCVD do not easily lend themselves to ultra-high vacuum techniques. This is due to the fact that it is difficult to control the removal of gases from the chamber as they are not trapped by the liquid nitrogen cryoshield and can react with other materials present. Also, as the flow of gas required for impurity doping is so small it is difficult to find a mass flow controller (MFC) which can regulate this flow effectively. Therefore, the question of n-type dopant sources for MBE had to be considered. By far the best solution for MBE is to have source materials which remain solid at their respective operating temperatures. This also allows the sources to be mounted horizontally in the growth chamber thereby reducing the risk of source contamination by flakes of material from the cryoshield and source shutters dropping into the sources.

Due to their physical properties the pure group VII elements can immediately be discarded as sources of dopant. For instance, chlorine is a gas and bromide is a liquid at room temperature. Both are extremely volatile with the ability to etch metal and semiconductor surfaces. Iodine also has these problems as well as being able to form the highly volatile species TiI_4 when in contact with titanium which is used extensively in MBE for sublimation and ion pumps. In their elemental form the group VII elements are not appropriate but, in compound form these same dopants can be found as solid sources, for example $ZnCl_2$ and ZnI_2 can both be used as sources of iodine and chlorine respectively. Both of these compounds still require careful handling prior to charging in the MBE cell source to minimise the introduction of impurities.

Epilayers of ZnSe with carrier concentrations in excess of $1x10^{19}$ cm^{-3} have been achieved using $ZnCl_2$ as a source of dopant in conventional MBE.[12,13] Consequently, $ZnCl_2$ was largely adopted as the preferred donor dopant for n-type ZnSe by most MBE groups currently operating in the II-VI field and was used in the first reported ZnSe based lasers.[14]

Despite its success $ZnCl_2$ is still fraught with problems; it has a relatively high vapour pressure in comparison with other sources used and the operating temperature of the source cell is in the region of 130°C. This operating temperature is quite low making control of the cell temperature quite difficult, requiring a great deal of optimisation of the proportional, integrating and differentiating (PID) parameters of the controller to match the power supply to the cell heaters. It is also in the same temperature region as that used for bake-out of the chamber (110°C) resulting in $ZnCl_2$ deposition all around the chamber whenever the system is baked. Of course, any variation in temperature of the cell around the set point will result in dopant flux variations and leads to an inability to control doping levels below $5x10^{16}$ cm^{-3}.[15] Also, due to the inefficient radiative cooling of the cell rapid changes in the dopant flux are not possible due to the lag, or lead time between changing the set temperature on the PID controller and the temperature actually changing in the cell.

At Heriot-Watt the n-type dopant source used is an electrochemical iodine source which uses solid silver iodide pellets. The advantage this cell has over the thermally operated cell is the ability to rapidly change the dopant flux by changing the applied current to the pellet. Similar sources have been used in surface science studies[16] and for doping of GaAs using S.[17] The design and operation of this cell is described below.

6.3 ELECTROCHEMICAL IODINE CELL

As has been mentioned previously, the source of n-type dopant used was an electrochemical cell. In this cell current was passed through a silver-iodide pellet to provide a source of iodine. The design of this cell is similar to electrochemical cells used in other studies where a sulphur electrochemical cell has been used as a dopant[17,18] in III-V systems and more recently in the production of lattice matched ZnSSe.[19]

6.3.1 Chemical and Physical Properties of Silver Iodide.

Most crystalline materials have an ionic structure where the gap between the conduction and valence bands is too large for electrons to cross and hence contribute to electrical conductivity. However, there are a group of compounds known as solid electrolytes where it is the positive or negative ions and not electrons which can move freely through the lattice and cause conduction.

AgI is a super-ionic conductor and at low temperatures conduction is primarily achieved through Frenkel defects. However, at a transition temperature of 146°C a phase transition occurs which changes the structure of the crystal from hexagonal wurtzite to a body centred cubic arrangement. The iodide ions lie at the corner and body centre positions and are essentially fixed. This leaves the silver ions to move through the crystal in a liquid-like manner randomly occupying tetrahedrally co-ordinated interstitial positions.

It is due to this change in structure that the resistivity falls by up to four orders of magnitude. Iodine is a large and polarisable anion and so covalent bonds form readily

between the silver and the iodine. During conduction silver can move from one tetrahedral site to the next via an intermediate three-co-ordinate site. Covalent bonding at the intermediate site helps to stabilise it and reduce the activation energy for conduction. Hence, above the transition temperature the flux of iodine molecules evolved at the anode will be greatly increased. In practice the electrochemical cell is operated at an indicated temperature of 170°C. This is a good trade off point in terms of the MBE requirements as it is sufficiently above the phase transition temperature of AgI to ensure relatively low resistance, but below the temperature where re-evaporation can occur from deposits on the external surfaces of the cell and the level of thermally generated iodine from the pellet becomes significant.

6.3.2 Electrochemical Cell Construction

The main drawback of the present electrochemical cell is in its construction. In order for it to operate reliably there must be good electrical and thermal contact between the cell and the pellet. The cell used throughout this study is shown schematically in Figure 6-1. The main parts of the cell are constructed of machineable glass ceramic.

As can be seen from this diagram the heater elements are detached from the main body, which holds the pellets. The thermal coupling between the heater element and the pellet holder is poor due to the necessary clearance required for assembly. Also, as the thermocouple is embedded in the centre of the main body, it is insensitive to changes in the heater power. The effect of this is to introduce a significant thermal lag time (approx. 15 min) between the application of power to the heater and the temperature registering on the thermocouple. This leads to the cell being extremely difficult to control thermally as the operating temperature required is only in the region of 150°C.

Figure 6-1: Schematic of Iodine Cell

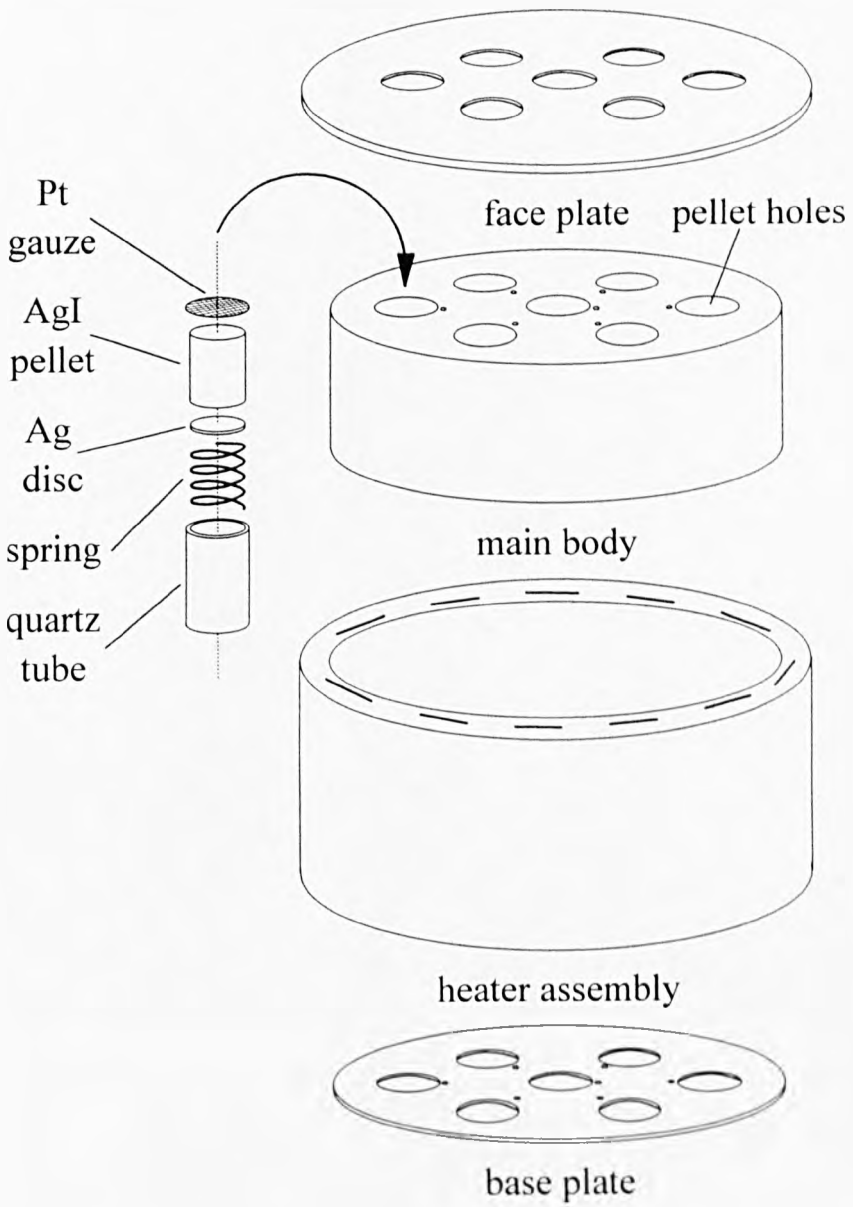

In practice this is not a large problem as once the cell is at its operating temperature there is no need for any adjustment to be made and any small temperature variations have no effect as the doping is controlled by the current passed through the pellet. In addition, the pellets themselves are held in glass sleeves which allow for their easy replacement, but which lead to even poorer thermal transfer. It is therefore difficult to ascertain the actual temperature of the pellets. However, this does not present a problem as all that is required is that the AgI pellets are kept above their phase transition temperature.

Electrical contact with the pellet is also poor as the pellet is, in effect, held by a spring between the platinum gauze and silver foil discs that form the front and rear contact respectively (Figure 6-2). Any free play allowed during assembly leads to poor contact and short operational lifetime of that particular pellet. Fortunately, the holder can accommodate up to seven pellets which increases the chance of obtaining a useful pellet.

The effect of passing a current through the pellet is to cause the I to migrate to the platinum gauze according to the following reactions:

$$Ag^{+} + e^{-} \rightarrow Ag_{(s)}$$

and

$$I^{-} \rightarrow I + e^{-}$$

Then on the platinum gauze at a steady state:

$$2I^{-} \rightarrow I_2 + 2e^{-}$$

From these reactions it is clear that as I accumulates at the front surface electrode, Ag accumulates at the rear silver electrode. The result of this is to form dendrites of Ag

Figure 6-2: Schematic of iodine pellet arrangement

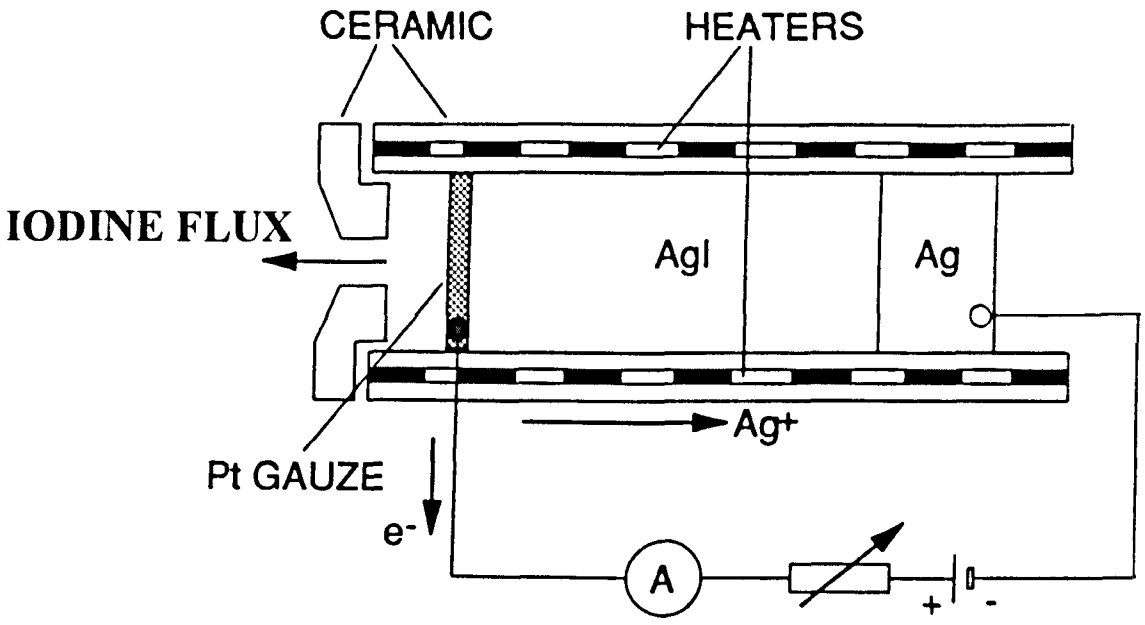

through the pellet. This ultimately limits the lifetime of the pellet. The accumulation of iodine at the front surface also meant that it was easier to change from a high current (10μA) to a low current (1μA) than vice versa. At low current the increased time taken to reach a steady state at the Pt electrode resulted in a graded doping flux as the source settled.

Another fundamental factor in the operation of the iodine cell is the formation of the pellet itself. At present the most consistent method of formation involves compressing the AgI powder in a press. Provided that the same amount of AgI material and pressure is used each time, satisfactory pellets can be produced. However, great care must be taken when compressing the pellets that the pressure exerted does not exceed that required to form the high pressure/low volume phase of AgI as when the pressure is released the pellet shatters.

Using the electrochemical cell it was possible to grow samples with a doping staircase profile as shown in Figure 6-3 where the doping steps corresponded to applied currents of 50μA, 5μA, 0.5μA and 0μA resulting in doping levels of 5×10^{18} cm^{-3}, 5×10^{17} cm^{-3}, 6×10^{16} cm^{-3} and 5×10^{16} cm^{-3}, respectively[20].

6.4 P-TYPE DOPANTS OR DOPING

As described above, nominally undoped ZnSe is n-type. This is due to the intrinsic electron-hole density, n_i being much smaller than that of one carrier species thermally generated from any defect levels which may be present, in this case electrons. This behaviour is common to most nominally undoped semiconductors. In II-VI

Figure 6-3: ZnSe:I doping staircase

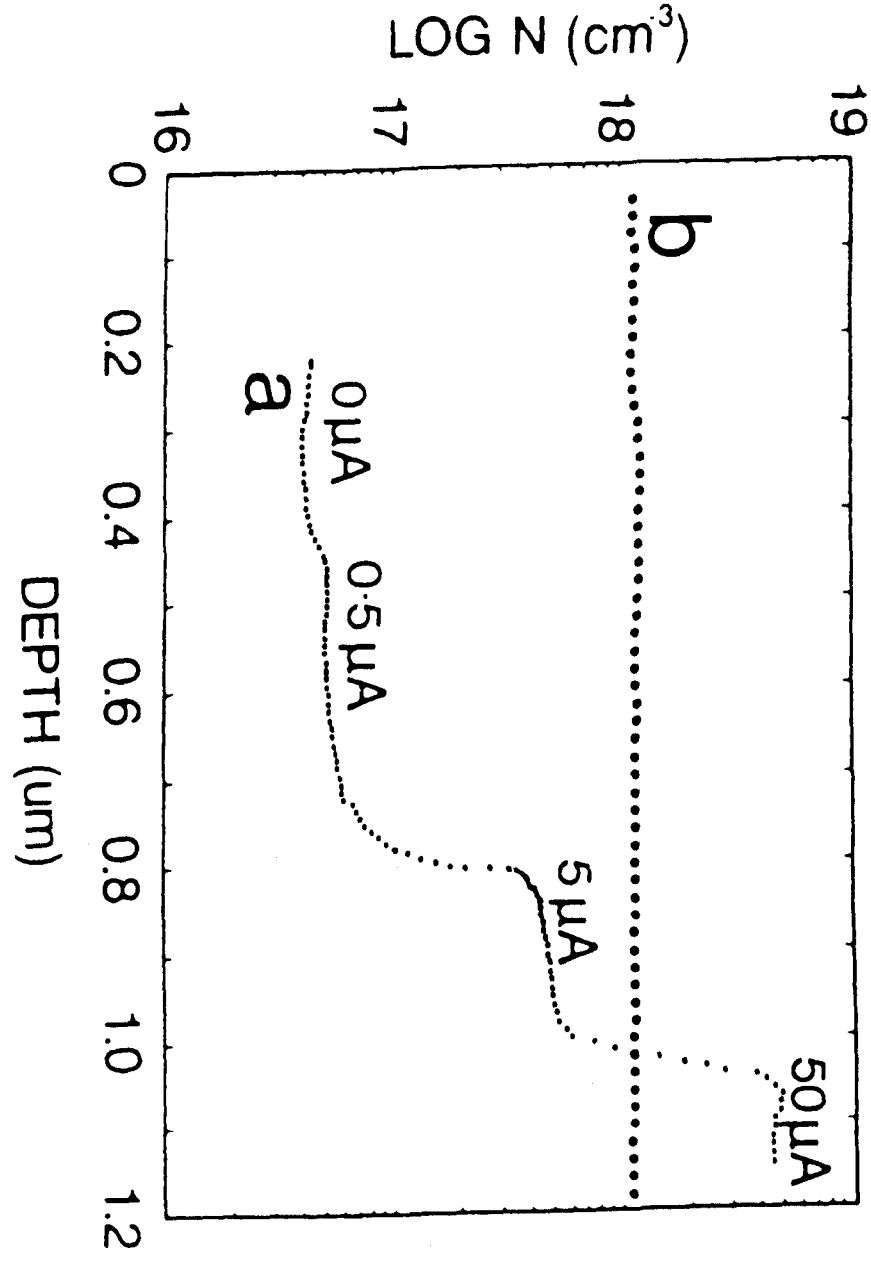

semiconductors ZnSe, ZnS, CdSe and CdS are all n-type but, ZnTe is p-type. This behaviour is determined from the defect levels which may arise as a result of lattice vacancies or intentional impurity doping.

The issue of intentionally doping a II-VI semiconductor is complicated by the phenomenon of self-compensation of the semiconductor, this is particularly evident when attempting to obtain relatively high carrier concentrations.

The occurrence of self-compensation in II-VI compounds but not elemental semiconductors such as silicon or III-V compounds such as GaAs is a consequence of their bonding type. The bonding in III-V compounds is predominantly covalent whilst the II-VI compounds have a much stronger ionic contribution.[21]

In the case of p-type dopants for ZnSe the elements which can be as acceptors are located in groups I and V of the periodic table. Group I elements are generally considered to be amphoteric.[22] In the case of ZnSe this means that when the element is incorporated substitutionally on a Zn site it acts an acceptor and as a donor when incorporated interstitially.

Lithium has proved to be the most successful of the group I elements for producing p-type material.[23] In MBE growth of ZnSe:Li, the highest hole concentrations were achieved under a selenium stabilised growth regime; with Zn:Se BPR's as high as 1:8 and substrate temperatures in the range 270-300 °C. These growth conditions yielded p-type layers with net acceptor concentrations in the mid 10^{16} to low 10^{17} cm^{-3}. However, in order to achieve this the lithium concentrations were as high as $5x10^{19}$ cm^{-3}.[23,24,25]

Greater net acceptor concentrations are limited due to the amphoteric nature of Li which results in compensation as more Li is incorporated (typically beyond concentrations of $1x10^{17}$ cm^{-3}) as predicted by Neumark.[26] Also, the compensating Li^{-} ion is highly mobile in the crystal lattice due to its relatively small size allowing it to rapidly diffuse through the lattice. These factors made the reliable production of p-type layers using Li difficult, but not impossible. However, the formation of a p-n junction requires a reasonably sharp interface which is very difficult using lithium due to its high mobility, Also, any thermal processing required post growth would also lead to smearing of any p-n junction.

Sodium has also been tried using ion-implantation into MOVPE grown nominally undoped ZnSe layers. Due to the lattice damage produced by this technique it is necessary to anneal the layers after implantation. Although the existence of a shallow acceptor due to the sodium was confirmed, during the anneal stage the donor bound exciton increased as the implantation damage was removed.[27] Na_2Se has also been used as a source of sodium in MBE growth of ZnSe.[25,28] Neither of these approaches were particularly successful as these samples, although exhibiting optical evidence for acceptor levels, did not produce electrically p-type material.

At Heriot-Watt the use of an electrochemical source of potassium was investigated. The principal of operation was similar to that of other more common electrochemical sources, such as iodine (Section 6.3). The p-type doping level N_a-N_d obtained using the electrochemical potassium source was in the range $3x10^{15}$ cm^{-3}.[29] This limit is possibly due to surface segregation during growth.[30]

The group V elements phosphorous (P), arsenic (As) and nitogen (N) have also been tried as possible anion site substitutional acceptors for ZnSe. Arsenic and phosphorous molecules, although having a smaller dissociation energy than nitrogen, did not produce p-type doping. This left nitrogen as the only remaining candidate for p-type doping.[31] However, the difficulty of finding a suitable source of nitrogen for MBE meant that the early work was mostly focused on MOCVD growth. Using ammonia as a source of N, p-type conduction was achieved with carrier concentrations of the order of 10^{14} cm^{-3}.[32]

The breakthrough for N doping in MBE came in 1990, when through the use of a R.F. plasma nitrogen source operating at 13.65 MHz yielded doped layers with N_a-N_d as high as 3-4x10^{17} cm^{-3}. [33,34] This level of acceptor concentrations allowed the fabrication of a ZnSe:N/ZnSe:Cl p-n junction LED's which exhibited dominant blue emission at room temperature, with an intensity peak at 465 nm.[33]

The nitrogen plasma source used at Heriot-Watt is of the same design (Figure 6-4). The maximum level of N_A-N_D achieved in conventional MBE growth techniques is 2x$10^{18}$$cm^{-3}$, as compensation effects dominate.[35]

6.4.1 Compensation in p-type ZnSe based Semiconductors

It has been shown that N_A-N_D increases with the concentration of nitrogen atoms, [N], until a plateau is reached. Typically, the peak N_A-N_D is around (5 to 10) x 10^{17} cm^{-3}.[35] Qiu et al.[36] Have shown that both [N] and N_A-N_D are a function of the II-VI ratio and the substrate temperature during growth, both quantities show maxima for VI:II ratios of approximately unity and increase monotonically with decreasing substrate temperature. At the start of the plateau region the fraction of the nitrogen which is electrically active can be high, typically over 80 to 90%, but any further increase in [N] sees a decrease in

Figure 6-4: Schematic diagram of OXFORD R.F. plasma source

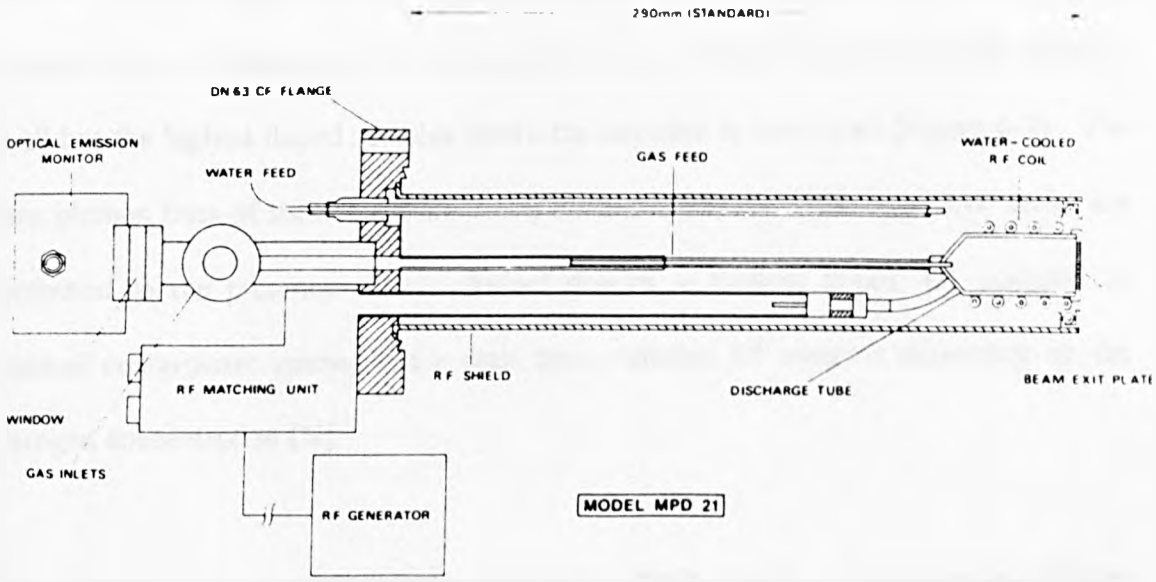

the activity in the highest doped samples to less than 10% (Figure 6-5). This has lead to the conclusion that for highly doped ZnSe:N samples, the material is highly compensated. The compensation mechanism in ZnSe:N has been reviewed in a number of articles in recent years.[37,38,39]

The PL spectra (Figure 6-6) of nitrogen doped ZnSe at Heriot-Watt clearly show evidence of two distinct sets of DAP transitions (zero phonon lines and phonon replicas) in all but the highest doped samples where the emission is too broad (Figure 6-7). The zero phonon lines of these DAP are 2.696 eV and 2.678 eV. The two DAP series are attributed to the presence of two distinct donors, a shallow donor, D^s, assigned to residual contaminant species and a deep donor labelled D^d which is dependent on the nitrogen concentration [N].

The recombination processes which result in these DAP emissions are as shown in Figure 6-8.[40] In this figure the shallow donor (26 meV) and the deep donor (44 meV) interact with the nitrogen acceptor. The model proposed by Hauksson for the deep donor was a complex, $[V_{Se}\text{-}Zn\text{-}N_{Se}]$,.[40] where this complex is a singly charged donor produced from the combining of a Se vacancy (a double donor) and the nitrogen acceptor.

The value obtained for the binding energy of the deep donor of 44 meV was subsequently revised in a study by Zhu[41], where under a more involved treatment the value was found to be 57 meV. As [N] increases the number of these complexes formed also increases resulting in compensation effects which severely limits the level of N_A-N_D which can be achieved.

Figure 6-5: Carrier concentration vs nitrogen incorporation

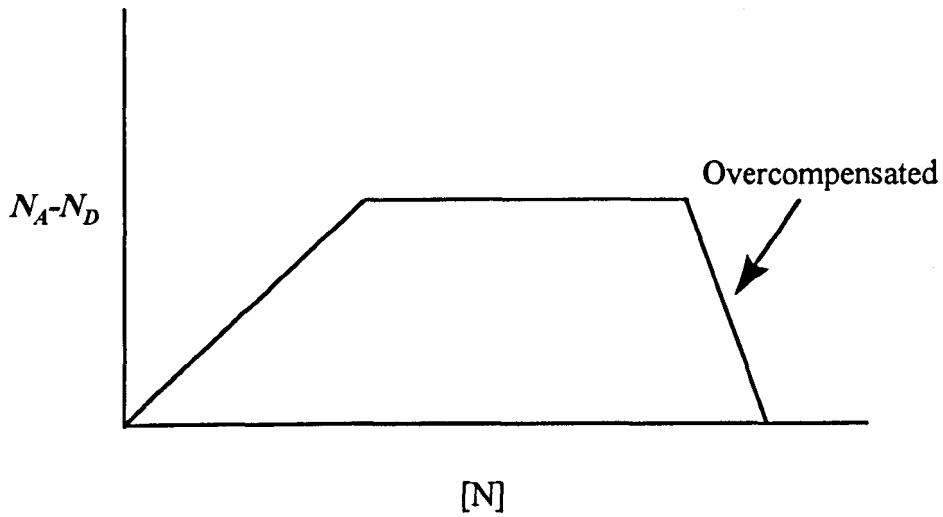

Figure 6-6: PL spectra showing shallow and deep DAP emission

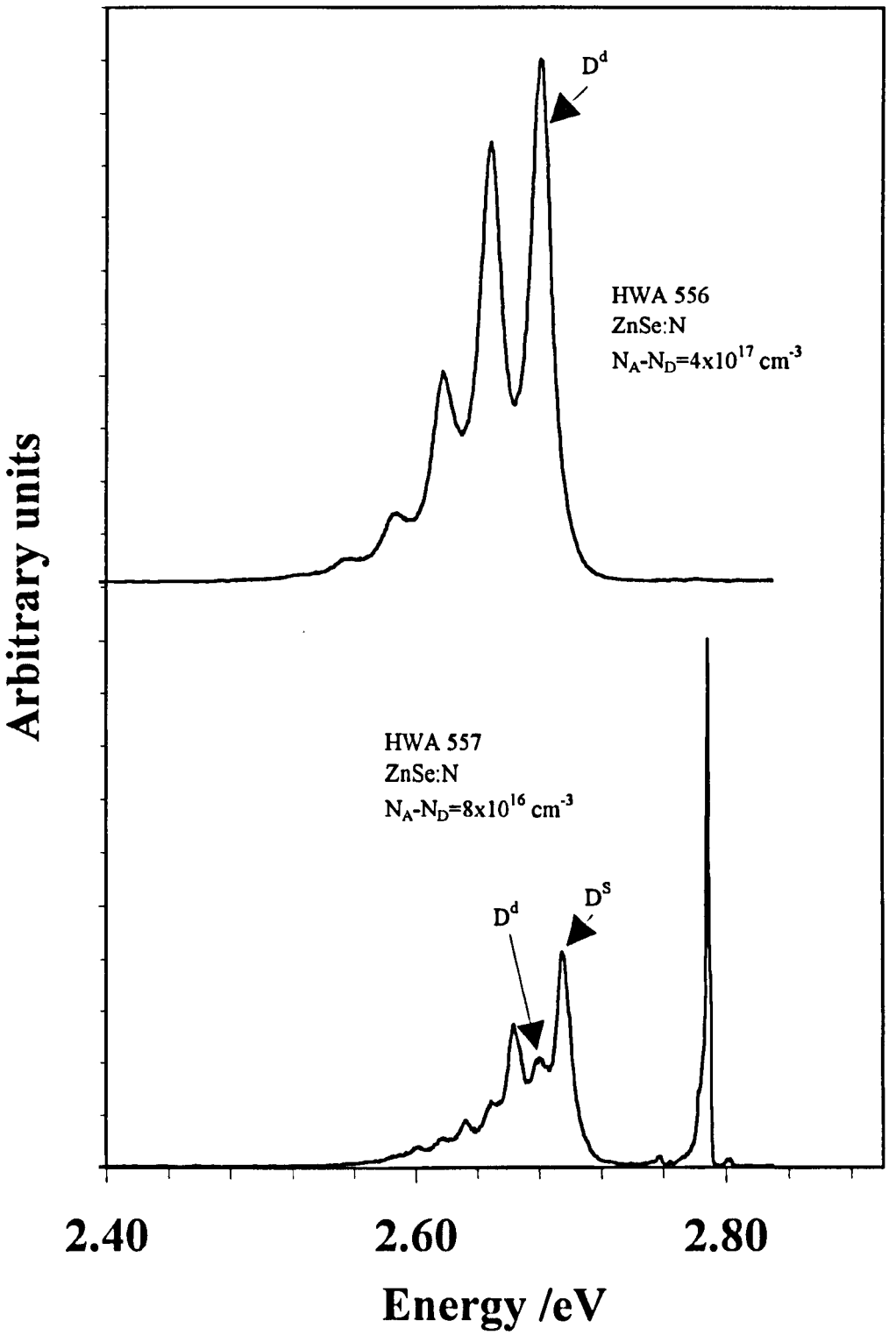

Figure 6-7: Overcompensated ZnSe:N showing broad DAP

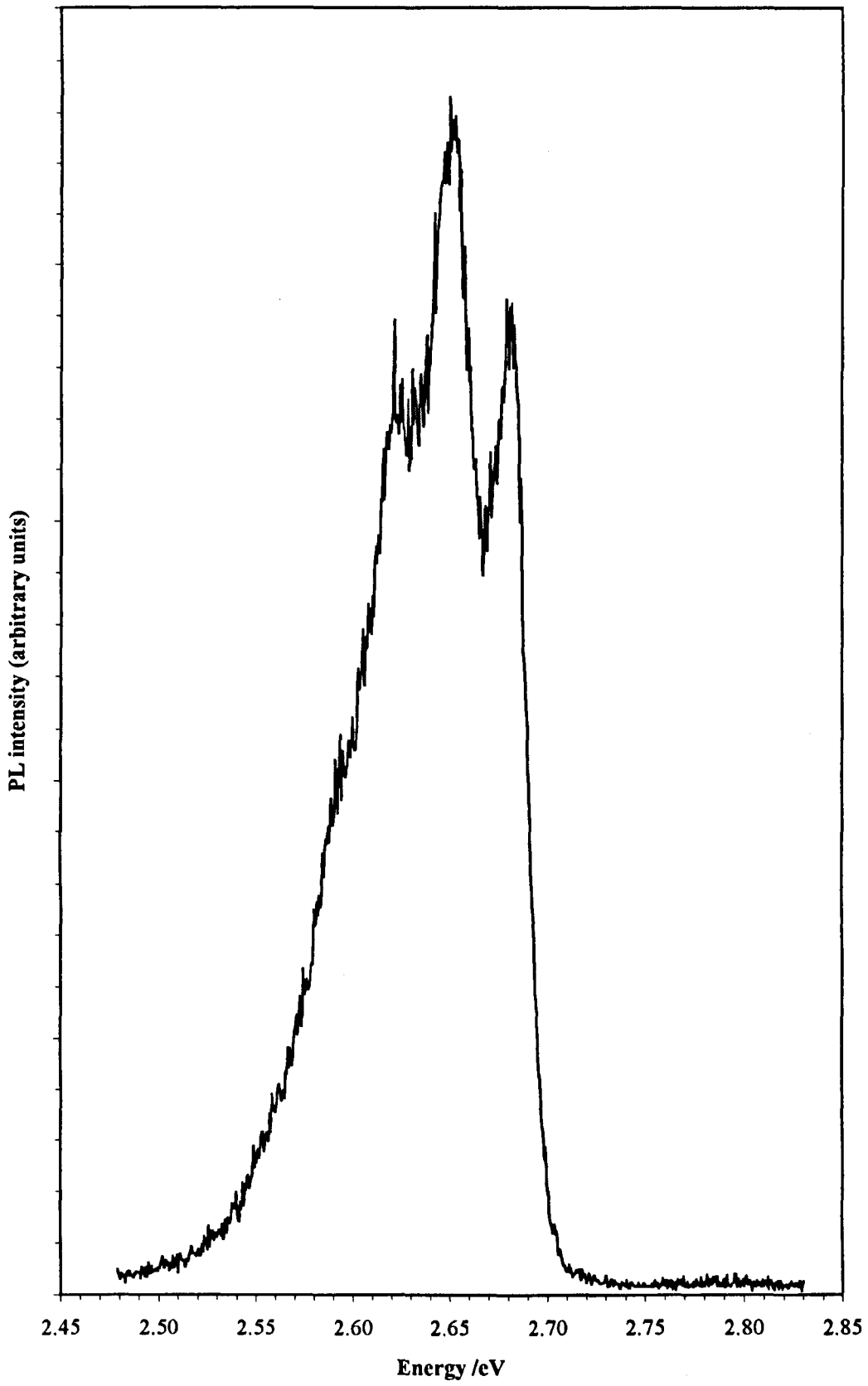

Figure 6-8: Recombination transitions in ZnSe:N

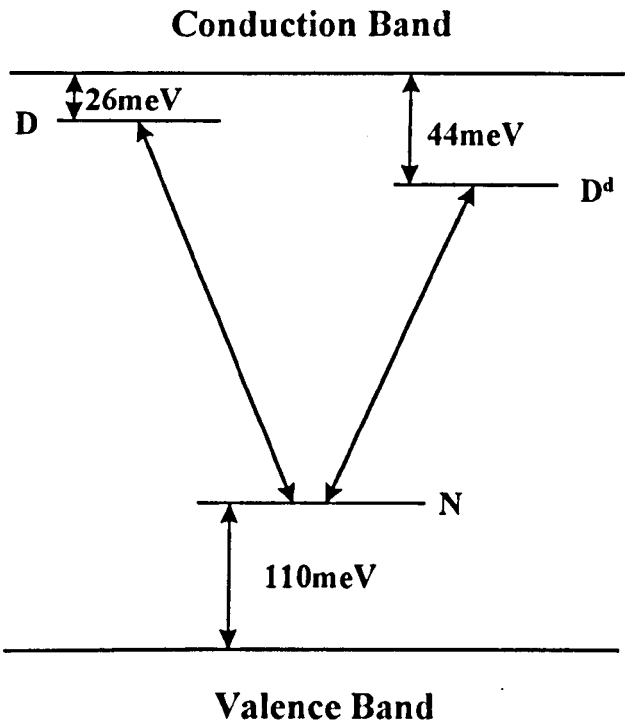

6.5 EXPERIMENTAL RESULTS FROM DOPED ZnSe AND ZnSe BASED COMPOUNDS

6.5.1 Typical Results from ZnSe:I and ZnSe:N

It is necessary to ensure that the doping profile through the layer is uniform and that changing from the n to p-type doping produces a suitably narrow junction region. In the case of LED's and semiconductor heterojunction lasers the pn junction coincides with an active region consisting of quantum wells.

In order to investigate the controllability of doping ZnSe, both n and p-type, a series of samples were planned covering the possible doping range. Throughout the doping series the Zn:Se flux ratio was maintained at unity and a substrate growth temperature of ~330°C as these conditions provided the best quality undoped ZnSe. The flux ratio was maintained by monitoring the RHEED to ensure that the mixed 2x1 & c(2x2) pattern was visible. All of the samples were grown on n-type GaAs substrates doped with Si to a level of 10^{19} cm^{-3}.

In the case of the n-type doping, control of the iodine flux was obtained by varying the current passed through the AgI pellets while maintaining a constant temperature of the iodine source. In this manner doping of ZnSe with iodine was obtained in the range N_d-N_a of 4×10^{16} cm^{-3} to 1.3×10^{19} cm^{-3}.

P-type doping control was achieved by varying the R.F. power applied to the nitrogen plasma source producing doping levels from 8×10^{16} cm^{-3} to 4×10^{17} cm^{-3} for a chamber pressure of 2×10^{-6} mbar.

Two reference samples were also grown under identical conditions to the respective doped samples. For the n-type doped a sample was grown with the iodine shutter open but with no current applied to the pellets and for the p-type a second sample was grown with a flow of nitrogen through the source to give a chamber pressure of 2×10^{-6} mbar but with no applied R.F. power to activate the nitrogen. From these two samples the nominally undoped level of ZnSe was compared and was found to be the same.

The variation of carrier concentration with applied current to the iodine electrochemical cell is as shown in Figure 6-9, from which it can be seen that the carrier concentration is a linear function of the applied current.

6.5.2 Photoluminescence and Capacitance-voltage Profiles for Doped ZnSe

As mentioned previously, not only must doping be to the required level but it must also be uniform throughout the layer. In Figure 6-10 the CV profile obtained using a BIORAD capacitance-voltage profiler for a ZnSe:I n-type layer (HWA 550) is shown. The doping profile for the layer is uniform with a carrier concentration of 1.4×10^{18} cm^{-3}. The higher level is due to the substrate doping which is doped at 10^{19} cm^{-3}. The dip at the interface between epilayer and substrate which is common with all of the samples in this series apart from the highest doped, is possibly due to an initial lag time for the production of iodine at the platinum electrode when using low current. Another possible explanation is As diffusion from the GaAs substrate.[42] However, the flat doping profiles were obtained over the rest of the sample range as can be seen from Figure 6-11 which shows the C-V profiles for HWA 547 and 553 with carrier concentrations of 1.1×10^{16} cm^{-3} and 1.3×10^{19} cm^{-3} respectively.

Figure 6-9: Carrier concentration vs iodine cell applied current

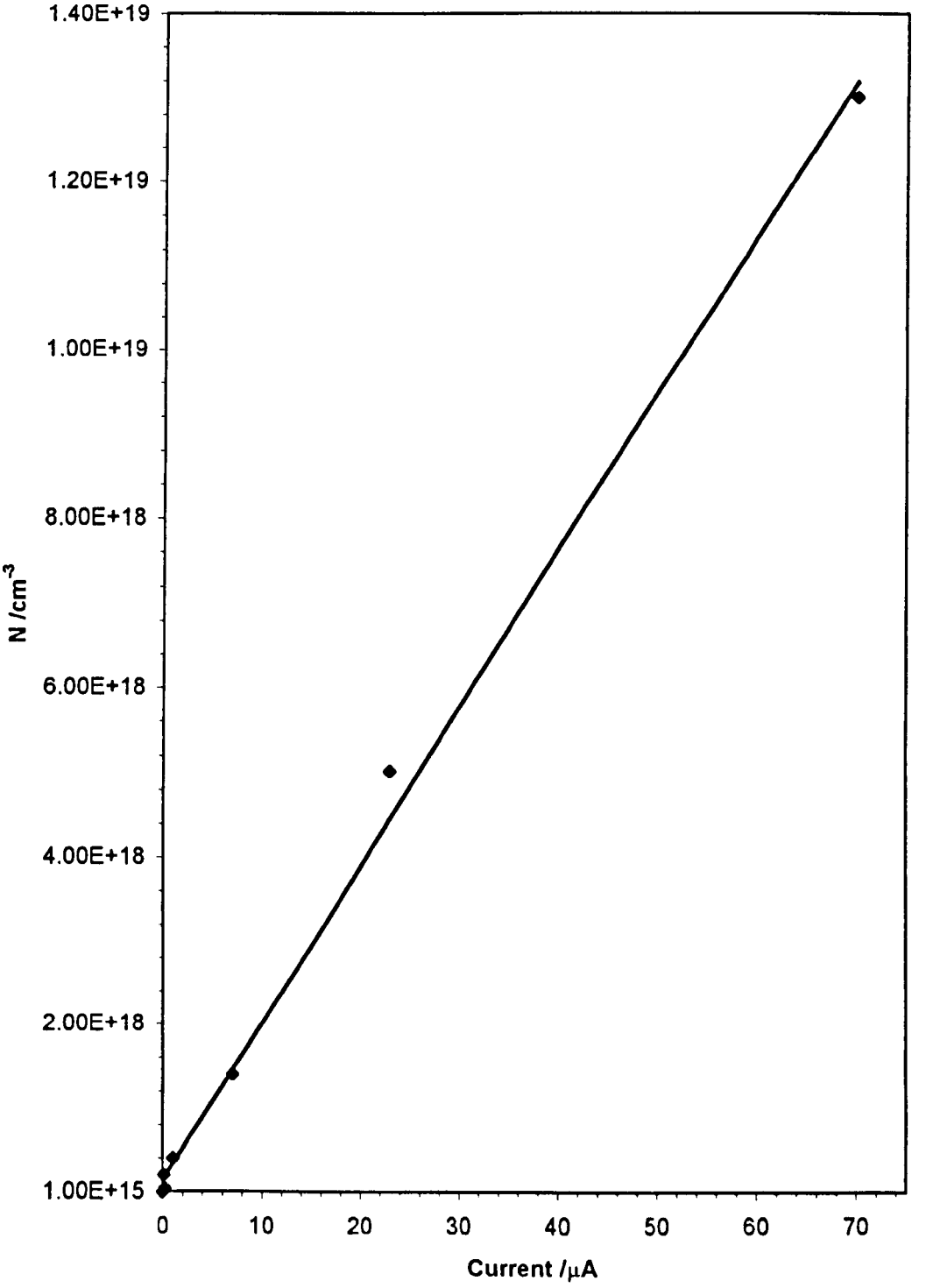

Figure 6-10: C-V profile of HWA 550

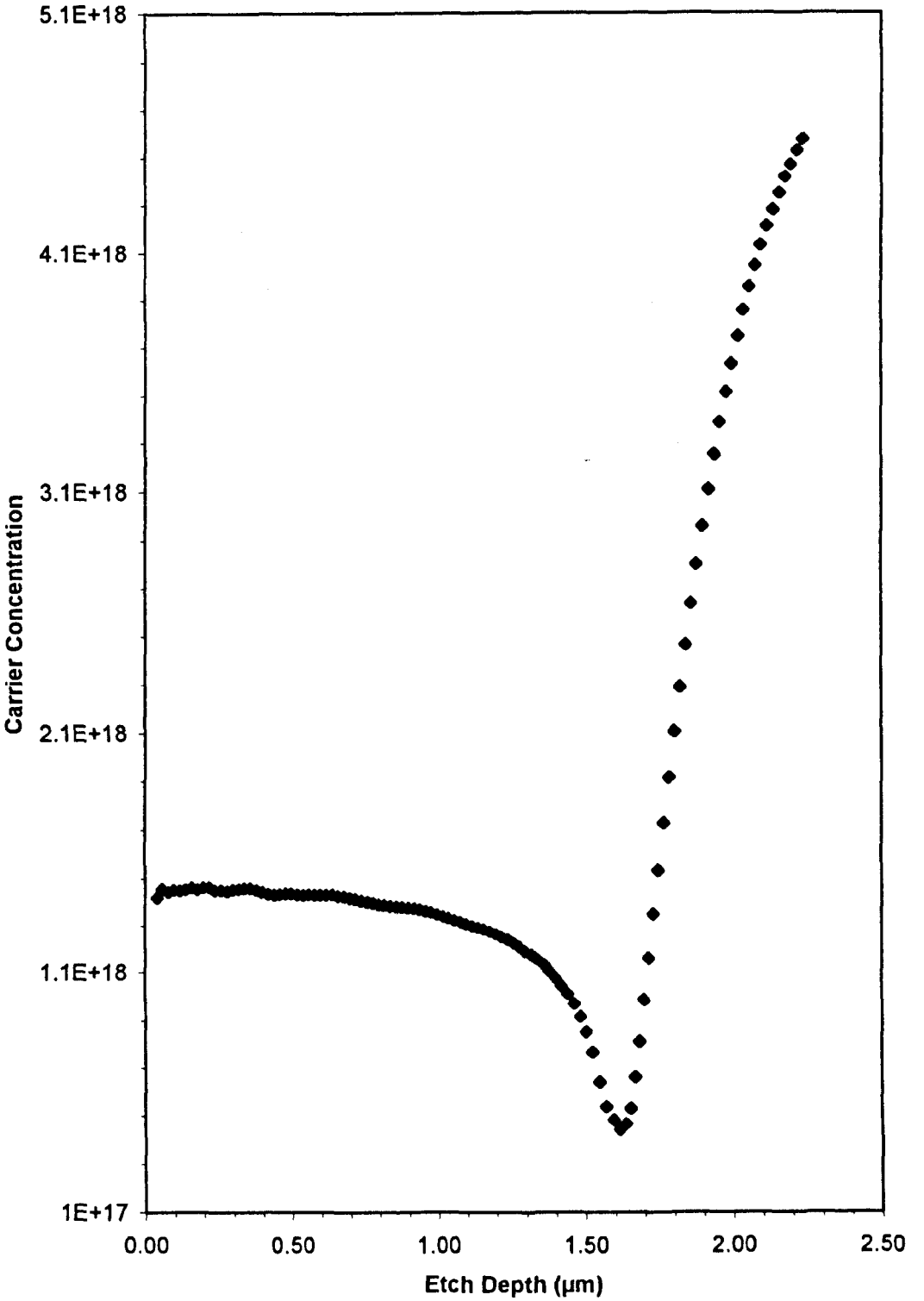

Figure 6-11: C-V profiles of HWA 547 and HWA 553 ZnSe:I epilayers

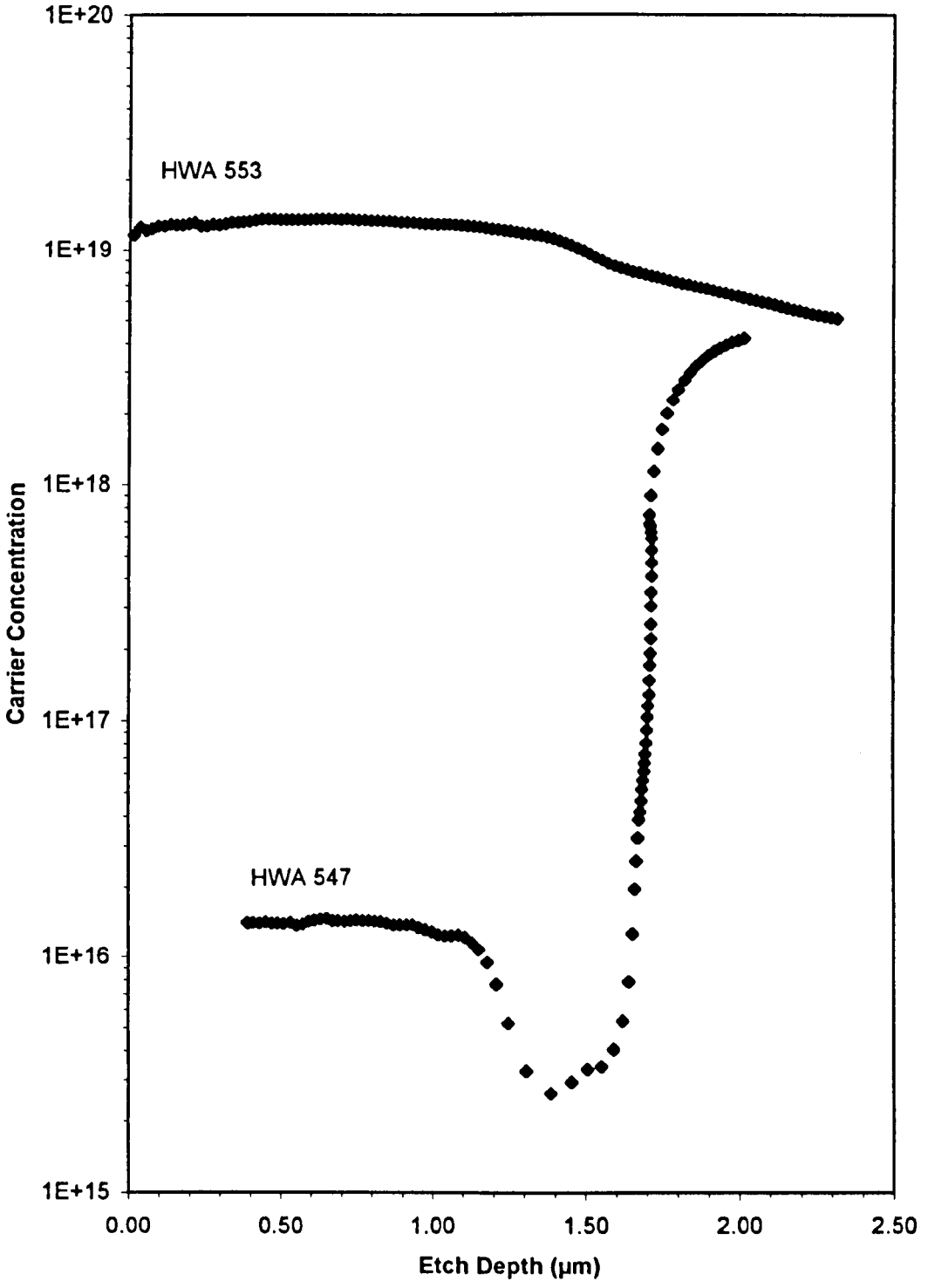

Photoluminescence spectra were also obtained for the samples and are shown in Figure 6-12, the PL from an undoped ZnSe layer is also included. As the carrier concentration increases it can be observed that the donor bound peak increases in intensity and broadens as well as exhibiting a blue shift. This blue shift has also been observed in Cl doped material[43] where it is attributed to a combination of the screening effect of donor electrons on excitons and the Stark effect due to charged impurities in bound excitons.

A CV profile obtained from p-type ZnSe:N is shown in Figure 6-13 shows a typically flat characteristic corresponding to a carrier concentration of 8×10^{16} cm^{-3}.

6.5.3 Doping of ZnSSe and ZnMgSSe

In order for the ternary and quaternary materials described in Chapter 5 to be incorporated in to electrically pumped laser structures, it is necessary to be able to dope ZnSSe and ZnMgSSe both n and p-type. As was described in Chapter 5 the best conditions for material quality is achieved at a VI:II ratio of 1:1 which provides the best morphology samples. It had been proved that the n and p-type doping of ZnMgSSe was possible using Cl and N, respectively.[44] The doping characteristics of ZnSSe had also been investigated and had already been used in a number of laser structures. The main problem which had been found was that as the bandgap of the quaternary alloy was increased the net acceptor concentration decreased. The maximum net acceptor level quoted for a ZnMgSSe layer with a bandgap of 3.05 eV was 2.5×10^{16} cm^{-3} which represents the upper limit for device fabrication as this is only one order of magnitude greater than the intrinsic level of $\sim 10^{15}$ cm^{-3}.[44] Also, as the A chamber of the Heriot-

Figure 6-12: PL of ZnSe:I samples

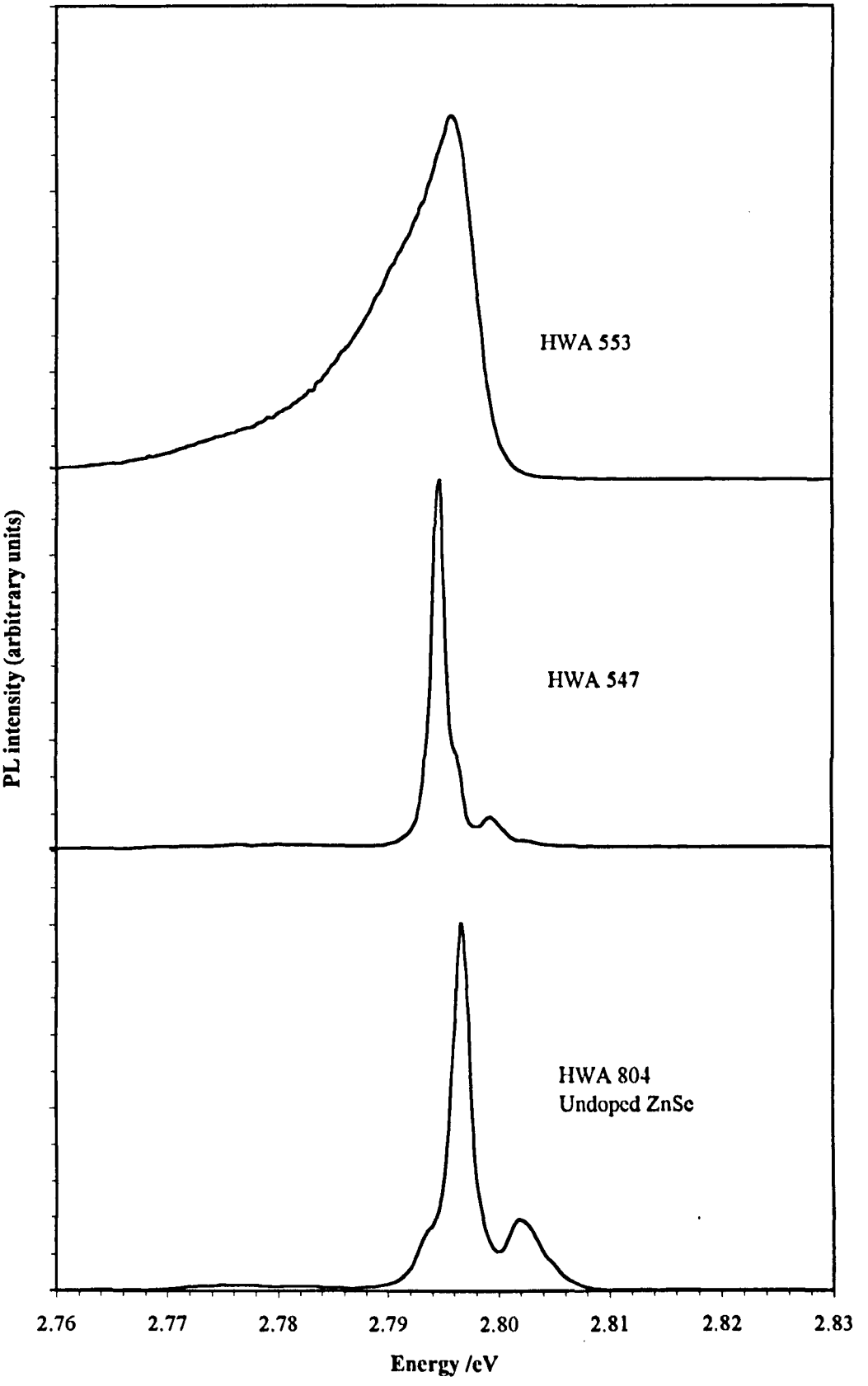

Figure 6-13: C-V of HWA 557 ZnSe:N

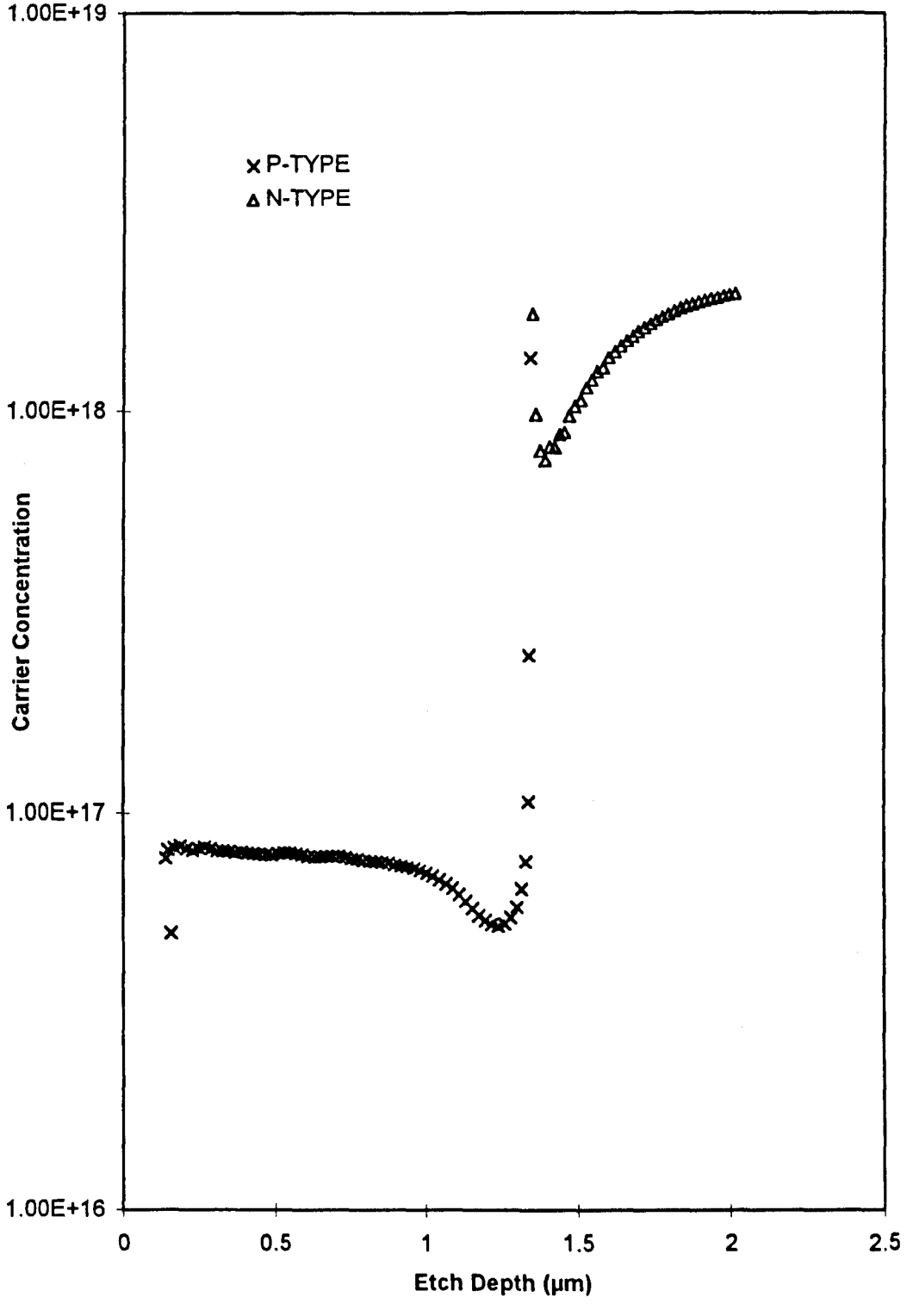

Watt growth machine only had an electrochemical iodine source as the n-type dopant it was necessary to confirm that doping of the quaternary was possible.

In the case of ZnSSe, the highest doped n-type sample grown was HWA 628, with a carrier concentration of 1.5 x 10^{18} cm^{-3}, grown at a substrate temperature of 280 °C (pyrometer) with a pellet current of 10 μA. The maximum p-type ZnSSe (HWA 626) had N_A-N_D of 2.2 x 10^{17} cm^{-3} grown with a R.F. power of 300W at a substrate temperature of 280 °C Therefore, it was possible to grow both n and p-type doped ZnSSe.

Similarly, for ZnMgSSe samples with a bandgap of ~2.9 eV at 4K were grown to investigate the doping characteristics. Again, using the iodine cell ZnMgSSe was obtained with carrier concentrations upto 8 x 10^{18} cm^{-3} at a substrate temperature of 280 °C. This proved once again that the iodine electrochemical cell provided a more than adequate alternative to Cl. The PL for sample HWA 649 shows the characteristic donor bound exciton emission common to heavily n-doped material.

Nitrogen doping of ZnMgSSe was achieved with N_A-N_D of 1.5 x 10^{17} cm^{-3} with sample HWA 675, the C-V profile of which is shown in Figure 6-14. This layer again had a bandgap of approximately 2.9 eV and was grown at 280 °C.

It was then possible to grow laser structures using the quaternary and ternary layers, the C-V profile of such a laser is shown in Figure 6-15. From this figure it can be seen that the laser structure sample HWA 640 had an average carrier concentration of 7 x 10^{18} cm^{-}

Figure 6-14: C-V of HWA 675 ZnMgSSe:N

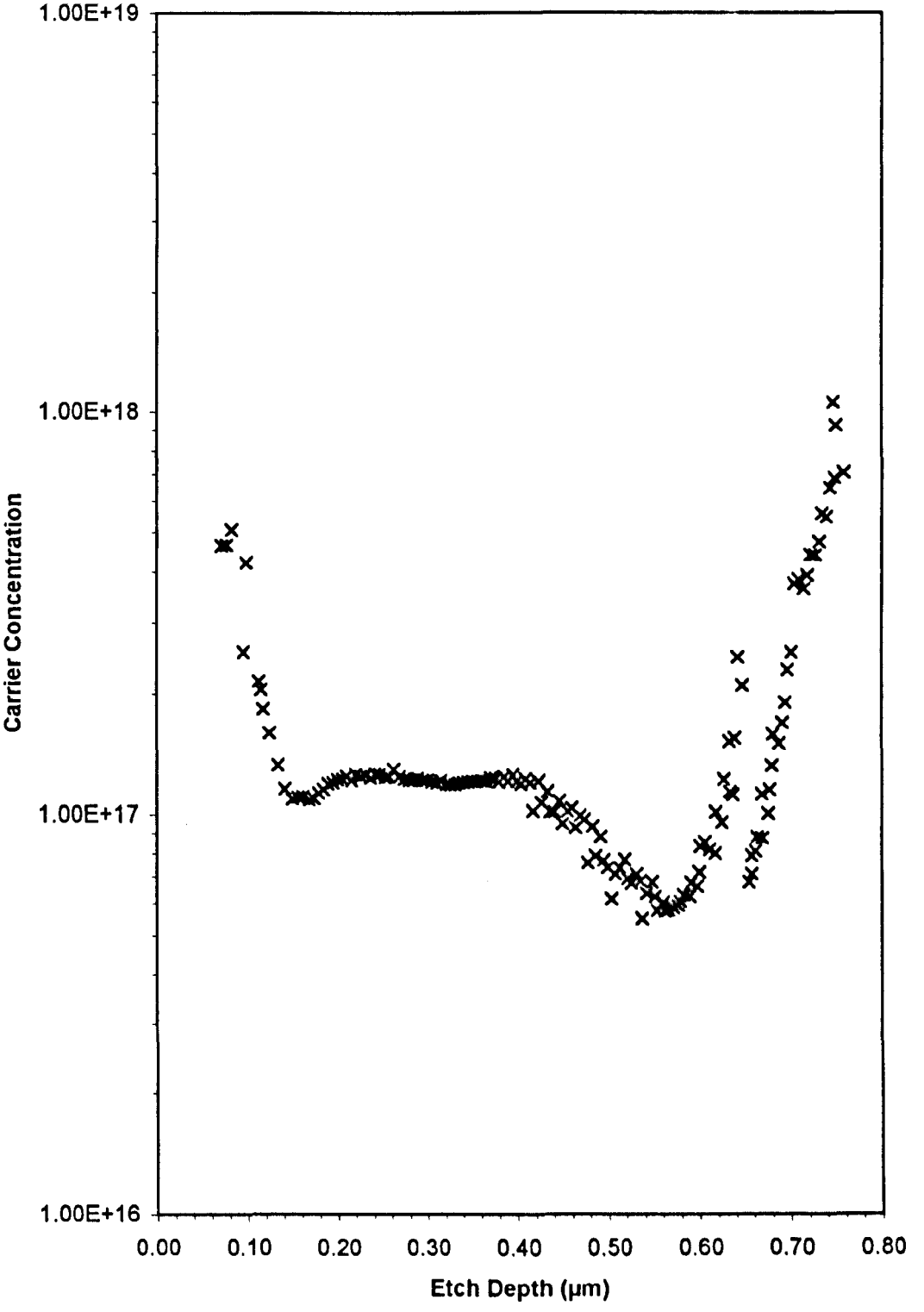

Figure 6-15: C-V profile of HWA 640 quaternary laser structure

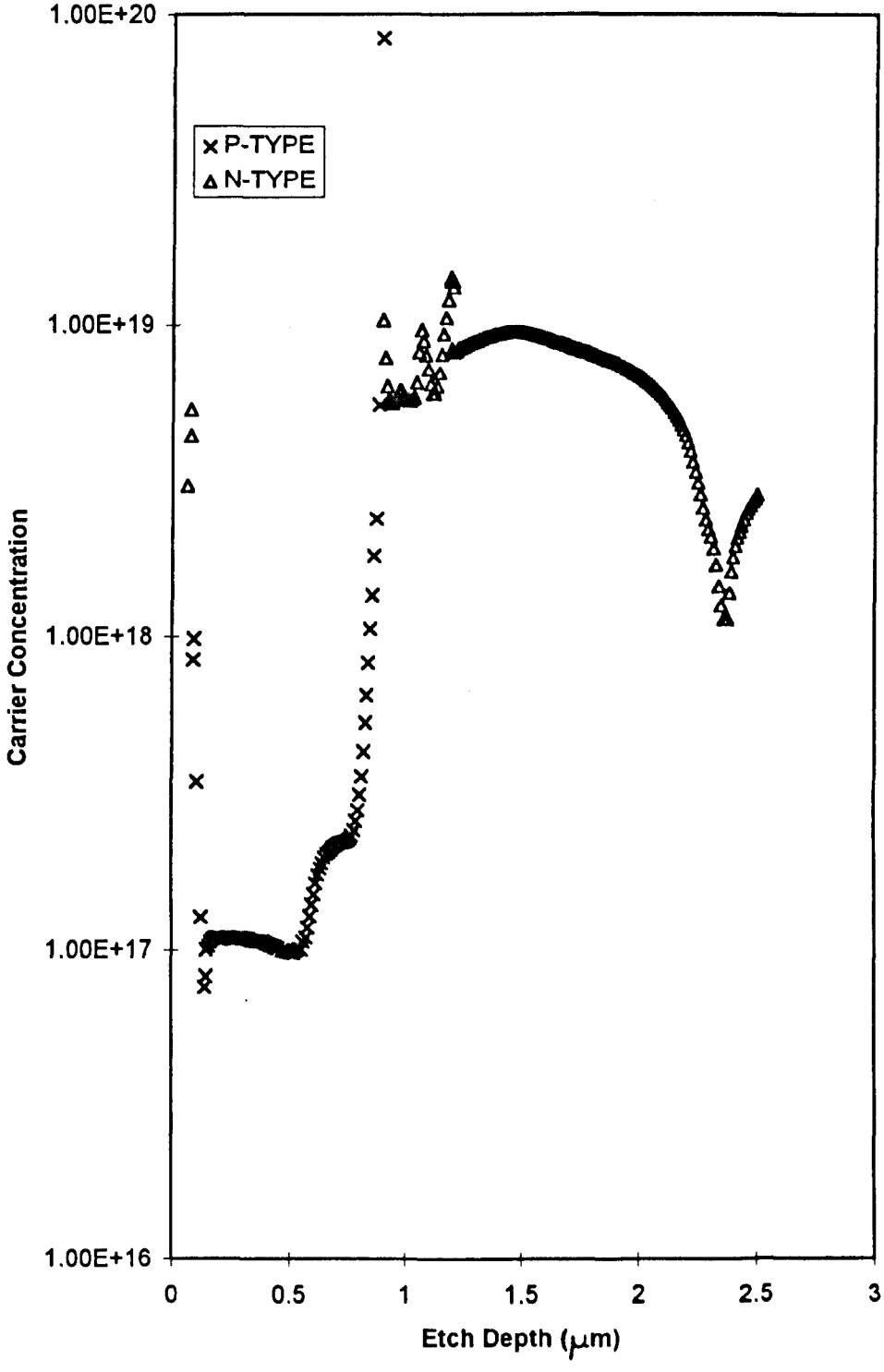

^{2} throughout the lower n-type layers, 3 x 10^{17} cm^{-2} for the ZnSSe layer, 1 x 10^{17} cm^{-2} in the ZnMgSSe layer and 5 x 10^{17} cm^{-2} in the ZnSe cap layer.

6.6 LASER PATTERNING OF DOPED ZnSe

As the Vacuum Generators 288 MBE system used at the start of this project was designed specifically to operate without rotation of the sample during growth, it was possible to investigate the effects of above bandgap irradiation of the growing ZnSe surface by illuminating a part or all of the sample during growth. Work at Heriot-Watt had previously shown that the generation and subsequent separation of electron-hole pairs can cause a change in the ZnSe layer grown, due to the arrival of holes at the semiconductor surface.

At high intensities (1-4 W cm^{-2}), selenium may be preferentially desorbed from the surface leading to a reduction in the growth rate[45,46] when the Se/Zn ratio at the growth surface falls below unity, while at lower intensities (~200 mW cm^{-2}) local reductions exceeding one order of magnitude occur in the donor concentration when iodine is used as a dopant.[47] This phenomenon could possibly be used to form isolation between devices. Therefore, given suitable imaging optics were available and machine limitations, such as vibration, were controllable then it should be possible to spatially pattern the doping of the ZnSe sample during growth.

The optical arrangement used is shown schematically in Figure 6-16. This was designed to project an optical grating onto the surface of the sample. A diffraction grating and cylindrical lens form a first order diffraction pattern comprising 8 lines of equal intensity

Figure 6-16: Optical arrangement used to produce doping patterns in ZnSe:I

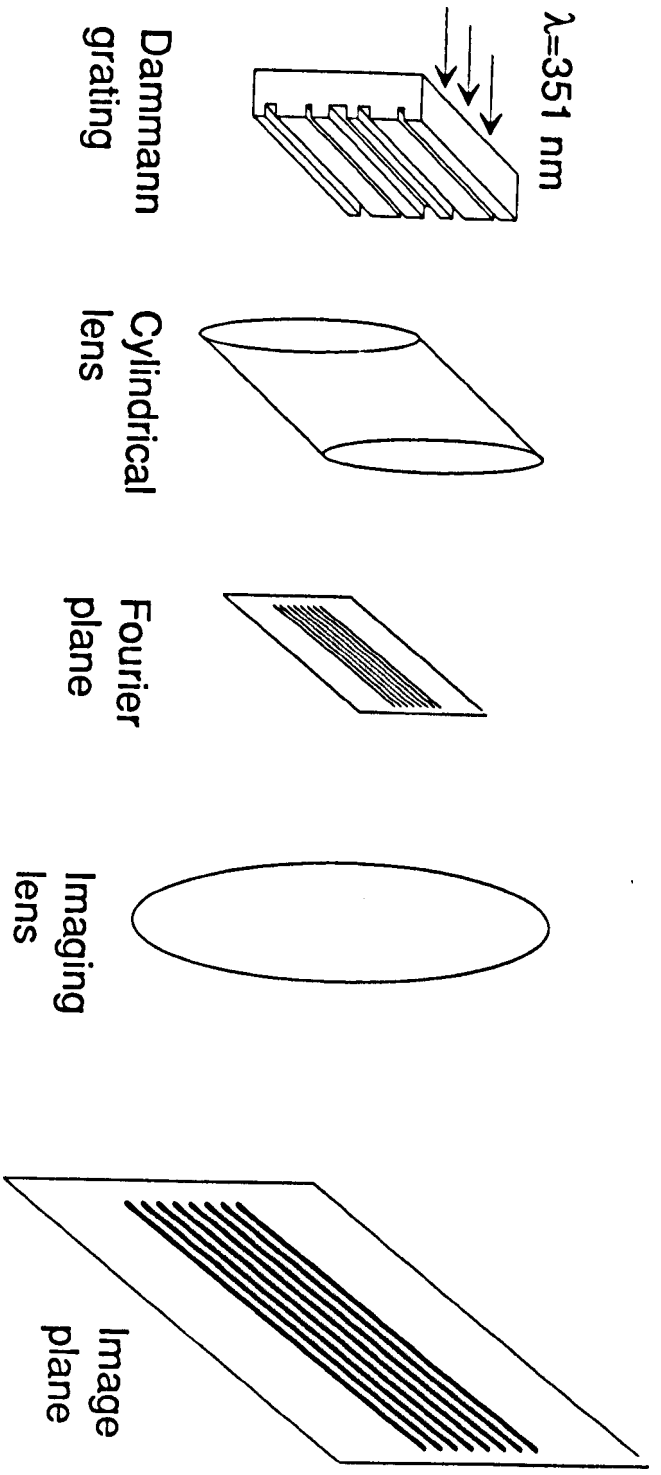

in the back focal plane of the cylindrical lens. Higher order diffraction patterns are also formed at either side. Then using an imaging lens this diffraction pattern is focused onto the surface of the sample Approximately 80% of the light incident on the grating is incorporated into the central first order pattern, with the remaining intensity falling into the higher orders.

The diffracted image was projected on to the sample through a purpose built viewport incorporating an internal heated window operated constantly at ~400°C (Figure 6-17). At this temperature, the internal window remained free of any deposits as any material on the window is re-evaporated ensuring that there were no scattering centres in the beam as this would produce a rough surface.

In order to investigate the resolution of the technique two ZnSe:I layers were grown at different intensities of incident light, the cathodoluminescence from these layers was then studied at 10 K using a Cambridge Stereoscan 150 Mk2 SEM equipped with a LaB_6 source operated at 10 kV as described in detail elsewhere[48].

The first sample (MBE 379) was grown at 280°C with a Se:Zn flux ratio of 1.5:1. A standard thermal desorption using RHEED was performed (as described in Chapter 3), the laser had been run for a number of hours previously in order to give a stable output of UV light. A Coherent Innova I200 Kr ion laser operating at 350.7nm was used to provide the high intensity radiation required. The power of the laser was adjusted to provide an average illumination intensity of 2 W cm^{-2} in the first order diffraction pattern, which had lines with FWHM of 128 μm. The photoluminescence observed from this sample was as shown in Figure 6-18. Close to the centre of the wafer was a clearly

Figure 6-17: Heated window arrangement

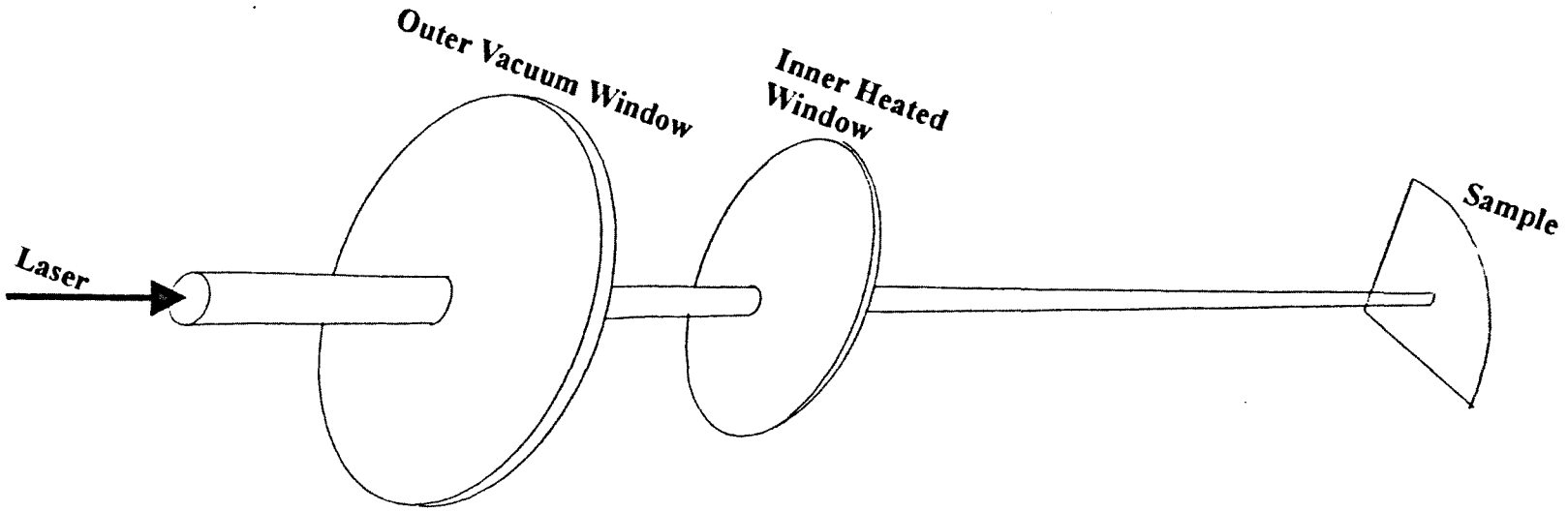

Figure 6-18: Photoluminescence from sample MBE 379 at room temperature

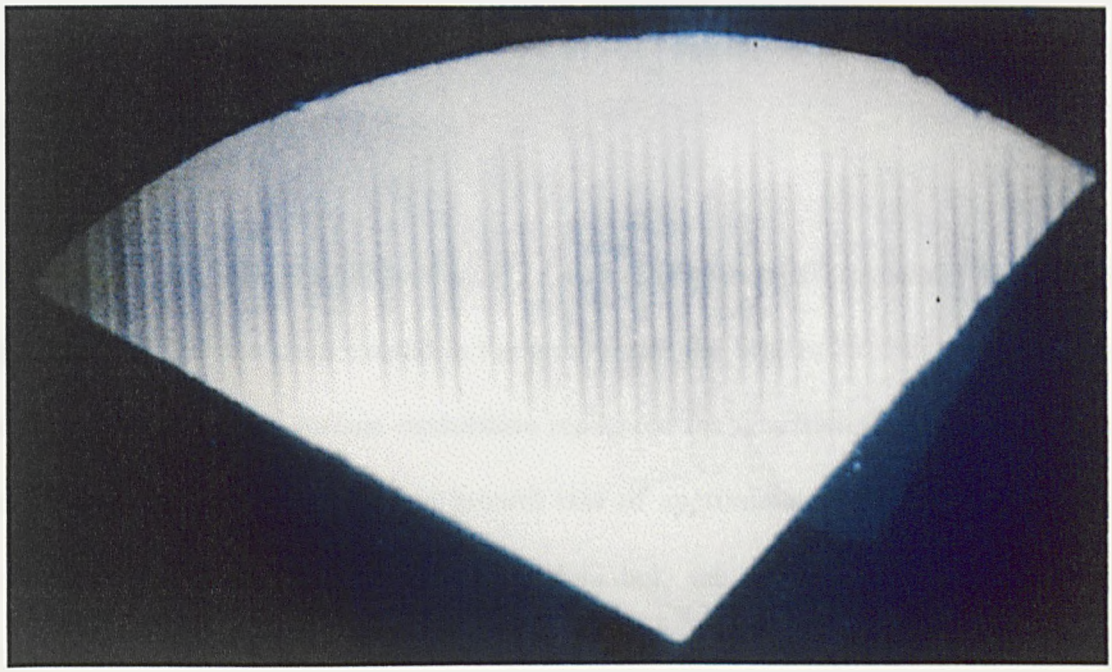

defined set of 8 dark lines with a period of 532 μm corresponding to a negative image of the first order diffraction pattern produced by the diffraction grating. At either side of this pattern were several sets of dark lines produced by the higher orders. The dark lines were areas where the donor concentration had been reduced by the incident illumination and the donor bound excitonic emission was weaker. The donor concentration of the bulk material, outwith the patterns, was $7x10^{17}$ cm^{-3} measured by capacitance-voltage profiling.

In addition to this, a DEKTAK profile of the surface (Figure 6-19) revealed that troughs approximately 200 nm deep existed in the area where the first order diffraction pattern had been focused. This surface modulation replicated the Gaussian profile of the beam and corresponded to a reduction in growth rate of approximately 20%. This growth modulation was repeated in the second orders but, the growth rate reduction was approximately 4%.

A second sample (MBE 380) was grown, where the illumination intensity was reduced to 0.4 W cm^{-2} at FWHM and the modulation period to 300 μm by readjusting the focus of the optics to project a pattern with a much smaller feature size. In this case the modulation of the sample surface was reduced to ~30 nm, a growth rate reduction of ~3% (Figure 6-20) which is far more acceptable than the 20% reduction previously obtained. From the cathodoluminescence image, Figure 6-21, it was observed that in addition to the intended 300 μm period stripes, a superimposed series of lines with a period of 40 μm are visible. These lines were unintentional and resulted from a slight mis-alignment of the optics. However, they show that with the proper imaging system, the possibility of patterning a structure on a scale of microns exists.

Figure 6-19: Surface profile of sample MBE 379

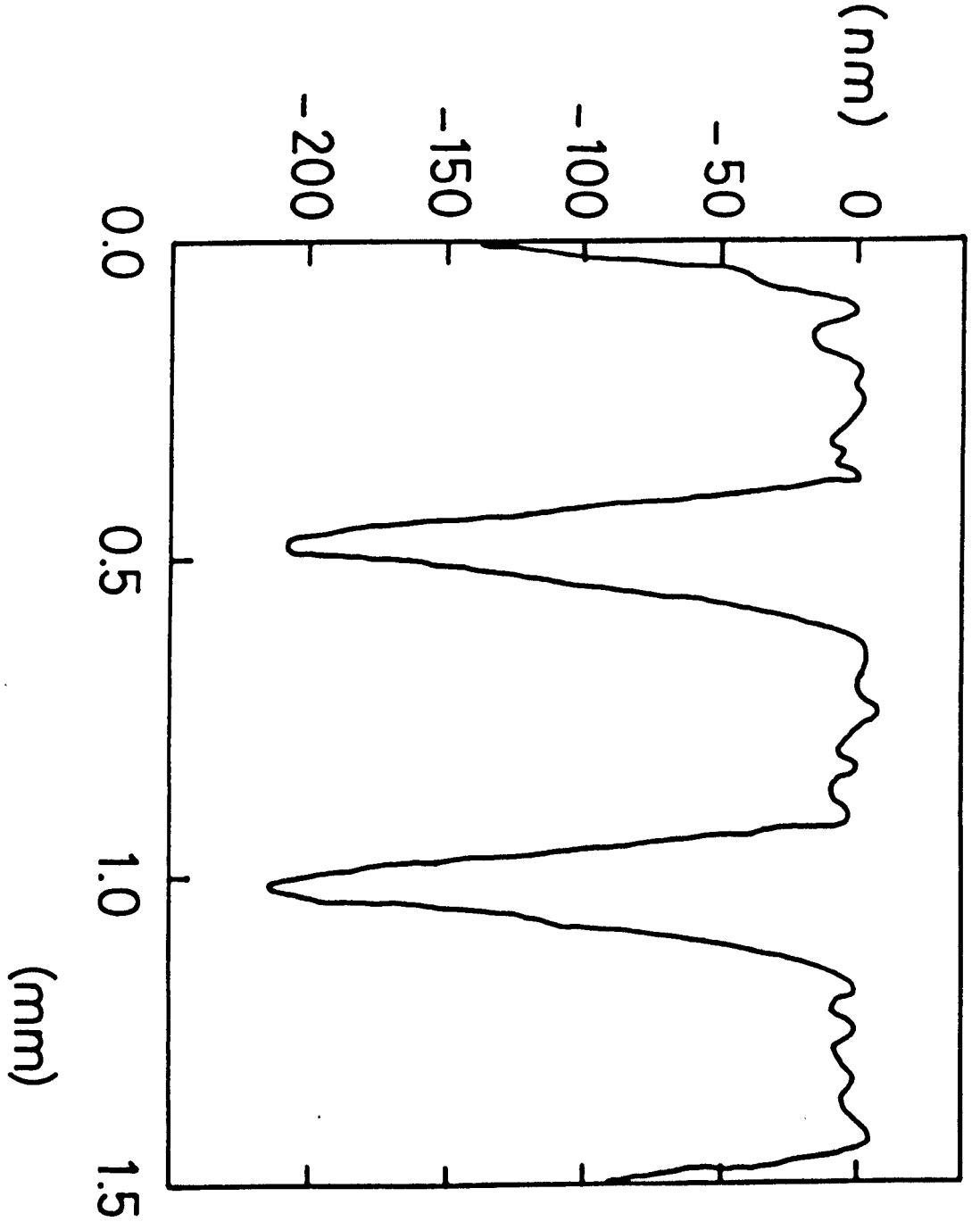

Figure 6-20: Surface profile of sample MBE 380

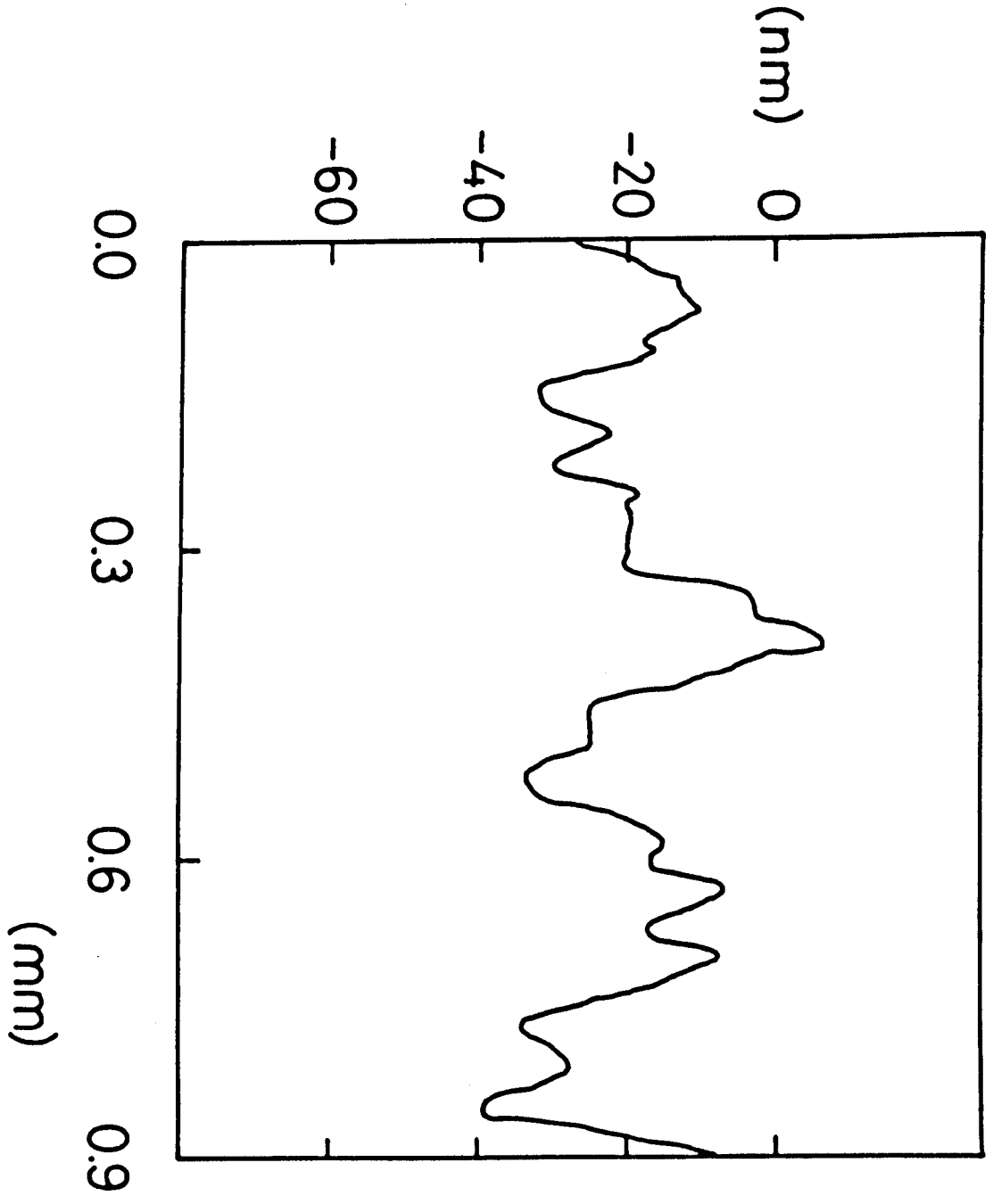

Figure 6-21: Cathodoluminescence from MBE 380

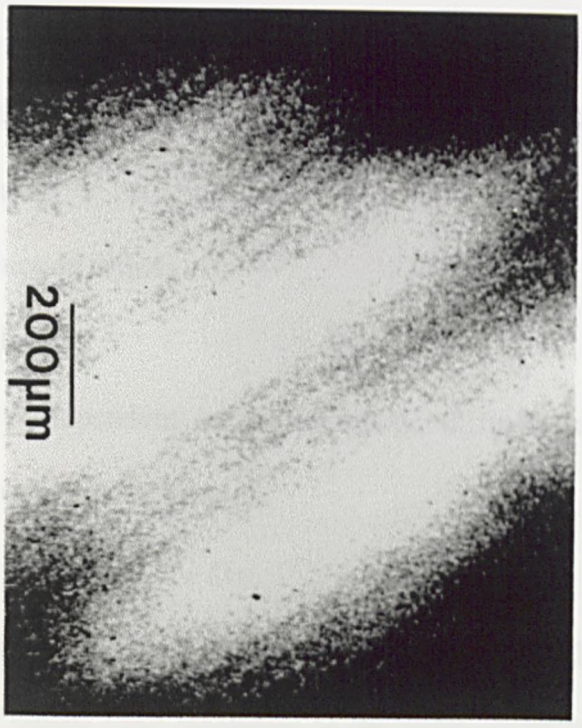

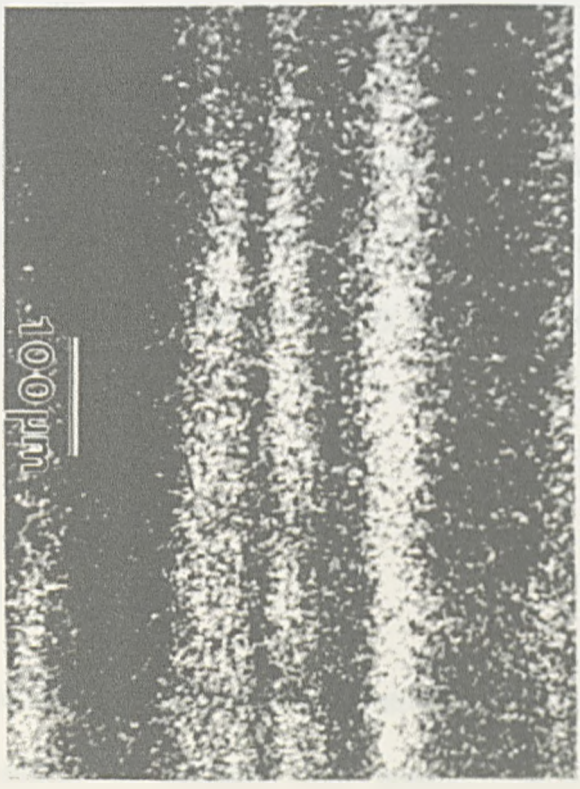

The samples were examined using an optical microscope to confirm that the specular morphology of the non-illuminated areas was maintained. This was found to be the case, highlighting the effectiveness of the heated window arrangement.

The ultimate resolution of this technique is dependent on three factors:

i) carrier diffusion

ii) optical diffraction effects

iii) machine vibration

The carrier diffusion is dependent on the ambipolar diffusion coefficent, D, and the carrier lifetime, τ, according to the relation:

$$x^2 = D\tau \qquad 6.2$$

where x is distance. In the case of ZnSe $D = 2.5$ cm^2s^{-1} and $\tau = 250$ ps[49] giving a value of 0.25 μm.[50] Diffraction effects limit resolution to the order of the wavelength of the light used, in this case 350.7 nm. In order to achieve such a spatial resolution, an incident beam of f/# ~ 1 would be required, however this has to be regarded as impractical using existing MBE technology. In this experiment, the spatial resolution obtained is limited by the low f/# optical system used (f/# ~ 20). Finally, the effects of machine vibration may be reduced to sub-micron levels as demonstrated by the use of electron beam writing in MBE.[51]

6.7 CONCLUSIONS

It has been demonstrated in this chapter that the control of doping of ZnSe using I and N is possible and a number of samples were produced with a range of carrier concentrations. The doping of ZnSSe and ZnMgSSe was also discussed.

The ability to pattern iodine doped layers was shown to be possible using the appropriate optics. Patterns with features of the order of a few 10's of microns were achieved and with some development it is felt that it should be possible to produce patterns in the micron scale with a possible view to device fabrication using such techniques.

6.8 REFERENCES

[1] T. Yao, Y. Makita and S. Maekawa, Appl. Phys. Letters 35 (1979), 97

[2] T. Yao, M. Ogura, S. Matsuoka and T. Morishita, Appl. Phys. Letters 43 (1983), 499

[3] I. Suemune, K. Ohmi, T. Kanda, K. Ykutake, Y. Kan and M. Yamanashi, Japan. J. Appl. Phys., 25 (1986), L827

[4] N. Kobayashi, Japan. J. Appl. Phys., 27 (1988), L1597

[5] W. Stutius, Appl. Phys. Lett., 38 (1981), 352

[6] W. Stutius, J. Cryst. Growth 59 (1982), 1

[7] A. Kamata, T. Uemoto, M Okajima, K. Hirahara, M. Kawzchia and T. Beppu, J. Cryst. Growth 86 (1988), 285

[8] S. Fujita, K. Terada, T. Sakamoto and S. Fujita, J. Cryst. Growth 92 (1989), 102

[9] H. Kukimoto in *Growth and Optical Properties of Wide-Gap II-VI Low Dimensional Semiconductors*, edited by T. C. McGill, C. M. Sotomayer Torres and W. Gebhardt (Plenum Press, New York 1989), 119

[10] N. Shibita, A. Ohki and A. Katsui, J. Cryst. Growth 95 (1989), 703

[11] H. Kukimoto, Materials Research Society Symp. Proc. Vol. 161, 91

[12] K. Ohkawa, T. Mitsuyu, and O. Yamakazi, J. Appl. Phys. 62 (1987), 3216

[13] H. Cheng, J. M. DePuydt, J. E. Potts and M. A. Haase, J. Cryst. Growth 95 (1989), 512

[14] M. A. Haase, J. Qui, J. M. DePuydt and H. Cheng, Appl. Phys. Lett. 59 (1991), 1272

[15] Z. Zhu Personal Communication.

[16] A. Mowbray and R. G. Jones, J. Vac. Sci. Technol. A7 (1989), 3373

[17] G. J. Davies, D. A. Andrews and R. Heckingbottom, J. Appl. Phys. 54 (1983), 7214

[18] D. A. Andrews, R. Heckingbottom and G. J. Davies, J. Appl. Phys. 54 (1983), 4421

[19] J. M. Wallace, K. A. Prior, B. C. Cavenett, J. J. Hunter, S. J. A. Adams and M. J. L. S. Haines, Mat. Res. Symp. Proc. 161 (1990), 163

[20] J. Simpson, J. M. Wallace, S. Y. Wang, H. Stewart, J. J. Hunter, S. J. A. Adams, K. A. Prior and B. C. Cavenett, Semicond. Sci. Technol. 7 (1992) 464

[21] M. S. Tyagi, in *Introduction to Semiconductor Materials and Devices*, published by John Wiley and Sons., 1991

[22] C. H. Henry, Phys. Rev. B4 (1971), 2453

[23] M. A. Haase, H. Cheng, J. M. DePuydt and J. E. Potts, J. Appl. Phys. 67 (1990), 448

[24] J. DePuydt, M. A. Haase, H. Cheng and J. E. Potts, Appl. Phys. Letters 55 (1989), 1103

[25] H. Cheng, J. M. DePuydt, J. E. Potts and M. A. Haase, J. Cryst. Growth 95 (1989), 512

[26] G. F. Neumark, J. Appl. Phys. 51(1980), 3383

[27] T. Yodo and K. Yamashita, Appl. Phys. Letters, 54 (1989), 1178

[28] T. Yao and T. Taguchi, Proceedings of 13th International Conference on Defects in Semiconductors (1984), 1221

[29] Helen Stewart, PhD Thesis 1996

[30] H. Stewart, J. Simpson, S. Y. Wang, I. Hauksson, S. J. A. Adams, K. A. Prior and B. C. Cavenett, J. Cryst. Growth, 127 (1993), 379

[31] R. N. Bhargava, J. Cryst. Growth 59 (1982)

[32] A. Ohki, N. Shibita and S. Zembutsu, Jap. J. Appl. Phys. 27 (1988), L909

[33] R. M. Park, M. B. Troffer, C. M. Rouleau, J. M. DePuydt and M. A. Haase, Appl. Phys. Lett. 57 (1990), 2127

[34] K. Ohkawa, T. Karawasa and T. Mitsuyu, J. Cryst. Growth 111 (1991), 797

[35] C. T. Walker, J. M. DePuydt, M. A. Haase, J. Qui and H. Gheng, Physica (Utrecht) 185B (1993), 27

[36] J. Qui, H. Cheng, J. M. DePuydt and M. A. Haase, J. Cryst. Growth 127 (1993), 279

[37] K. A. Prior, Phys. Stat. Sol. (b), 187 (1995), 379

[38] T. Yao and Z. Zhu, Phys. Stat. Sol. (b), 187 (1995), 387

[39] T. Yao, Z. Zhu, Y. H. Wu, C. D. Song, F. Nishimaya, K. Kimura, H. Kajiyama, S. Miwa, and T. Yasuda, J. Cryst. Growth, 159 (1996), 214

[40] I. S. Hauksson, J. Simpson, S. Y. Wang, K. A. Prior and B. C. Cavenett, Appl. Phys. Lett., 61 (1992), 2208

[41] Z. Zhu, G. D. Brownlie, P. J. Thompson, K. A. Prior and B. C. Cavenett, Appl. Phys. Lett., 67 (1995), 3762

[42] I. M. Dharmadasa, private communication

[43] K. Okhawa, T. Mitsuyu and O. Yamakazi, J. Appl. Phys. 62 (1987), p3216

[44] H. Okuyama, Y. Kishita, T. Miyajima, A. Ishibashi and K. Akimoto, Appl. Phys. Lett., 64 (1994), 904

[45] J. Simpson, S.J.A. Adams, J.M. Wallace, K.A. Prior, and B.C. Cavenett, Semicond. Sci. Technol. 7 (1992) 460.

[46] J. Simpson, S.Y. Wang, I. Hauksson, H. Stewart, S.J.A. Adams, K.A. Prior and B.C. Cavenett, J. Crystal Growth 127 (1993) 327.

[47] J. Simpson, S.J.A. Adams, S.Y. Wang, J.M. Wallace, K.A. Prior, and B.C. Cavenett, , J. Crystal Growth 117 (1992) 134.

[48] G.M. Williams et al, Microscopy of Semiconducting Materials 1991, Inst. Of Phys Conf. Ser. 117, Eds. A.G. Cullis and N.J. Long (Inst. Phys., Bristol, 1991) p. 695.

[49] J. S. Massa, G. S. Buller, A. C. Walker, J. Simpson, K. A. Prior and B. C. Cavenett, Appl. Phys. Lett. 64 (1994), 589

[50] J. A. Bolger, A. K. Kar, B. S. Wherrett, K. A. Prior, J. Simpson, S. Y. Wang and B. C. Cavenett, Appl. Phys. Lett. 63 (1993), 571

[51] E. Linfield, Personal communication

7. CONCLUSIONS AND FURTHER WORK

7.1 INTRODUCTION

Over the duration of this study a number of advances were made in the attempt to produce a room temperature blue laser diode from II-VI based semiconductors. The most successful group were Sony, who in 1996 reported a CW room temperature laser with a lifetime of 100 hours using a structure containing ZnSSe and ZnMgSSe layers.[1]

At Heriot-Watt, by 1993 it became clear that the MB 288 MBE system being used was no longer capable of effectively competing in this field due to limitations on the number of K-cell sources which could be used. A more modern replacement system was purchased, a V 80H twin chamber MBE machine. As this system had previously been used for III-V research it required considerable cleaning and refurbishment. After this work had been carried out and after initial characterisation of the system, the V 80H produced high quality II-VI epilayers. As well as research towards the realisation of a quaternary laser structure, studies into the heteroepitaxial growth and doping of ZnSe were undertaken. The results and conclusions drawn from these studies are summarised in this chapter as well as a discussion of suggested further work.

7.2 ZnSe/GaAs HETEROINTERFACE

Transmission electron microscope (TEM) studies were performed on very thin layers of ZnSe grown on (100) GaAs substrates. From the thinnest of these samples, HWA 475, (estimated 0.2 nm) the TEM results, although not able to confirm the presence of ZnSe, did highlight the occurrence of etch pits in the GaAs substrate. The density of etch pits was estimated to be 200 μm^{-1}. An attempt to confirm the presence of any ZnSe on the surface by EDX also failed to provide conclusive results. However, in the case of a 2 nm sample, (HWA 476), EDX studies did confirm the presence of ZnSe at the surface. Also, from the TEM analysis of this layer it was not possible to observe any etch pits in the GaAs surface. It was unclear whether the difference between this sample and the previous one which showed etch pits was due to a substrate etch problem or due to initial growth under group II and VI excess. However, these results did lead to a standardisation of GaAs substrate etch procedures within the group to ensure consistency between samples and growers.

A plan view TEM of HWA 476 revealed that no island formation could be observed on this sample, despite the fact that the thickness across the sample varied between 0.57 and 3.97 nm. The implication of this is that the layer may have been at the boundary of two-dimensional layer by layer growth.

7.3 DOUBLE CRYSTAL X-RAY DIFFRACTOMETRY

During this research a double crystal X-ray diffraction (DCXRD) system was purchased. The benefit of such a system to the grower is in its ability to provide rapid non-

destructive feedback regarding the quality and composition of epilayers. An indication of the structural quality of the epilayer can be found from the FWHM of the DCXRD rocking curves obtained. Also, in the case of multiple quantum well structures used for the production of modulators the interference pattern observed in the rocking curve can be used to determine the period of the quantum wells.

In a heteroepitaxial system, the difference in lattice parameters between the layer and the substrate results in a misfit strain. As DCXRD uses the diffraction of X-rays from the crystallographic planes within a crystal it is the ideal tool for observing the effects of misfit strain. It is also possible to simulate the effects of strain on the epilayer FWHM versus layer thickness through the use of simulation packages commercially available. From the results obtained it was observed that for pseudomorphic material, the FWHM versus layer thickness agrees with the theoretically predicted values but, for material epilayer thickness exceeding the critical layer thickness the FWHM is much higher than predicted. This discrepancy was due to the level of dislocations present in the material ($\sim 8 \times 10^7$ cm^{-2} for fully relaxed material) which could not be simulated using the package available.

An indication of the high quality of the ZnSe being produced at Heriot-Watt was the observation of thickness fringes (periodic oscillations) in the rocking curves for pseudomorphic ZnSe which can be used to calculate the thickness of the epilayer.

7.4 DOUBLE CRYSTAL X-RAY TOPOGRAPHY

Although the critical thickness of ZnSe on GaAs had been determined from other techniques such as DCXRD and photoluminescence (PL) to be of the order of 150 nm. However, the definition of the critical thickness is that thickness where the first misfit dislocation is formed. Unlike double crystal X-ray topography, (DCXRT), techniques previously used were unable to image this first defect directly but, instead relied on the change of some other parameter with strain to estimate the critical thickness. Using the synchrotron facility at Daresbury, DCXRT was performed on a number of pseudomorphic ZnSe layers. For the first time misfit dislocations in ZnSe grown on GaAs substrates were observed and the critical thickness was determined to be 100±5 nm. This was significantly less than previous estimates.

The implication of this greatly reduced critical thickness extends to ternary and quaternary layers, for example the critical thickness of ZnCdSe may be proportionately less resulting in the possibility that a quantum well of 60 Å may already be relaxed with a high number of dislocations. In this case the active layer of any device may already have high numbers of defects which would severely limit the lifetime and performance.

7.5 GROWTH OF ZnSSe AND ZnMgSSe

The V 80H system enabled the Heriot-Watt group to investigate the growth of ZnMgSSe for the first time. Although ZnSSe had been grown on the MB 288 using an electrochemical sulphur source, in order to produce layers with a S content anywhere near the 6% required for lattice matching the growth rate had to be reduced to 0.05

μm/hr. This growth rate was approximately 10 times less than normal which is at the limits of practicality.[2] Therefore, for this study the source of sulphur was chosen to be the compound ZnS in a normal K-cell.

One of the problems encountered with the use of ZnS was due to its low vapour pressure which required the cell operating temperature to be in the region of 750°C. When at operating temperature it was not possible to obtain the 4x3 RHEED pattern of GaAs expected after thermal desorption of the oxide layer. This led to the first ZnSSe and ZnMgSSe layers produced to be of poor quality with high XRD FWHM and poor PL characteristics. Firstly, this problem was addressed by keeping the ZnS cell approximately 100°C below its operating value during thermal desorption of the GaAs then ramping the ZnS cell temperature while the substrate cooled to growth temperature. This approach worked and good quality lattice matched material was grown. Indeed, using this method laser structures were grown which operated just below room temperature under pulsed operation. The second method involved the use of a liquid nitrogen cooled shutter. This allowed the ZnS cell to be left at operating temperature during the oxide thermal desorption of the GaAs substrate, preventing the oscillations in ZnS flux due to the rapid temperature change occasioned by the first method. Better quality samples were obtained using this method as determined by the XRD FWHM. Unfortunately, there was not enough time in this study to incorporate these new techniques in a laser structure in order to determine if these improvements in the epilayers would have had any effect on device performance.

7.6 DOPING OF ZnSe AND ZnSe BASED COMPOUNDS

A number of ZnSe samples were grown using an iodine electrochemical cell and a nitrogen R.F. plasma source for n and p-type doping, respectively. The purpose of these samples was to investigate the controllability of the doping of ZnSe. It was found that controllable n-type doping was possible between 1.1 x 10^{16} cm^{-2} and 1.3 x 10^{19} cm^{-2} by varying the current applied to the electrochemical cell. In the case of p-type doping the range was 8 x 10^{16} cm^{-2} to 4 x 10^{17} cm^{-2} by changing the applied R.F. power.

The doping of ZnSSe and ZnMgSSe was also confirmed using the iodine electrochemical cell, n-type doping levels in the mid 10^{18} cm^{-2} range could easily be accomplished for both materials.

A novel method of patterning ZnSe:I during growth using above bandgap radiation was investigated. It had previously been shown that the use of U.V. illumination during the growth, producing electron-hole pairs, results in Se desorption from the surface and a reduction in the incorporation of iodine into the layer.[3,4] Using suitable optics, a diffraction pattern was projected onto the surface of a ZnSe:I sample during growth. A pattern corresponding to the image was visible, under U.V. illumination, on the sample after growth with a period of 532 μm. There was also a reduction in growth rate of approximately 20% in the illuminated areas. The illumination intensity was 2 W cm^{-2}.

A second sample was grown with a lower illumination power of 0.4 W cm^{-2} and the optics focused to produce a modulation period of 300 μm. The lower power resulted in a growth rate reduction of only 3% which was far more acceptable. In addition, due to a

slight mis-alignment of the optics a second pattern was superimposed with the intended 300 μm image. This pattern had a modulation period of 40 μm. These results showed that with the proper optical set-up patterning of the surface would be possible on a micron scale which would allow the possibility of patterning ridge waveguide lasers without the need for damaging post processing techniques. Unfortunately, this work could only be carried out on the MB 288 due to its static growth ability. To attempt this type of work on the V 80H, which is designed for rotation of the substrate during growth, it would be necessary to rotate the external optics at exactly the same frequency as the substrate.

7.7 FURTHER WORK

With the increasing use of non-(100) substrates becoming more common due to the possibility of producing devices utilising the piezoelectric effect, a continuation of the TEM studies on very thin layers in order to investigate the initiation of growth on such surfaces could prove valuable. For substrate orientations such as (111) the surface has a mixture of both (100) and (111) planes exposed and by changing the growth conditions it may be possible to make the epilayer either hexagonal or cubic in nature.

In this study the measurement of the critical thickness of ZnSe using DCXRT was performed. How these results affect ZnSe based ternary and quaternary materials is unclear. For materials such as ZnCdSe which are commonly used as the active quantum well region for devices an investigation of the critical thickness versus the composition would be of benefit in the design of such devices to ensure that the active region is as free from defects as possible. It could also provide an indication of the tolerance to

which nominally lattice matched material could be grown before relaxation of the structure occurs.

Although the iodine electrochemical cell used throughout this study has been proved to be more than a viable alternative to the $ZnCl_2$ source more commonly used, there is still a question over its reliability. The design of the cell is not ideal as there is limited thermal contact with the pellet and the electrical contact is weak. A replacement cell was designed before the end of this study which will hopefully address these problems. The new design is more compact, with provision for only three pellets rather than the seven of the previous design and the thermocouple is closer to each pellet allowing for better temperature control. At the time of writing this thesis, the revised design is being tested as part of a final year project.

7.8 CONCLUDING REMARKS

Recently, at the end of 1997 the race to produce a commercially viable blue semiconductor laser diode has been won by Nichia chemicals using GaN based technology. Reports indicate that a 10,000 hour laser operating at 50°C has been achieved and that the same company hopes to market the device by the end of 1998.[5] Although this would appear to mark the end of II-VI involvement in blue laser diodes there are still plenty of interesting devices possible with II-VI wide bandgap materials. These include SEED's, modulators and piezoelectric devices as well as returning to many of the compounds which were developed and fully researching their physical properties.

7.9 REFERENCES

[1] S. Taniguchi, T. Hino, S. Itoh, K. Nakano, N. Nakayama, A. Ishibashi and M. Ikeda, Electron. Lett. 32 (1996), 552

[2] J. M. Wallace, PhD Thesis 1992, 6-10

[3] J. Simpson and J. O. Williams, J. Appl. Phys. 70 (1991), 2001

[4] J. Simpson, S. J. A. Adams, S. Y. Wang, J. M. Wallace, K. A. Prior and B. C. Cavenett, J. Cryst. Growth, (1991)

[5] W. Meredith, Personal communication